

**PROTEIN ENGINEERING APPLICATIONS ON *Candida methylica*
FORMATE DEHYDROGENASE TO ELUCIDATE FOLDING
MECHANISMS AND TO INCREASE THE THERMOSTABILITY**

**PhD. Thesis by
Emel ORDU**

Department : Advanced Technologies

Programme : Molecular Biology-Genetics and Biotechnology

APRIL 2010

**PROTEIN ENGINEERING APPLICATIONS ON *Candida methylica*
FORMATE DEHYDROGENASE TO ELUCIDATE FOLDING
MECHANISMS AND TO INCREASE THE THERMOSTABILITY**

**PhD. Thesis by
Emel ORDU
(521042204)**

Date of submission : 27 January 2010

Date of defence examination: 26 April 2010

Supervisor (Chairman): Asist.Prof.Dr.Nevin Gül KARAGÜLER (ITU)
Members of the Examining Committee: Doç.Dr.Ayten Yazgan KARATAŞ (ITU)
Doç.Dr.Cenk SELÇUKİ (EU)
Prof.Dr. Melek TÜTER (ITU)
Asist. Prof. Dr. Negahan ERSOY (HU)

APRIL 2010

**PROTEİN MÜHENDİSLİĞİ İLE *Candida methylica* FORMAT
DEHİDROGENAZ ENZİMİNİN KATLANMA MEKANİZMASININ
AYDINLATILMASI VE TERMOSTABİLİTESİNİN ARTTIRILMASI**

DOKTORA TEZİ
Emel ORDU
(521042204)

Tezin Enstitüye Verildiği Tarih : 27 Ocak 2010
Tezin Savunulduğu Tarih : 26 Nisan 2010

Tez Danışmanı : Yrd.Doç.Dr. Nevin Gül KARAGÜLER (İTÜ)
Diğer Jüri Üyeleri : Doç.Dr. Ayten Yazgan KARATAŞ (İTÜ)
Doç.Dr. Cenk SELÇUKİ (EÜ)
Prof.Dr. Melek TÜTER (İTÜ)
Yrd.Doç.Dr. Nagehan ERSOY (HÜ)

NİSAN 2010

FOREWORD

I would like to thank my advisors, Assist. Prof. Dr. Nevin Gül Karagüler and Prof. Dr. Anthony R. Clarke for their valuable scientific and moral supports. I would like to extend my thanks to Dr. Richard Sessions for his useful support in the homology modelling studies.

I would also like to thank Head of Biology Department in Yıldız Technical University, Prof. Dr. Nezhun Gören, for her insightful approach during my thesis work and Assist. Prof. Dr. Şenay Vural Korkut and Assist. Prof. Dr. Nehir Özdemir, for their supports.

I would like to thank all friends from Protein Engineering Research Group in İstanbul Technical University, and Gus Cameron and Kathleen Moreton from C101 Lab. of Department of Biochemistry in University of Bristol.

I must thank my mother, Emine Bıçakçı, father, Şahabettin Bıçakçı and brother, Engin Bıçakçı, who have always been supported my goals.

Finally, I must thank my husband, Levent Ordu, for his constant love, support, and encouragement throughout my thesis work.

I would like to thank the funding agencies for their financial support throughout my PhD research: This thesis was partly supported by ITU Institute of Science and Technology (Project no: 33309), Turkish State Planning Organization (Project no: 90188), Turkish State Planning Organisation in Advanced Technologies Program and TUBITAK (Project no: 107T684).

December 2009

Emel ORDU

TABLE OF CONTENTS

	<u>Page</u>
FOREWORD	xvii
TABLE OF CONTENTS	vii
ABBREVIATIONS	ix
LIST OF TABLES	xi
LIST OF FIGURES	xiii
SUMMARY	xvii
ÖZET	xix
1. INTRODUCTION	1
1.1 Purpose of the Thesis.....	2
1.2 Background.....	5
1.2.1 Protein Folding and Stability.....	5
1.2.2 Folding mechanism in the globular proteins.....	6
1.2.3 Thermostability of globular proteins.....	8
1.2.4 Electrostatic interactions.....	11
1.2.5 Disulphide bridges.....	13
1.2.6 Protein engineering.....	15
1.2.7 Molecular modeling.....	19
1.2.8 Homology modeling.....	20
1.2.9 NAD ⁺ dependent formate dehydrogenase.....	23
1.2.10 Enzymatic regeneration of NAD(P)H.....	25
1.2.11 Thermostability studies of NAD ⁺ -dependent formate dehydrogenase.....	27
2. MATERIALS and METHODS	31
2.1 Molecular Biological Techniques.....	31
2.1.1 Bacterial strains.....	31
2.1.2 Cloning and expression of the <i>cmFDH</i> gene into pQE-2 vector.....	31
2.1.3 Site directed mutagenesis.....	32
2.1.4 Site saturation mutagenesis.....	32
2.1.5 Growth and expression.....	35
2.2 Enzymological Techniques.....	35
2.2.1 Purification of <i>cmFDH</i> protein by using 6xHis-tag system.....	35
2.2.2 Digestion of histidine tag.....	36
2.2.3 Purification by a two-step standard chromatographic technique.....	36
2.3 Kinetic and Thermodynamic Characterization Experiments.....	37
2.3.1 Steady state kinetics.....	37
2.3.2 Equilibrium unfolding assay of <i>cmFDH</i>	37
2.3.3 Stopped flow unfolding experiments of <i>cmFDH</i>	38
2.3.4 Refolding activity assay.....	39
2.3.5 Thermal denaturation.....	39
2.4 Homology Modeling.....	40
2.4.1 Computer simulation protocol.....	41
3. RESULTS and DISCUSSIONS	43

3.1 Improving the Purification of <i>cm</i> FDH by Affinity Tag.....	43
3.2 Kinetic and Thermodynamic Properties of the Folding and Assembly of Formate Dehydrogenase	51
3.2.1 Equilibrium unfolding.....	51
3.2.2 Thermodynamics of the folding-unfolding transition of native <i>cm</i> FDH ..	52
3.2.3 Kinetics of folding and unfolding	58
3.2.4 Construction of a quantitative mechanism	61
3.2.5 A simple analytical method for approximating folding and assembly rates	62
3.2.6 Thermal denaturation	63
3.3 Designed Mutants by Homology Modeling	66
3.3.1 Optimization of protein surface electrostatic interactions.....	66
3.3.2 Disulphide bridge engineering.....	69
3.4 Optimization of Surface Electrostatic Interactions.....	79
3.4.1 Steady state kinetics	79
3.4.2 Irreversible thermal denaturation of electrostatic interaction mutants.....	84
3.4.3 Thermodynamics of the folding-unfolding transition.....	92
3.4.4 Refolding Analysis.....	134
3.5 Introduction of disulphide bridges into <i>cm</i> FDH structure	138
3.6 Site Saturation mutagenesis application on first residue of <i>cm</i> FDH	149
4. CONCLUSION.....	153
REFERENCES	157
APPENDICES	175
CURRICULUM VITAE	179

ABBREVIATIONS

FDH	: Formate Dehydrogenase
cmFDH	: <i>Candida methylca</i> FDH
cbFDH	: <i>Candida boidinii</i> FDH
psFDH	: <i>Pseudomonas</i> sp. 101 FDH
NAD	: Nicotinamide Adenine Dinucleotide
NADP	: Nicotinamide Adenine Dinucleotide Phosphate
SDM	: Site Directed Mutagenesis
PCR	: Polymerase Chain Reaction
DNA	: Deoxyribonucleic Acid
dNTP	: Deoxyribonucleotide Triphosphates
NBT	: Nitroblue Tetrazolium
PMS	: Phenazine Methosulfate
Ni-NTA	: Nickel-Nitrilotriacetic Acid.
IMAC	: Immobilized-Metal Affinity Chromatography
SDS-PAGE	: Sodium Dodecyl Sulphate-Poliacrylamide Gel Electrophoresis
3D	: Three Dimensional
PDB	: Protein Data Bank

LIST OF TABLES

	<u>Page</u>
Table 2.1: Primers to construct the designed mutations by site directed mutagenesis.....	33
Table 2.2: Degenerate primers to construct cmFDH mutant library.....	33
Table 3.1: TAGZyme pQE-2–FDH expression constructs.	45
Table 3.2: Purification protocol of FDH from crude extract of <i>Candida methylca</i> . 46	46
Table 3.3: His-tag digestion conditions for small scale and preparative amount.....	49
Table 3.4: Protein concentrations during digestion procedure.....	49
Table 3.5: Kinetic measurements of His-tagged and digested His-tagged FDH.....	50
Table 3.6: m, K_w , ΔG and [den.] _{0.5} results of native cmFDH from GdnHCl.....	54
Table 3.7: m, K_w , ΔG and [den.] _{0.5} results of native cmFDH from urea.....	56
Table 3.8: Comparison equilibrium and kinetic parameters of some large proteins. 60	60
Table 3.9: Summarise the activity differences in different pH conditions	83
Table 3.10: Comparison of temperatures that provides 50 % inactivation	88
Table 3.11: Residual activities of native cmFDH and mutant enzymes after.	89
Table 3.12: Analysis of thermal denaturation experiments by Arrhenius relationship.	91
Table 3.13: Analysis of thermal denaturation experiments by van't Hoff equation. 91	91
Table 3.14: m, K_w , ΔG and [den.] _{0.5} results of mutant H13E from GdnHCl.....	93
Table 3.15: m, K_w , ΔG and [den.] _{0.5} results of mutant N187E from GdnHCl.....	94
Table 3.16: m, K_w , ΔG and [den.] _{0.5} results of mutant N147R from GdnHCl.....	96
Table 3.17: m, K_w , ΔG and [den.] _{0.5} results of mutant Q105R from GdnHCl.....	98
Table 3.18: m, K_w , ΔG and [den.] _{0.5} results of mutant N187E/Q105R from GdnHCl	100
Table 3.19: m, K_w , ΔG and [den.] _{0.5} results of mutant N187E/N147R from GdnHCl	102
Table 3.20: m, K_w , ΔG and [den.] _{0.5} results of mutant Y160E from GdnHCl.....	104
Table 3.21: m, K_w , ΔG and [den.] _{0.5} results of mutant Y160R from GdnHCl.....	106
Table 3.22: m, K_w , ΔG and [den.] _{0.5} results of mutant Y302R from GdnHCl	108
Table 3.23: [GdnHCl] _{0.5} , m value, free energy changes recorded at 25°C to compare native and mutant cmFDHs.	110
Table 3.24: Thermodynamic properties of the native and surface electrostatic interaction mutants of cmFDH	111
Table 3.25: m, K_w , ΔG and [den.] _{0.5} results of mutant H13E from urea	113
Table 3.26: m, K_w , ΔG and [den.] _{0.5} results of mutant N187E from urea	114
Table 3.27: m, K_w , ΔG and [den.] _{0.5} results of mutant N147R from urea	116
Table 3.28: m, K_w , ΔG and [den.] _{0.5} results of mutant Q105R from urea	118
Table 3.29: m, K_w , ΔG and [den.] _{0.5} results of mutant N187E/Q105R from urea ..	120
Table 3.30: m, K_w , ΔG and [den.] _{0.5} results of mutant N187E/N147R from urea ..	122
Table 3.31: m, K_w , ΔG and [den.] _{0.5} results of mutant Y160E from urea induced..	124
Table 3.32: m, K_w , ΔG and [den.] _{0.5} results of mutant Y160R from urea	126

Table 3.33: m, K_w , ΔG and $[\text{den.}]_{0.5}$ results of mutant Y302R from urea	128
Table 3.34: $[\text{urea}]_{0.5}$, m values and free energy changes recorded at 25°C to compare native and mutant <i>cmFDHs</i>	130
Table 3.35: Thermodynamic properties of the native and surface electrostatic interaction mutants of <i>cmFDH</i>	131
Table 3.36: Unimolecular folding and bimolecular association rate constants of all mutants	137
Table 3.37: Some examples of disulfide bridges	138
Table 3.38: Activity properties of disulphide bridge mutants in oxidised and reduced conditions.....	141
Table 3.39: Thermodynamic parameters for the cysteine mutants in oxidising and reducing conditions	144
Table 3.40: m, K_w , dG and $[\text{den.}]_{0.5}$ results of mutant M1C from GdnHCl induced denaturation experiments.....	145
Table 3.41: m, K_w , dG and $[\text{den.}]_{0.5}$ results of mutant M1C from urea induced denaturation experiments.....	147
Table 3.42: Activity and $T_{0.5}$ values of site saturation mutants on M1 position of <i>cmFDH</i>	149
Table 3.43: Residual activities of native <i>cmFDH</i> and mutant enzymes	151
Table 3.44: Thermodynamic parameters for the site saturation mutants.....	152

LIST OF FIGURES

	<u>Page</u>
Figure 1.1 : The reaction catalyzed by FDH.	24
Figure 1.2 : NAD(P)H regeneration	26
Figure 2.1 : Alignment of <i>Candia methylica</i> and <i>Candida boidinii</i> formate dehydrogenase amino acid sequences	42
Figure 2.2 : Alignment of <i>Candia methylica</i> and <i>Pseudomonas</i> sp 101 formate dehydrogenase.....	42
Figure 3.1 :1094 bp DNA fragment and example of plasmid which has FDH gene	44
Figure 3.2 : Blast homology result of insert.....	45
Figure 3.3 : Overexpression of <i>cmFDH</i> gene.....	46
Figure 3.4 : His-tag (A) and two-steps of standard (B) purification of <i>cmFDH</i>	47
Figure 3.5 : Purified FDH protein.	48
Figure 3.6 : Comassi dying of digested His-tagged FDH with Excess DAPase,	49
Figure 3.7 : Kinetic measurement graph of 6xHis-tagged <i>cmFDH</i>	50
Figure 3.8 : Equilibrium unfolding curves.....	52
Figure 3.9 : GdnHCl-induced equilibrium unfolding curves of native <i>cmFDH</i>	53
Figure 3.10 : Thermodynamics of unfolding of <i>cmFDH</i>	54
Figure 3.11 : Urea-induced equilibrium unfolding curves of native <i>cmFDH</i>	56
Figure 3.12 : Thermodynamics of unfolding of <i>cmFDH</i>	57
Figure 3.13 : Unfolding kinetics of <i>cmFDH</i>	58
Figure 3.14 : Refolding of <i>cmFDH</i> followed by regain of activity.	59
Figure 3.15 : The relationship between the half-time of refolding and reactant concentration.....	62
Figure 3.16 : Heat inactivation of <i>cmFDH</i>	64
Figure 3.17 : Thermodynamic analysis of the unfolding barrier.....	65
Figure 3.18 : Positions of mutations created on the <i>cmFDH</i> gene.	71
Figure 3.19 : Positions of mutants determined by homology modelling based on <i>psFDH</i> and <i>cbFDH</i> 3D structures..	72
Figure 3.20 : Homology model of salt bridge formation between Glu300 and Arg147.....	73
Figure 3.21 : Homology model of salt bridge formation between Arg160 and Asp318.....	74
Figure 3.22 : Homology model of salt bridge formation between Glu160 and Arg277.....	75
Figure 3.23 : Homology model of salt bridge formation between Arg302 and Asp16	76
Figure 3.24 : Homology model of salt bridge formation between Glu302 and Lys19	77
Figure 3.25 : Homology model of disulphide bridge formation between Cys1 and Cys62.....	78

Figure 3.26 : Enzyme kinetic data of native and mutant <i>cmFDH</i>	81
Figure 3.27 : Enzyme kinetic data of native and mutant <i>cmFDH</i>	82
Figure 3.28 : Heat inactivation of N187E mutant of <i>cmFDH</i>	84
Figure 3.29 : Heat inactivation of H13E mutant of <i>cmFDH</i>	85
Figure 3.30 : Heat inactivation of Q105R mutant of <i>cmFDH</i>	85
Figure 3.31 : Heat inactivation of N147R mutant of <i>cmFDH</i>	86
Figure 3.32 : Heat inactivation of Y160E mutant of <i>cmFDH</i>	86
Figure 3.33 : Heat inactivation of Y160R mutant of <i>cmFDH</i>	86
Figure 3.34 : Heat inactivation of Y302R mutant of <i>cmFDH</i>	87
Figure 3.35 : Heat inactivation of N187E/Q105R mutant of <i>cmFDH</i>	87
Figure 3.36 : Heat inactivation of N187E/N147R mutant of <i>cmFDH</i>	87
Figure 3.37 : Bar graph presentation of residual activities of native <i>cmFDH</i> and mutant enzymes.	90
Figure 3.38 : GdnHCl-induced equilibrium unfolding transition of mutant H13E ..	92
Figure 3.39 : Thermodynamics of unfolding of mutant <i>cmFDH</i> , H13E.	93
Figure 3.40 : GdnHCl-induced equilibrium unfolding transition of mutant N187E	94
Figure 3.41 : Thermodynamics of unfolding of mutant <i>cmFDH</i> , N187E.	95
Figure 3.42 : GdnHCl-induced equilibrium unfolding transition of mutant N147R	96
Figure 3.43 : Thermodynamics of unfolding of mutant <i>cmFDH</i> , N147R.	97
Figure 3.44 : GdnHCl-induced equilibrium unfolding transition of mutant Q105R	98
Figure 3.45 : Thermodynamics of unfolding of mutant <i>cmFDH</i> , Q105R.	99
Figure 3.46 : GdnHCl-induced equilibrium unfolding transition of mutant N187E/Q105R	100
Figure 3.47 : Thermodynamics of unfolding of mutant <i>cmFDH</i> , N187E/Q105R..	101
Figure 3.48 : GdnHCl-induced equilibrium unfolding transtion of mutant N187E/N147R	102
Figure 3.49 : Thermodynamics of unfolding of mutant <i>cmFDH</i> , N187E/N147R..	103
Figure 3.50 : GdnHCl-induced equilibrium unfolding transition of mutant Y160E	104
Figure 3.51 : Thermodynamics of unfolding of mutant <i>cmFDH</i> , Y160E.	105
Figure 3.52 : GdnHCl-induced equilibrium unfolding transition of mutant Y160R	106
Figure 3.53 : Thermodynamics of unfolding of mutant <i>cmFDH</i> , Y160R.	107
Figure 3.54 : GdnHCl-induced equilibrium unfolding transition of mutant Y302R	108
Figure 3.55 : Thermodynamics of unfolding of mutant <i>cmFDH</i> , Y302R.	109
Figure 3.56 : Unfolding pattern of native <i>cmFDH</i>	110
Figure 3.57 : Urea-induced equilibrium unfolding transition of mutant H13E.....	112
Figure 3.58 : Thermodynamics of unfolding of mutant <i>cmFDH</i> , H13E.	113
Figure 3.59 : Urea-induced equilibrium unfolding transition of mutant N187E....	114
Figure 3.60 : Thermodynamics of unfolding of mutant <i>cmFDH</i> , N187E.	115
Figure 3.61 : Figure urea-induced equilibrium unfolding transition of mutant N147R	116
Figure 3.62 : Thermodynamics of unfolding of mutant <i>cmFDH</i> , N147R..	117
Figure 3.63 : Figure urea-induced equilibrium unfolding transition of mutant Q105R	118
Figure 3.64 : Thermodynamics of unfolding of mutant <i>cmFDH</i> , Q105R.	119
Figure 3.65 : Figure urea-induced equilibrium unfolding transition of mutant N187E/Q105R.	120
Figure 3.66 : Thermodynamics of unfolding of mutant <i>cmFDH</i> , N187E/Q105R..	121

Figure 3.67 : Figure urea-induced equilibrium unfolding transition of mutant N187E/N147R.....	122
Figure 3.68 : Thermodynamics of unfolding of mutant <i>cmFDH</i> , N187E/N147R. .	123
Figure 3.69 : Figure urea-induced equilibrium unfolding transition of mutant 160E	124
Figure 3.70 : Thermodynamics of unfolding of mutant <i>cmFDH</i> , Y160E.....	125
Figure 3.71 : Figure urea-induced equilibrium unfolding transition of mutant Y160R	126
Figure 3.72 : Thermodynamics of unfolding of mutant <i>cmFDH</i> , Y160R.	127
Figure 3.73 : Figure urea-induced equilibrium unfolding transition of mutant Y302R	128
Figure 3.74 : Thermodynamics of unfolding of mutant <i>cmFDH</i> , Y302R.	129
Figure 3.75 : GdnHCl and urea induced unfolding of native and mutant <i>cmFDH</i> s.	133
Figure 3.76 : Refolding of H13E mutant <i>cmFDH</i> followed by regain of activity. .	134
Figure 3.77 : Refolding of N187E mutant <i>cmFDH</i> followed by regain of activity.	134
Figure 3.78 : Refolding of N147R mutant <i>cmFDH</i> followed by regain of activity.	135
Figure 3.79 : Refolding of N187E/N147R mutant <i>cmFDH</i> followed by regain of .	135
Figure 3.80 : Refolding of Y160E mutant <i>cmFDH</i> followed by regain of activity.	135
Figure 3.81 : Refolding of Y302R mutant <i>cmFDH</i> followed by regain of activity.	136
Figure 3.82 : The relationship between the half-time of refolding and reactant concentration.....	137
Figure 3.83 : Activity of disulphide bridge mutant M1C/D62C.	140
Figure 3.84 : Activity of single mutants, M1C, D62C, in oxidised and reduced conditions.....	140
Figure 3.85 : The heat denaturation of M1C/D62C mutant	142
Figure 3.86 : The heat denaturation of M1C mutant	142
Figure 3.87 : GdnHCl -induced equilibrium unfolding curves of mutant M1C	145
Figure 3.88 : Thermodynamics of unfolding of mutant <i>cmFDH</i> , M1C.....	146
Figure 3.89 : Urea-induced equilibrium unfolding curves of mutant M1C.....	147
Figure 3.90 : Thermodynamics of unfolding of mutant <i>cmFDH</i> , M1C.....	148
Figure 3.91 : Bar graph presentation of residual activities of native <i>cmFDH</i> and site saturation mutants.	151
Figure A.1 : TAGZyme™ pQE-2 expression vector.....	178

PROTEIN ENGINEERING APPLICATIONS ON *Candida methylica* FORMATE DEHYDROGENASE TO ELUCIDATE FOLDING MECHANISMS AND TO INCREASE THE THERMOSTABILITY

SUMMARY

The NAD⁺-dependent formate dehydrogenases (FDHs) catalyze the oxidation of formate to carbon dioxide, coupled with reduction of NAD⁺ to NADH thus they are widely used to regenerate the expensive NAD(P)H coenzyme which is essential for all NAD(P)H-dependent oxidoreductases. The limitation in the thermostability of FDH enzyme is a crucial problem, despite of its advantages. In this study a simple and efficient method was described to improve the purification of NAD⁺-dependent FDH from yeast *Candida methylica* (*cm*FDH) to allow us to easily purify the designed and constructed mutants. After the optimization of protein purification, the folding mechanism and stability of dimeric *cm*FDH were analysed. Equilibrium denaturation data yielded a dissociation constant of about 10⁻¹³ M. Findings showed that homodimeric *cm*FDH unfolds by two state single transition model without intermediates in equilibrium. In the equilibrium one dimer is equal to two unfolded monomers including both folding and dissociation processes.

The kinetics of refolding and unfolding reactions revealed that the overall process comprises 2 steps, folding and assembly, representing a irreversible unimolecular-bimolecular kinetic model. In the first step a marginally stable folded monomeric state is formed at a rate (k_1) of about $2 \times 10^{-3} \text{ s}^{-1}$ (by deduction k_{-1} is about 10^{-4} s^{-1}) and assembles into the active dimeric state with a bimolecular rate constant (k_2) of about $2 \times 10^4 \text{ M}^{-1} \text{ s}^{-1}$. The rate of dissociation of the dimeric state in physiological conditions is extremely slow ($k_{-2} \sim 3 \times 10^{-7} \text{ s}^{-1}$).

Homology modelling has been used to design a more thermostable enzyme by optimizing electrostatic interactions on the protein surface and introduction a disulphide bridge into protein structure. Site directed and site saturation mutagenesis techniques have been applied to the original *cm*FDH enzyme to construct mutant enzymes. The effects of site-specific engineering on the stability of this molecule was analysed according to minimal model of folding and assembly reaction and deduced equilibrium properties of the native system with respect to its thermal and denaturant sensitivities. It was observed that mutations did not change the unfolding pattern of native *cm*FDH and increased numbers of electrostatic interactions can cause either stabilizing or destabilizing effect on the thermostability of this protein. Except relatively improved mutants, M1C, N147R, N187E and Q105R mutations increased the melting temperature on the average of 2, 2.75, 6, 2.75 °C. The most dramatic increase in the stability was observed for the N187E mutants which has about 6 °C greater than that of the native *cm*FDH.

PROTEİN MÜHENDİSLİĞİ İLE *Candida methylica* FORMAT DEHİDROGENAZ ENZİMİN KATLANMA MEKANİZMASININ AYDINLATILMASI VE TERMOSTABİLİTESİNİN ARTTIRILMASI

ÖZET

NAD⁺-bağımlı format dehidrogenazlar (FDHs) karbondioksidin formata oksidasyonunu katalizlerken NAD⁺'yi NADH'e indirgerler. Bu özelliklerinden dolayı FDH'ler tüm NAD(P)H-bağımlı oksidoredüktazlar tarafından kullanılan ve oldukça pahalı bir koenzim olan NAD(P)H'in rejenerasyonunda yaygın olarak kullanılmaktadır. Birçok avantajına rağmen düşük termostabilitesi FDH enzimin en önemli dezavantajıdır. Bu çalışmada öncelikle protein mühendisliği çalışmalarında oluşturulacak mutant enzimlerin kolay ve verimli saflaştırılabilmesi amacıyla *Candida methylica* mayasından klonlanmış olan NAD⁺-bağımlı format dehidrogenaz (*cmFDH*) enzimi için basit ve etkili bir protein saflaştırma metodu geliştirilmiştir. Saflaştırma işleminin optimize edilmesinin ardından *cmFDH* enziminin katlanma mekanizması ve stabilitesi incelenmiştir. Protein dissosiyasyon sabitinin 10⁻¹³ M olarak hesaplandığı denge denaturasyon deneyleri homodimerik *cmFDH* yapısının herhangi bir ara yapı oluşturmadan iki yapıya tek adım geçiş modeline göre katlanmamış hale geçtiğini göstermiştir. Denge durumunda bir dimer iki katlanmamış monomere eşittir ve katlanma ve birleşme işlemlerinin her ikisini de içerir.

Kinetik deneyleri katlanma işleminin iki adımda gerçekleştiğini göstermiştir. Birinci adımda kararlı halde katlanmış monomerik yapı (k_1) 2x10⁻³s⁻¹ hız sabiti ile oluşmakta ve ikinci adımda aktif dimerik yapı yaklaşık 2x10⁴ M⁻¹s⁻¹ olarak hesaplanan (k_2) bimoleküler hız sabiti ile biraraya gelmektedir. Fizyolojik koşullarda dimerik yapının dissosiyasyon sabiti oldukça yavaştır (3x10⁻⁷ s⁻¹).

Daha kararlı bir enzim dizayn etmek üzere protein yüzeyindeki elektrostatik etkileşimlerin optimizasyonu ve disülfid köprüsü oluşturulması için homoloji modellemesi kullanılmıştır. Dizayn edilen mutantlar bölgeye özel ve saturasyon mutasyon teknikleri ile oluşturulmuştur. Bölgeye özel değişikliklerin molekülün stabilitesi üzerindeki etkileri rekombinant yabancı tip enzim için elde edilen minimal katlanma ve birleşme modeline ve rekombinant yabancı tip enzime termal ve kimyasal denaturasyon uygulanılarak elde edilen denge özelliklerine göre analiz edilmiştir. Sonuçlar uygulanan mutasyonların enzimin katlanma özelliklerini değiştirmediğini ortaya çıkarırken, elektrostatik etkileşimlerin arttırılmasının bu proteinin termostabilitesi üzerinde olumlu ya da olumsuz etkileri olabileceğini göstermiştir. Bağlı olarak stabilitesi arttırılmış mutantlar dışında M1C, N147R, N187E ve Q105R mutasyonları *cmFDH* enziminin erime sıcaklığını sırasıyla ortalama 2, 2.75, 6 ve 2.75 °C arttırmıştır. En dikkat çekici artış rekombinant yabancı tip enzimden 6 °C daha yüksek T_m değerine sahip olan N187E mutantında gözlenmiştir.

1. INTRODUCTION

It is arguable that efforts to control the stability of proteins by genetic modification of sequence could be laid on a firmer foundation such that we would understand better the full mechanism of folding and unfolding of the active system. This, ideally, requires elucidation of the kinetic and equilibrium properties of each step and, in addition, it would be illuminating to know the temperature-dependence of the system so that its classical thermodynamic properties can be derived. With such a foundation, it might be possible to target certain critical steps in the process, so that sequence engineering would be more rationally directed.

While there is a wealth of data on the kinetics and thermodynamics of folding in single-chain proteins (Rumfelt *et al*, 2008), our understanding of folding and assembly processes in multi-chain proteins is less comprehensive. Clearly, it is more demanding to study such systems, owing to their greater complexity and the frequently encountered inefficiency of self-assembly of oligomeric structures. However, many of the proteins of interest in biotechnology are oligomeric, as are many of the structures in biological systems where we want to understand the dynamics of assembly and disassembly and for these reasons it is useful to examine such mechanisms with a view to provide a framework for their analysis. Also monomeric protein folding studies provide information about the relationship between amino acid sequence and secondary or tertiary structure in theory, but quaternary structural information can only be obtained from oligomeric protein studies (Maity *et al.*, 2005).

In this thesis we used *Candida methylica* formate dehydrogenase (*cmFDH*), cloned and overproduced by Allen and Holbrook (1998), as a study object owing to its potential in industrial scale and the ease of measuring its regain of activity. While there has been much empirical work on stabilizing FDHs against elevated temperatures and other environmental factors such as oxidation (Wu *et al*, 2009; Andreadeli *et al*, 2008; Thiskov and Popov, 2006), the thermodynamic and kinetic properties of its folding and unfolding pathways have not been dissected in detail. In

this thesis, firstly, we defined the rates of steps in the minimal model of folding and assembly reaction and deduced the equilibrium properties of the system with respect to its thermal and denaturant sensitivities. After the characterization of folding and unfolding properties of the *cmFDH*, these results were used as a basis for understanding the effect of site-specific engineering on the thermostability of this molecule.

Although there are several successful examples of stabilization of proteins, general methods of increasing protein stability are not available, since the mechanism of thermostabilization is not yet clearly understood (Kumar *et al.* 2000). Results found in the literature show that studies to increase protein thermostability are mainly concentrated on optimizing the electrostatic interactions on the protein surface and generating disulphide bridges strategies by using rational and semirational design (Arolas *et al.*, 2009; Haung *et al.*, 2009; Hyun *et al.*, 2009; Roca *et al.*, 2007; Permyakov *et al.*, 2005; Eijsink *et al.*, 2004; Kumar and Nussinov, 2001).

Several strategies have been applied to increase the thermostability of FDH from bacteria and yeast (Tishkov and Popov 2006, Karagüler, 2007a). However, effect of surface electrostatic interactions on the FDH from a yeast source has not been investigated yet. On the other hand generating disulphide bridge have not given expected results on the *cmFDH* so far. Here, after the characterization of folding and assembly properties of *cmFDH*, we attempted to overcome thermostability problem by using two strategies mentioned above and to investigate the effect of surface electrostatic interactions on the folding characteristics of *Candida methylica* FDH. Site directed mutagenesis and site saturation mutagenesis methods were used to obtain desired mutations.

1.1 Purpose of the Thesis

Production of optically pure compounds is important for product quality and customer safety in industry. Racemic mixtures, which contain both forms of optically active compounds, are a problem in the synthesis of chiral molecules. In the pharmaceutical industry, when only one enantiomer has the appropriate physiological activity, problems from side effects can arise like the case of thalidomide. While the R-enantiomer of thalidomide has an analgesic activity, the S-enantiomer causes defects in the fetus (Davies and Teng, 2003; Muller, 1997;

Eriksson, 1995; Dunn et al, 1991). In food industry, chiral molecules are indicator of quality and purity of products. Natural food components are optically pure but extreme industrial process like high pH, temperature and irradiation cause racemic mixture in the food. Chirality is also important in taste and odour application in food industry. For example, while the L-form of asparagine, tryptophan, tyrosine and isoleucine are characterized by bitter taste, they are characterized as sweet taste in the D-form (Wojtasiak, 2006).

Enzymatic reactions catalyzed by oxidoreductases (e.g. lactate dehydrogenase, hydroxyisocaproate dehydrogenase, xylitol dehydrogenase, mannitol dehydrogenase and limone monooxygenase) are highly stereospecific and very important for the production of chirally pure products. Enzymatic synthesis of the final product may reach 100 %, while the processes based on chemical synthesis of racemic mixtures can only provide the theoretical yield of 50 %. Lactate dehydrogenase and hydroxyisocaproate dehydrogenase can be used in the production of optically pure hydroxyacids which are used for the production of semi synthetic antibiotic (S - α -hydroxyisocaproic acid) and medical diagnosis (S – phenyl pyruvate in diagnosis of phenylketonuria and S – ketoisocaproic acid for some urine disease) (Van der Donk and Zhao, 2003; Nakamura, 1988). Xylitol dehydrogenase and mannitol dehydrogenase are used in D-xylitol and D-mannitol synthesis, respectively and limone monooxygenase used in aroma synthesis also provides stereospecific compounds in the food industry (Kaup et al, 2005; Mayer et al, 2002). However use of these enzymes and similars is still limited because of the requirement for stoichiometric amounts of the very expensive NAD(P)H coenzyme. It is possible to recover used coenzymes via recycling reactions, however, existing methods for regenerating NAD(P)H are still a significant expense and are not cost-effective in the manufacturing process. Therefore, there is a need for a low-priced method of coenzyme regeneration (Liu and Wang, 2007; Patel, 2004; Vrtis,2002).

There are several approaches for the regeneration of nicotinamide coenzymes including, chemical, photochemical, electrochemical and enzymatic methods. NAD(P)H regeneration with enzymatic methods is the most promising among the methods examined (Eckstein, 2004; Nakamura, 1988). Many enzymes like phosphite dehydrogenase (PTDH) (Johannes et al., 2007; Woodyer et al., 2006), glucose dehydrogenase (GDH) (Xu et al, 2007) and formate dehydrogenase (FDH) (Wu et al,

2009; Andreadeli, 2008; Bolivar et al., 2007; Karagüler et al., 2001) were studied and used for NAD(P)H regeneration in processes of enzymatic chiral molecule synthesis. Studies showed that FDH is the best and widely used enzyme for regenerating NADH in enzymatic synthesis of optically active compounds. FDH offers several advantages over other dehydrogenases. It is available and low cost and has a favourable thermodynamic equilibrium. Reaction results in a 99–100 % yield of the final product. The reaction of FDH is essentially irreversible and the final product (CO₂) can be easily removed from the reaction system. Formate or CO₂ will not inhibit the other reaction and interfere with the purification of the final product. FDH also has a wide range pH optimums so that it can work with lots of different enzymes (Thiskov and Popov, 2006).

The number of studies on FDH and its application for coenzyme regeneration in the processes of chiral synthesis with NAD(P)H-dependent enzymes is getting large year by year. Studies show that methylotrophic yeast and bacterial FDHs are more stable and cheaper and easier to produce. In laboratory scale experiments, FDH was used for NADH regeneration with several enzyme like lactate dehydrogenase, xylitol dehydrogenase and mannitol dehydrogenase in the production of hydroxyacids, xylitol and mannitol, respectively, (Van der Donk and Zhao, 2003; Kaup, 2005; Mayer, 2002). FDH from the yeast *Candida boidinii* was used in the first commercial scale process of chiral synthesis of tert-L-leucine with leucine dehydrogenase by German Degussa company (Popov and Thiskov, 2003).

Unfortunately, native FDHs have some disadvantages. These are low k_{cat} , high K_M , its limited coenzyme specificity and solvent tolerance and lack of thermostability (Karagüler, 2007). Hence it is important to improve, the stability of FDH to cope with the harsh conditions like high temperature, pressure or pH required for the most of manufacturing processes in food or pharmaceutical industries. The most significant parameter to affect enzyme stability during the manufacturing process is high temperature. For example in the starch sector, which is one of the largest users of enzymes, conversion of starch include liquefaction and saccharification steps. The temperature has to be 105-110 °C during these processes. Otherwise, below 105 °C, gelatinisation of starch granules is not achieved successfully and causes filtration problems in the other steps (Synowiecki, 2006; Haki, 2003). This causes an economical challenge for the manufacturer. If such problems can be solved by high

temperature, any FDH enzyme that would be used for NAD(P)H regeneration in this kind of high temperature process would need to be thermostable.

In brief, our aim is to contribute towards the economical regeneration system for NAD(P)H coenzyme which is important for enzymatic synthesis of chiral products, by increasing the thermal stability of formate dehydrogenase from *Candida methylca* yeast. Protein engineering is a promising approach to enhance the thermostability of FDH but care has to be taken not to decrease the specific activity of the enzyme. By using these techniques industrial important protease, amylase, lipase and cellulase enzymes have been enhanced and produced in large scale (Rubingh, 1996; Decklerck, 1995; Martinelle, 1996; Koivula, 1996). Mutations performed to obtain desired properties also give valuable information to elucidate *cm*FDH structure and relationship between folding and stability.

1.2 Background

1.2.1 Protein Folding and Stability

Protein stability, in other words the capacity of protein to protect its native and functional structure is essential to life. All biological processes depend on the native state of proteins which are stable and in the appropriate and unique folded conformation. While polypeptide chain is folding it also increases the stability. It is important to know how proteins fold into their biologically functional states, and how these functional active states are stabilized. The driving forces responsible for protein folding and protein stabilization are the same (Jaenicke, 2000), therefore protein stability and folding studies are not separate from each other.

The folding process of a polypeptide chain to a unique three dimensional structure is required to have a functional protein according to physiological needs of an organism. How a protein folds into its native and active state, what forces stabilize protein structure and the relationship among stability, folding and function are still unsolved and challenging problems. Proteins are synthesized as linear polymers that organize themselves into specific three dimensional structures through a series of intermediate states. Amino acid sequence, in other words genetic codes of proteins, determine their three-dimensional structures, consequently protein stability and protein folding mechanisms (Baker, 2000). For the first time Anfinsen et al. (1973)

demonstrated this keystone information by experiments on the folding of RNaseA. While many studies have been performed since Anfinsen's work, using new approaches and tools improving day by day, there are no accurate rules for this phenomena. How to predict the three-dimensional structure of a protein from a known amino acid sequence is still the main concern of several research disciplines like protein stability, genome research, drug design or protein conformational disorders etc.

1.2.2 Folding mechanism in the globular proteins

During the folding process, an unfolded polypeptide chain finds its functional structure, amongst an large set of possible conformations typically in a milliseconds-to-seconds time scale, typically. This time scale is much faster than the rate estimated for randomly searching all possible conformations, and is known as the Levinthal paradox (Leach, 2001; Chen et al., 2008). Based upon this knowledge about the folding rate, Levinthal proposed that there can not be a random search to reach the three dimensional active conformation, folding must proceed along a defined pathway where the polypeptide is driven, both thermodynamically and kinetically, through an ordered series of distinct, transiently populated intermediates (Zwanaing et al., 1992).

In the folding of globular proteins the folding process is thought of as an energy funnel; a rapid hydrophobic collapse phase of linear polypeptide followed by a slower second phase that often consists of a compact secondary structure "molten globule" intermediate. Subsequently, the tertiary structure evolves simultaneously with or without population of intermediates (Uversky, 2003). In the literature, some proteins which were unfolded in vitro have shown the accumulation of at least one kind of intermediate state, but some proteins have shown none (Riley et al., 2007; Went et al., 2004). The folding process like many biological processes comprise a mixture of first order and second order transitions during the conversion of the polypeptide chain from a disordered, nonnative state to the ordered native state (Privalov, 1996).

In the case of oligomeric proteins that fold with the assistance of chaperones, in vivo, oligomerization may occur after release of the folded subunits from the chaperone or vice versa (Ali and Imperiali, 2005). In some proteins such as P22 tailspike protein

and bacterial luciferase, the subunit association occurs before folding is completed. In other proteins such as aspartokinase I, homoserine dehydrogenase I, and malate dehydrogenase, each subunit is first folded and then the folded subunits associate into a larger complex (Doyle et al., 2000).

The formate dehydrogenase (FDH) enzyme used in our work is a homodimeric protein. Folding mechanisms of dimeric proteins have been studied with several proteins like coagulation Factor XI (Riley et al., 2007), Mge1p (Moro and Muga, 2006), *Erythrina indica* lectin (Ghosh and Mandal, 2006), dimeric variant Cro F58W (Maity et al., 2005), Arc repressor (Milla and Sauer, 1999), Trp aporepressor (Mann and Matthews, 1993). Studies on these proteins suggest that the folding mechanism involves, in some cases, the presence of folded and partially folded monomeric and dimeric intermediates and, in other cases, involves native dimeric and unfolded monomeric forms (Maity et al., 2005).

1.2.2.1 Diseases related to protein folding

Understanding of protein folding is also related to neurodegenerative diseases and give valuable information for drug development research.

The folding of a protein depends on its environment. Stress conditions like heat shock and reactive oxygen species or genetic defects cause some errors in the protein folding process. These errors lead to aggregation instead of native protein structure which has minimum hydrophobic surface area and could promote ordered fibrillar intermediate aggregation (Wickner et al., 1999). Sometimes the crowded environment in the cytosol also increases the propensity of incompletely folded chains to misfold, partly fold or aggregate (Ellis, 2003; Stagg, 2007).

Misfolded or partially unfolded fibrilizing proteins cause functional deficits such as cystic fibrosis, Alzheimer diseases, Parkinson diseases, osteogenesis imperfecta, prion based diseases, amyloidosis etc. (Banavar and Maritan, 2007).

The amyloidoses comprise a large group of diseases caused by an alteration in the conformation and metabolism of several globular proteins which deposit as insoluble amyloid fibril structures. Amyloid fibrils are hydrophobically collapsed species containing different degrees of secondary and tertiary structure formation. They have protease resistant structures characterized by a high content of β sheets (Bellotti et al., 2007; Radford et al., 2005). Although all fibrils share some common

morphological features, like reduced folding stability, tendency to get several conformations, they have not conserved amino acid sequence motif (McParland et al., 2000). Fibrillation and protein deposition diseases have been related to destabilized native structures and increased steady state concentration of partially folded conformers. Thus the aggregation of fibrillar proteins can be reduced by increasing stability of the native protein.

Some cytosolic enzymes and molecular chaperones often assist protein folding *in vivo* to prevent fibrillation and aggregation. They prevent aggregation by promoting proper folding (Prosinecki, 2007; Young et al., 2004; Hartl, 2002; Jaenicke, 1991). Chaperones are important molecules in the efficient folding and assembly and transportation of newly synthesized proteins and their refolding under denaturing stress conditions. Different chaperone proteins cooperate with each other to control polypeptides at all stage of folding by binding to first stage polypeptide chains in the very complex cell environment. Folding and degradation of a cytosolic protein are determined by some chaperone pathways. Irreversibly, misfolded proteins that could escape from the chaperone system are degraded by the proteasomes (McClellan, 2005). Both chaperones and proteases select the hydrophobic regions of unfolded polypeptides. The chaperone activities of heat shock proteins enable folding of newly synthesized proteins and assist protein translocation across intracellular membranes. The heat shock proteins undertakes in the signaling pathways to regulate growth and development of folded proteins. Hsp90 and Hsp70 are associated with a number of signaling molecules, including v-Src, Raf1, Akt and steroid receptors (Nollen and Morimoto, 2002; Young et al., 2001).

1.2.3 Thermostability of globular proteins

During the evolution, several organisms have managed to live in their natural environment, from boiling waters of hot springs to cold sea of South Pole Sea; from the highest parts of earth to deep sea and absolute dark caves, by means of mutations that trigger new and improved phenotypes (Bloom et al., 2006). Organisms adapted to extremes of pH, salinity, pressure and temperature are generally called extremophiles and they have drawn attention of many scientists to understand how extremophiles are able to stay alive while their mesophilic counterparts cannot in extraordinary conditions. Proteins are the best candidates to evolve because they may

change their biochemical function with just a few mutations (Razvi and Scholtz, 2006). These molecules have evolved by different strategies to protect their stability and function under unusual conditions.

The main forces which are responsible for protein stability comprise the covalent bonds in the peptide backbone, disulphide bridges and noncovalent interactions between residues and interactions between water and residues. The major stabilizing noncovalent forces are cumulative effect of van der Waals interactions, hydrophobic interactions, interactions between charged groups (electrostatic interactions or salt bridges) and between polar groups (hydrogen bonds). The balance of these forces is known as the conformational stability of a protein and is defined thermodynamically as the Gibbs free energy change, ΔG , for the transition from the native structure to unfolded structureless polypeptide chain.

Protein stability studies have been performed against to several denaturing agents like extremes of pH, salinity, pressure and temperature. Among these extreme conditions, high temperature stability (thermostability) is particularly important in the industrial and biotechnological enzymatic production process where the enzymes are often inactivated due to high temperature (please see section 1.1) The lack of thermostability of proteins is one of the limiting factor for development of biotechnological and industrial processes.

Therefore, one purpose of protein engineering is the molecular redesign of proteins to be stable against heat. Thermostability can be investigated both as thermodynamic and kinetic stability. In order to increase the stability of proteins, folding and unfolding mechanism should be known both kinetically and thermodynamically. Kinetic stability depends on the activation energy of unfolding and it refers to the enzyme activity even under denaturing conditions. The thermodynamic stability depends on the equilibrium between the native and denatured state and is temperature dependent. It is represented by the conformational stabilities (enthalpy, entropy and free energy) and by the midpoint transition temperatures for unfolding (i.e., T_m). The thermodynamic description allows generating a stability curve for a protein that defines how the conformational stability varies with temperature only when the protein denatures reversibly. If the protein denaturation is irreversible kinetic characterization can be made by measuring the rate of thermally induced

activity loss at set of temperatures. Therefore, it is important to investigate kinetic stability and equilibrium stability separately.

In the thermodynamic characterization studies, measuring ΔG as a function of temperature generates a parabolic curve, crossing zero at both high and low temperatures. The temperature that protein shows maximum stability is between these high and low temperature points. On this curve, the point at which ΔG of protein unfolding is zero defines the melting temperatures (T_m) under a given set of conditions. The thermodynamic parameters; enthalpy changes (ΔH), entropy changes (ΔS) and changes in heat capacity (ΔC_p) are determined by fitting this curve to modified version of the Gibbs–Helmholtz equation ($\Delta G = \Delta H + \Delta C_p \cdot (T - T_o) - T \cdot \Delta S - \Delta C_p \cdot T \cdot \ln(T/T_o)$) at a chosen reference temperature (T_o).

In order to understand thermostability, differences between thermophilic and mesophilic proteins have been compared in many studies. Comparison of stability curves of thermophilic and mesophilic proteins show that thermophilic proteins achieve stability at high temperatures via 3 different strategies either in combination or separately. Firstly, the melting temperature (T_m) may be increased by raising the stability curve to higher ΔG ; secondly the curve may be broadened by decreasing the slope to reach higher T_m ; finally, the curve may be shifted to the right towards higher temperatures (Razvi and Scholtz, 2006; Kumar and Nussinov, 2001).

The results of protein stability studies and the shapes of the curves obtained depend on the sequence–structure–stability relationship at the molecular level. Sequence defines protein structure, and interactions in the structure determine stability. For instance, in strategy one, ΔG can be increased by changing the electrostatic interactions, salt bridges, hydrogen bonds, or hydrophobic interactions etc, by adding single amino acid mutations at the molecular level (Razvi and Scholtz, 2006).

Studies in the literature also show that thermophilic proteins typically have increased number of van der Waals interactions, hydrogen bonds, salt bridges, dipole-dipole interactions, disulphide bridges and hydrophobic interactions, aromatic stacking interactions improved core packing, shorter and/or tighter surface loops, enhanced secondary structure propensities, decreased conformational entropy of the unfolded state and oligomerization at the molecular level (Karshikoff and Ladenstein, 1998; Kumar et al., 2000; Robinson-Rechavi et al., 2006). According to these observations

several efforts have been attempted to identify the most efficient method to enhance thermostability of a mesophilic protein by using site directed mutagenesis (Annaluru et al., 2006; Yokoigawa et al., 2003; Rodriguez et al., 2000). However, since there is no single factor that contributes towards protein stability, strategies may not be transferable among several families.

After the determination of importance of hydrophobic interaction by Langmuir (1938), hydrophobic interactions are one of the widely studied and observed driving forces behind the folding and stability of globular proteins (Dill, 1990; Reiersen and Rees, 2000; Folch, et al., 2008). Recent results show that two other strategies have attracted attention to increase protein thermostability. One of them is improving the electrostatic interactions on the protein surface to optimize the surface electrostatic interactions (Takita et al., 2008; Roca et al., 2007; Kundrotas and Karshikoff, 2002; Trejo et al., 2001, Kumar and Nussinov, 2001; Eijsink, 2004. The second one is the introduction of disulphide bonds between Cys residues (Rajagopalan et al., 2007; Russo et al., 2002; Tigerström, 2004; Mason et al., 2005; Hamza and Engel, 2007; Yang et al., 2007; Chu et al., 2007). Although the contribution of surface electrostatics or disulphide bridges to protein stability is still not fully understood, it is clear that these interactions are important in protein stability.

1.2.4 Electrostatic interactions

Optimization of the electrostatic interactions on the protein surface has become an attractive way to increase the thermostability of a protein as mentioned above. Changes in electrostatic interaction of charged side chains of residues are critical for protein folding and stability, consequently biological activity of the protein. Strong electrostatic interactions have been shown on the folding pathway of several proteins (Cho and Raleigh, 2006; Oliveberg and Fersht, 1999). Although electrostatic interactions like hydrogen bonds and salt bridges contribute to stability less than hydrophobic interactions, salt bridges buried within the hydrophobic folding units provide a specificity to the fold. (Waldburg et al, 1995; Spector et al., 2000). Electrostatic interactions also provide the specificity of protein-protein interactions at subunit interface (Stevens et al., Biochem., 2000). Analysis of protein-protein interfaces also shows the stabilizing effect of more hydrogen bonds and salt bridges across the interfaces (Kumar and Nussinov, 2002). Relative locations and

geometrical orientations of electrostatic interactions respect to one another and their environment are important, as well as the number of them, for protein stability. (Loladze et al., 1999; Kumar and Nussinov, 2001).

When mesophilic and thermophilic or hyperthermophilic orthologous protein groups were compared it was shown that hyperthermophilic and thermophilic proteins have greater electrostatic interactions than their mesophilic homologous on the surface. Compared with positions buried in the core, stabilizing surface mutations are less likely to disrupt the tertiary structure, therefore surface mutations occur frequently during evolution (Xiao and Hoing, 1999; Alsop et al., 2003, Loladze and Makhatadze, 2002).

Experiments performed to calculate electrostatic contribution of salt bridges to protein stability show that character and position of salt bridging groups affect the helix formation (Hendsch and Tidor, 1994). Salt bridges are often formed in protein secondary structural elements. Although there have been relatively fewer studies on salt-bridge formation in β sheets, salt bridges stabilize the β sheets to similar extents as the α helices (Kumar and Nussinov, 2002).

Electrostatic interactions affect the protein flexibility which implies movement of atoms, residues, and fragments of the protein with respect to one another. Therefore it is important for protein-protein, protein-ligand, enzyme-substrate, antigen-antibody binding or protein folding processes. Proteins show a general flexibility in side chain and main chain atoms of the native state and a partial flexibility in response to a molecular event related to the protein function. Close range electrostatic interactions allow protein flexibilities by breaking and reforming easily (Kumar et al., 2001).

The electrostatic interactions are pH-dependent. Proteins generally become unstable at extreme pH values because increased acidity or basicity affects the overall charge on the molecule, generally leading to increased charge repulsion which destabilizes the folded form (Whitten and Moreno, 2000; Matthews, 1993). Formation or breakage of salt bridges may be accompanied by changes in the pK_a of the charged-residue side chains and in protein stability (Kumar et al., 2001; Kortemme et al., 2000).

Ionizable groups have structural and functional roles in proteins and they contribute to a single electrostatic network including interactions over all relevant distances

(Xiao and Honig, 1999). Electrostatic interactions such as salt bridges and their network may destabilize the proteins in some cases (Hendsch and Tidor, 1994; Trejo et al., 2001). The most remarkable point of Hendsch and Tidor's work is that nearly all 21 salt bridges studied are electrostatically destabilizing by an important amount, roughly 2.5-6.0 kcal/mol. While a 4.0 Å distance between the charged groups is stabilizing to proteins, at distances exceeding 4.0 Å they largely contribute to destabilization of the protein structure (Loladze et al., 1999; Perl and Schmid, 2001).

On the other hand lots of studies have shown that an increase in the proportion of charged residues and optimized electrostatic interactions appear to be most consistent among the factors enhancing protein thermostability. This relationship between thermostability and electrostatic interaction has been shown for several proteins including pig cytosolic malate dehydrogenase (cMDH) (Trejo et al., 2001), ubiquitin (Loladze and Makhatadze, 2002), the holo azurin enzyme from *Pseudomonas aeruginosa* (Tigerstem et al., 2004), Ribonuclease T1 (Grimsley et al., 1999), bovine calbindin D (Akke and Forsen., 1990), cytochrome P450 (Maves and Sligar, 2001), cold shock and CheY protein families (Dominy et al., 2004).

Although the strategy of optimization of electrostatic interactions by engineering mesophilic proteins to achieve thermal stability is complex and not fully understood, there is a broad agreement between scientists that surface charged residues are important for the stability of proteins.

1.2.5 Disulphide bridges

Before the discovery of large numbers of proteins containing disulphide bonds in microorganisms living at extreme temperature conditions it was thought that disulphide bonds have no effect on thermostability because they are prone to oxidative degradation at high temperatures. However, results in the literature show that covalent bonding of thiol groups can provide protein stabilization as much as cumulative non-covalent interactions in terms of free energy (Ladenstain and Ren, 2006). Disulphides are also essential to folding, global structure, stability, and function but only have a minimal effect on dimer formation (Rajagopalan, 2007).

Using the strategy of site directed mutagenesis of residues to cysteine allows the formation of covalent intermediates which may be isolated and characterized structurally and the investigation of rates of disulphide-bond formation and reduction

factors which can be varied without altering other interactions in the protein (Pecher and Arnold, 2009; Thangudu et al., 2008). This basic approach encouraged the researchers to investigate the effect of disulphide bonds on protein stabilization and the folding pathways of numerous proteins. After the studies of Anfinsen on the reduction and reformation of protein disulphide bonds of ribonuclease in 1961, the role of disulphides has been extensively studied on monomeric proteins. Therefore recent studies have been concentrated on oligomeric proteins (Fernandez-Lafuente, 2009; Cabra, 2008; Das, 2007; Mason, 2005; Russo, 2002)

Intra or intermolecular disulphide bonds play an important role in the folding pathway and stabilize the proteins in the folded native structure. Structural disulphide bonds usually connect nonadjacent cysteine residues which are most frequently buried inside proteins. The introduction of a disulphide bond generally increases the free energy of unfolded state by reducing its configurational entropy and also affects interactions among residues of entire protein by tying two residues together (Wedemeyer, 2000). Disulphide bonds may also stabilize the folded state enthalpically through favorable local interactions, especially in flexible regions suggesting that enthalpic N-state effects may dominate negative entropic considerations (Betz, 1993; Wedemeyer, 2000). Because of the importance of disulphides in the protein structure and function they are usually conserved in different degrees among homologous proteins during evolution (Thangudu, 2008).

Many proteins unfold when their disulphide bonds are reduced (Clarke, 1995). Deletion of intramolecular disulphide in the dimeric protein interleukin-8 (IL-8) results in mutant proteins which have reduced stability. On the other hand, disulphide bond mutation can affect the protein activity without changing the structure, significantly (Rajagopalan, 2007).

The stabilization by engineering disulphide bonds is not always successful in practice. While the introduction of disulphide bonds can stabilize some proteins, on the other hand this mutation can destabilise others (Thangudu, 2008; Das et al. 2007; Chu, 2007; Bjork, 2003). A possible reason why a disulfide bond does not stabilize a protein is that the disulfide bond may introduce strain in the folded form that can reduce or reverse the stabilizing effect due to the reduction in the chain entropy of the unfolded form (Lee and Vasmatsiz, 1997).

1.2.6 Protein engineering

Many enzymes isolated from mesophilic organisms are used in industry, but they easily denature under the conditions required for industrial process like heat, organic solvents, and high pressure etc. Enzymes from thermophiles are generally more stable to such conditions than those from mesophiles. However, the use of thermophilic enzymes depends on their availability. Identification and purification of new industrial enzymes suitable to these kinds of harsh conditions is not always straightforward. Therefore, improving wild type enzymes for a desired function or increased stability by using protein engineering is an important approach to overcome this restriction. Proteins from thermophilic organisms are widely used as model system to improve less stable homologous organisms (Lill, 2004). Understanding the mechanisms of thermophilic proteins at such high temperatures will also help to optimize and design new thermostable proteins for biotechnological applications (Robic et al., 2003). On the other hand, in protein engineering studies, many amino acid substitutions do not have large effects on stability. Proteins tolerate substitutions because some substitutions preserve critical interactions; some interactions do not make large contributions to stability, and protein structures can compensate for changes in sequence. The effect of an amino acid substitution is a combination of its intrinsic effects on the folded and unfolded states. (Alber, 1989). However, it may not be possible to design amino acid substitutions that will eliminate one type of interaction (e.g. electrostatic) without simultaneously affecting other types of interactions like van der Waals, hydrophobic, or hydrogen-bonding. It is important to determine the contributions of individual amino acids to the stability of a specific protein as a function of desired environmental conditions such as high temperature (Matthews, 1993). The capability of protein engineering is the reason that enzymes may be improved, on the other hand this technology can be also employed to better understand the molecular basis of enzyme functions. Hence, as time goes on, more protein engineering studies will improve our understanding of protein redesign and improve our ability to produce enzymes that can be used to synthesize novel products in non-native environments.

Protein engineering methods comprise three main strategies; rational design, directed evolution and a combination of both methods, site saturation mutagenesis (semi rational design). Extreme enzymes in nature have appeared through mutations and

recombinations in the DNA sequence. Although each approach has some limitations, all have been applied successfully in several studies for changing substrate specificity, cofactor specificity, enantioselectivity and improving stability or basic understanding of enzyme properties. Informations obtained from random mutagenesis and rational protein engineering studies provide information which can be applied to each other (Chen, 2001).

1.2.6.1 Directed Evolution

Unlike rational design, directed evolution (in vitro evolution or random mutagenesis) does not require any knowledge about sequence, structure or function of proteins. Directed evolution mimicks natural evolution *in vitro* by reducing the time scale of evolution from millions of years to months or weeks. This method has been used since 1980s to enhance or alter various enzyme functions (Frances, 2001; Tao and Cornish, 2002; Chen and Arnold, 1993). It has become a powerful technology through the work of Arnold and Stemmer in the 1990's which enhance the existing methods (Marshall, 2003). Today, directed evolution methods can be divided into two classes; (i) non-recombinative, random mutagenesis of genes (SM, Error Prone PCR) and (ii) recombinative methods, recombination of gene fragments of homologous enzymes from different sources (DNA Shuffling, Family DNA Shuffling, StEP, RACHITT, ITCHY, ADO, SCHEMA) (Bornscheuer and Pohl, 2001; Williams et al., 2004). Recombination of homologous enzymes genes which are evolved from a common ancestor cause significant diversity, and with a higher frequency of novel and functional proteins (Arnold, 1998).

Directed evolution requires two essential steps; one is the generation of random genetic libraries and the other one is screening and selection of variant enzymes that possess the desired characteristics, for example increased catalytic activity, enhanced selectivity or improved stability. Choice of the right strategy for both steps is very important to achieve the desired goal. In order to select a target protein from a large pool of mutant proteins, an efficient screening strategy, such as high-throughput solid phase digital imaging, phage display and other different screening techniques, is the most important requirement for the success of this method. The disadvantage of this method is the time-consuming process of screening and the selection of desired mutants and generally it requires robotic equipment to screen large libraries of

enzyme variants (Turner, 2003). Screening of libraries on the order of 10^3 - 10^4 variants seems sufficient for reliable selection (Tao and Cornish, 2002).

1.2.6.2 Rational design and site directed mutagenesis

Rational design in other words computational design of proteins requires the amino acid sequence, 3D structure and function knowledge of the protein of interest. This method provides controllable amino acid sequence changes (insertion, deletion or substitution). Controlled changes are important to determine the effect of individual residue changes on the protein structure, folding, stability or function.

When mutants obtained and characterized from both computational and random mutagenesis methods have been compared, it is often found that the best mutants obtained from both methods have the same residue changes. On the other hand strongly destabilized mutants obtained from the computational method can not be found by random mutagenesis. This explains the advantages of rational design in terms of either increasing stability or determination of individual residue effect on the protein stability, folding or function (Wunderlich et al., 2002).

The first step in rational design is the development of a molecular model by using an appropriate algorithm. This is followed by experimental construction and analysis of the properties of the designed protein. Besides the improvement of several enzyme properties like coenzyme and substrate specificity (Chul Lee et al., 2009), stability towards to oxidative stress (Slusarczyk et al., 2000), rational protein design has also been applied to improving the thermostability of several cases (Annaluru et al., 2006; Spadiut et al., 2009; Wei et al., 2009; Voutilainen et al., 2009).

Mechanisms for altering these properties include manipulation of the primary structure. Just a single point mutation may cause significant structural or functional changes in the protein. There are many rational strategies to change protein characteristics as discussed in section 1.2.5, introducing disulfide bridges, optimization of electrostatic interactions, improved core packing, shorter and/or tighter surface loops etc. These changes are put in practice by site-directed mutagenesis.

Site directed mutagenesis:

Rational protein design by site-directed mutagenesis (SDM) is a very effective strategy to produce improved enzymes and to elucidate enzyme mechanisms. In this

technique, mutations are created at computationally defined sites in the gene sequence via PCR using primers containing nucleic acid changes which correspond to the desired amino acid changes (Walker and Rapley, 2008).

Two types of PCR methods are used to create mutations (i) in the overlap extension method, two separate PCRs are performed by using 4 primers, two of them containing the mutant codon, (ii) in the whole plasmid method, only one PCR is performed using 2 primers, one of them containing the mutant codon. After the methylation reaction, template DNA is amplified with two overlapping primers and then PCR reaction is transformed into *mcrBC* wild type *E. coli*. The methylated template DNA is digested by the host. A single in vivo endonuclease digestion provides the elimination of parental methylated wild type plasmid and the plasmid DNA contain mutant region can be purified. If *mcrBC* type cells do not use, original gene and mutated gene can be selected by digesting the PCR reaction with DpnI methylase endonuclease (Url-1).

1.2.6.3 Semirational Design-Site Saturation Mutagenesis

Although either rational design or directed evolution gives effective results, to overcome the time consuming screening and selection process of directed evolution and the necessity of amino acid sequence and 3D information for rational design, a new approach was needed. A combination of both strategies represented the new route to improve the properties and function of an enzyme (Chen, 2001; Bommaris, 2006; Hilvert, 2001).

Site saturation mutagenesis method has some advantages when it is compared to other directed evolution methods. In directed evolution methods such as DNA shuffling (Stemmer 1994) or error-prone PCR (epPCR) (Leung vd., 1989; Wong vd., 2004), random or targeted mutations in the whole sequence coding for the protein generates a large mutant library which is very time consuming to screen. With saturation mutagenesis, it is possible to create a library of mutants containing all possible combination of 22 different amino acids at one or more pre-determined target positions in a gene. Choice of the correct mutagenesis, positions that can be responsible for desired changes is determined by homology modelling which requires 3D information (Lehmann and Wyss, 2001).

Because of the rational approach of this method, it is possible to obtain more effective results by combining it with high throughput screening methods. In combination with high-throughput screening methods, site saturation mutagenesis has been successfully used to improve several enzymatic properties as well as thermostability (Wu et al., 2009; Andreadeli et al., 2008; Reetz et al. 2006; Zheng, 2004).

1.2.7 Molecular modeling

Several genome projects are continuously providing amino acid sequence of proteins by creating huge databases such as SwissProt/TrEMBL. According to records of May 2008 UniProtKB/Swiss-Prot and TrEMBL contains 385721 and 5814087 sequence entries respectively. Nevertheless these sequence information databases can be of limited use without understanding the function of these new proteins. Knowledge of three-dimensional structure is a key for understanding the biological function. Although an understanding of 3D structure of proteins is crucial in terms of their function, only about 1 % of proteins (50,000 proteins with known structures have accumulated in the PDB database in the date of April 2008) for which the amino acid sequence is known had their 3D structure determined because of the time consuming nature and difficulty of crystallographic experimental methods. (Rutgers University 2008; Sanchez and Sail, 1997). As a result, the gap between the numbers of known sequences and structures continuously grows. In addition to enlarging databases, improvements in sequence comparison, fold recognition and protein modelling algorithms have supported the enhancement of protein structure prediction studies based on computer modelling methods to bridge this gap (Hillisch, 2004).

To date, the most successful and reliable computer models have been predicted by homology modelling methods based on amino acid sequence similarity. Although the other structure prediction methods, de novo or ab initio, which have to be used for proteins have no similarity with any known structure in the databases, constantly get better, it should be noted that most of current template-free modelling methods rely on template-based methods by using local sequence matching (Chen and Kihara, 2008; Mass et al., 1998). It is obvious that homology modelling is already the most promising and easiest technique among the computer based structure prediction

methods (Sali and Blundel, 1993). Therefore the importance of homology or comparative modelling which can provide a useful 3D models for many proteins is steadily increasing (Suarez, 2009).

1.2.8 Homology modeling

Homology modelling is used to predict the 3D structure of a target protein by using an experimentally (x-ray crystallography or NMR) determined protein structures as a template (Sanchez and Sail, 1997). This means that homology modelling techniques require the availability of high resolution 3D protein structure data of the template protein and knowledge of amino acid sequence of the target protein. The amino acid sequence of proteins determines their unique three dimensional structure, and hence their functions. Similar sequences adopt similar structures during evolution. A small change in the protein sequence usually results in a small change in its 3D structure (Baker, 2000; Chothial and Lesk, 1986). Consequently, homology modelling which is structured on this basic order provides the nearest model of real 3D structure of homologous proteins. It is understandable that quality of modelled protein structure and its applicability firmly depends on the score of the sequence similarity between the template protein and target protein to be modelled (Moult, 2005; Tramontano, 1993).

When target and template sequence have greater than ~50% of sequence identity, modelled structures are frequently of sufficient quality to be used in the prediction of detailed studies such as structure-based drug design, analysis of protein function, interactions, antigenic behaviour, and rational design of proteins with increased stability or novel functions (Sali and Blundel, 1993). Modelling with 50 % sequence identity tends to have approximately 1 Å RMS error for the main-chain atoms. This accuracy is very close to a medium resolution NMR structure or a low-resolution X-ray structure (Jacobson and Sali, 2004). If the sequence identity between template and target proteins is greater than 30 %, algorithms used for homology modelling will provide reliable results. A least 30% identity can be evidence of evolutionary related 3D structures arising from a common ancestor (Hillisch, 2004). Although different methods such as 3D-coffee, Staccato or SAlign are being developed to be able to make a reliable model in the case of low sequence identity, if the sequence

identity is between 15% and 30% conventional alignment methods are not sufficiently reliable and modelling becomes speculative (Dalton and Jackson, 2007).

One of the important applications of homology modelling is the design of site directed mutants. Improving some desired properties of proteins and determining the amino acids which are important structurally or functionally via introducing point mutations is a common approach in molecular biology. In this study, homology modelling has been used for both the prediction and analysis of mutant proteins with specific properties. In order to obtain mutant *cmFDHs*, site-directed and site-saturation mutagenesis methods were employed to create the amino acid substitutions.

Modelling studies were performed by using Insight II which is a comprehensive graphics and molecular modelling program with a combination of molecular mechanics/dynamics program Discover developed by Accelrys. Dr. Richard Sessions in the University of Bristol Department of Biochemistry helped with computer simulations for all designed mutations.

1.2.8.1 Molecular Mechanics/Dynamics

When a model structure of a molecule is made, it usually needs to be refined to reach the minimum potential energy corresponding to a stable, sterically acceptable state of the system. This refinement process is called minimization. The classical approach to calculate the energy of the modeled structure and to find a minimum of an empirical potential energy function is known as *Molecular Mechanics (MM)*. Molecular mechanics can be described by the summation of individual potential energy functions:

$$E_{\text{total}} = E_{\text{bond length}} + E_{\text{bond angles}} + E_{\text{torsion angles}} + E_{\text{hydrogen bonding}} + E_{\text{van der Waals}} + E_{\text{electrostatic}}$$

The potential energy of the system incorporate two types of parameters in the function; bonded forces in terms of bond length, angles and torsions are internal energy terms and correspond to the deviation from equilibrium positions of each atom, and non-bonded forces describe the van der Waals forces, hydrogen bonding and coulombic forces between interacting atoms. The combination of these parameters with the functional forms of the individual energy terms is known as a *forcefield*. The accuracy of the forcefield used for the modeled molecule affects calculations in molecular mechanics. The better forcefield used, it gives models that

more closely match experimentally determined structures (Url-2; Laech, 2001a). The Constant Valance Force Field (CVFF), Version 2, is a high quality forcefield and the default forcefield of the Discover 2.95 package, was used in these studies.

The optimum geometry of a molecule modelled using molecular mechanics is a motionless state. In reality, molecules change their geometry through the effect of thermal motions. *Molecular Dynamics*, (*MD*), and *Monte Carlo*, (*MC*) are based on principles of statistical mechanics and allow calculation of thermodynamic properties of molecular systems. MD simulates these thermal fluctuations of geometry as a function of time and corresponding energies. Molecular mechanics is preferred for the calculation of large molecule like proteins, because it is computationally inexpensive compared with quantum mechanics. MD uses the molecular mechanics energy description of the structure as described above and is initialized by assigning random velocities to atoms according to a given temperature, the forces acting on the atoms can be evaluated (Url-3) and the MD trajectory numerically integrated over time.

1.2.8.2 Energy Minimisation

Energy minimization is the basis of molecular mechanics energy calculations. The forces acting on each atom in the system can be determined from the potential energy surface or derivatives of it. The potential energy of the system incorporate bonded and non-bonded forces as described above. The minimization of the potential energy function involves a search for the minimum of this function and corresponds to an optimum geometry of molecule. Atomic co-ordinates (cartesian coordinates, internal coordinates, as appropriate) are moved in a stepwise manner in response to the forces which act on them to locate the minimum energy. This process continues until the minimum energy has been found. Energy minimisation approaches can be classified as methods which use derivatives of the potential energy function and non-derivative methods.

Derivative Approaches / First-order Minimisation Methods:

The energy of the system can be lowered by moving each atom in response to the force acting on it. This process continues until all first derivatives reach zero and the energy minimum has been found. Steepest descents and conjugate gradients are the most frequently employed methods in first-order minimization.

Steepest descent minimization is often used when the structure is far from a minimum because the method is extremely robust. It searches for the closest minimum by following the direction of the first derivative. If a given step locates a lower energy, the next step is made in the same direction. If the step causes the energy to increase, the step size is reduced and the direction of the next step is reversed.

Conjugate gradient minimisation is typically applied after the steepest descent method for large system, once the energy minimum has been approached. In this method, minimization combines both the previous and current gradients (or first derivatives) to produce a more efficient descent path.

Derivative Approaches / Second-order Minimisation Methods:

These methods are only applied to small molecules, since the calculations are very large. They use both first order and second order derivatives to find the energy surface in a few steps. Newton-Raphson is the simplest and most popular one.

Non-derivative Approaches:

This method follows only values of the function itself and locates a minimum by moving around on the potential energy surface. They are usually used as initial step because they always find a minimum in spite of their slow performance. SIMPLEX is the most employed algorithm in these methods.

The most appropriate energy minimisation method can be selected according to its speed and demand on computer memory. Most of the minimization methods are iterative and require on input some initial estimate for the position of the minimum. There is no optimum single minimisation method to answer all modelling problems (Leach, 2001b; Url-4; Url-5).

1.2.9 NAD⁺ dependent formate dehydrogenase

NAD⁺-dependent formate dehydrogenase (FDH, EC 1.2.1.2) is an abundant enzyme in many organisms, including methylotrophic yeasts, bacteria (Allen 1995, Thiskov and Popov, 1994; Watanabe et al., 2005; Chistoserdova et al., 2007) and plants (Francs Small 1993; Olson, 2000; Andreadeli et al., 2009). The methylotrophic microorganisms using methanol as carbon and energy source contain an NAD⁺-dependent FDH which catalyse the terminal step in the oxidation of methanol to

CO₂. Plant FDH is responsible for the oxidation of formate in the dark and it is induced by Fe deficiency and anaerobic stress (Suzuki, 1998).

NAD⁺-dependent FDH is a dimeric enzyme with two identical subunits each has an independent active site, containing no metal ions or prosthetic groups. They are unable to use one-electron carriers as oxidizers, and are highly specific to both formate and NAD⁺. FDH catalyzes the oxidation of formate to carbon dioxide coupled with reduction of NAD⁺ to NADH (Tishkov and Popov 2004, Tishkov and Popov, 2006):

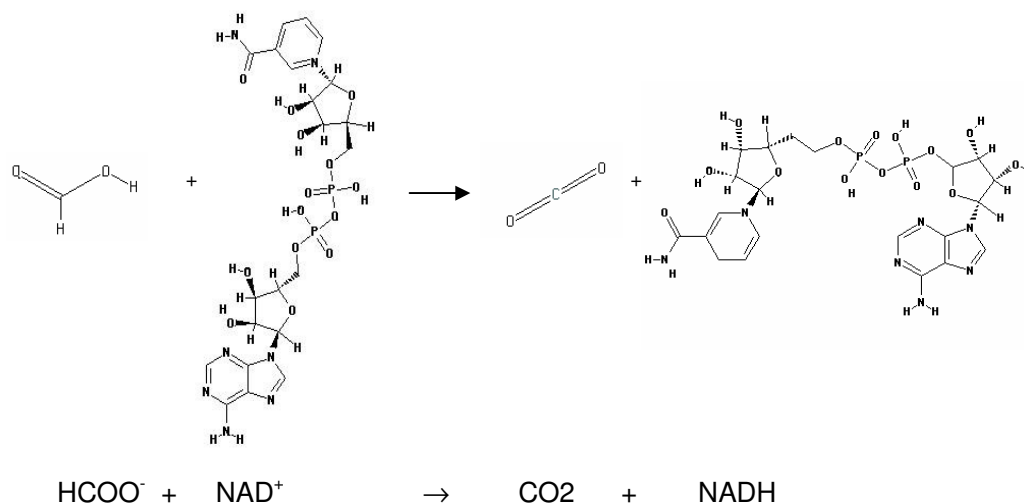


Figure 1.1 : The reaction catalyzed by FDH.

The FDH enzyme was first discovered in 1950 (Uversky, 2003) but it has attracted attention in recent years due to its practical application in the regeneration of NAD(P)H in the enzymatic processes of chiral synthesis. FDH is widely used for coenzyme regeneration with enzymes used for optically pure product synthesis in the pharmaceutical, food, cosmetic and agriculture industries (Patel, 2004; Jormakka et al., 2003). The FDH catalysed reaction is also a suitable model for investigating the general mechanism of hydride ion transfer because of direct transfer of hydride ion from the substrate onto the C4-atom of the nicotinamide moiety of NAD⁺ without stages of acid-base catalysis (Serov et al., 2002).

In the last decades active sequencing of genomes resulted in the discovery of FDH genes in various organisms such as *Staphylococcus aureus*, *Mycobacterium avium* subsp. *paratuberculosis* str.k10, different strains of *Bordetella*, and *Legionella*, *Francisella tularensis* subsp. *tularensis* SCHU S4, *Histoplasma capsulatum*,

Cryptococcus neoformans var. neoformans JEC21, *A. thaliana*, potato, rice, barley, cotton plant, English oak, *Mesembryanthemum crystallinum*, (*S. cerevisiae*, *C. boidinii*, *C. methylica*, *Hansenula polymorpha*, and *Pichia pastoris*, *A. nidulans*, *N. crassa*, *G. zeae* PH-1, *M. grisea*, *M. graminicola*, *U. Maydis* (Url-6).

Among the large number of microorganisms that have formate dehydrogenase, attention has been mainly focused on the yeasts. In yeast, the ability to utilize methanol as the sole carbon source is limited to members of 4 genera, namely *Candida*, *Hansenula*, *Pichia* and *Torulopsis*. An investigation of FDHs led to the selection of *Candida* species FDH as the best candidate for the NADH regeneration system because it is stable and it has relatively good activity. However, while several FDH enzymes have been isolated, crystal structures of FDHs from the bacterium *Pseudomonas sp.*101 and yeast *Candida boidinii* have only recently been solved (Lamzin et al., 1992; Schirwitz et al., 2007)

The native form of *cm*FDH is a dimer and each subunit has 364 residues folded into two distinct domains, each comprising a parallel β -sheet core surrounded by α -helices arranged in a Rossmann-type fold. One domain is functionally defined by co-enzyme binding, the other domain is for catalysis; coenzyme and substrate are encapsulated in the inter-domain cleft during the catalytic reaction. The molecule dimerizes by 2-fold symmetrical interactions between the co-enzyme-binding domains while the catalytic domains are distal to the dimer interface (Schirwitz et al., 2007).

1.2.10 Enzymatic regeneration of NAD(P)H

Enzymes remain unchanged after the reaction is completed, but coenzymes react with the substrate chemically and they are usually more expensive than desired product. Therefore improving an efficient regeneration system to reuse coenzymes is economically very important. A proficient regeneration system has to provide simplified product isolation and, prevent product inhibition by the other components in the reaction medium.

Several approaches including chemical, electrochemical, photochemical, microbial and enzymatic synthesis have been investigated for coenzyme regeneration. Enzymatic regeneration is the most promising one in the industrial process due to its

high selectivity, efficiency, aqueous solvent as operational medium and environmentally safe waste (Van der Donk and Zhao, 2005).

There are two different approaches for enzymatic regeneration. One of them is substrate coupled reaction systems in which one enzyme that reacts with both the reduced and oxidized forms a coenzyme to catalyze both the desired synthesis of the product from one substrate and the coenzyme regeneration with a second substrate. But in this system it is difficult to find thermodynamically favourable conditions for both reactions in the same medium. The other approach is the usage of second enzyme to catalyze the coenzyme regeneration (Fig. 1.2) (Eckstain et al., 2004; Popov and Thiskov, 2003). In this way second substrate must be very cheap or can be regenerated easily.

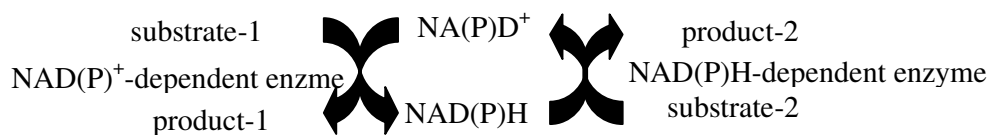


Figure 1.2 : NAD(P)H regeneration.

Several enzymes have been studied for NAD(P)H regeneration based on enzyme coupled approach. Formate dehydrogenase-FDH (Seelbach et al., 1996; Gül-Karagüler et al., 2001; Tishkov and Popov, 2004; Bolivar et al., 2007), phosphite dehydrogenase-PTDH (Vrtis et al., 2002; Relyea et al., 2005; Woodyer et al., 2006; Johannes et al., 2007), alcohol dehydrogenase-ADH, glucose-6 phosphate dehydrogenase, glucose dehydrogenase-GDH (Endo and Koizumi, 2001; Xu, 2007) are currently available systems. Among them FDH is the best and most widely used enzyme (Shaked and Whitesides, 1980; Kula and Wandrey, 1987; Hummel and Kula, 1989; Liese and Villela, 1999; Burton, 2003; Liese, 2005; Wichmann and Vasic-Racki, 2005; Johannes et al., 2007; Tishkov and Popov, 2006).

PTDH, catalyzes the oxidation of phosphite to phosphate by reducing the NAD⁺ to NADH, works in very narrow pH range (pH 7.0-7.6) and destabilize above 35°C. Although the cost of phosphite is cheaper than formate, which is the substrate of FDH, 90 g phosphite is necessary to regenerate 1 mol NADH by PTDH while formate dehydrogenase needs only 45 g formate to produce 1 mol NADH. GDH which catalyzes the hydrolyzation of gluconolactone to gluconic acid has both coenzyme specificity, NAD⁺ and NADP⁺. Although this enzyme has higher specific activity than

FDH (FDH, 2,5-10U/mg; GDH, 20-100U/mg), 172 g glucose is needed for reduction of 1 mol NAD(P) to 1 mol NAD(P)H. Moreover, gluconic acid should be removed from the reaction medium to produce pure chiral product. When FDH is compared to other studied dehydrogenases it offers several advantages. It is available at low cost and has a favourable thermodynamic equilibrium. Its reaction results in a 99–100 % yield of the final product. Since the reaction of FDH is essentially irreversible and the product (CO₂) can be easily removed from the reaction system and formate or CO₂ does not inhibit the other reaction and interfere with the purification of the final product. FDH also has a wide range pH optima so that it can work with lots of different enzymes (Popov and Thiskov, 2003).

In laboratory scale, FDH was used for NADH regeneration with several enzyme like lactate dehydrogenase, xylitol dehydrogenase and mannitol dehydrogenase in the production of hydroxyacids, xylitol and mannitol, respectively, (Van der Donk and Zhao, 2003; Mayer et al., 2002; Kaup, 2005). FDH from the yeast *Candida boidinii* was used in the first commercial scale process of chiral synthesis of tert-L-leucine with leucine dehydrogenase by German Degussa company (Popov and Thiskov, 2003). NADP-dependent enzymes are less common than their NAD-dependent counterparts. Engineered FDH is also a favourite enzyme to regenerate NADPH among other investigated enzymes such as ADH and glucose-6 phosphate dehydrogenase because of its cheap substrate. Engineered FDH that can accept NADP⁺ and it is preferred over glucose-6 phosphate dehydrogenase given the expense of its substrate (Wu et al., 2009; Andreadeli et al., 2008). The number of studies on FDH and its application for coenzyme regeneration in the processes of chiral synthesis with NAD(P)H-dependent enzymes is getting larger year by year (Holbrook et al., 2000; Yamamoto et al., 2005; Tishkov and Zaitseva, 2008).

1.2.11 Thermostability studies of NAD⁺-dependent formate dehydrogenase

Stability and folding studies have been focused mainly on monomeric proteins. In order to understand the quaternary structure and subunit or domain interactions, oligomeric proteins must be investigated. Oligomerization is also one of the protein stability strategies observed in the thermophilic organisms (Ragone, 2000). Over the past years the use of genetically altered proteins has become an important tool for studying the physical principles that determine the thermodynamic stabilities and

folding mechanisms of proteins. This is also critical for designing efficient enzymes that can work at high temperatures requiring for several industrial application such as pharmaceutical, food, detergent etc.

FDH makes the production of NAD(P)H coenzyme available and has strong potential for practical applications in several industries. Analysis of the stability and folding mechanism of homodimeric FDH is important both to improve the properties of this enzyme for industrial use or to obtain information on the mechanisms of protein stability and folding. While there is no detailed study of the folding mechanism of FDH in the literature, several studies have been performed to improve properties of FDH such as coenzyme specificity (Wu et al., 2009; Andreadeli et al., 2008) and thermostability (Karaguler, 2007; Thiskov and Popov, 2006). The lack of thermostability is the most important disadvantage of FDH. Studies in the literature with the aim of improving the thermostability of FDH have been focused on *Pseudomonas* sp 101 which has the best thermostability among the known FDHs and the FDH from *Candida boidini* by using rational design or directed evolution. The FDH enzymes from these organisms have the advantage of solved crystal structures. Odintseva et al. (2002) have engineered Cys residues in an attempt to increase the stability of *ps*FDH, obtaining mutants that showed the same kinetic parameters as the wild type enzyme, but its thermal stability dropped four-fold. Fedorchuk et al. (2002) tried to optimize electrostatic interactions by engineering residues in positions 43 and 61 of *ps*FDH by comparison to the *Mycobacterium vaccae* N10 FDH that only differs in two amino acid residues but has a lower stability than *ps*FDH. They showed the thermostability effect of loop regions of bacterial formate dehydrogenases which are absent in analogous eukaryotic enzyme and the replacement of Asp43 and in the *Pse*FDH molecule does not result in an increase in stability. Rojkova et al. (1999) applied the hydrophobization of alpha helix strategy. They selected the 5 serine residues occupying positions 131, 160, 163, 184 and 222 of *ps*FDH. Their results showed that a combination of mutations had an additive effect to FDH stabilization and obtained a four-point mutant FDH which has a thermal stability 1.5 times higher, compared to the wild type enzyme. Serov et al. (2005) tried to optimize the polypeptide chain conformation to increase thermostability of *ps*FDH. Slusarczyk et al. (2000) have engineered the Cys residues of *cb*FDH, they showed that mutations affecting Cys23 are more effective than

Cys262 on the stability. In the case of FDH from *Candida methylica*, an attempt was made to produce a more thermostable enzyme by the DNA shuffling method because the 3D structure of FDH from *C. methylica* is not yet solved. In DNA shuffling, the ability to select an improved protein from a large pool of protein variants depend on sensitive screening or selection methods. In this study host proteins could not be inactivated through a heat step screening method. In the light of this problem a homology model of *cm*FDH was generated on the basis of *ps*FDH 3D structure and a strategy of disulfide bridge introduction was applied to *cm*FDH by site directed mutagenesis to generate a thermostable *cm*FDH (Gül Karagüler, 2007). Experimental studies in the literature on the thermostability of FDH have not shown a significant increase in thermal stability until now.

2. MATERIALS and METHODS

2.1 Molecular Biological Techniques

2.1.1 Bacterial strains

Two different bacterial strains are used in this work namely, *JM105* {F' traD36 proA⁺ proB⁺ lacIq lacZΔM15/Δ (lac-pro) X111 thi rpsL (Strr) endA sbcB supE hsdR9} as a host cell and DH5αTM -T1^R competent cells ([Fϕ80lacZΔM15 Δ(lacZYA-argF)U169 recA1 endA1 hsdR17(r_k⁻, m_k⁺) phoA supE44 thi-1 gyrA96 relA1 tonA]) which is supplied with Invitrogen GeneTailorTM Site-Directed Mutagenesis System.

2.1.2 Cloning and expression of the *cmFDH* gene into pQE-2 vector

In order to eliminate difficulties in the purification of FDH and to produce quick and highly purified - homogeneous - recombinant protein, FDH was subcloned into pQE-2 expression vector.

The wild type gene in pKK223-3 was amplified according to standard PCR methods (95°C for 4 min, 95°C for 1.30 min, 60°C for 1min, 72°C for 2.5 min) in the presence of 0.2 mM of each dNTPs (Fermentas), 0.8 pmol of each primer and 0.6 U Pfu DNA Polymerase (Fermentas). Following oligonucleotides were used as PCR primers (N-terminus; 5'-CGCGTGAGCTCAAATGAAGATCGTTTTAGTC-3' and C-terminus; 5'-ACCGCTGCAGTTATTTCTTATCGTGTTTACC-3') in order to introduce new restriction enzyme sites which are suitable for pQE-2 expression vector (purchased from Qiagen). The amplified PCR product was cut with restriction enzymes *SacI* and *PstI* and ligated into similarly digested pQE-2 expression vector by using T4 ligase. Ligation product was transformed into *E.coli JM105* and selected on LB agar containing 100 μg / ml as described by Sambrook et al. After the plasmid isolation by using Qiagen - QIAprep Plasmid Isolation Kit, the double stranded DNA was sequenced to check for the correct amino acid change using the ABI Prism 3100 Avant automated sequencer at Molecular Biology and Genetics Dept., ITU.

2.1.3 Site directed mutagenesis

Invitrogen Gene Tailor™ Site-Directed Mutagenesis System was applied to introduce the mutations into *cmFDH* gene at required positions according to the manufacturer's protocol. Designed primers were synthesized commercially (Tab. 2.1). Base changes are in boldface. Double stranded of plasmid DNA was isolated and methylated with 4 units of DNA methylase. Methylated DNA was amplified with two overlapping primers to produce linear double stranded DNA. The PCR reaction (at 94 °C for 2 min initial denaturation, 94°C for 30 sec, 55 °C for 30 sec, 68 °C for 5 min 30 sec, 30 cycles, and at 68°C for 10 min final extension) was carried out to obtain linear plasmid of *cmFDH* gene with the desired change on it in the presence of 0.3 mM of each dNTP, 0.3 pmol of each primer and 0,02 unit of Platinum® *Taq* High Fidelity polymerase. The mutagenesis mixture was transformed into DH5α-T1 cells (supplied by kit). The host cell circularizes the linear mutated DNA, and *McrBC* endonuclease in the host cell digests the methylated template DNA, leaving only unmethylated, mutated product. The double-stranded DNA extracted from mutated *cmFDH* gene was sequenced in the region of the mutation to check for correct base deletion. Purified DNA samples were sequenced using ABI Prism 3100-Avant automated sequencer at Molecular Biology and Genetics Dept, ITU. pQE-2 expression vector containing His-tagged FDH gene was transformed into JM105 cells for over-expression of NAD⁺-dependent FDH protein.

2.1.4 Site saturation mutagenesis

This method is a mixture of the site directed mutagenesis technique of rational design and the high throughput screening of directed evolution methods. In the first step, libraries containing 22 amino acid changes of the desired residue positions are generated. In the second step positive mutants are selected by screening methods.

2.1.4.1 Generation of a mutant library

Degenerate primers containing mutant codons on both forward and reverse directions were designed as follows (Tab. 2.2).

Table 2.1: Primers to construct the designed mutations by site directed mutagenesis.

mutant	Primers		GC %	T _m (°C)
N187E	F-primer	5'- AAAGATTACTCCCATTT GA ACCAAAAAGAA-3'	31	57.4
N187E	R-primer	5'- AAATGGGAGTAATCTTTCCAAGACTCTG-3'	39	60.1
H13E	F-primer	5'-TTATATGATGCTGGTA AGGA AGCTGCTGATG-3'	41	65.2
H13E	R-primer	5'- CTTACCAGCATCATATAAGACTAAAACGATC-3'	31	60.0
Q105R	F-primer	5'- GATTTAGATTATATTAAT AGA ACAGGTAAG-3'	23	51.8
Q105R	R-primer	5' - ATTAATATAATCTAAATCAATGTGATCAG-3'	20	52.1
N300E	F-primer	5'ACCCATGGAGAGATATGAGAG AAAA ATATGGTG3'	39	64.2
N300E	R-primer	5'- TCTCATATCTCTCCATGGGTGATCCTTTGG-3'	46	66.1
N147R	F-primer	5'-AGCACATGAACAAATTATT AGAC ACGATTGGG-3'	37	63.5
N147R	R-primer	5'- AATAATTTGTTTCATGTGCTGGAACGAAATTTTC-3'	31	60.1
Y160R	F-primer	5'- GCTATCGCTAAGGATGCT AGAG ATATCGAAG-3'	45	65.0
Y160R	R-primer	5'- AGCATCCTTAGCGATAGCAGCAACCTCC-3'	53	69.0
Y302R	F-primer	5'-GGAGAGATATGAGAAATA AAAAG AGGTGCTGGTA-3'	39	63.5
Y302R	R-primer	5'- TTTATTTCTCATATCTCTCCATGGGTGATC-3'	36	60.8
Y160E	F-primer	5'- GCTATCGCTAAGGATGCT GAAG ATATCGAAG-3'	45	65.3
Y160E	R-primer	5'- AGCATCCTTAGCGATAGCAGCAACCTCC-3'	53	69.0
Y302E	F-primer	5'- GGAGAGATATGAGAAATA AGAAG GTGCTGGTA-3'	35	61.4
Y302E	R-primer	5'- TTTATTTCTCATATCTCTCCATGGGTG ATC-3'	36	60.8
M1C	F-primer	5'- ATATGCATGCGGGAGCTCAAT TGTA AGATCGTTTT-3'	42	68.3
M1C	R-primer	5'-TTGAGCTCCCGCATGCATATGGTGATGGTG-3'	53	71.6
D62C	F-primer	5'- ATAAACATATCCCAGATGCT TGT ATTATCATCAC-3'	32	61.9
D62C	R-primer	5'- AGCATCTGGGATATGTTTATCCAATTCACCTTG-3'	37	63.2

Table 2.2: Degenerate primers to construct *cmFDH* mutant library on the position of first residue of enzyme. Base changes are in boldface. N is A, T, G or C; K is G or T; M is A or C.

mut	primers		GC %	T _m (°C)
M1	F-p	5'- CATATGCATGCGGGAGCTCAANN K AAGATCGTTTTAG-3'	44	67
M1	R-p	5'-CTAAAACGATCTT MN NTTGAGCTCCCGCATGCATATG-3'	44	67

Double stranded plasmid DNA containing the native *cmFDH* gene was isolated and used as template DNA. The PCR reaction (at 94 °C for 2 min initial denaturation, 95°C for 2 min, 50 °C for 2 min, 72 °C for 8 min, 30 cycles, and at 72°C for 10 min final extension) was carried out to obtain linear plasmids of the *cmFDH* gene with

the desired change, in the presence of 50 ng template DNA, 0.3 mM of each dNTP, 0.3 pmol of each primer and 0.02 unit of Pfu[®] *Taq* polymerase.

PCR products were digested with Roche- *DpnI* endonuclease restriction enzyme in the presence of 10 unit of *DpnI* by incubating at 37°C for 4 hours. *DpnI* endonuclease cuts the methylated adenine (N6-methyladenine) sites at only G^m ATC sequences eliminating nonmutant original *cmFDH* genes. Such methylated sequences are produced by *dam* methylase. Our template DNA (pQE-2 vector containing *cmFDH* gene) was purified from bacteria expressing the *dam*-encoded methylase, making it susceptible to digestion with the restriction endonuclease *DpnI*. Consequently, only mutated *cmFDH* genes are present in the PCR reaction to use for transformation. The PCR products, containing site saturation mutants on the first residue (M1) were transformed into BL21 electrocompetent cells (New England Biolabs). To establish the mutant library, transformed colonies were grown in 96 well culture plates containing 100 µl Invitrogen Magic Media *E.coli* expression medium and 100 mg/ml ampicillin by incubating at 37 °C for 18 hours. After the growth period, cell cultures containing 20 % glycerol in stock plates were stored at -80 °C.

2.1.4.2 Screening of the library

A colorimetric method was used to screen for positive mutants. Firstly, cells were grown in 96 well culture plates containing 200 µl Invitrogen Magic Media *E.coli* expression medium and 100 mg/ml ampicillin by incubating at 37 °C for 22 hours. Cultures were centrifuged at 4000xg for 20 min to remove medium and collect cells. Pellets were resuspended by using 50 µl “BugBuster” (Novagen) lysis buffer and plates were incubated by shaking at room temperature for 20 min to digest cells and obtain enzymes. After this incubation period cells were centrifuged at 4000xg again to remove cell debris. Cleared lysates were taken in new 96 well plates to use for colorimetric screening assay.

Colorimetric assays were repeated three times for all mutants in 200 µl reaction medium containing 20 µl lysate, 20 µl (10 mM) NAD, 20 µl (200 mM) formate and 140 µl reaction solution (50 mM Tris-HCl containing 0.13 % gelatin, pH 8.0, 300 µM NBT and 30 µM PMS which generates a blue-purple formazan that can be quantified by monitoring absorbance at 598 nm). Lysate was added as last component to start reaction and increasing blue-purple color was followed at 580 nm

to measure activity, indirectly. To determine the thermostability of mutant colonies this assay was performed before and after heat treatment at 55°C for 10 min. Empty Magic Media *E. coli* expression medium, cells which did not contain the *cmFDH* gene and native *cmFDH* protein were used as controls. After the comparison of mutants to controls, the most promising mutant colonies were selected for further characterization studies.

2.1.5 Growth and expression

Growth and expression procedures were adapted from The Qiaexpressionist™ protocols. After small scale optimization studies, *JM105* cells containing His-tagged FDH gene inserted to pQE-2 expression vector were grown overnight at 37 °C with shaking at 250 rpm. 50 ml of the overnight culture was inoculated into 1000 ml LB medium containing ampicillin (100µg/ml) and grown at 37 °C until the OD₆₀₀ reach to 0.6. The culture was induced by adding 1 mM of isopropyl-β-D-thiogalactopyranoside (IPTG) to a final concentration of 1 mM for 4 hours at 37 °C and then harvested by centrifugation (at 4000 g for 20 min). The pelleted cells were stored at -80 °C.

2.2 Enzymological Techniques

2.2.1 Purification of *cmFDH* protein by using 6xHis-tag system

Cells, centrifuged from 1000 ml of culture, were suspended in 20 ml of lysis buffer. Lysozyme was added to 1 mg / ml and the cell suspension was incubated on ice for 30 min before sonication with bursts at 200–300 W with a 10 s cooling period between each burst. 50 µl of sample was collected for determination of total protein expression. The remaining cell suspension was centrifuged at 15000 g for 15 min at 4 °C. 1 ml of the 50 % Ni-NTA slurry was added to 20 ml of cleared lysate and mixed gently by shaking (50 rpm on a horizontal shaker) at 4°C for 60 min. The mixture was centrifuged at 13000 rpm for 1 min, 50 µl of sample was saved as a control and remaining supernatant was discarded. Pelleted resin was washed twice with 3 ml of wash buffer by centrifugation at 13000 rpm for 1 min and 50 µl of sample was saved as a control for each repeat. His-tagged proteins were eluted 6 times with 100 µl of elution buffer by centrifugation at 13000 rpm for 1 min.

Collected samples from each step and eluted proteins were analyzed by SDS polyacrylamide gel (%12 w / v) electrophoresis. SDS-PAGE and Coomassie Brilliant Blue staining showed the protein to be >95 % pure after purification. Protein concentration was determined by the method of Bradford (1976) using bovine serum albumin as a standard and expressed in terms of the monomeric protein concentration using monomer mass of 42000 Da. His-tagged proteins were analyzed by using Invitrogen InVision™ His-tag In gel Stain which is capable of detecting C-terminal, N-terminal or internal oligohistidine tag on fusion proteins.

2.2.2 Digestion of histidine tag

To digest the His-tag from His-tagged purified protein, TAGZyme™ procedure works well at pH 6.3-7.5 in the absence of imidazole which is used for elution of His-tagged proteins from Ni-NTA matrices. Therefore purified target should be desalted by ultrafiltration before starting the TAGZyme™ procedure. After the desalting procedure, Bradford protein assay was performed to determine the concentration of purified and desalted FDH. Several DAPase-Qcyclase digestion conditions were tested and subtractive IMAC was performed to eliminate undigested proteins. Digested proteins were analyzed by using Invitrogen InVision™ His-tag In gel Stain which is capable of detecting C-terminal, N-terminal or internal oligohistidine tags on fusion proteins.

2.2.3 Purification by a two-step standard chromatographic technique

The cells were resuspended in a minimum volume of 50 mM Tris/ethanolamine buffer at pH 8 (buffer A). The cells were sonicated (3 _ 10 s bursts) then centrifuged. The protein was precipitated by adding 0.43 g (NH₄)₂SO₄ per ml of supernatant and recovered by centrifugation. The resulting pellet was dissolved in a minimum volume of buffer A and dialysed against the same buffer overnight at 48°C. After dialysis, the protein solution was loaded onto a Blue Sepharose column (Sigma) equilibrated in buffer A and eluted with 2 volumes of (150 ml) buffer A containing 1 mM NAD. Next, the protein sample was applied to a Q-Sepharose ion-exchange column in buffer A. FDH was eluted using a gradient of 0 to 0.2 M NaCl in buffer A.

2.3 Kinetic and Thermodynamic Characterization Experiments

2.3.1 Steady state kinetics

The steady-state kinetic experiments of recombinant native and mutant *cmFDHs* were carried out at Shimadzu 1700 double beam (10 mm path length) UV-VIS spectrophotometer using a 25 °C in a reaction mixture containing 20 mM Tris Buffer at pH 8, 1 mM NAD⁺, 0–40 mM formate and 0.4 μM enzyme (Mr 42000). Initial rates were determined at 340 nm by measuring the NADH production and fitted using the Grafit 5 Kinetics Software.

2.3.1.1 Steady state kinetics of disulphide bridge mutants

Kinetic studies for disulfide bridge mutants were performed on both reduced and oxidised forms of the mutant proteins. Hence disulphide bridges were broken by incubating the protein for 1 hr in 30 mM of DTT and 5 mM of EDTA before assay (Creighton 1993). Likewise, disulphide bridges were formed by incubating the protein with 50 μM of zinc chloride for 30 min before assay (Rainer et al. 1989).

2.3.2 Equilibrium unfolding assay of *cmFDH*

Unfolding experiments were performed by using 0.1 and 1 μM protein to determine the dependence of the folding process on protein concentration, at the beginning of studies. Protein samples were incubated in 20 mM Tris, pH 8 at a series of GdnHCl concentrations (from 0 to 1.5 M by 0.05 interval) at 25 °C.

According to results of preliminary experiments, the following unfolding studies were carried on with 0.1 μM protein. All experiments were performed in unfolding buffer including 20 mM Tris and 5mM DTT, pH 8. Protein samples were incubated in unfolding buffer containing a series of GdnHCl and urea denaturants at different temperatures (25, 30, 35, 40, 45 °C) for 4 hours. Urea stock solution was prepared freshly just before the experiment. The protein fluorescence intensity of each sample was measured between 300-400 nm using an excitation wavelength of 285 nm in a Spex Fluoromax spectrofluorometer. Maximum emission was obtained at 350 nm. For each sample three scans were averaged for final spectrum. Denaturation curves were analyzed by assuming a two-state mechanism. Fluorescence values obtained from both denaturant at each temperature were fitted equation 2.1 to calculate K_w by fixing the m at the mean value for all transitions with Grafit 5.

$$K=K_w \cdot \exp(m \cdot D) \quad (2.1)$$

$$a= 1$$

$$b= -(2+1/(2 \cdot K \cdot Mo))$$

$$c= 1$$

$$\alpha_D = (-b - (b^2 - 4 \cdot a \cdot c)^{0.5}) / (2 \cdot a)$$

$$Y = \text{sig}_D \cdot \alpha_D + \text{sig}_M \cdot (1 - \alpha_D)$$

Where K_w is the D/M in water, Sig_D is the signal for folded state, Sig_M is the signal for unfolded state and Mo is the monomer concentration as a constant. For the analysis of equilibrium data, guanidinium hydrochloride (equation 2.2) and urea (equation 2.3) concentrations were converted to molar denaturant activity (D), according to the following relationship.

$$D = ([\text{GdnHCl}] \cdot C_{0.5}) / ([\text{GdnHCl}] + C_{0.5}), \quad (2.2)$$

where $C_{0.5}$ is a denaturation constant with a value of 7.5 M.

$$D = (C_{0.5} \cdot [\text{urea}]) / (C_{0.5} + [\text{urea}]) \quad (2.3)$$

where $C_{0.5}$ is a denaturation constant with a value of 25.3 M.

After obtaining K_w values from equation 2.1, the change in free energy between the folded and unfolded states in the absence of denaturant, ΔG_w , was calculated for each temperature (25, 30, 35, 45), using the $\Delta G = -RT \ln K_w$ relationship. For the free-energy change associated with a particular transition with temperature, data were fitted to the following equation 2.4:

$$\Delta G = \Delta H + \Delta C_p \cdot (T - T_0) - T \cdot \Delta S - \Delta C_p \cdot T \cdot \ln(T/T_0) \quad (2.4)$$

where $\Delta H(T_0)$, $\Delta S(T_0)$ and ΔC_p are the enthalpy, entropy and heat capacity changes, respectively, at a defined reference temperature (T_0). All data were fitted using the Grafit 5 analysis software (Erithracus software, U.K.).

2.3.3 Stopped flow unfolding experiments of *cmFDH*

The rate constant for unfolding at a particular concentration of GdnHCl was measured using stopped flow fluorometer (Applied Photophysics (05-109) pbp Spectra Kinetic Monochromator). 1 μM protein is jumped into 4, 4.5, 5, 5.5 and 6 M GdnHCl concentrations and the fluorescence decay was measured against time. The

protein was excited by monochromatic light at 285 nm and the resulting fluorescence was selected with a WG320 cut-off filter. Each recorded transient was an average of at least three individual reactions. Reactions were recorded at 25 °C. Data were fitted to single exponential decay pattern. The rate constants were plotted as a function of denaturant activity to extract the rate constant for unfolding in the absence of denaturant ($k_{u(w)}$) according to the following equation:

$$k_u = k_{u(w)} \cdot \exp(-m \cdot D) \quad (2.5)$$

2.3.4 Refolding activity assay

*cm*FDH enzyme was unfolded in the unfolding buffer containing 4M GdnHCl and 20 mM DTT in 20 mM Tris pH 8, at room temperature for 2 hours. The refolding assay was initiated by the dilution of 16.6 μ M unfolded FDH to 0.1, 0.2, 0.3, 0.5 and 1 μ M concentrations in the refolding assay buffer containing 20 mM Tris pH 8, 5 mM DTT, 20 mM formate, 1 mM NAD. The production of NADH was monitored by following the increase in absorption at 340 nm spectrophotometrically to assess the refolding yield at different concentrations of FDH. Measurements were performed by using UV/VIS Spectrometer Lambda 2 for 60 min in 1 ml cuvette. For numerical analysis of the refolding curves data were globally fitted using a numerical method (Kuzmic, 1996) to the system 2U \rightarrow 2M \rightarrow D.

2.3.5 Thermal denaturation

The proteins (wild type and mutant FDHs) were aliquoted and incubated at different temperatures with 2 °C intervals for 20 min. in triplicate. Remaining activity measurements were performed at 25 °C in a reaction mixture containing 20 mM Tris Buffer at pH 8, 1 mM NAD⁺, 2 mM formate and 0.4 μ M enzyme. Rate constants (k) were derived directly from the residual activity (A) by the following relationship:

$$A = A_0 \cdot \exp(-k \cdot t_{inc}) \quad (2.6)$$

Where t_{inc} is the period of incubation (in our case 1200 s) and A_0 is the initial activity. Using this relationship we obtain a relationship between k and T from which we can calculate the free-energy barrier for unfolding as a function of temperature by the relationship:

$$k = k_0 \cdot \exp(-\Delta G / (R \cdot T)) \quad (2.7)$$

where ΔG is the free energy of activation [$\Delta G = \Delta H + \Delta C_p \cdot (T - T_0) - T \cdot \Delta S - \Delta C_p \cdot T \cdot \ln(T/T_0)$] and k_0 is the rate of an unfolding reaction in the absence of an activation barrier (a value of 10^7 s^{-1} was taken for our analysis, see Discussion).

Values for temperatures where 50 % activity remained ($T_{0.5}$) under these conditions were also analysed by using Grafit 5 Kinetics Software.

2.4 Homology Modeling

To increase the thermostability and to investigate the effect of surface electrostatic interactions on the folding mechanisms of *cmFDH*, mutations were designed on a homology model of *cmFDH*. In order to generate homology model of *Candida methylica*, crystal structures of FDH from *Pseudomonas sp.101* (Lamzin et al., 1992) which has 49 % amino acid sequence identity with *cmFDH* and *Candida boidinii* which has about 90% identity with *cmFDH* (Schirwitz *et al.*) were used as the basis of model (Fig. 2.1 and 2.2). Amino acid changes were performed using InsightII 2005 (Accelrys), according to the amino acid sequence alignment as shown figures 2.1 and 2.2. All the differences (insertions and/or deletions) between template (*Pseudomonas sp.101* and *Candida boidinii*) and target (*Candida methylica*) sequences in the alignment appeared at the surface of the structure, the loop building facility in InsightII was used to model these differences in the protein backbone.

Energy minimization of modelled native *cmFDH* and various mutant FDHs were carried out using the steepest descents and conjugate gradients methods to minimize the energy because of the large number of atoms in FDH protein from *Candida methylica*. All energy minimizations were calculated using Discover, Version 2.95 (Accelrys) on a Linux workstation, which can be used for minimization and molecular dynamic simulations.

The model was set up for energy calculations in the following way: hydrogen atoms were added, consistent with a pH of 7; the azide was replaced with formate; water molecules were added to a depth of 5 Å around the surface of protein dimer.

2.4.1 Computer simulation protocol

The following procedure was used for the simulations of protein structure:

The system's energy was minimised by tethering all the protein atoms to their initial positions with a force constant of $100 \text{ kcal mol}^{-1} \text{ \AA}^{-2}$. The minimisation was carried out with 500 cycles of steepest descents to reduce any bad van der Waals contacts introduced by the mutations, in a controlled manner. The minimisation was continued for an additional 200 cycles of steepest descents while reducing the heavy atom tethering to $50 \text{ kcal mol}^{-1} \text{ \AA}^{-2}$. Tethering was reduced to $10 \text{ kcal mol}^{-1} \text{ \AA}^{-2}$ to refine the structure and minimisation was continued for 200 cycles of conjugate gradients. Heavy atoms were tethered with a force constant of only $5 \text{ kcal mol}^{-1} \text{ \AA}^{-2}$ for a further 200 cycles of conjugate gradients. All tethering was removed and the protein structure refined with 500 cycles of conjugate gradients. Finally, 200 cycles of conjugate gradient were performed to produce the fully refined structure including cross terms and Morse potentials.

3. RESULTS and DISCUSSIONS

3.1 Improving the Purification of *cm*FDH by Affinity Tag

The NAD⁺-dependent FDH from *Candida methylica* was previously isolated by Allen (1995). Its N-terminal amino acid sequence was determined and it was cloned into pKK223-3. Then it was transformed into *Escherichia coli* and the enzyme was overproduced. Since then, the recombinant FDH from *Candida methylica* was intensively studied (Karagüler et al., 2001; Karagüler et al., 2004) to improve the properties for the NAD(P)H regeneration by using site directed mutagenesis. The mutated novel FDH proteins were produced and purified by using two step chromatographic methods namely; Blue Sepharose affinity column and Q-Sepharose ion-exchange chromatographies, respectively (Karagüler, 2001). Although relatively pure proteins were obtained, the procedure was rather time consuming with low yield of recovery of typically below 50 % of the starting material. Therefore, the first part of the this thesis describes a simple and efficient method to improve the purification of NAD⁺-dependent formate dehydrogenase from *Candida methylica* and the results compared with the standard two step chromatographic methods.

Since the affinity tags are highly efficient tools for protein purification, they have been widely used in several areas of research. Although there are few different approaches available, TAGZyme™ system is considered as the most efficient one as it allows us to remove the unwanted affinity tag in the recombinant protein following the purification. The exopeptidase cleavage of the his-tag is provided by DAPase, a recombinant rat dipeptidyl aminopeptidase that is part of the TAGZyme™ system. This enzyme removes the dipeptides from the N-terminus until encountering a stop position in the sequence. This approach enables the purification of any protein and its production with the native N-terminus. The pQE-2 expression vector is based on the T5 promoter transcription–translation system for the high level expression of 6 x His-tagged proteins and multiple cloning site sequences that allows complete and convenient removal of N-terminal His tags.

In order to eliminate difficulties in the purification of FDH and to produce quick and highly purified - homogeneous - recombinant protein, FDH was subcloned into pQE-2 expression vector through the PCR method by using FDH gene in the pKK223-3 vector as a template. As a result of the PCR reaction 1094 bp fragment was obtained (Fig. 3.1A). The PCR product was extracted from agarose gel. pQE-2 vector and PCR product were digested with *SacI* and *PstI*. Ligation was performed with T4 ligase. *JM105* chemically competent cells were transformed with this ligation reaction mixture. Colonies were screened in terms of plasmid and insert content (Fig. 3.1B).

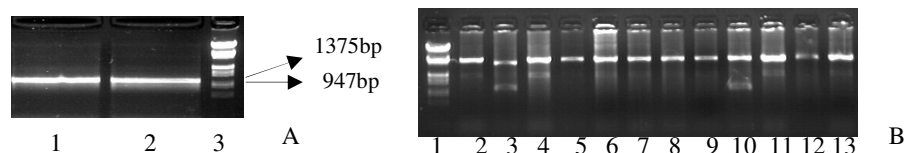


Figure 3.1 : A. lane 1 and 2 show the 1094 bp DNA fragment with *SacI* and *PstI* ends obtained via PCR, lane 3 is DNA marker (Fermentase Lambda DNA/EcoRI + HindIII marker, 3) B. Lane 1 is DNA marker (Fermentase Lambda DNA/EcoRI + HindIII marker, 3), lane 3 and 10 are examples of plasmid which has FDH gene.

FDH gene contain 6xHis-tag in the N-terminal was checked by sequencing with 3 sequence primer (pQETypeIII, pQEPromoter and pQERReverse) of pQE-2 vector and BLAST homology (Fig. 3.2). Sequence analysis result confirmed that the FDH gene was cloned into pQE-2 expression vector but there is an extra G base insertion which changes the open reading frame and damages the 6xHis-tag. To overcome the frameshift problem of the desired protein, the inserted one purin base was removed by using Invitrogen Gene Tailor Site Directed Mutagenesis Kit". This system was applied to delete the one extra "G" base insertion of *cmFDH* gene at required positions according to the manufacturer`s protocol. Following oligonucleotides,

Forward: 5'-CCATCACCATATGCATGCGGGAGCTCAAATG-3`

Reverse: 5'-CGCATGCATATGGTGATGGTGATGGTGATG-3`

were designed and synthesized in order to delete "G" base insertion. Base changes are in boldface. Generated construct (Tab. 3.1) was used for following studies.

```

gi|1181203|emb|X81129.1|CMNADDFD C.methylica gene for NAD-dependent formate
dehydrogenase Length=1256
Score = 1207 bits (609), Expect = 0.0 Identities = 668/677 (98%),
Gaps = 5/677 (0%) Strand=Plus/Plus

Query 34 AAATGAAGATCGTTTTAGTCTTATATGATGCTGGTAAGCACGCTGCTGATGAAGAAAAAT 93
          |||
Sbjct 124 AAATGAAGATCGTTTTAGTCTTATATGATGCTGGTAAGCACGCTGCTGATGAAGAAAAAT 183

Query 94 TATATGGTTGTTACTGAAAATAAATTAGGTATTGCTAATTGGTTAAAAGATCAAGGTCATG 153
          |||
Sbjct 184 TATATGGTTGTTACTGAAAATAAATTAGGTATTGCTAATTGGTTAAAAGATCAAGGTCATG 243

Query 154 AACTAATTACTACTTCTGATAAAGAAGGTGAAACAAGTGAATTGGATAAACATATCCCAG 213
          |||
Sbjct 244 AACTAATTACTACTTCTGATAAAGAAGGTGAAACAAGTGAATTGGATAAACATATCCCAG 303

Query 214 ATGCTGATATTATCATCACCCTCTTTCCATCCTGCTTATATCACTAAGGAAAGACTTG 273
          |||
Sbjct 304 ATGCTGATATTATCATCACCCTCTTTCCATCCTGCTTATATCACTAAGGAAAGACTTG 363

Query 274 ACAAGGCTAAGAACTTAAAATTAGTCGTTGTCGCTGGTGGTTCTGATCACATTGATT 333
          |||
Sbjct 364 ACAAGGCTAAGAACTTAAAATCAGTCGTTGTCGCTGGTGGTTCTGATCACATTGATT 423

Query 334 TAGATTATATTAATCAAACAGGTAAGAAAATCTCAGTCCTGGAAGTTACAGGTTCTAATG 393
          |||
Sbjct 424 TAGATTATATTAATCAAACAGGTAAGAAAATCTCAGTCCTGGAAGTTACAGGTTCTAATG 483

Query 394 TTGTCTCTGTTGCTGAACACGTTGTCATGACCATGCTTGTCTTGGTTAGAAATTCGTTT 453
          |||
Sbjct 484 TTGTCTCTGTTGCTGAACACGTTGTCATGACCATGCTTGTCTTGGTTAGAAATTCGTTT 543

Query 454 CAGCACATGAACAAATTAATTAACCACGATTGGGAGGTTGCTGCTATCGCTAAGGATGCTT 513
          |||
Sbjct 544 CAGCACATGAACAAATTAATTAACCACGATTGGGAGGTTGCTGCTATCGCTAAGGATGCTT 603

Query 514 ACGATATCGAAGGTAAAACATACGCTACCATTGGTGTGCTGGTAGAATTGGTTACAGAGTCT 573
          |||
Sbjct 604 ACGATATCGAAGGTAAAACATACGCTACCATTGGTGTGCTGGTAGAATTGGTTACAGAGTCT 663

Query 574 TGGAAAGATTACTCCCATTTAATCC-AAAGAATTATTATACTACGATTATCAAGCTTTAC 632
          |||
Sbjct 664 TGGAAAGATTACTCCCATTTAATCCAAAAGAATTATTATACTACGATTATCAAGCTTTAC 723

Query 633 C-AAAGAAGCTG-AAANAAAAGTTGGTGTGCTAGAAGAGTTGAAAATATTGAA-AATTAGTTG 689
          | |
Sbjct 724 CAAAAGAAGCTGAAGAAAAGTTGGTGTGCTAGAAGAGTTGAAAATATTGAAGAATTAGTTG 783

Query 690 CNC-AGCTGATATCGTT 705
          | |
Sbjct 784 CTCAAGCTGATATCGTT 800

```

Figure 3.2 : Blast homology result of inserted *Candida methylica* FDH gene into pQE-2 expression vector.

Table 3.1: TAGZyme pQE-2–FDH expression construct. First amino acid of the native protein sequence in bold. (↓) is DAPase stop point.

Construct	Size of insert (bp)	Size of protein (aas)	Size of tag	Expressed protein N-terminus
6xHis FDH	1094	364	45bp 15aa	MKH6HMHAGA↓QMKIVL....

After the verification of the DNA sequence of the 6xHis-tagged FDH gene, the protein was overexpressed (Fig. 3.3) in *E. coli JM105* cells and purification was

performed as mentioned in section 2.2.1 (Tab. 3.2). While 1.2 mg/ml protein was obtained from 6xHis-tag purification, 0.45 mg/ml protein was measured at the end of the two step purification method (Fig. 3.4).

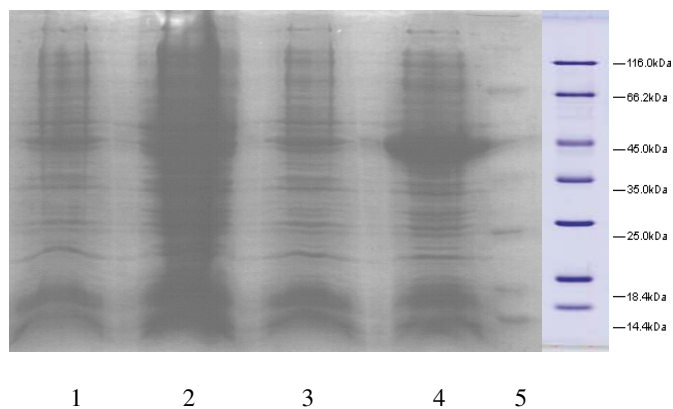


Figure 3.3 : Overexpression of *cmFDH* gene. 1. Noninduced pQE-2 vector (t0), 2. Induced pQE-2 vector (t4), 3. Noninduced pQE-2 vector carrying *cmFDH* gene (t0), 4. Induced pQE-2 carrying *cmFDH* gene (t4), 5. Unstained Protein Molecular Weight Marker (Fermentas).

Table 3.2: Purification protocol of FDH from crude extract of *Candida methylica*.

Purification Steps	Activity (U / ml)	Protein (mg / ml)	Specific Activity (U / mg)	% Yield	Purification Factor
crude extract	0.45	1.36	0.33	100	1
Ni-NTA resin and ultrafiltration	4.8	1.2	4	88	12

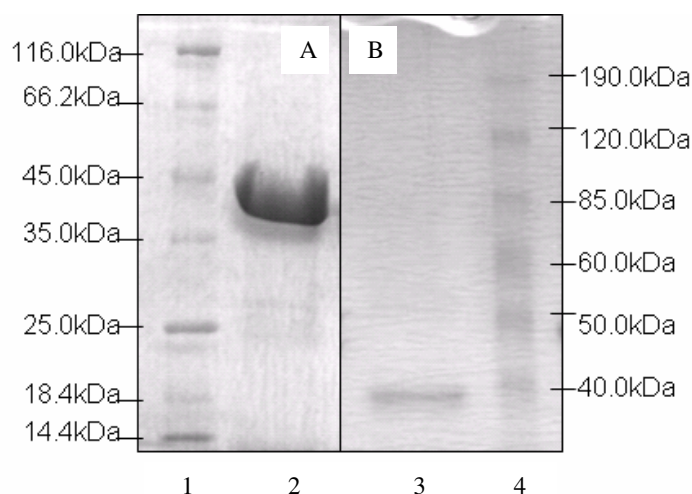


Figure 3.4 : His-tag (A) and two-step of standard (B) purification of *cmFDH*: 1. Unstained protein molecular weight marker (Fermentas), 2. Purified histagged FDH from pQE-2 vector, 3. Purified FDH from pKK223-3 vector, 4. BenchMark- Pre-Stained Protein Ladder (Invitrogen).

Purification of individual enzymes is a time consuming and costly process. Therefore, decreasing the production cost and improving the yield of purified enzymes are important goals. Production of target proteins using recombinant *E. coli* strains has some advantages compared with the systems based on wild strains. Recombinant systems could be employed for the production of different mutant FDHs with desired properties and large scale production with reduced cost by using protein engineering technology (Thiskov and Popov, 2006). The 6xHis-tagged purification method described here provides a quick and efficient purification procedure for recombinant His-tagged wild type FDH from *E. coli*. Obtaining 1.2 mg/ml (Tab. 3.2) of purified protein takes only three hours compared with a week of standard chromatographic methods. Additionally, the amount of protein is also improved from 0.45 mg / ml as shown in figure 3.4. The pQE-2 expression vector used in this study for His-tagged purification strategy has multiple cloning site that allow complete and convenient removal of N-terminal His tags to obtain original amino acid sequence of cloned FDH gene. In order to use this feature of the vector, several DAPase and Qcyclase digestion conditions were tested and digested proteins were analyzed by dying with Invitrogen InVision™ His-tag In gel Stain which is capable of detecting a C-terminal, N-terminal or internal oligohistidine tag on fusion proteins.

TAGZyme enzymes, DAPase and Qcyclase, work well at pH 6.3-7.5 in the absence of imidazole which is used for elution of His-tagged proteins. The presence of imidazole decrease the cleavage rate because of its inhibitory effect on DAPase catalysis. Therefore, to digest the 6xHis-tag a desalting procedure must be done before starting the TAGZyme procedure. Dialysis and ultrafiltration methods were tested for this purpose. After the desalting procedures, the proteins were analysed by SDS-PAGE (Fig. 3.5). We observed that the most amount of purified protein were lost after dialysis. Hence ultrafiltration (using a 10.000 cutoff membrane) was found to be the most suitable method for desalting.

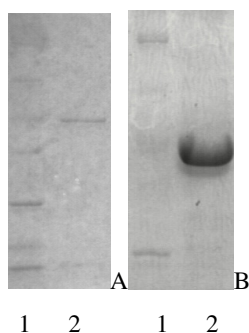


Figure 3.5 : (A) 1. Unstained protein molecular weight marker (Fermentas), 2. Purified FDH protein after dialysis, (B) 1. Unstained protein molecular weight marker (Fermentas), 2. Purified FDH protein after ultrafiltration.

After the desalting procedure using ultrafiltration, several DAPase+Qcyclase digestion conditions were tested and digestion reactions were performed in the following conditions (Tab. 3.3). Subtractive Immobilized-Metal Affinity Chromatography (IMAC) was performed to eliminate undigested proteins and enzymes used for digestion reaction. These recombinant enzymes bound to Ni-NTA matrix because of their C-terminal His tag and thus are removed from the reaction solution by IMAC.

Table 3.3: His-tag digestion conditions for small scale and preparative amount.

Digestion conditions for 50µg FDH in 1xTAGZyme Buffer	DAPase	10µl (1U/ml)	o/n at 37C
	Cysteamine HCl	20µl (2mM)	
	Qcyclase	12µl (50U/ml)	
Buffer	Cysteamine HCl	4µl (2mM)	2 hour at 37C
	pGAPase	4µl (25U/ml)	
Digestion conditions for 1mg FDH in 1xTAGZyme Buffer	DAPase	10µl (10U/ml)	o/n at 37C
	Cysteamine HCl	10µl (20mM)	
	Qcyclase	12µl (50U/ml)	
Buffer	Cysteamine HCl	4µl (20mM)	o/n at 37C
	pGAPase	40µl (25U/ml)	

It was observed that the molecular weights of digested and undigested FDHs are different by SDS-PAGE analysis (Fig. 3.6) hence confirming the success of digestion reaction.

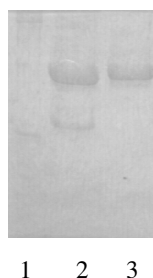


Figure 3.6 : Comassie staining of digested His-tagged FDH with Excess DAPase, 1. Unstained protein molecular weight marker (Fermentas), 2. Excess digested FDH, 3. Undigested FDH.

Almost 40% of purified protein were lost during first and second subtractive IMAC which is a process to eliminate 6xHis-tag undigested enzymes. Concentrations of purified FDH before and after digestion were given at table 3.4.

Table 3.4: Protein concentrations during 6xHis-tag digestion procedure.

Undigested (His-tagged FDH)	1.3 mg/ml
After DAPase+Qcyclase Digestion and first IMAC	0.8 mg/ml
After pGAPase Digestion and second IMAC	0.5 mg/ml

After the optimization of 6xHis-tag digestion conditions, enzyme activity studies were performed for total protein extract, undigested and digested FDH. Before the activity measurements 1xTAGZyme buffer was changed with pH 8, 20 mM Tris

buffer because the FDH enzyme gives the best activity in 20 mM Tris or TAE Buffer at pH 8. Kinetic measurements were carried out at 25 °C in a reaction mixture containing 20 mM Tris Buffer at pH 8, 1 mM NAD⁺, 0–40 mM formate and 0.4 μM enzyme (Mr 40344). Data were analysed using Grafit5 Kinetics Software and K_m values of undigested and digested 6xHis-tagged *cm*FDH and *cm*FDH purified by two step chromatography, see table 3.5.

Table 3.5: Kinetic measurements of His-tagged and digested His-tagged FDH from pQE-2 and FDH from pKK223-3 vector.

<i>cm</i> FDH	K _m (mM)	k _{cat} (sn ⁻¹)	k _{cat} / K _m (sn ⁻¹ mM ⁻¹)
Pure His-tagged FDH before digestion	4.75±0.3	1.13±0.1	0.24
Pure FDH after the digestion of His-tag	4.9±0.6	0.5±0.1	0.1
Pure FDH after 2 step standart chromatography	5.5±0.4	1.4±0.1	0.25

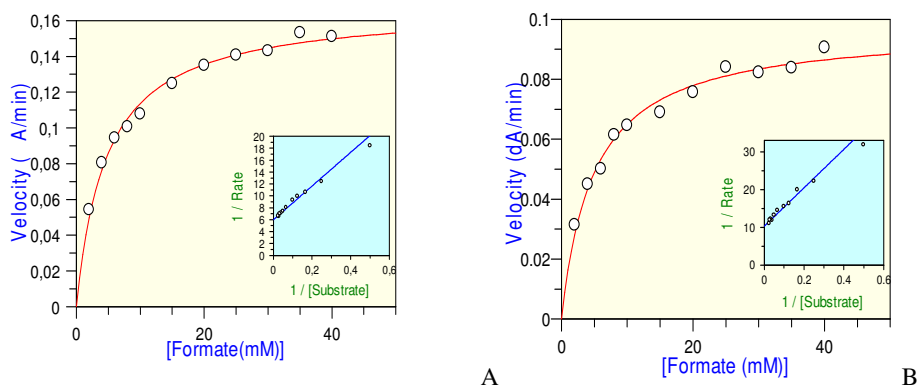


Figure 3.7 : Kinetic measurement graph of A. undigested and B. digested 6xHis-tagged *cm*FDH.

It was observed that the N-terminally His tagged FDH has similar activity to the FDH enzyme without the His-tag after digestion with exopeptidases (Tab. 3.5). The results in literature support our data, an N-terminal Histidin tag does not influence the activity of lactate dehydrogenase and amelogenin activities (Halliwell et al., 2001; Svensson et al., 2006). Therefore, activity studies have been carried out with His tagged FDH. The K_m value for formate was measured as 4.75 mM. which is within the range of 3-10 mM found in (Thiskov and Popov, 2004; Karagüler, 2004)

for *Candida methylica* FDH. The kinetic behaviour of the N-terminally His tagged FDH enzyme is shown in figure 3.7 and table 3.5.

As the conclusion, the purification procedure of *cm*FDH has been improved by subcloning it into pQE-2 vector. This will allow us to easily purify designed and constructed mutants of FDH for protein engineering studies.

3.2 Kinetic and Thermodynamic Properties of the Folding and Assembly of Formate Dehydrogenase

3.2.1 Equilibrium unfolding

To measure the free energy of folding of 364 aa dimeric FDH, we analysed the guanidinium chloride (GdnHCl)-induced denaturation of the enzyme at equilibrium. Denaturation reactions were monitored by using fluorescence spectroscopy measuring the fluorescence spectra of intrinsic tryptophan residues which are typically used as a very sensitive probe to the tertiary structure of proteins. The position of the maximum of a tryptophan fluorescence spectrum reflects the extent to Trp residue exposed to solvent (Baryshnikova et al., 2005; Ladokhin A. S., 2000). *cm*FDH has 5 tryptophan residues in the monomer. When excited at 285 nm, it exhibited an emission maximum at 350 nm in unfolding buffer containing 5mM DTT.

Upon unfolding there is a large (~70 %) quench of the native tryptophan fluorescence and the transition to the unfolded state occurs in a single step, without intermediates as shown in Fig. 3.8. As denaturation of the dimer requires dissociation of the component subunits, this transition must be dependent upon protein concentration. To confirm this we, collected equilibrium unfolding curves at two protein concentrations an order of magnitude apart and found that at the higher concentration the midpoint of the curve was shifted to higher concentrations of denaturant (Fig. 3.8). The data have been fitted to the dimer dissociation equation shown in materials and methods (equation 2.1) as a function of GdnHCl denaturant activity. For the 1 μ M protein K_w and m values were found to be $1.4 \pm 0.6 \times 10^{13} \text{ M}^{-1}$, -17.7 ± 1.0 , respectively. For the 0.1 μ M protein K_w and m values were found as $1.5 \pm 0.8 \times 10^{13} \text{ M}^{-1}$, -17.2 ± 1.2 , i.e. irrespective of concentration the curves fit with the same parameters. Owing to the equation accounting for the effect of protein

concentration on the denaturation transition, both of the fit-lines produce the same value for the apparent association constant (K_a), i.e. about 10^{13} M^{-1} . Note that this represents the equilibrium: 1 dimer is equal to 2 unfolded monomers, so includes both folding and dissociation processes.

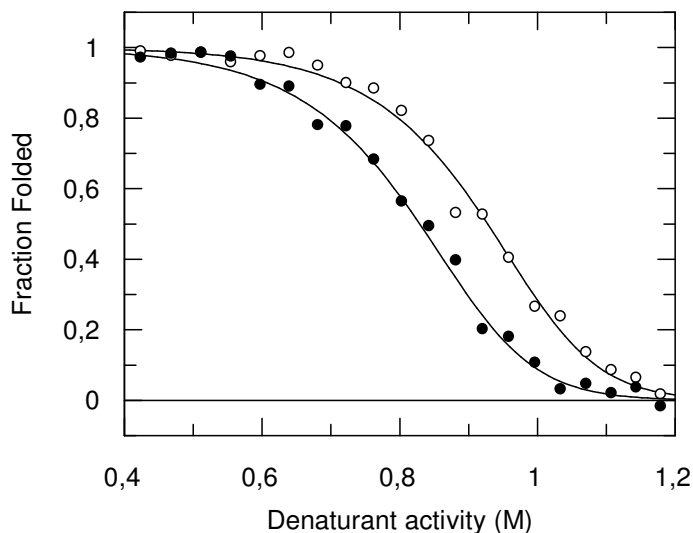


Figure 3.8 : Equilibrium unfolding curves: Normalized equilibrium unfolding curves of $1 \mu\text{M}$ (open circles) and $0.1 \mu\text{M}$ (closed circles) of *cmFDH*. Fluorescence intensity of 5 tryptophan residue of *cmFDH* was measured at increasing concentrations of the guanidinium hydrochloride at $25 \text{ }^\circ\text{C}$.

3.2.2 Thermodynamics of the folding-unfolding transition of native *cmFDH*

The equilibrium unfolding experiment was performed at a series of temperatures in order to extract the thermal dependence of the equilibrium unfolding transition. A concentration of $0.1 \mu\text{M}$ protein was used in the unfolding reactions based on the previous experiment. Protein samples were incubated in 20 mM Tris, $\text{pH } 8$ at a series of denaturant concentrations as mentioned in material method section 2.3.2. *cmFDH* was analysed by using two chemical denaturants, urea and GdnHCl which are the most common chemical denaturants in use for probing protein conformation in stability and unfolding studies. These denaturants show different behaviour towards the same protein. GdnHCl is a stronger denaturant than urea due to its charge. As a result, it can be possible to observe the different stabilisation states with different chemical denaturants. Therefore, comparing the results recorded from different denaturants is more elucidative to define folding intermediates (Monera et al., 1994; Dar et al., 2007).

3.2.2.1 GdnHCl induced denaturation

Protein samples were incubated in unfolding buffer containing a series (0-1.4 M by 0.05 intervals) of GdnHCl denaturant at different temperatures (25, 30, 35, 40, 45 °C) for 4 hours and fluorescence signals were recorded for each reaction. Curves generated according to fluorescence spectrum versus GdnHCl concentration in Fig. 3.9 show the equilibrium profile of native *cm*FDH at different temperatures. At the same time the concentration of GdnHCl which denatures the half concentration of protein can be extracted from the data shown in Fig. 3.9. Table 3.6 shows the $[GdnHCl]_{0.5}$ values obtained in different temperatures. Data obtained from these experiments were fitted to equation 1 to calculate K_w and the $\Delta G = -RT \ln K_w$ relationship was used to calculate ΔG values (Tab. 3.6).

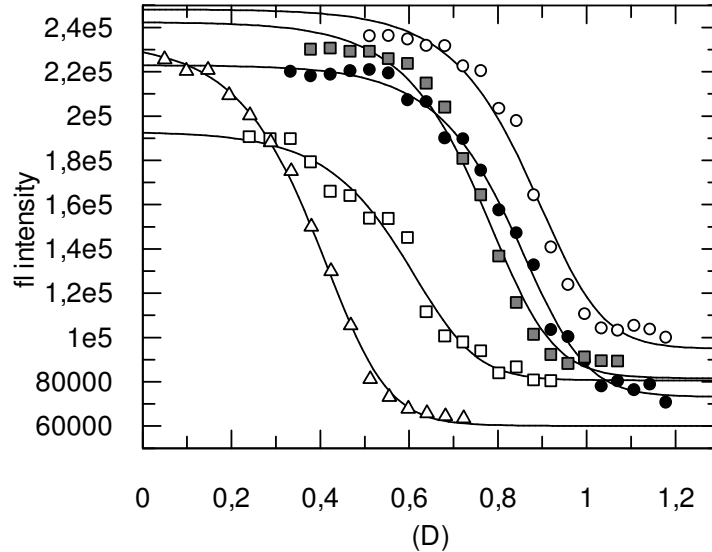


Figure 3.9 : GdnHCl-induced equilibrium unfolding curves of native *cm*FDH in different temperatures: 25°C is open circles, 30°C is closed circles, 35°C is grey square, 40°C is open square and 45°C is open triangle.

Table 3.6: K_w , m , ΔG and $[\text{denaturant}]_{0.5}$ results of native *cm*FDH from GdnHCl induced denaturation experiments.

Temp (K)	K_w	ΔG (cal/mol)	m (cal/mol M)	$[\text{GdnHCl}]_{0.5}$ (M)
298	1.52×10^{13}	-17963		0.85 ± 0.008
303	4.08×10^{13}	-18678		0.85 ± 0.004
308	5.95×10^{12}	-17836	-4.2 ± 0.07	0.77 ± 0.003
313	2.86×10^{11}	-16274		0.61 ± 0.02
318	8.78×10^9	-14370		0.4 ± 0.009

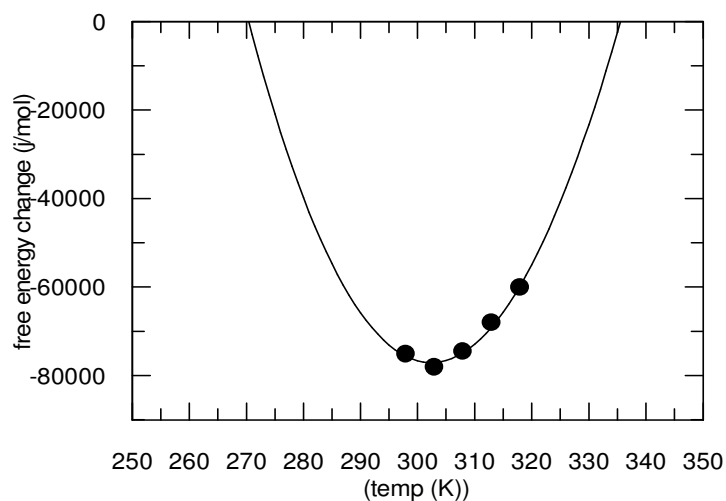


Figure 3.10 : Thermodynamics of unfolding of *cm*FDH. The free energy changes of unfolding in water (ΔG_w) over a range of temperatures (T) were determined from GdnHCl-induced equilibrium denaturation data and fitted to the equation 4, at a reference temperature of $T_0=298$ K.

The plot in Fig. 3.10 shows the free-energy change (i.e. $-RT \cdot \ln K_a$) for this transition as a function of temperature fitted to the Gibbs-Helmholtz equation as described in Materials and Methods (equation 2.4). The data show that, at the reference temperature of 25°C the enthalpy change on folding (ΔH) is unfavourable (approximately $+27 \pm 18$ kcal/mol), while the entropy change is favourable ($-T\Delta S = -46 \pm 18$) kcal/mol). The heat capacity change (ΔC_p) is -10.5 ± 1.8 kcal/mol/K; a value that is dominated by the degree of desolvation of non-polar surface during the folding process. Hence, ΔC_p is dependent on the chain-length of the protein and can be empirically estimated by the formula (Robertson and Murphy, 1997): $\Delta C_p = N \times -0.015 + 0.13$ kcal/mol/K.

The enzyme unfolds in a single transition involving two subunits of 364 residues hence the expected value is -10.8 kcal/mol/K, extremely close to the value of -10.5 derived from the data shown in Fig. 3.10.

On the curve in figure 3.10, the point at which ΔG of protein unfolding is zero define the melting temperatures (T_m) under a given set of conditions and T_m was found to be 63°C.

3.2.2.2 Urea induced denaturation

The fluorescence intensity of 0.1 μ M native *cmFDH* protein at different temperatures (25 °C, 30 °C, 35 °C, 40 °C, 45 °C and 25°C) and different urea concentrations (50°C 0→2 M urea (0.1 interval); 45°C 0→2 M urea (0.1 interval); 40° 0→2.5 M urea (0.125 interval); 35°C 0→4 M urea (0.2 interval; 30°C 0→5 M urea (0.25 interval; 25°C 0→5 M (0.25 interval) were measured by monitoring the changes in fluorescence intensity via the intrinsic fluorescence probe tryptophan. Curves generated according to the fluorescence spectrum versus urea concentration in Fig. 3.11 show the urea-induced equilibrium profile of native *cmFDH* at different temperatures.

Data obtained from these experiments were fitted to equation 1 to calculate K_w and the $\Delta G = -RT \ln K_w$ relationship was used to calculate ΔG values (Tab. 3.7). Table 3.7 also shows the concentration of urea which denature the half concentration of protein at different temperatures.

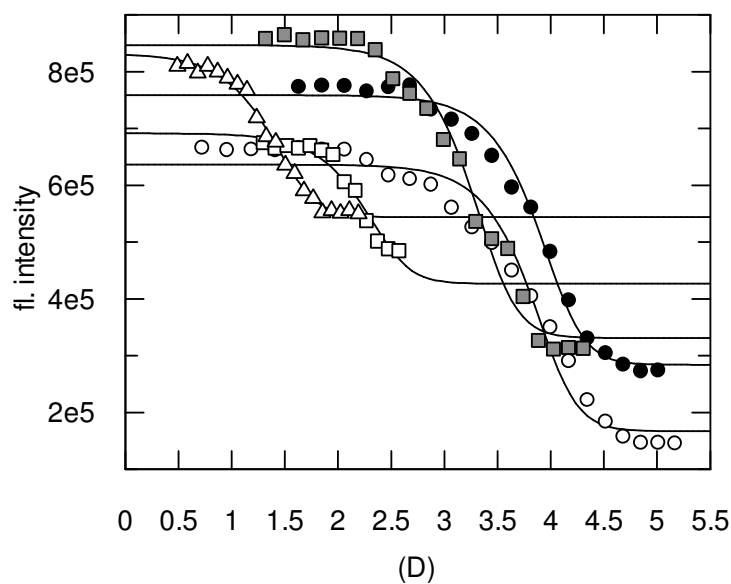


Figure 3.11 : Urea-induced equilibrium unfolding curves of native *cmFDH* in different temperatures: 25°C is open circles, 30°C is closed circles, 35°C is grey squares, 40°C is open squares and 45°C is open triangles.

Table 3.7: m , K_w , ΔG and $[\text{denaturant}]_{0.5}$ results of native *cmFDH* from urea induced denaturation experiments.

Temp (K)	K_w	ΔG (cal/mol)	m (cal/mol M)	$[\text{urea}]_{0.5}$ (M)
298	8.09×10^{17}	-24409		3.93 ± 0.05
303	1.22×10^{18}	-25054		3.92 ± 0.04
308	1.97×10^{16}	-22949	-1.57 ± 0.6	3.36 ± 0.05
313	2.57×10^{13}	-19195		2.18 ± 0.01
318	7.84×10^{10}	-15840		1.39 ± 0.02

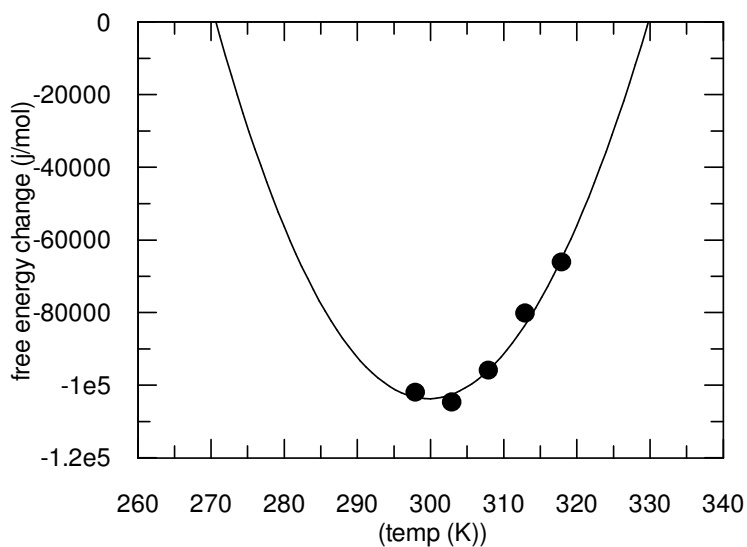


Figure 3.12 : Thermodynamics of unfolding of *cmFDH*. The free energy changes of unfolding in water (ΔG_w) over a range of temperatures (T) were determined from urea-induced equilibrium denaturation data and fitted to the same equation with GdnHCl experiment (equation 2), at a reference temperature of $T_0=298$ K.

The plot in Fig. 3.12 shows the free-energy change for the urea-induced transition as a function of temperature fitted to the Gibbs-Helmholtz equation (equation 4). The data show that, at the reference temperature of 25°C the enthalpy change on folding (ΔH) is approximately $+5 \pm 4.8$ kcal/mol and the heat capacity change (ΔC_p) is -17 ± 4.6 kcal/mol/K. The entropy change at 25°C is favourable ($-T\Delta S = -30 \pm 0.16$ kcal/mol). T_m was found to be 57°C .

While the free energy change of native *cmFDH* is found as 19 kcal/mol from GdnHCl-induced equilibrium experiments, analysis of the unfolding transition of native *cmFDH* induced by urea shows 24 kcal/mol free energy change at 25°C . The T_m value of native *cmFDH* was found to be 63°C and 57°C from GdnHCl and urea-induced experiments, respectively. These difference can be explained in terms of masking effect of Gdn^+ and Cl^- ions of GdnHCl on electrostatic repulsion that might be present in the protein (Huang and Quiñones, 2008). The T_m value obtained by the urea-induced experiment (57°C) is also identical to the $T_{0.5}$ value obtained from thermal denaturation experiment.

3.2.3 Kinetics of folding and unfolding

The rate constant for unfolding in the absence of denaturant can be estimated from the data shown in Fig. 3.13. In these experiments the folded protein was mixed in a stopped-flow apparatus with a series of denaturing concentrations of GdnHCl and the rate constant for unfolding measured by recording the decrease in indole fluorescence as a function of time. Extrapolation to zero denaturant yields a value for the rate constant of $3.4 (\pm 1.5) \times 10^{-7} \text{ s}^{-1}$ and the Δm -value for the linear free-energy relationship, which relates to the change in solvent exposure between the folded dimeric ground state and the transition state for unfolding, is 4.6 ± 0.1 .

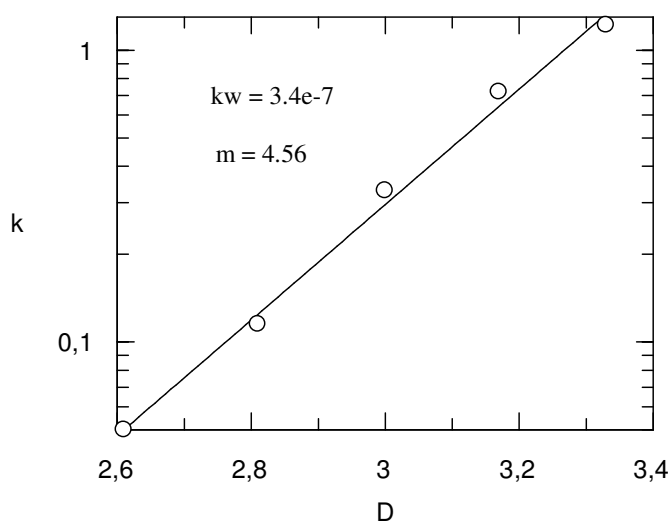


Figure 3.13 : Unfolding kinetics of *cmFDH*. Enzyme was unfolded in a stopped-flow fluorimeter and the rate constant recorded by analysis of the decrease in fluorescence. The plot shows the variation with denaturant activity fitted to the equation described in materials and methods.

To analyse the folding kinetics, we followed the renaturation process and measured the rate of regain of enzymatic activity from the fully unfolded state as a function of time. Shown in Fig. 3.14 is a plot of activity against time for refolding reactions performed at a series of protein concentrations. The reactivation curves have distinct lag phases showing that the refolding process is rate-limited by at least two steps occurring on the same time scale. Further, one of these steps must be multi-molecular since the half-time of refolding is clearly sensitive to the protein concentration. At zero time the tangents to the refolding curves are zero, showing that the intermediate state (or states) lying between the two rate-limiting steps is devoid of activity. In any

dimeric system, at least two processes must occur before the individual unfolded chains can form the active state, i.e. folding and association (Mei et al., 2005).

The simplest model that accounts for the data is an essentially irreversible unimolecular-bimolecular reaction: $2U \rightarrow 2M \rightarrow D$, where U is the unfolded chain, M the folded monomer and D the active dimer. In this system M has no enzymatic activity.

Using numerical methods we globally, i.e. simultaneously, fitted the progress curves to the above kinetic model which yielded values of $1.9 (\pm 0.4) \times 10^{-3} \text{ s}^{-1}$ for the unimolecular folding step and $1.6 (\pm 0.5) \times 10^4 \text{ M}^{-1}\text{s}^{-1}$ for the bimolecular association of subunits. The results show a close agreement between model and data over a wide concentration range.

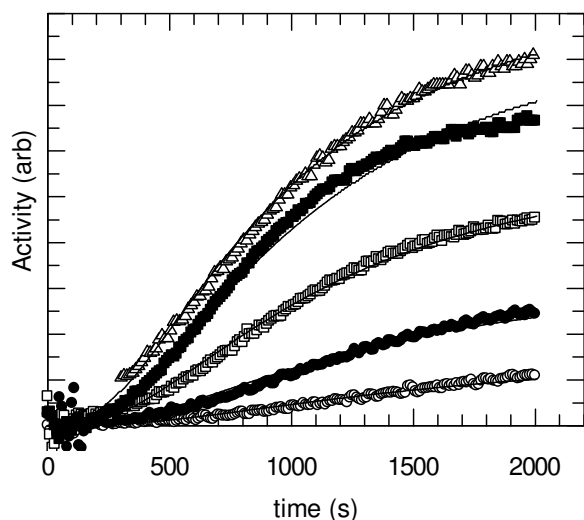


Figure 3.14 : Refolding of *cmFDH* followed by regain of activity. Activity was measured as a function of time for refolding reactions measured at a series of protein concentrations. The data were globally fitted using a numerical method to the system $2U \rightarrow 2M \rightarrow D$.

The monomeric intermediate of *cmFDH* forms active dimers at a rate which is slower than expected for a process limited by subunit diffusion in solution. Considerations based on orientational constraints and Brownian diffusion for protein associations have suggested that the basal rate should lie in the range of 10^5 – $10^6 \text{ M}^{-1}\text{s}^{-1}$ (Northrup, and Erickson, 1992; Zhou et al., 1997; Schlosshauer and Baker, 2004). Electrostatic attractions can enhance this rate significantly, as shown experimentally in the formation of the barnase:barstar complex (Schreiber and Fersht, 1996) and the colicin:Im9 interaction (Wallis et al., 1998). In addition such charge effects have

been predicted with reasonable accuracy by models developed by Alsallaq and Zhou (2007). In these studies association rates greater than $10^9 \text{ M}^{-1}\text{s}^{-1}$ were observed, which accords with the value for dimerization of the apo form of superoxide dismutase (Tab. 3.8) where the second-order rate constant is $2 \times 10^9 \text{ M}^{-1}\text{s}^{-1}$. Comparisons with other large proteins that fold through a unimolecular / bimolecular mechanism and for which all steps have been defined are shown in table 3.8 (Mallam and Jackson, 2007; Najera et al., 2003; Svensson et al., 2006; Vassall et al., 2006).

Table 3.8: Comparison of equilibrium and kinetic parameters of some large proteins that fold through a unimolecular / bimolecular mechanism.

Protein (residues)	$\Delta G \text{ U} \rightarrow \text{M} /$ $\Delta G^\circ \text{ M} \rightarrow \text{D}$ (kcal.mol ⁻¹)	k_f (s ⁻¹)	k_u (s ⁻¹)	k_{ass} (M ⁻¹ s ⁻¹)	k_{dis} (s ⁻¹)
YbeA (155)	-2.8 / -13.3	1.6e-1	8.1e-4	3.9e4	4.3e-4
yTIM (247)	-4.0 / -16.8	1.4e-2	3.6e-6	6.7e5	3.5e-8
apo-SOD (153)	-2.6 / -17.3	8.0e-2	9.5e-4	2.0e9	2.4e-4
FDH (364)	-1.7 / -14.6	1.9e-3	1.1e-4	1.6e4	3.4e-7

k_f and k_u : rate constant of unimolecular folding and unfolding, respectively

k_{ass} and k_{diss} : rate constant of bimolecular association and dissociation, respectively

At the level of simple reaction kinetics, there are at least three explanations that can account for the apparently slow association rates of the formate dehydrogenase monomers. Firstly, and most straightforwardly, the bimolecular rate might be genuinely $10^4 \text{ M}^{-1}\text{s}^{-1}$ owing to some unusually stringent orientational requirement for securing a productive interaction or owing to charge repulsion between monomers. Secondly, the monomer may be an ensemble of conformations in rapid equilibrium with each other. If only a minority population can dimerize then the apparent bimolecular rate will appear to be slower than the real value. For instance if only 1/10th of the population were competent at any one time, then the apparent second-order rate constant would be 100-fold slower than the real bimolecular constant, i.e. a real rate constant of $10^6 \text{ M}^{-1}\text{s}^{-1}$ would appear to be only $10^4 \text{ M}^{-1}\text{s}^{-1}$. Thirdly, and least intuitively, an unstable dimeric state might be formed with a rapid bimolecular constant, but be unstable at the experimentally accessible concentration of subunits. If there is a rate-limiting unimolecular isomerization of this encounter complex to form the active dimer, then the progress curve will appear second-order because of

the depletion of monomers as the reaction progresses. For instance, if the bimolecular rate constant were $10^6 \text{ M}^{-1}\text{s}^{-1}$ and the dissociation rate 10^1 s^{-1} , the K_d for this rapid equilibrium would be 10^{-5} M . With a unimolecular rate constant for isomerization of 10^{-1}s^{-1} and a concentration of 10^{-6} M monomer (i.e. the proportion of dimer in the rapid equilibrium is $1/10^{\text{th}}$), then the renaturation reaction would be closely approximate to a second-order process with an apparent bimolecular rate constant of $10^4 \text{ M}^{-1}\text{s}^{-1}$.

The relatively slow bimolecular rate constant is combined with a slow rate of dissociation to yield a high stability for the native dimer ($\Delta G^{\circ} = -14.6 \text{ kcal/mol}$), in keeping with other dimeric proteins of high molecular weight. This level of stability ($K_d \sim 10^{-13} \text{ M}$) means that at a micromolar concentration, less than one millionth of the enzyme is in the inactive and unstable monomeric state. It is interesting to note that the rate constant for FDH dissociation (Fig. 3.13) is so slow that, once formed, the dimer has a dissociative half-life of one and a half years.

3.2.4 Construction of a quantitative mechanism

For the simplest model there are two steps; a unimolecular folding process defined by k_1 and k_{-1} in the forward ($U \rightarrow M$) and reverse direction respectively and a bimolecular process defined by k_2 and k_{-2} . The overall equilibrium constant K_a defines the distribution D/U^2 , hence is the product of the two steps. However, since it requires two unfolded chains to form the dimer then:

$$K_a = (k_1/k_{-1})^2 \cdot k_2/k_{-2} \quad (3.1)$$

Making the assumption that the rate-limiting step in denaturation is dissociation (k_{-2}) then the only value in this system that is not experimentally defined is k_{-1} . This value can be deduced as follows:

$$k_{-1} = ((k_1^2 \cdot k_2) / (K_a \cdot k_{-2}))^{0.5} \quad (3.2)$$

Given values of $1.5 \times 10^{13} \text{ M}^{-1}$ for K_a , $1.9 \times 10^{-3} \text{ s}^{-1}$ for k_1 , $1.6 \times 10^4 \text{ M}^{-1}\text{s}^{-1}$ for k_2 and $3.4 \times 10^{-7} \text{ s}^{-1}$ for k_{-2} , this relationship provides a value for the $M \rightarrow U$ step of about $1 \times 10^{-4} \text{ s}^{-1}$. In this system M has no enzymatic activity and its stability is marginal, the free-energy change for this step being only 1.7 kcal/mol .

3.2.5 A simple analytical method for approximating folding and assembly rates

The formal analytical equation for fitting a uni-bi kinetic systems is extremely unwieldy, therefore, to extract the values for rate constants in the renaturation reaction we have used numerical fitting procedures. The numerical fitting technique employed to extract the forward rate constants in the renaturation process required good time-resolution in the data and a simultaneous analysis of the progress curves. However, in the analysis of such data, it is interesting to note that summing the individual half-lives for a bi-molecular step ($t_{1/2} = 1/(k_{bi} \times M_o)$) and a unimolecular step ($t_{1/2} = \ln 2 \times k_{uni}$) provides a tolerably close approximation to the overall half-time of refolding. If we use the approximation that the measured $t_{1/2} = 1/(k_{bi} \times M_o) + \ln 2 \times k_{uni}$ then the data sets shown in Fig. 3.14 can be re-analysed in terms of $t_{1/2}$ versus total monomer concentration. Such a plot is shown in figure 3.15 and the fitting procedure yields a value for k_{bi} of $2.4 \times 10^4 \text{ M}^{-1} \cdot \text{s}^{-1}$ and a value for k_{uni} of $1.6 \times 10^{-3} \text{ s}^{-1}$; remarkably close to the values arrived at from global numerical fitting, i.e. $1.6 \times 10^4 \text{ M}^{-1} \cdot \text{s}^{-1}$ and $1.9 \times 10^{-3} \text{ s}^{-1}$, respectively. The k_{uni} measured in such reactions might be a compound of two or more unimolecular steps in a more complex mechanism; in this case $1/k_{uni} = \tau_{uni} = \tau_1 + \tau_2 + \dots + \tau_n$.

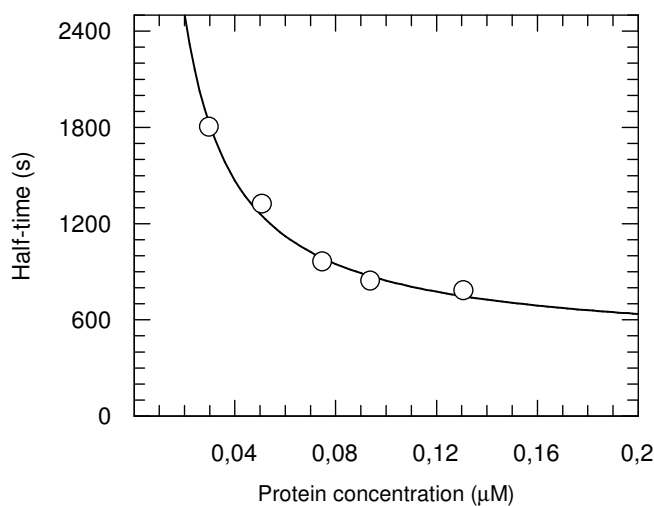


Figure 3.15 : The relationship between the half-time of refolding and reactant concentration. The refolding half times were fitted to the equation; $t_{1/2} = 1/(k_{bi} \times M_o) + \ln 2 \times k_{uni}$ The shown fit yields values of $1.6 \times 10^{-3} \text{ s}^{-1}$ and $2.4 \times 10^4 \text{ M}^{-1} \text{ s}^{-1}$, respectively, for the unimolecular folding and bimolecular association rate constants.

3.2.6 Thermal denaturation

Shown in Fig. 3.16 are denaturation data derived from an experiment in which the enzyme was incubated at a series of temperatures for a period of 20 minutes and the residual activity recorded. The heat inactivation of *cmFDH*, as for most proteins, is not reversible and follows a first-order decay (Sarmiento et al., 2009; Rudra et al., 2008; Ying and Zhang, 2008). As a result of this, denaturation cannot be formally treated as an equilibrium system to which the orthodox analysis can be applied, rather it should be thought of as being defined by a temperature-sensitive rate constant for the irreversible step. These data can be treated as representing rate constants of denaturation as a function of temperature, i.e. the rate constant (k) can be derived directly from the residual activity (A) as described in equation 2.6 (see Mat and Met). The variation of rate constant with temperature can be described by the Arrhenius relationship:

$$k = k_0 \cdot \exp(E_a/RT) \quad (3.3)$$

where E_a is the activation enthalpy. When the data in Fig. 3.16A are fitted to this relationship we obtain a value for k_0 of $2 \times 10^{57} \text{ s}^{-1}$ and for E_a a value of 91 kcal/mol.

However, in the knowledge that protein folding involves large changes in heat capacity, it is more realistic to fit the data to the integrated form of the van't Hoff relationship (equation 2.7) where the free-energy barrier for unfolding is related to temperature. For the purposes of this analysis, we take a value of 10^7 s^{-1} as the upper rate of rearrangements involved in protein folding or unfolding (Parker et al., 1998).

In Fig. 3.16B the deduced ΔG for activation is plotted against the temperature. The relationship between the height of the free-energy barrier and the temperature defines the changes in heat capacity, enthalpy and entropy between the folded state and the transition state according to equation 2.4. Combining the above equations allows a direct fit of residual activity against ΔH , ΔC_p and ΔS as shown by the fit line in Fig. 3.16A which is superimposed on the original data. This analysis gives an enthalpic barrier of 25 kcal/mol, a favourable entropic term (-5.5 kcal/mol at 298K) and a heat capacity change of 2.0 kcal/mol/K.

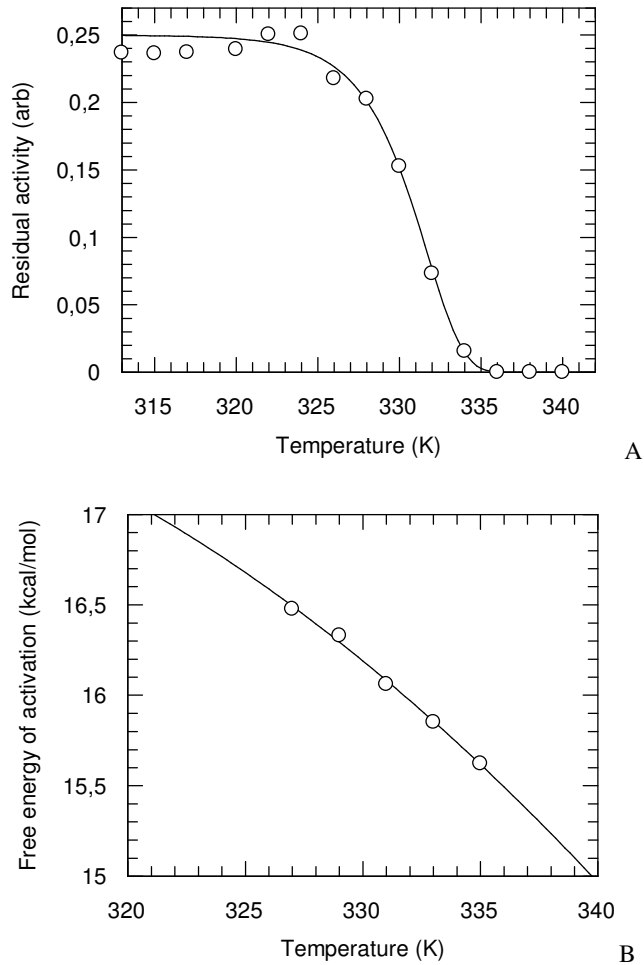


Figure 3.16 : Heat inactivation of *cmFDH* (A) The thermal denaturation of *cmFDH* was measured by incubating the enzyme at varying temperatures for 20 minutes. After this period the residual activity was recorded. The method for fitting the residual activity data is described in Materials and Methods. The plot shown in (B) shows the deduced ΔG for activation against the temperature.

Measurements of unfolding rate constants as a function of temperature yielded similar values for ΔH , ΔC_p and ΔS i.e. 31 kcal/mol, 1.6 kcal/mol/K. and -11 kcal/mol at 298K (Fig. 3. 17).

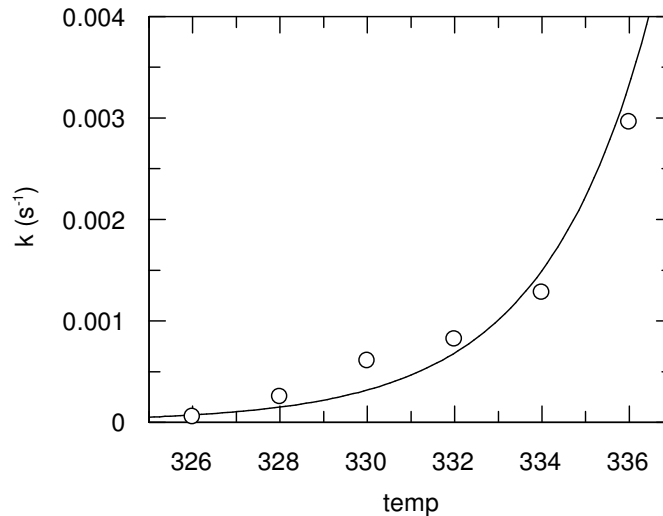


Figure 3.17 : Thermodynamic analysis of the unfolding barrier. Samples of FDH (50 μM) were incubated at the temperatures shown and aliquots removed for assay at a series of times. The resultant data (residual activity v time) were well described by single-exponential decays and the rate constants were extracted. The plot show rate constant as a function of temperature fitted to the equation: $k_o \cdot \exp(-\Delta G/(R \cdot T))$ where $\Delta G = \Delta H + \Delta C_p \cdot (T - T_o) - T \cdot \Delta S - \Delta C_p \cdot T \cdot \ln(T/T_o)$ as described in Materials and Methods.

Interestingly, these values are comparable to those for the barrier to the unfolding of phosphoglycerate kinase (N-domain) (N-PGK) which shows a favourable entropy term (-6.3 kcal/mol at 298K) and an unfavourable enthalpy (+18.4 kcal/mol) (Parker et al., 1998). A further similarity can be seen in the heat capacity change in attaining the transition state in unfolding folding which in the case of FDH and N-PGK is about 20% of the ΔC_p for complete unfolding, i.e. the transition state is about 80% folded as measured by solvent exposure. It is also intriguing to note that for chemical denaturation of FDH, according to the Δm -value for the transition state (~ 4.5 , Fig. 3.13) and the overall Δm value for unfolding (~ 17.5 , Fig. 3.9), the transition state is about 75 % folded. Indeed, using the thermodynamic parameters derived from the rates of thermal denaturation, we would predict the rate of unfolding at 25°C to be $6 \times 10^{-7} \text{ s}^{-1}$, a value remarkably close to $3 \times 10^{-7} \text{ s}^{-1}$ derived from orthodox denaturant analysis.

3.3 Designed Mutants by Homology Modeling

In order to improve the thermal stability of *cmFDH*, two different strategies were applied. Optimization of the protein surface electrostatic interactions has been used as initial strategy and mutations were designed on the basis of *Pseudomonas sp.101* and *Candida boidinii* crystal structures as template molecule. All designed mutations in the literature to improve any kind of properties of *cmFDH* were performed by using a homology model based on the crystal structure of *Pseudomonas sp.101* (Lamzin, 1992), which has 49 % identity with *cmFDH* (Thiskov and Popov, 2006). After the publication of crystal structure of *Candida boidini*, in 2007 (Schirwitz et al., 2007), new electrostatic interaction mutants have been designed according to a homology model of *cmFDH* based on the *Candida boidini* crystal structure as described in this thesis. Disulphide bridge engineering was used as second strategy and these mutants were designed according to this new homology model. The primary sequence of this protein is 97 % identical with that of *cmFDH* and will provide a better model for rational design. Nevertheless, the *cmFDH* model based on the *Pseudomonas sp. 101* crystal structure is of reasonable quality apart from a poor loop prediction between residues 10 and 19. Hence the $C\alpha$ root mean square deviations between *cbFDH* and this *cmFDH* model are: complete dimer, 2.9 Å (1 Å = 0.1 nm); NAD-binding domain, 1.4 Å; catalytic domain 2.2 Å; catalytic domain without loop 10–19, 1.7 Å (Karagüler et al., 2007).

3.3.1 Optimization of protein surface electrostatic interactions

Surface electrostatics are related to protein stability and optimization of the electrostatic surface is an attractive mechanism for increasing the thermostability of a protein as discussed above in section 1.2.5.1 in detail. The mutation of polar groups to charged ones on the protein surface may lead to structure stabilization even in the absence of the salt-bridge partners of the mutated group (Berezovsky, 2008).

3.3.1.1 Mutations designed according to homology model based on *Pseudomonas sp 101* crystal structure

According to the homology model generated based on *psFDH* 3D structure 5 mutations were chosen in terms of optimization of protein surface electrostatic interactions. Except for glutamine (Gln) residue at the position 105, all other residues chosen are on intersubunit region of the dimer. Three asparagine (Asn) residues on

the NAD binding domain, one histidine (His) residue on the dimerization helix of catalytic domain and one Gln residue on the catalytic domain were selected to be changed (Fig. 3.19). Arginine (Arg) and glutamic acid (Glu) residues are usually found on the surface of globular proteins because of their polar character. The polar and uncharged Asn residues were replaced by Arg residue which is a large polar molecule with a positive charge at the position 147 and by negatively charged Glu residue at positions 187 and 300. The polar and uncharged Gln residue was also replaced by Arg at position 105 and positively charged His residue changed to Glu at position 13 (Figure 3.19).

Asn147Arg and Gln105Arg

cmFDH is a homodimer and the NAD binding domains are employed to hold together the dimer. The 19 residue long helix turn helix motif between F138 and K157 of the NAD binding domain is an important part of the interactions between subunits (Schirwitz et al., 2007). Asparagine 147 was chosen since it is located in this connecting loop on intersubunit contact region. Uncharged Asn works as a chain crosslinker via hydrogen bond formation or it can hydrogen bond to water at the protein surface. Replacement of an uncharged Asn residue at the position 147 by an Arg residue will result in the increased close range electrostatic interactions. It is expected to form a salt bridge between Arg147 and Asp297 residues.

We decided to change the 105th residue by replacing this polar uncharged Gln residue with the positively charged polar residue, Arg. Introduction of a positive charge at this position may increase the protein stability by interacting with negatively charged aspartate and glutamate residues in the vicinity. It is expected to form a salt bridge between Arg105 and Glu125 residues. Arg, which contains guanidium group in its side chain, acts as a connector in such networks (Kumar and Nussinov, 2002).

Asn187Glu, Asn300Glu and His13Glu

Asn 187 and 300 are on the loop region between α -helix and β -strand structures of the NAD binding domain of *cmFDH*. These positions are good candidates to change because of being on an apparently flexible loop and in a critical position for protein dimerization. Residue Asn187 is on the loop between α -helix and β -strand that contains the NAD⁺ binding residues Asp195, Tyr196, Gln197. This helix related to

NAD binding, is structurally matching in *psFDH* and *cbFDH* but strand structure is shorter in *cbFDH*. Therefore, it is thought that this loop provides the location of NAD binding residues which make contact with the hydroxyl groups of the NAD adenine ribose. Residue 300 is located on a loop structure in the cofactor binding domain. It is thought that Asn300 interacts with the N-terminal helix which is its dimerization partner. Residue His13 is also in the N-terminal dimerization helix which holds together the dimer structure. It was planned to increase the proportion of charged residues by replacing uncharged Asn residue with the negatively charged Glu at the position 187 and 300 to optimize electrostatic interactions on the protein surface. Likewise, H13 was chosen to be replaced by a negatively charged glutamic acid residue. The pKa of histidine residues is typically about 6; hence, it is expected to be neutral under the standard experimental conditions used to study FDH in this work. By replacing the residues 187, 300 and 13 to negatively charged Glu it is expected to form a salt bridges between Glu187 and Arg322; Glu300 and K19; Glu13 and Arg296.

Asn147Arg/Asn300Glu

In order to observe the effect of both NAD binding domain mutations on the dimerization, the construction of double mutant at positions 147 and 300 on the dimerization helix were planned to form a salt bridge between them (Fig. 3.20).

It is expected that charged residues will form cooperative salt bridge networks, additional salt bridges can protect the integrity of the active site at high temperatures (Kumar et al., 2000) and salt bridges formed between subunits are usually stabilizing interactions (Kumar and Nussinov, 2002).

3.3.1.2 Mutations designed from homology model based on *Candida boidinii* crystal structure

Four mutations were designed according to the homology model generated based on *cbFDH* 3D structure. In order to optimize the protein surface electrostatic interactions two different residue were selected to alter, (tyrosine) Tyr160 and Tyr302, because there are large amount of hydrogen bonds around these positions to constitute salt bridges (Fig. 3.19). Therefore, aromatic Tyr residue which could be involved in a pairwise interaction at both positions were replaced with the polar and negatively charged Glu, and polar and positively charged Arg.

Tyr160Glu and Tyr160Arg

The Tyr160 position occupies a region on the loop which is next to the dimerization helix of the NAD binding site. At the same time this loop has a role in NAD-binding groove region. Therefore it is important both in terms of protein integrity and activity. When the Tyr residue at the position 160 is replaced by Arg it is planned to construct a salt bridge between Arg160 and Asp318 residues (Fig. 3.21). When this Tyr residue is replaced by Glu residue a salt bridge between Glu160 and Arg277 (Fig. 3.22) is anticipated.

Tyr302Glu and Tyr302Arg

The Tyr302 residue is located in the NAD binding domain and it interacts with the N-terminal dimerization helix of the catalytic domain in the dimer structure. It has a significant role to keep the dimers together. By changing Tyr by Glu and Arg in this position, the effect of charged residues in terms of formation of an electrostatic interaction network can be examined. When the Tyr residue at the position 302 is replaced by Arg it is planned to construct a salt bridge between Arg302 and Asp16 residues (Fig. 3.23). When this Tyr residue is replaced by Glu residue a salt bridge between Glu302 and Lys19 is anticipated (Fig. 3.24).

All mutation sites mentioned in sections 6.1.1 and 6.1.2 were selected in or around the active site, NAD-binding site or substrate binding site, and dimerization site. While designing all these mutants it was aimed to increase the stability of *cmFDH* at high temperatures and at the same time protect its flexibility that is essential for enzyme activity.

3.3.2 Disulphide bridge engineering

According to studies that have compared mesophilic and thermophilic enzymes, the formation of disulphide bridges is one of the important strategies developed during evolution to stabilize proteins. Disulphide bridges are strongly related to protein 3D structure, stability and function. The native *cmFDH* does not contain a disulphide bridge, hence it is a good candidate for attempted stabilisation by this approach. Cysteine residues have been introduced into the N-terminal domain of *cmFDH* to construct a disulphide bridge mutant.

Met1Cys/Asp62Cys

Residues at positions 1 next to the N-terminal dimerization helix and 62 next to the functionally relevant residue 68 were selected. These lie on the start point of two different β -strand, hence this is a good position to introduce a disulphide bridge in the N-terminal of catalytic domain of *cmFDH* for stabilizing the structure (Fig. 3.25). Both single mutants and the disulphide bridge mutant containing double point mutation were constructed and characterized separately.

The locations of all mutants, which were designed using homology models based on *psFDH* or *cbFDH*, on the nucleic acid sequence of the *cmFDH* gene are shown in Figure 3. 18.

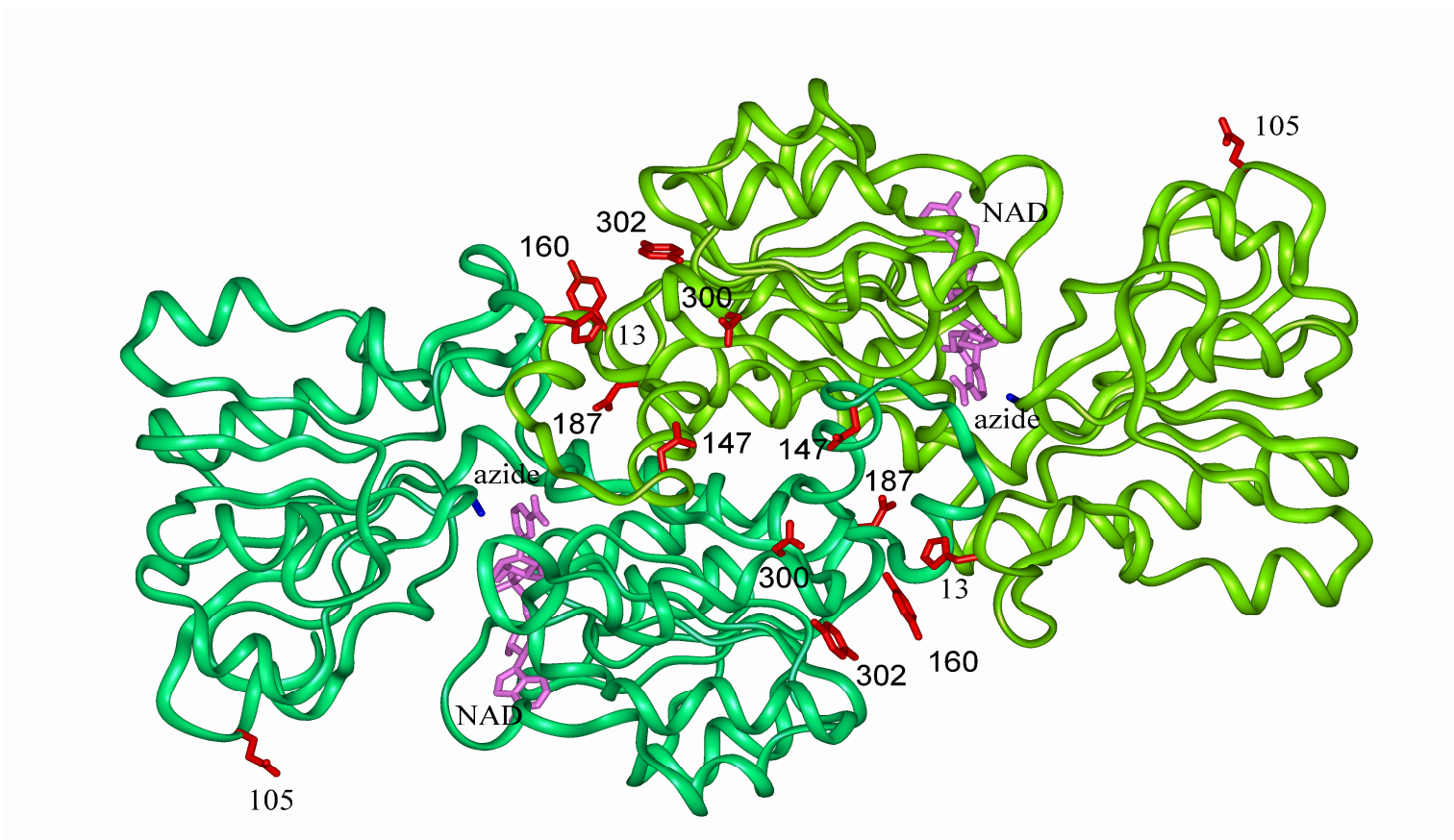


Figure 3.19 : Positions of mutants determined by homology modelling based on *ps*FDH and *cb*FDH 3D structures. N147, N187, N300, H13, Q105, Y160 and Y302 All residues to be changed were selected on the dimerization regions of active sites or related to dimerization helix.

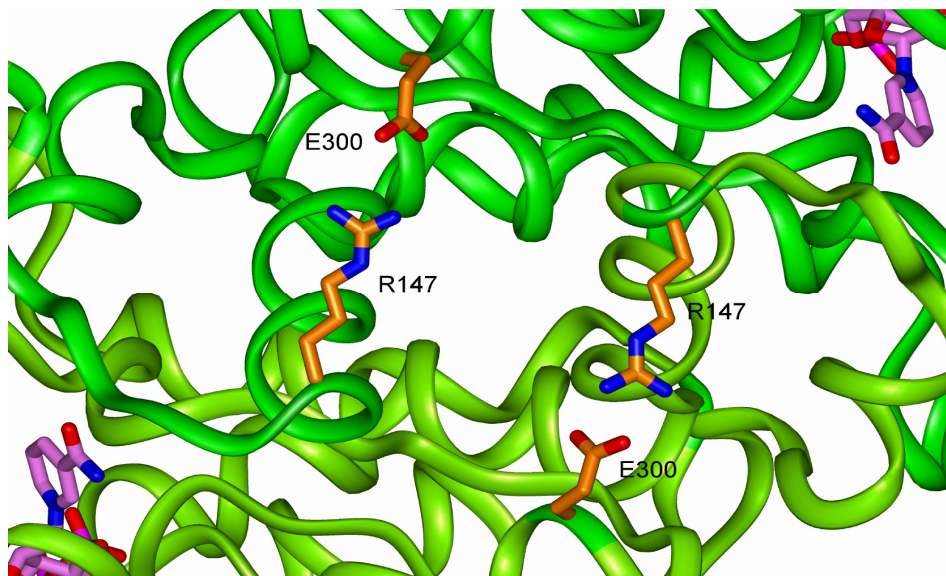


Figure 3.20 : Homology model of salt bridge formation between Glu300 and Arg147 on NAD binding domain.

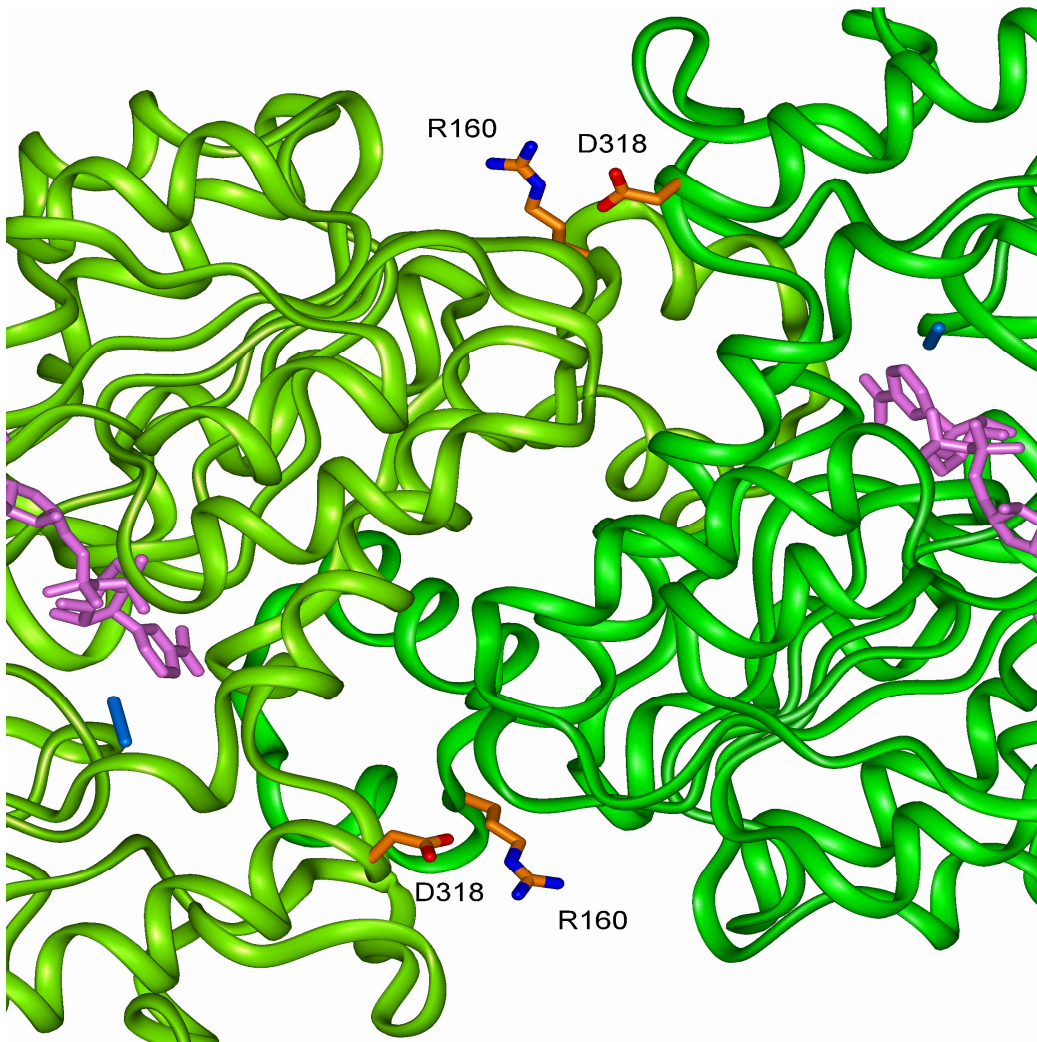


Figure 3.21 : Homology model of salt bridge formation between Arg160 - Asp318.

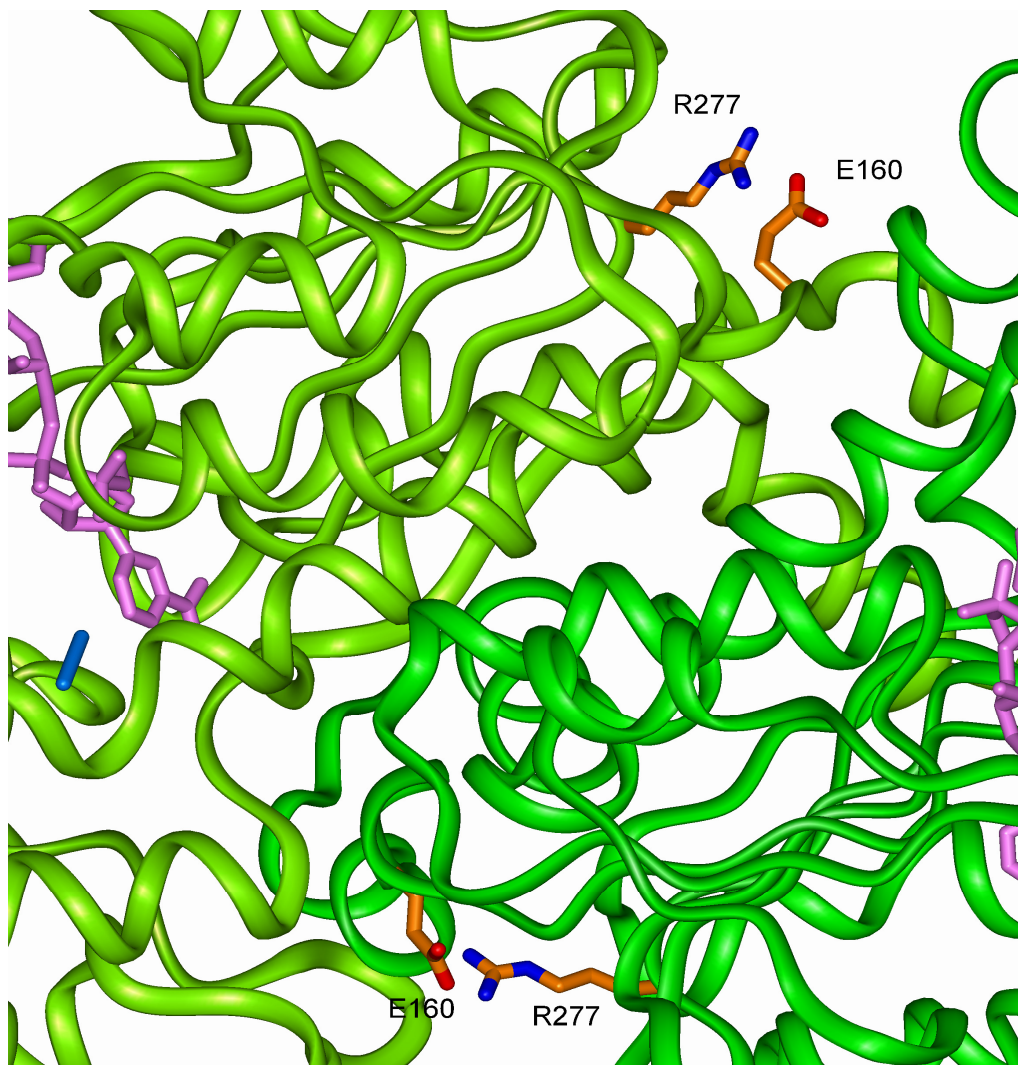


Figure 3.22 : Homology model of salt bridge formation between Glu160 - Arg277.

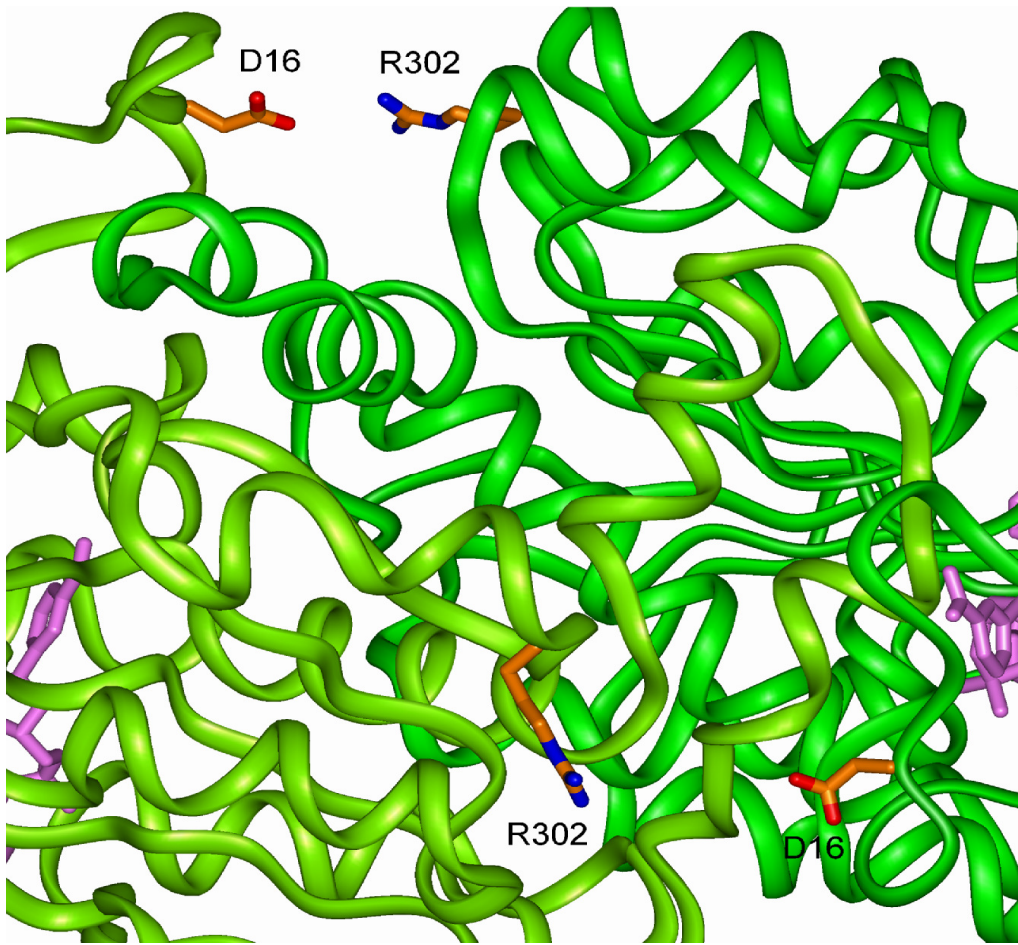


Figure 3.23 : Homology model of salt bridge formation between Arg302 - Asp16.

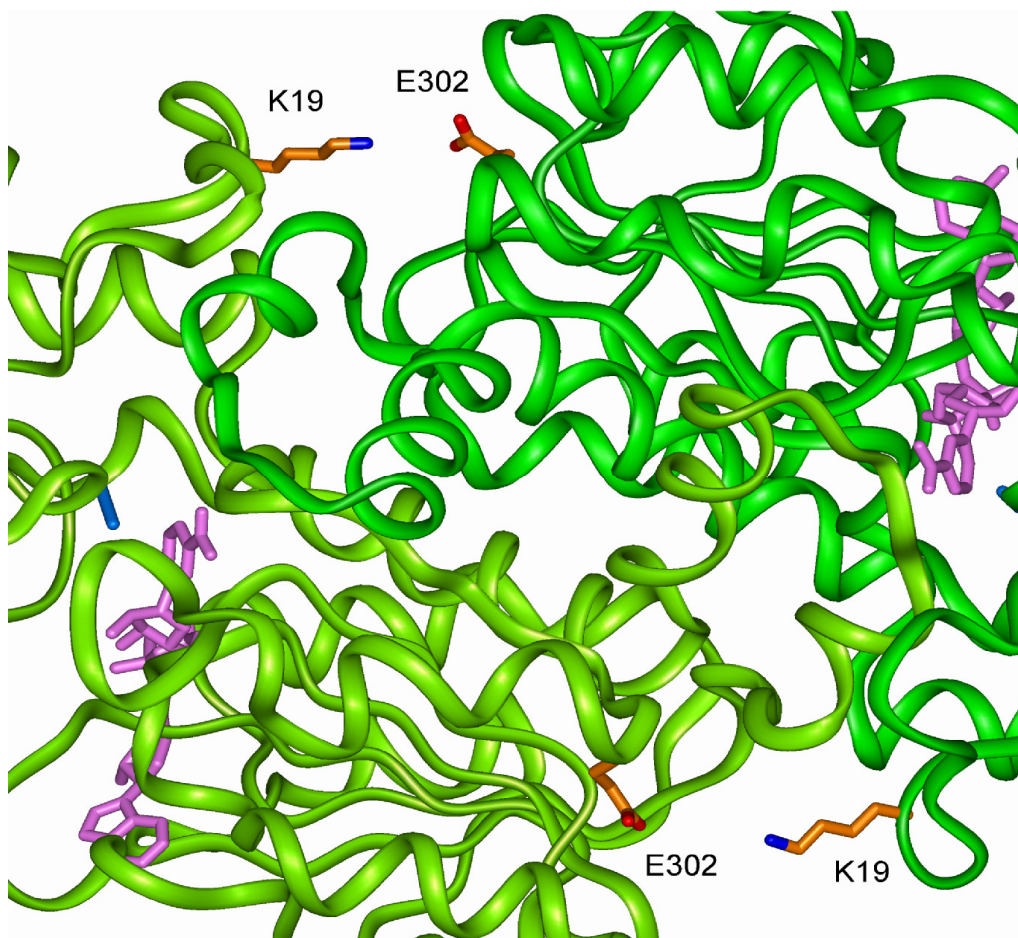


Figure 3.24 : Homology model of salt bridge formation between Glu302 and Lys19.

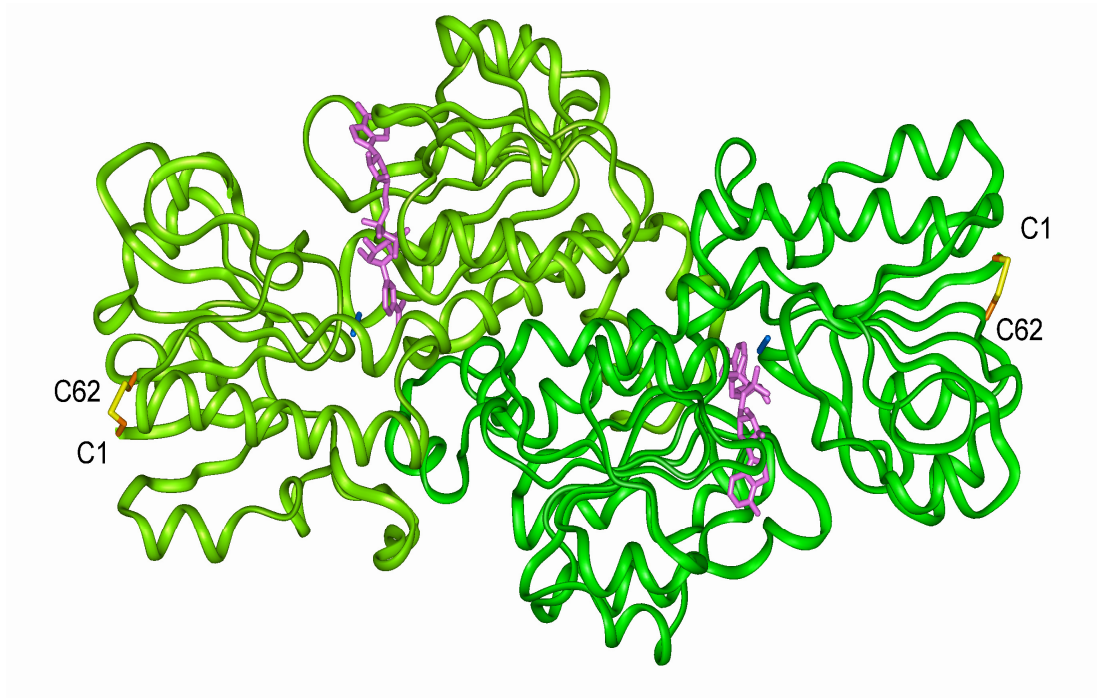


Figure 3.25 : Homology model of disulphide bridge formation between Cys1 and Cys62.

3.4 Optimization of Surface Electrostatic Interactions

In recent years, engineering of surface electrostatic interactions is one of the most attractive methods to increase thermostability as mentioned in section 1.2.4. Electrostatic interactions on the protein surface are important especially for the intermediate stages of oligomer formation in multidimeric globular proteins as well as protein-protein interactions or binding affinity (Yun et al., 2007, Baldwin, 2007). Therefore, all residues to be changed were selected in the dimerization regions of the protein or related to the dimerization helix. According to homology models generated based on *psFDH* and *cbFDH* 3D structures, 12 mutants (9 of them are single and 3 of them are double mutants) were chosen to optimize electrostatic interactions on *cmFDH* surface. While designing all these mutants it was aimed to increase the stability of *cmFDH* at high temperatures and at the same time protect its flexibility that is essential for enzyme activity. Figures 3.19 shows the positions of the mutations, on the homology model of *cmFDH*. The mutants (N147R; N187E; N300E; H13E; Q105R; Y160E; Y160R; Y302E; Y302R; N300E/N147R; N187E/Q105R; N187E/N147R) were constructed by the use of “Invitrogen Gene Tailor Site Directed Mutagenesis Kit”.

After purification on a nickel–agarose column, on average 1.2 mg/ml of native and all mutant *cmFDH* proteins of >95 % purity were obtained. No formate-dehydrogenase enzymatic activity could be measured for mutants, N300E, N300E/N147R and Y302E. Positions of N300 and Y302 are on the loop region between α helix and β -strand structures of the NAD binding domain of *cmFDH*. These residues have a role in the stabilizing of β -strand structure and presumably alteration of these residues to glutamic acid (N300E and Y302E) have distorted the structure of the FDH dimer to such an extent that the coenzyme binding machinery is rendered ineffective. Inactive N300E/N147R double mutant can be explain with the negative effect of N300E mutation because N147R is a kinetically active single mutant.

3.4.1 Steady state kinetics

Enzyme catalytic activity is affected by the pH of the medium due to the presence of amino acids which can be charged or uncharged dependent on pH. In the enzyme

engineering studies when an amino acid changed with another one especially at the active site, it is important to control whether or not the mutation has altered pH-activity profiles. The difference of the kinetic parameters with the pH reflects the alteration of ionization profile of changed amino acid sequence of enzyme. (Lutz and Bornscheuer, 2009). Therefore pH dependent catalytic characterization of mutant enzymes were performed over a pH range from 6.0 to 9.0. Figures 3.26 and 3.27 show activity profiles of enzymes in pH 6, 7, 8 and 9.

Results show that the best activity of native and all surface electrostatic interaction mutants is obtained in pH 8 as described in the literature for native enzyme (Karagüler 2001). According to these results, further studies were carried out at pH 8. Comparison of K_m and k_{cat} values of native and mutant proteins are shown in table 3.9.

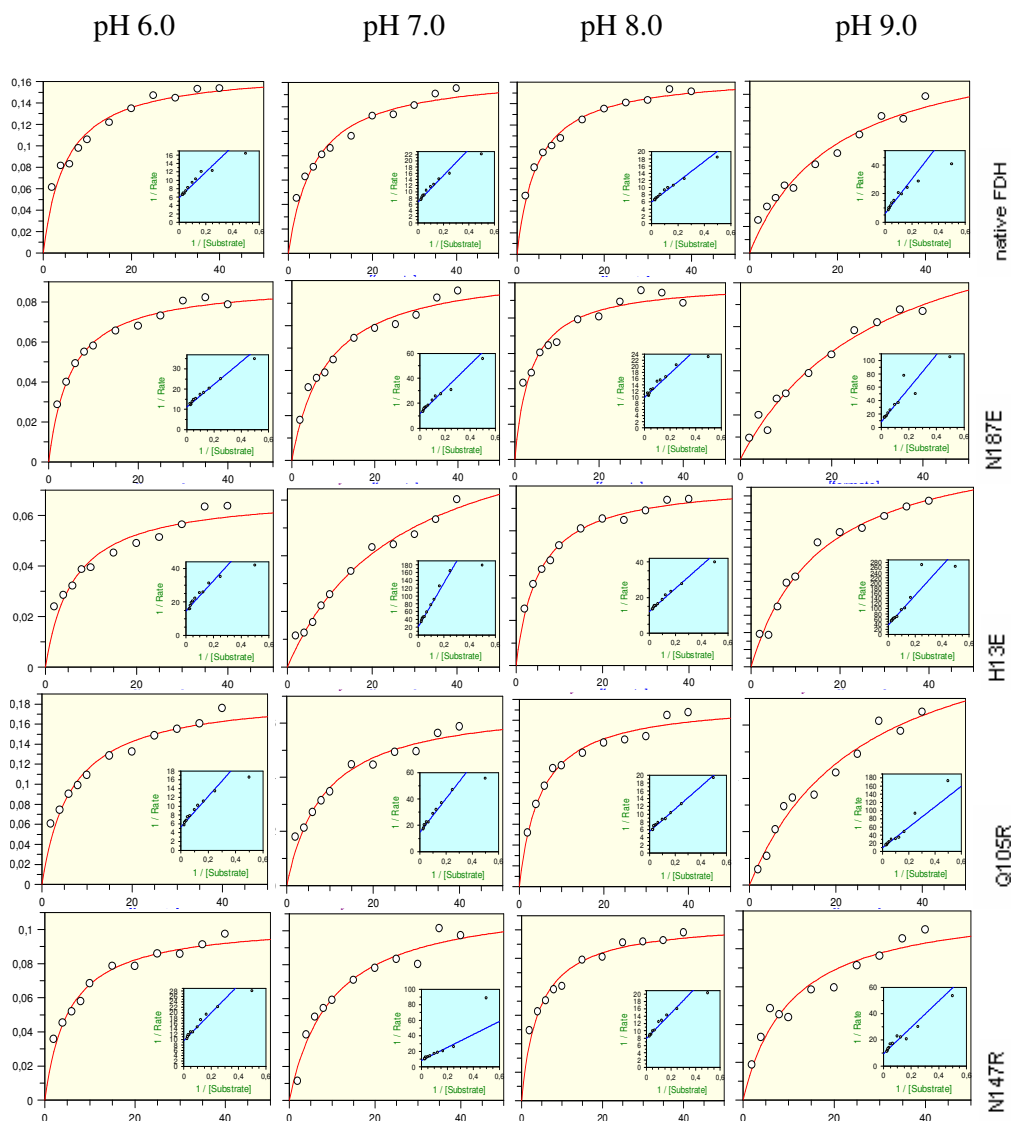


Figure 3.26 : Enzyme kinetic data of native and mutant *cm*FDH designed according to *ps*FDH crystal structure, in pH6, 7, 8 and 9.

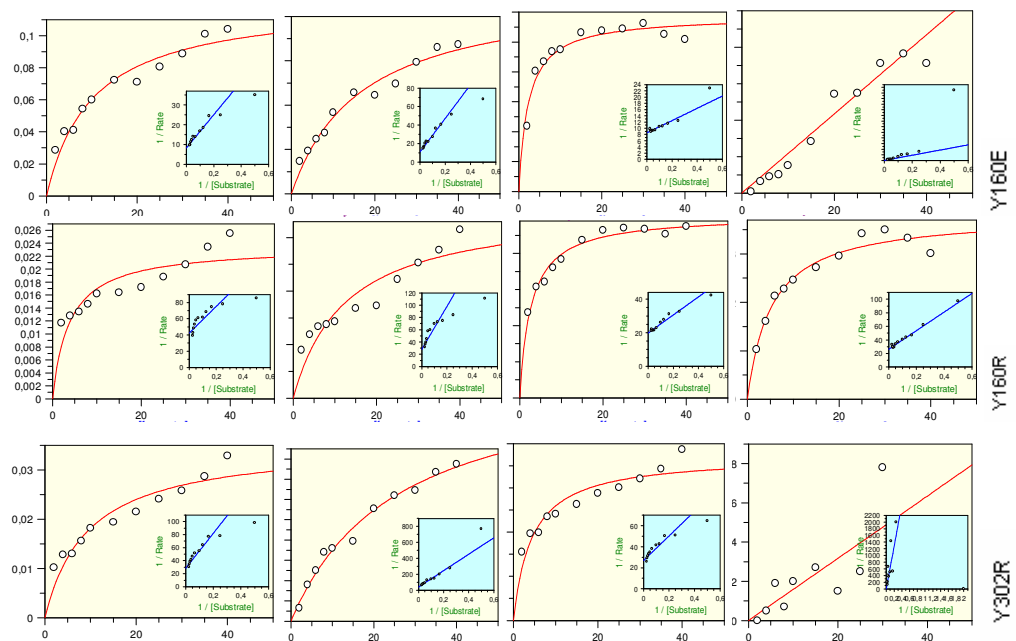


Figure 3.27 : Enzyme kinetic data of native and mutant *cmFDH* designed according to *cbFDH* crystal structure, in pH6, 7, 8 and 9.

Table 3.9: Summarise the activity differences between native and mutant *Candida methylica* FDH enzymes in different pH conditions.

mutants	pH6			pH7			pH8			pH9		
	K_m (mM)	k_{cat} (sn^{-1})	k_{cat}/K_m ($sn^{-1} mM^{-1}$)	K_m (mM)	k_{cat} (sn^{-1})	k_{cat}/K_m ($sn^{-1} mM^{-1}$)	K_m (mM)	k_{cat} (sn^{-1})	k_{cat}/K_m ($sn^{-1} mM^{-1}$)	K_m (mM)	k_{cat} (sn^{-1})	k_{cat}/K_m ($sn^{-1} mM^{-1}$)
Native	5.22±0.7	1.15±0.2	0.22	6.3±0.8	0.99±0.005	0.16	4.75±0.3	1.13±0.1	0.24	19.8±4	1.1±0.01	0.056
N187E	5±0.4	0.6±0.02	0.12	8.5±1	0.58±0.004	0.07	3.9±0.6	0.68±0.004	0.17	31.3±6	0.83±0.01	0.03
H13E	6.2±1.1	0.45±0.003	0.07	26.6±4.3	0.33±0.004	0.01	5.33±0.4	0.55±0.002	0.10	15.7±2.2	0.18±0.02	0.01
Q105R	6.6±0.9	1.28±0.008	0.19	8.6±1.2	0.45±0.003	0.05	5.1±0.5	1.2±0.005	0.24	26.3±5.7	0.7±0.01	0.03
N147R	5.4±0.6	0.7±0.003	0.13	9.9±1.7	0.8±0.007	0.08	4.37±0.5	0.85±0.004	0.19	10.5±2.4	0.7±0.009	0.07
160E	10.3±1.9	0.83±0.008	0.08	16.9±3.2	0.63±0.008	0.04	2.31±0.7	0.78±0.005	0.34	-	-	-
160R	3.9±1.2	0.16±0.002	0.04	12.6±4.2	0.24±0.004	0.02	2.73±0.2	0.33±8.10 ⁻⁴	0.12	5.2±0.8	0.25±0.00	0.05
302R	9.5±2.4	0.24±0.003	0.025	25.7±4	0.17±0.002	0.007	4.36±1	0.25±0.002	0.06	-	-	-
187E/ Q105R							5.48±0.2	0.59±6.10 ⁻⁴	0.18			
187E/ N147R							5.88±0.3	0.46±0.001	0.08			

3.4.2 Irreversible thermal denaturation of electrostatic interaction mutants

One of the approaches in the literature to characterize enzyme thermostability is to measure the residual enzyme activity upon incubation at a fixed temperature for a fixed time (Thiskov and Popov, 2006). In this study, enzyme was aliquoted and incubated at a series of temperatures for a period of 20 minutes and the residual activity was recorded by using UV spectrophotometer. Figures 3.28 to 3.36 demonstrate the thermal inactivation profile of mutants N87E, H13E, Q105R, N147R, Y160E, Y160R and Y302R, N187E/Q105R and N187E/N147R respectively. The temperature which is required for 50 % reduction of initial activity of enzyme ($T_{0.5}$) was determined from these data. Table 3.10 illustrates the half life of mutants compare to native *cm*FDH.

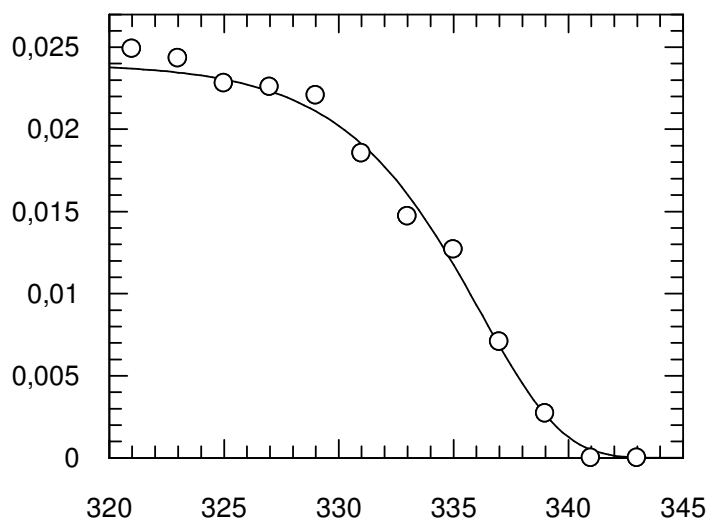


Figure 3.28 : Heat inactivation of N187E mutant of *Candida methylica* FDH.

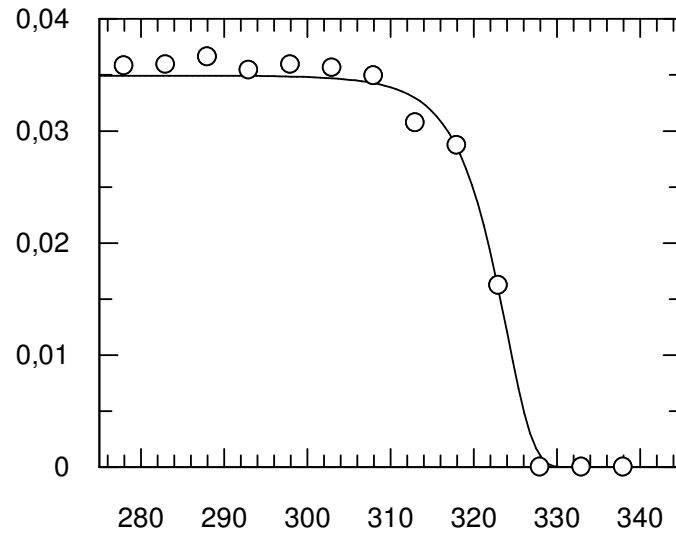


Figure 3.29 : Heat inactivation of H13E mutant of *Candida methylica* FDH.

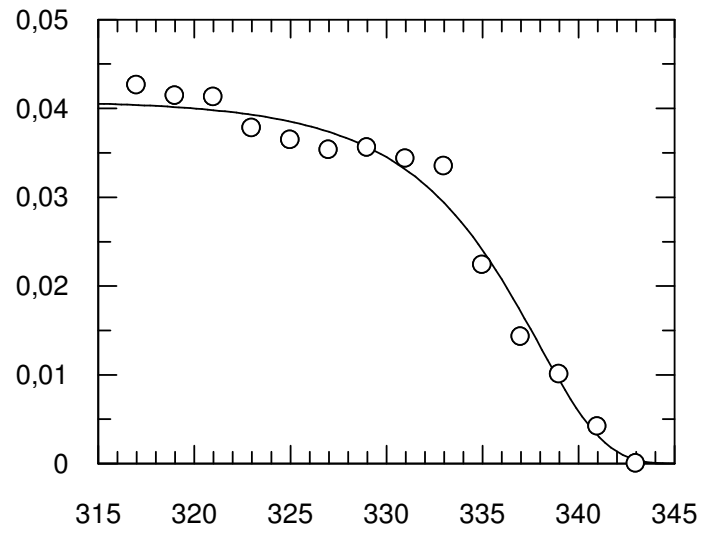


Figure 3.30 : Heat inactivation of Q105R mutant of *Candida methylica* FDH.

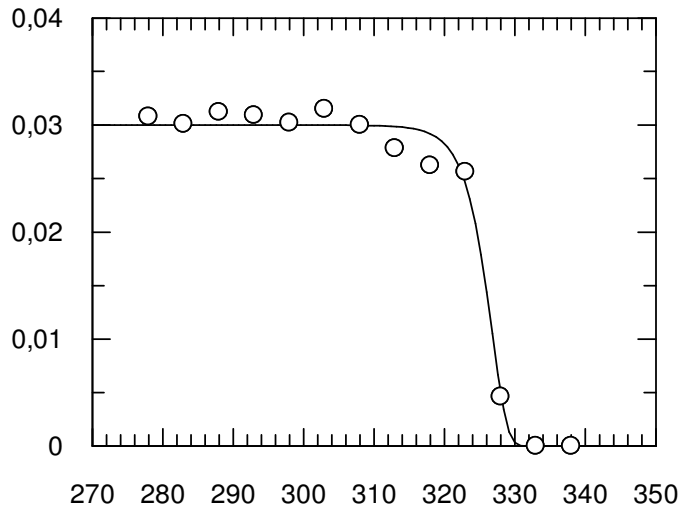


Figure 3.31 : Heat inactivation of N147R mutant of *Candida methylica* FDH.

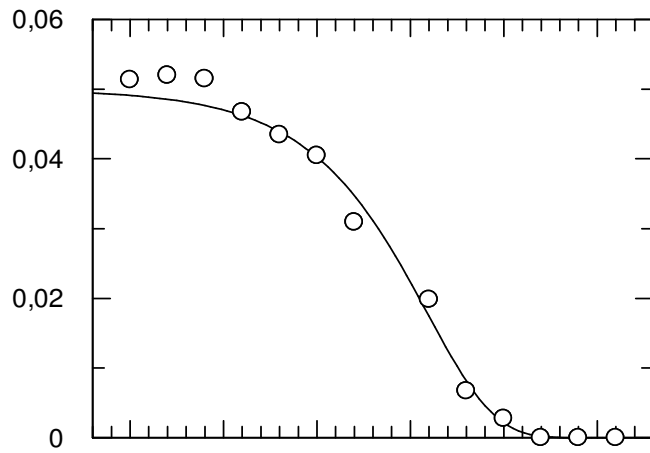


Figure 3.32 : Heat inactivation of Y160E mutant of *Candida methylica* FDH.

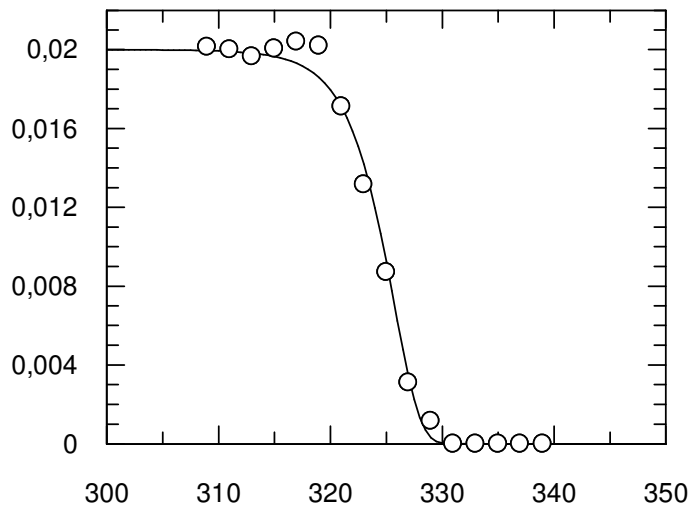


Figure 3.33 : Heat inactivation of Y160R mutant of *Candida methylica* FDH.

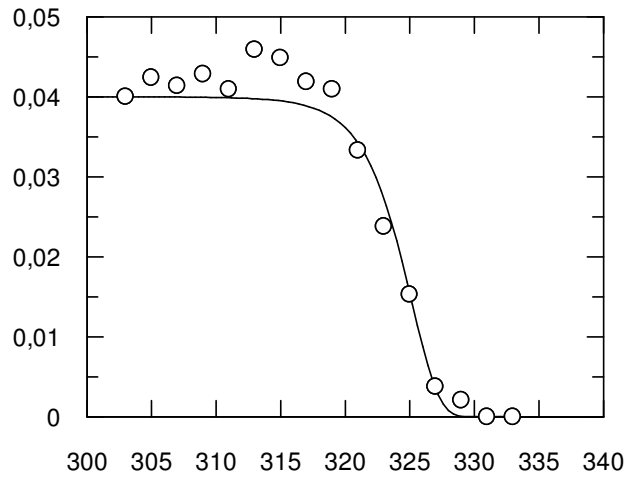


Figure 3.34 : Heat inactivation of Y302R mutant of *Candida methylica* FDH.

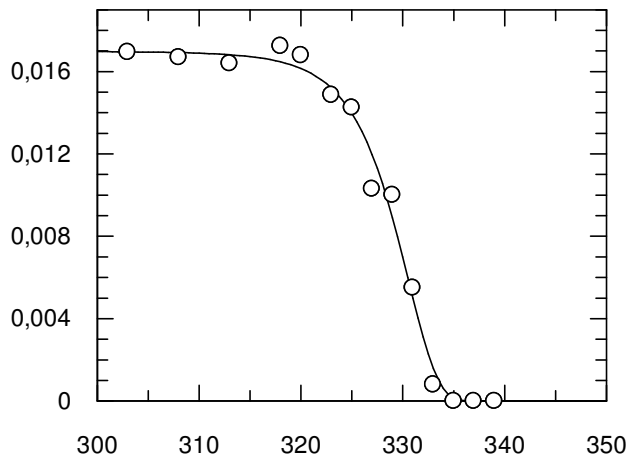


Figure 3.35 : Heat inactivation of N187E/Q105R mutant of *Candida methylica* FDH.

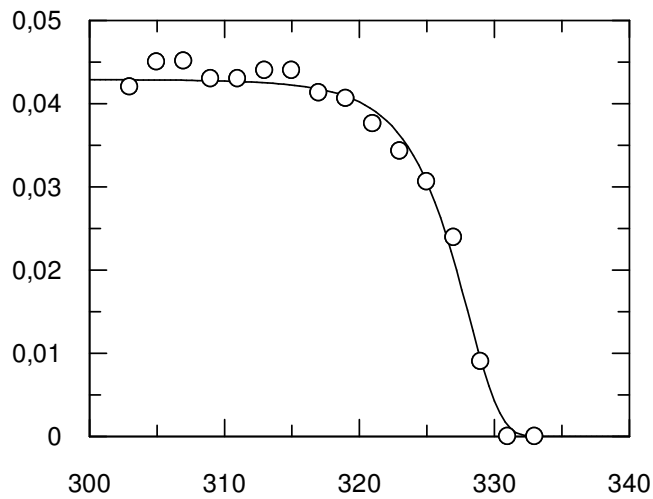


Figure 3.36 : Heat inactivation of N187E/N147R mutant of *Candida methylica* FDH

Table 3.10: Comparison of temperatures that provides 50 % inactivation of native and electrostatic interaction mutants of *cmFDH* enzyme in 20 min.

Enzymes	T _{0.5}	ΔT _{0.5}
native <i>cmFDH</i>	56.7±0.2	0
H13E	49.5±0.6	-7.2
N147R	51.2±0.5	-5.5
N187E	56±0.5	-0.7
Q105R	56.4±1	-0.3
N187E/Q105R	55.12±0.2	-1.6
N187E/N147R	54.8±0.8	-1.9
Y160E	45±0.2	-11.7
Y160R	51±0.3	-5.7
Y302R	50.5±0.3	-6.2

Results showed that the catalytic efficiency (k_{cat}/K_m) of Q105R is equal to native *cmFDH* and alteration of Q105 residue with arginine amino acid do not change the T_{0.5} value (56.4). Only one mutant, Y160E has higher catalytic efficiency than native. However, while this mutant has a higher k_{cat}/K_m , the alteration of Y160 to glutamic acid decreases the thermal inactivation temperature of enzyme, such that it has the lowest T_{0.5}, 11.7°C lower than native.

All other mutant enzymes show around half of the catalytic efficiency of native *cmFDH*. When we analyze k_{cat} and K_m individually, results show that N187E, N147R, Y160E, Y160R and Y302R mutants have lower K_m than native, and consequently better formate affinity. The K_m of mutants at residue 160 is about half of the K_m of native, hence these mutants have a two fold better affinity for formate. Another important mutation in terms of T_{0.5} value is N187E, although it has two fold lower catalytic efficiency than native it has almost the same T_{0.5} with the native *cmFDH* enzyme. The overall comparison of T_{0.5} values between mutant enzymes and native enzyme is in the range of 11.7-0.3. T_{0.5} significantly changed by replacing Tyr by Glu at position 160 and, His by Glu at the position 13 (Tab. 3.10).

When the stability is considered in terms of relative residual activity, the results showed that N187E retains full activity after incubation at 50 °C like native *cmFDH*. The activity of H13E and 160E decrease below 50 % and other mutants Q105R (88.6

%), N147R (83 %), N187E/Q105R (87.5 %), N187E/N147R (81.6 %), 160R (65.4 %) and 302R (59.4 %) retain activities above 50 % under these conditions. After incubation at 55 °C, the stability of Q105R and native *cmFDH* is very similar while the N87E mutant is 5.5 % more stable than native enzyme. The stability of other mutants towards incubation at 55 °C for 20 min. are all below 40 % except for N187E/Q105R which has 59 % residual activity. The most clear results for increased stability of N187E and Q105R was observed after incubation of enzymes at 60 °C for 20 min. While the N87E and Q105R retain activities of 60.5 % and 78.5 % respectively, native *cmFDH* retains only 6.5 % of its activity. While increased stability of N147R and the double mutants N187E/Q105R, N187E/N147R was observed after incubation at 50 °C, they lost serious activity after incubation at 55 °C and 60 °C significantly.

The major result of the thermal inactivation experiments, when comparing percentages of residual activity, is the observation that the N187E and Q105R electrostatic interaction mutants retain more activity than native *cmFDH* after incubation at 60 °C. Table 3.11 and figure 3.37 summarize the residual activities of enzymes after incubation at 50, 55 and 60 °C.

Table 3.11: Residual activities of native *cmFDH* and mutant enzymes after incubation in 50, 55 and 60 °C for 20 min. Residual activities were expressed relative to activities in room temperature (25 °C).

Temp (°C)	native <i>cmFDH</i>	N187E	H13E	Q105R	N147R	N187E/Q105R	N187E/N147R	Y160E	Y160R	Y302R
50	100	100	45	88.6	83	87.5	81.6	13	65.4	59.4
55	85.5	91	0	83	14.9	59	38.5	0	10	0
60	6.58	60.5	0	78.5	0	4.7	0	0	0	0

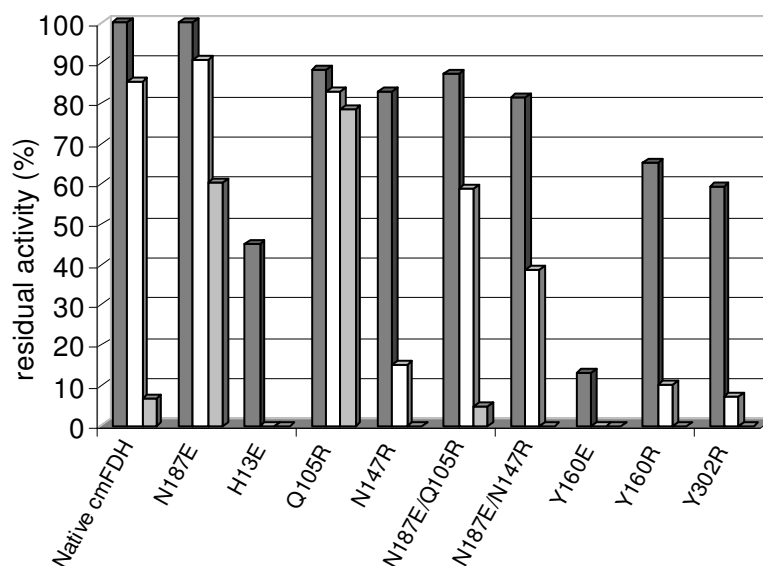


Figure 3.37 : Bar graph presentation of residual activities of native *cmFDH* and mutant enzymes after incubation in 50 (dark grey), 55 (white) and 60 °C (light grey) for 20 min. Residual activities were expressed relative to activities in room temperature (25 °C).

In order to obtain more detailed information from these experiments, residual activity data was also treated as representing rate constants of denaturation as a function of temperature. Rate constant of unfolding reaction in the absence of an activation barrier (k_0) and activation enthalpy (E_a) values were obtained (Tab. 3.12) by fitting the thermal denaturation data to Arrhenius relationship (equation 3.3).

The results show that, while the rate constants of the unfolding reactions of N187E and Y160E decrease, the rate constant of N147R and Y302R increase. The rate constants of other mutants are similar. The lowest E_a was observed for N187E and Y160E which have the lowest k_0 .

In order to describe the protein unfolding more realistically, data were fitted to van't Hoff relationship (2.7), k value was taken as 10^7 s^{-1} as described in the experiment performed with native *cmFDH*. The deduced ΔG for activation was plotted against the temperature. Combining the equations 2.4, 2.6 and 2.7 allows a direct fit of residual activity against enthalpic barrier (ΔH), heat capacity changes (ΔC_p) and entropic term ($-T\Delta S$) (Tab. 3.13). Residual activity data was fitted as described before in section 3.2.1.

Table 3.12: Analysis of thermal denaturation experiments by Arrhenius relationship.

	E_a (kcal/mol)	k_o (s^{-1})
native <i>cm</i> FDH	91±0.7	2x10 ⁵⁷
H13E	90.22±0.2	3.1x10 ⁵⁷
N147R	94.8±1.2	8x10 ⁵⁹
N187E	88.8±0.5	1.9x10 ⁵⁴
Q105R	93.6±1.8	1.9x10 ⁵⁷
N187E/Q105R	91.35±0.17	1x10 ⁵⁷
N187E/N147R	91±0.12	1.6x10 ⁵⁷
Y160E	87.8±0.3	2.2x10 ⁵⁶
Y160R	90.7±0.2	2.7x10 ⁵⁷
Y302R	91.8±0.6	1.7x10 ⁵⁸

Table 3.13: Analysis of thermal denaturation experiments by van't Hoff equation.

	ΔH (kcal/mol)	$-T\Delta S$ (kcal/mol)	ΔC_p (kcal/mol/K)
native <i>cm</i> FDH	25±10	-5.5±0.003	2.0±0.5
H13E	21.6±1.1	-4.5±0.004	1.52±0.2
N147R	31.2±6	-12±0.02	2.23±0.6
N187E	53.4±2	-33±0.06	0.28±0.13
Q105R	-30.8±5	+45±0.1	2.23±1.4
N187E/Q105R	11.3±9.6	+6±0.03	1.82±0.3
N187E/N147R	-1.4±1	+18±0.05	2.82±07
Y160E	38±6	-21±0.02	0.76±0.4
Y160R	38.1±8.5	-18±0.03	1.8±0.5
Y302R	47.5±15	-27±0.05	1.87±1.8

We could not observe any clear trend between native and mutant enzymes in terms of van't Hoff relationship.

3.4.3 Thermodynamics of the folding-unfolding transition

In order to analyse the thermal dependence of folding-unfolding transition equilibrium unfolding experiments was performed at a series of temperatures. Thermodynamic stabilities were compared using two different chemical denaturants, GdnHCl and urea.

3.4.3.1 GdnHCl induced denaturation

Experiments were performed as described in section 3.2.2.1. for each kinetically active mutant. The equilibrium unfolding transitions of mutants at different temperatures are shown in the following figures (Fig. 3.38-3.54). Data were fitted to equation 2.1 to extract K_w and $\Delta G = -RT \ln K_w$ was used to calculate ΔG values (Tab. 3.14 to 3.22). The plots show the free-energy change of mutants for GdnHCl-induced unfolding transition as a function of temperature fitted to equation 2.4 as previous (figures 3.39, 41, 43, 45, 47, 49, 51, 53, 55).

The data obtained at different temperatures for all mutants are given in the following part of this section, sequentially (H13E, N187E, Q105R, N147R, Y160E, Y160R and Y302R).

H13E

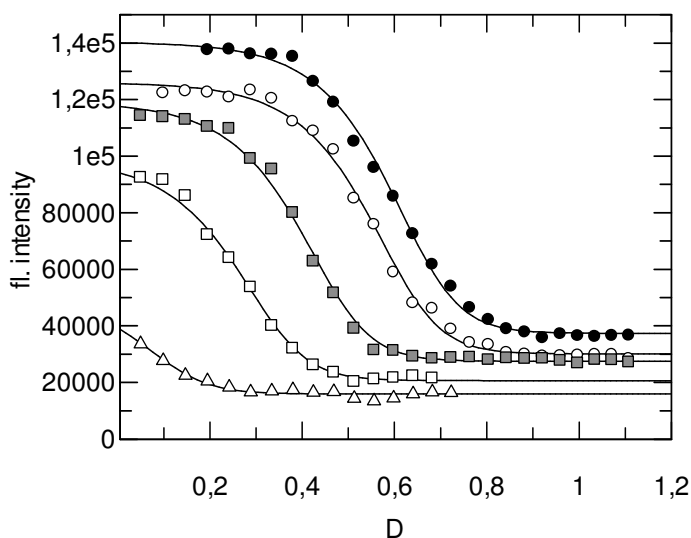


Figure 3.38 : GdnHCl-induced equilibrium unfolding transition of mutant H13E in different temperatures: 25°C is closed circles, 30°C is open circles, 35°C is grey square, 40°C is open square and 45°C is open triangle.

Table 3.14: m , K_w , ΔG and $[\text{denaturant}]_{0.5}$ results of mutant H13E from GdnHCl induced denaturation experiments.

Temp (K)	K_w	ΔG (cal/mol)	m (cal/mol M)	$[\text{GdnHCl}]_{0.5}$ (M)
298	6.82×10^{11}	-16125		0.59 ± 0.004
303	3.09×10^{11}	-15916		0.55 ± 0.003
308	1.83×10^{10}	-14455	-4.52 ± 1	0.4 ± 0.003
313	1.37×10^9	-13080		0.27 ± 0.007
318	2.3×10^7	-10718		0.1 ± 0.008

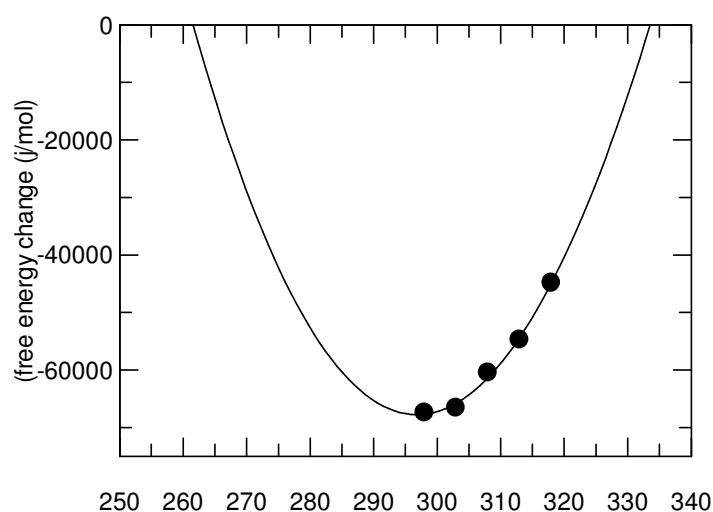


Figure 3.39 : Thermodynamics of unfolding of mutant *cmFDH*, H13E. The free energy changes of unfolding in water (ΔG_w) over a range of temperatures (T) were determined from GdnHCl-induced equilibrium denaturation data and fitted to the equation 2, at a reference temperature of $T_0=298$ K.

The free energy change of H13E decreases with increasing temperature. It has a T_m of 60.5 °C, a 2.5 °C decrease in the stability compared to that of the native protein, which corresponds to an decrease in the thermodynamic stability of 1.8 kcal/mol at 25 °C.

The results show that, at the reference temperature of 25 °C the enthalpy change on folding (ΔH) is favourable (-25 ± 14) kcal/mol) and the heat capacity change (ΔC_p) is -7.4 ± 1.3 kcal/mol/K. The entropy change at 25 °C is unfavourable ($-T\Delta S = +8.6 \pm 0.04$ kcal/mol) (Fig. 3.39). Insertion of a negative charge instead of a neutral

histidine residue causes a favourable enthalpy change and unfavourable entropy change. This is accompanied by a decrease in stability, compared to native *cmFDH*.

N187E

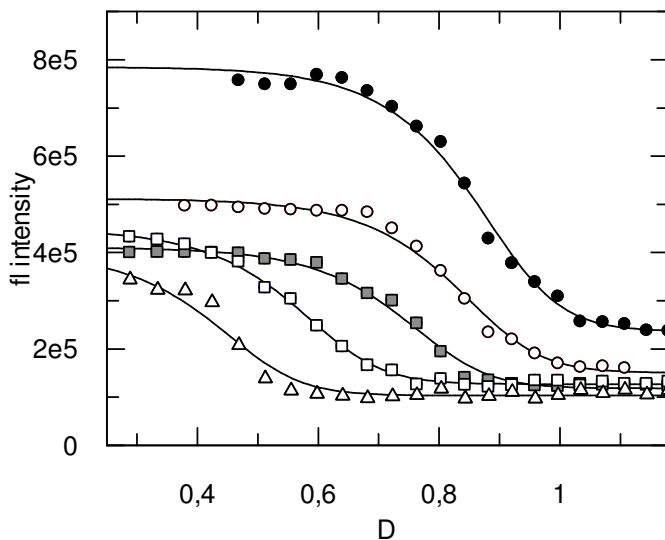


Figure 3.40 : GdnHCl-induced equilibrium unfolding transition of mutant N187E in different temperatures: 25°C is closed circles, 30°C is open circles, 35°C is grey square, 40°C is open square and 45°C is open triangle.

Table 3.15: m , K_w , ΔG and $[\text{denaturant}]_{0.5}$ results of mutant N187E from GdnHCl induced denaturation experiments.

Temp (K)	K_w	ΔG (cal/mol)	m (cal/mol M)	$[\text{GdnHCl}]_{0.5}$ (M)
298	2.42×10^{14}	-19600		0.86 ± 0.004
303	1.29×10^{14}	-19549		0.83 ± 0.003
308	2.34×10^{13}	-18828	-4.73 ± 0.38	0.74 ± 0.006
313	6.97×10^{11}	-16953		0.57 ± 0.005
318	4.84×10^{10}	-15535		0.46 ± 0.003

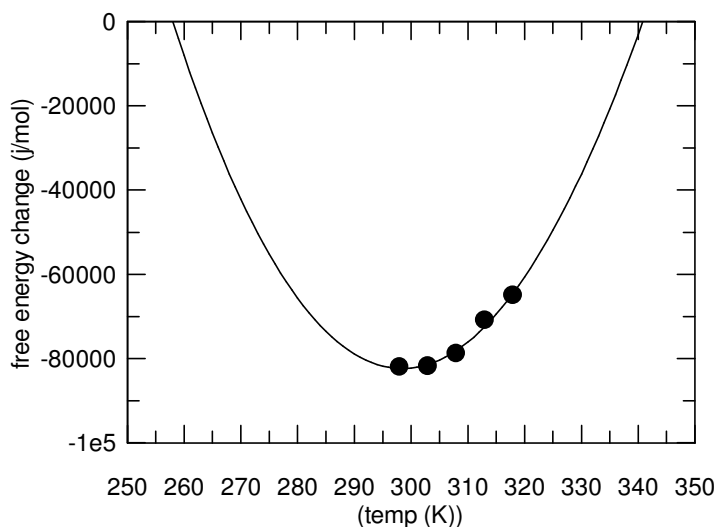


Figure 3.41 : Thermodynamics of unfolding of mutant *cmFDH*, N187E. The free energy changes of unfolding in water (ΔG_w) over a range of temperatures (T) were determined from GdnHCl-induced equilibrium denaturation data and fitted to the equation 2, at a reference temperature of $T_0=298$ K.

The free energy change of N187E decreases with increasing temperature. It has a T_m of 68 °C, a 5 °C increase in the stability compared to that of the native protein, which corresponds to an increase in the thermodynamic stability of 1.7 kcal/mol at 25 °C.

The results show that, at the reference temperature of 25 °C the enthalpy change on folding (ΔH) is favourable (-16.5 ± 2) kcal/mol) and the heat capacity change (ΔC_p) is -7 ± 2 kcal/mol/K. The entropy change at 25 °C is favourable ($-T\Delta S = -3.13 \pm 0.06$ kcal/mol) (Fig. 3.41). Insertion of a negatively charged glutamic acid instead of uncharged asparagine residue causes a favourable enthalpy change and favourable entropy changes accompanied by an increase in stability.

N147R

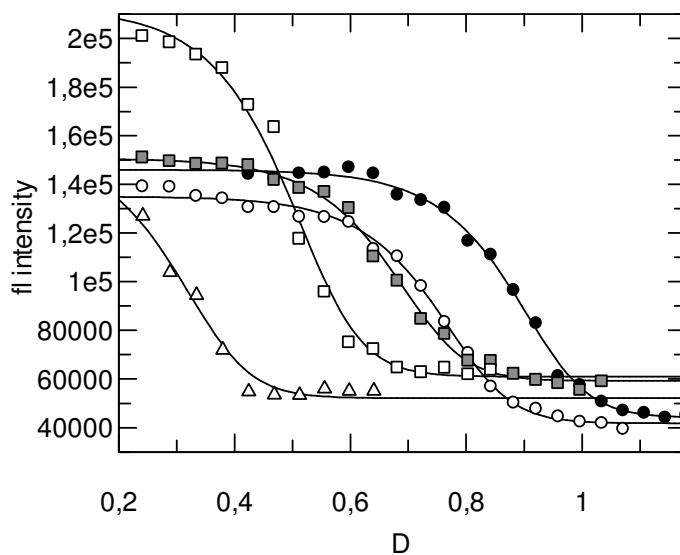


Figure 3.42 : Figure GdnHCl-induced equilibrium unfolding transition of mutant N147R in different temperatures: 25°C is closed circles, 30°C is open circles, 35°C is grey square, 40°C is open square and 45°C is open triangle.

Table 3.16: m , K_w , ΔG and $[\text{denaturant}]_{0.5}$ results of mutant N147R from GdnHCl induced denaturation experiments.

Temp (K)	K_w	ΔG (cal/mol)	m (cal/mol M)	$[\text{GdnHCl}]_{0.5}$ (M)
298	3.18×10^{15}	-21123		0.89 ± 0.006
303	1.66×10^{14}	-19698		0.75 ± 0.008
308	2.86×10^{13}	-18950	-5.3 ± 1.3	0.67 ± 0.005
313	5.43×10^{11}	-16798		0.5 ± 0.005
318	7.73×10^9	-14377		0.3 ± 0.008

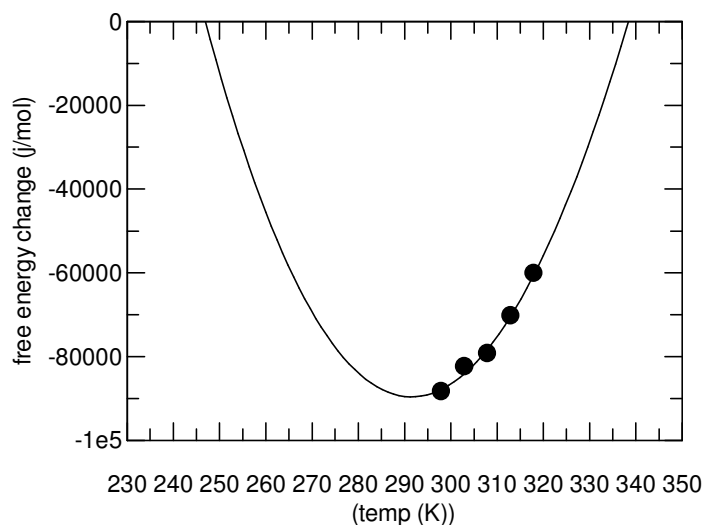


Figure 3.43 : Thermodynamics of unfolding of mutant *cmFDH*, N147R. The free energy changes of unfolding in water (ΔG_w) over a range of temperatures (T) were determined from GdnHCl-induced equilibrium denaturation data and fitted to the equation 2, at a reference temperature of $T_0=298$ K.

The free energy change of N147R decreases with increasing temperature. It has a T_m of 65.5 °C, a 2.5 °C increase in the stability compared to that of the native protein, which corresponds to an increase in the thermodynamic stability of 3.2 kcal/mol at 25 °C.

The results show that, at the reference temperature of 25 °C the enthalpy change on folding (ΔH) is favourable (-60 ± 22 kcal/mol) and the heat capacity change (ΔC_p) is -6 ± 2.1 kcal/mol/K. The entropy change at 25 °C is unfavourable ($-T\Delta S = +39.3 \pm 0.07$ kcal/mol) (Fig. 3.43). Insertion of a positively charged arginine residue instead of uncharged asparagine residue causes a favourable enthalpy change and an unfavourable entropy change accompanied by an increase in stability.

Q105R

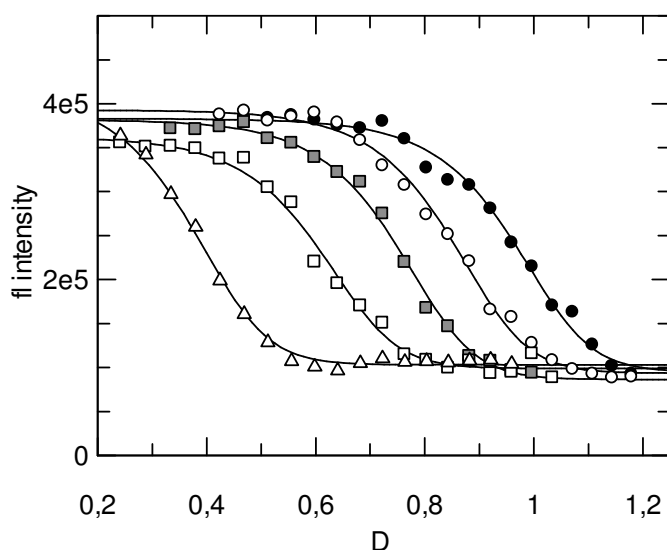


Figure 3.44 : GdnHCl-induced equilibrium unfolding transition of mutant Q105R in different temperatures: 25°C is closed circles, 30°C is open circles, 35°C is grey square, 40°C is open square and 45°C is open triangle.

Table 3.17: m , K_w , ΔG and $[\text{denaturant}]_{0.5}$ results of mutant Q105R from GdnHCl induced denaturation experiments.

Temp (K)	K_w	ΔG (cal/mol)	m (cal/mol M)	$[\text{GdnHCl}]_{0.5}$ (M)
298	3.42×10^{15}	-21166		1 ± 0.02
303	3.25×10^{14}	-20102		0.86 ± 0.006
308	4.42×10^{13}	-19217	-4.85 ± 0.9	0.76 ± 0.007
313	2.44×10^{12}	-17733		0.6 ± 0.006
318	1.97×10^{10}	-14969		0.39 ± 0.005

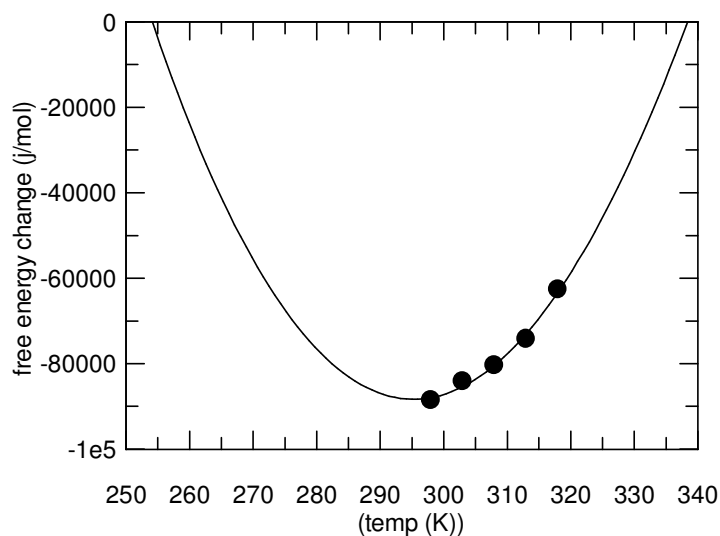


Figure 3.45 : Thermodynamics of unfolding of mutant *cmFDH*, Q105R. The free energy changes of unfolding in water (ΔG_w) over a range of temperatures (T) were determined from GdnHCl-induced equilibrium denaturation data and fitted to the equation 2, at a reference temperature of $T_0=298$ K.

The free energy change of Q105R decreases with increasing temperature. It has a T_m of 65.5 °C, a 2.5 °C increase in the stability compared to that of the native protein, which corresponds to an increase in the thermodynamic stability of 3.3 kcal/mol at 25 °C.

The results show that, at the reference temperature of 25 °C the enthalpy change on folding (ΔH) is favourable (-40 ± 23 kcal/mol) and the heat capacity change (ΔC_p) is -7 ± 2.2 kcal/mol/K. The entropy change at 25 °C is unfavourable ($-T\Delta S = +19.3 \pm 0.07$ kcal/mol) (Fig. 3.45). Insertion of a positively charged arginine residue instead of uncharged glutamine residue causes a favourable enthalpy change and an unfavourable entropy change accompanied by an increase in stability, compared to native *cmFDH*.

N187E/Q105R

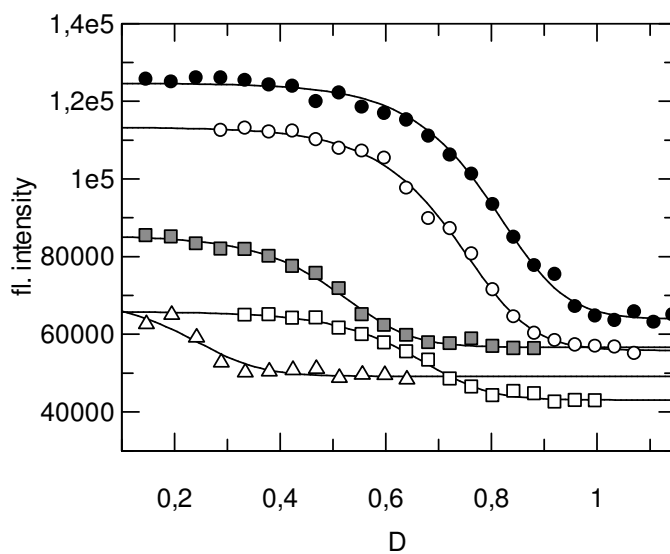


Figure 3.46 : GdnHCl-induced equilibrium unfolding transition of mutant N187E/Q105R in different temperatures: 25°C is closed circles, 30°C is open circles, 35°C is grey square, 40°C is open square and 45°C is open triangle.

Table 3.18: m , K_w , ΔG and $[\text{denaturant}]_{0.5}$ results of mutant N187E/Q105R from GdnHCl induced denaturation experiments.

Temp (K)	K_w	ΔG (cal/mol)	m (cal/mol M)	$[\text{GdnHCl}]_{0.5}$ (M)
298	7.40×10^{12}	-17536		0.84 ± 0.009
303	2.42×10^{14}	-19923		0.74 ± 0.007
308	3.34×10^{13}	-19046	-4.7 ± 0.5	0.65 ± 0.01
313	1.89×10^{13}	-17575		0.51 ± 0.009
318	7.74×10^8	-12924		0.25 ± 0.008

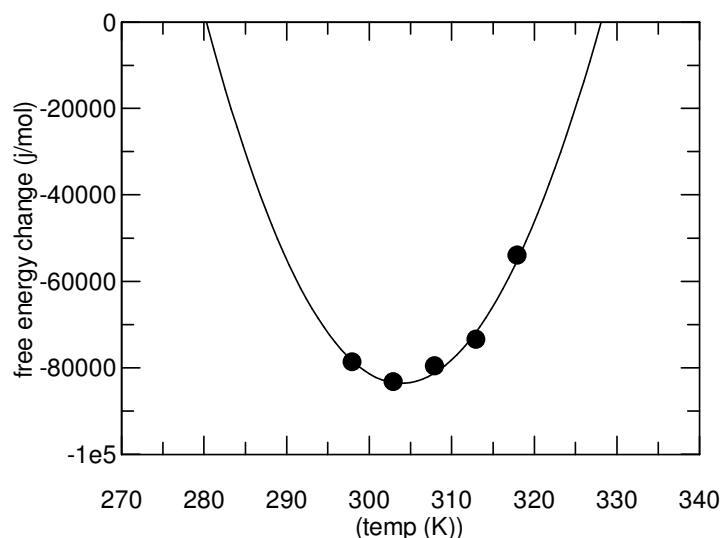


Figure 3.47 : Thermodynamics of unfolding of mutant *cmFDH*, N187E/Q105R. The free energy changes of unfolding in water (ΔG_w) over a range of temperatures (T) were determined from GdnHCl-induced equilibrium denaturation data and fitted to the equation 2, at a reference temperature of $T_o=298$ K.

The free energy change of N187E/Q105R decreases above 35°C (308K). It has a T_m of 55°C , a 8°C decrease in the stability compared to that of the native protein, which corresponds to an decrease in the thermodynamic stability of 0.4 kcal/mol at 25°C .

Results show that, at the reference temperature of 25°C the enthalpy change on folding (ΔH) is unfavourable ($+166 \pm 29$ kcal/mol) and the heat capacity change (ΔC_p) is -25.8 ± 2.8 kcal/mol/K. The entropy change at 25°C is favourable ($-T\Delta S = -178 \pm 0.1$) kcal/mol) (Fig. 3.47).

In this double mutant, insertion of negatively charged glutamic acid and positively charged arginine residues instead of uncharged asparagine and glutamine residues causes a unfavourable enthalpy change and an unfavourable entropy change accompanied by a decrease in stability. This is the largest (three fold) changes of enthalpy and entropy compared to native *cmFDH* and correspondence to the minimum change in the free energy change among mutants. The greater enthalpy change is probably derived from greater electrostatic interactions. It is puzzling that the single mutations N187E and Q105R increase the stability individually, but they are actually destabilising as the double mutant. We might speculate that these residues in the double mutant are somehow responsible for destabilising the unfolded state of the protein.

N187E/N147R

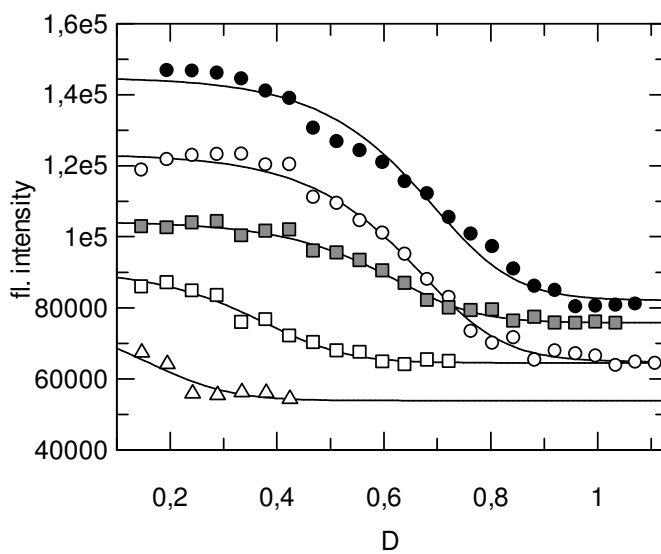


Figure 3.48 : GdnHCl-induced equilibrium unfolding transition of mutant N187E/N147R in different temperatures: 25°C is closed circles, 30°C is open circles, 35°C is grey square, 40°C is open square and 45°C is open triangle.

Table 3.19: m , K_w , ΔG and $[\text{denaturant}]_{0.5}$ results of mutant N187E/N147R from GdnHCl induced denaturation experiments.

Temp (K)	K_w	ΔG (cal/mol)	m (cal/mol M)	$[\text{GdnHCl}]_{0.5}$ (M)
298	3.59×10^{11}	-15745		0.72 ± 0.03
303	2.55×10^{11}	-15799		0.65 ± 0.009
308	1.18×10^{11}	-15595	-3.78 ± 0.77	0.6 ± 0.01
313	2.50×10^9	-13454		0.38 ± 0.01
318	7.75×10^7	-11470		0.2 ± 0.006

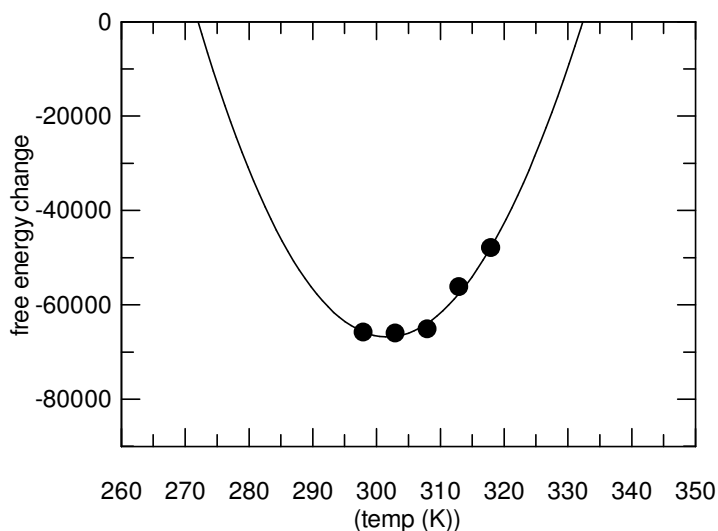


Figure 3.49 : Thermodynamics of unfolding of mutant *cmFDH*, N187E/N147R. The free energy changes of unfolding in water (ΔG_w) over a range of temperatures (T) were determined from GdnHCl-induced equilibrium denaturation data and fitted to the equation 2, at a reference temperature of $T_0=298$ K.

The free energy change of N187E/N147R decreases with increasing temperature. It has a T_m of 59.5 °C, a 3.5 °C decrease in the thermostability compared to that of the native protein, which corresponds to an decrease in the thermodynamic stability of 2.2 kcal/mol at 25 °C.

The results show that, at the reference temperature of 25 °C the enthalpy change on folding (ΔH) is unfavourable approximately +23 \pm 2 kcal/mol) and the heat capacity change (ΔC_p) is -10.5 \pm 2.17 kcal/mol/K. The entropy change at 25 °C is favourable ($-T\Delta S = -38.4 \pm 0.07$ kcal/mol) (Fig. 3.49).

In this double mutant, insertion of negatively charged glutamic acid and positively charged arginine residues instead of uncharged asparagine residues in two different positions causes a unfavourable enthalpy change and favourable entropy changes accompanied by decreasing stability. However, the heat capacity change is the same as native *cmFDH*, the decrease of 4.5 and 8 kcal/mol in enthalpy and entropy, respectively, causes the decrease of 2.2 kcal/mol in stability.

Y160E

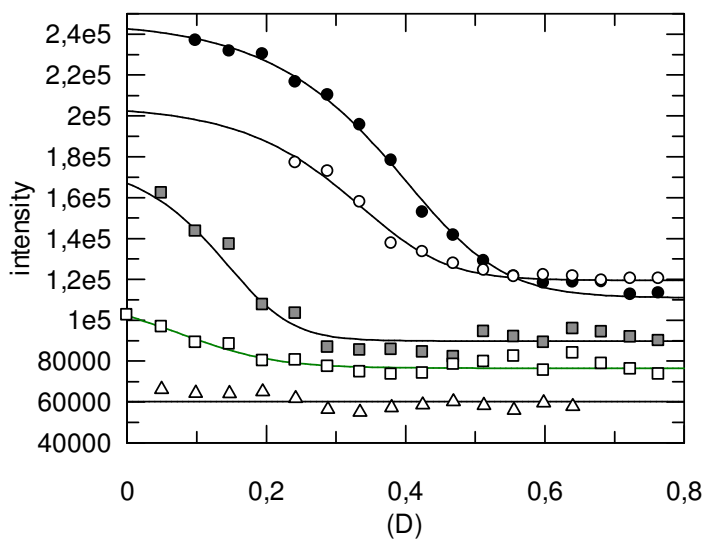


Figure 3.50 : GdnHCl-induced equilibrium unfolding transition of mutant Y160E in different temperatures: 25°C is closed circles, 30°C is open circles, 35°C is grey square, 40°C is open square and 45°C is open triangle.

Table 3.20: m , K_w , ΔG and $[\text{denaturant}]_{0.5}$ results of mutant Y160E from GdnHCl induced denaturation experiments.

Temp (K)	K_w	ΔG (cal/mol)	m (cal/mol M)	$[\text{GdnHCl}]_{0.5}$ (M)
298	6.41×10^9	-13362		0.39 ± 0.004
303	1.39×10^9	-12677		0.35 ± 0.008
308	2.65×10^8	-11862	-4.06 ± 0.83	0.24 ± 0.01
313	2.10×10^7	-10482		0.17 ± 0.02
318	1.55×10^6	-9004		0.1 ± 0.03

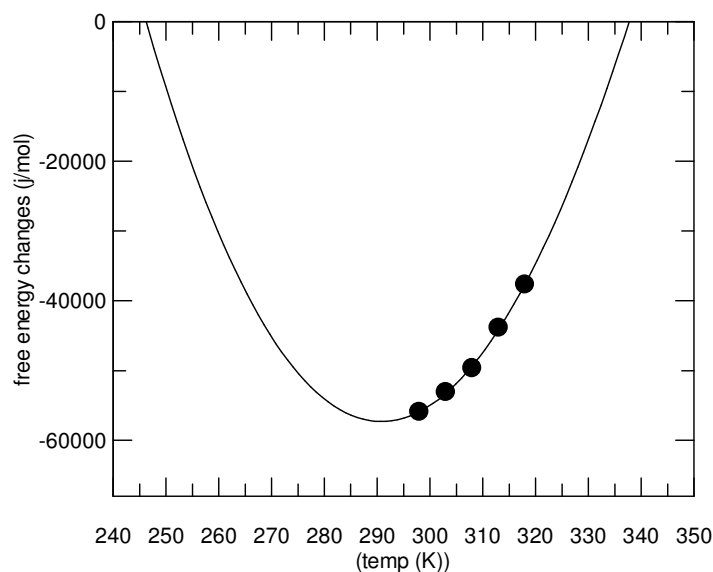


Figure 3.51 : Thermodynamics of unfolding of mutant *cmFDH*, Y160E. The free energy changes of unfolding in water (ΔG_w) over a range of temperatures (T) were determined from GdnHCl-induced equilibrium denaturation data and fitted to the equation 2, at a reference temperature of $T_0=298$ K.

The free energy change of Y160E decreases with increasing temperature. It has a T_m of 51 °C, a 12 °C decrease in the stability compared to that of the native protein, which corresponds to an decrease in the thermodynamic stability of 4.5 kcal/mol at 25 °C.

The results show that, at the reference temperature of 25 °C the enthalpy change on folding (ΔH) is unfavourable $+2.2 \pm 4.9$ kcal/mol and the heat capacity change (ΔC_p) is -13.3 ± 0.48 kcal/mol/K. The entropy change at 25 °C is favourable ($-T\Delta S = -14.9 \pm 0.02$ kcal/mol) (Fig. 3.51).

Insertion of a negatively charged glutamic acid residue instead of the aromatic tyrosine residue causes an unfavourable enthalpy change and a favourable entropy change accompanied by a decrease in stability.

Y160R

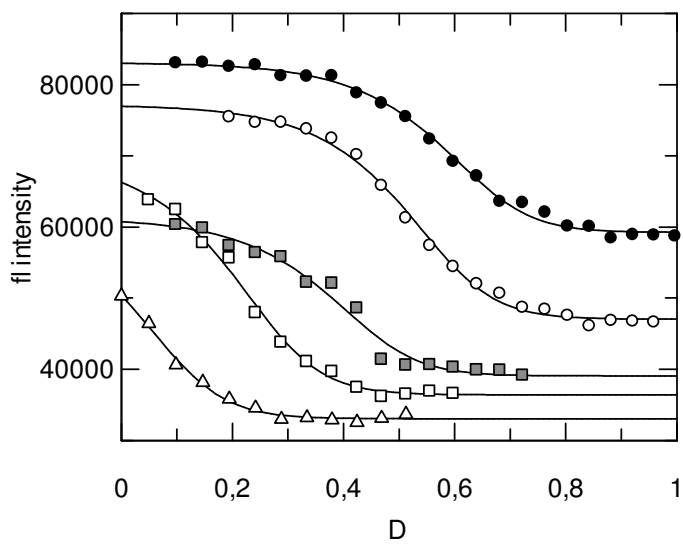


Figure 3.52 : GdnHCl-induced equilibrium unfolding transition of mutant Y160R in different temperatures: 25°C is closed circles, 30°C is open circles, 35°C is grey square, 40°C is open square and 45°C is open triangle.

Table 3.21: m , K_w , ΔG and $[\text{denaturant}]_{0.5}$ results of mutant Y160R from GdnHCl induced denaturation experiments.

Temp (K)	K_w	ΔG (cal/mol)	m (cal/mol M)	$[\text{GdnHCl}]_{0.5}$ (M)
298	3.71×10^{11}	-15765		0.59 ± 0.006
303	1.13×10^{11}	-15315		0.52 ± 0.003
308	9.48×10^9	-14050	-4.35 ± 0.55	0.4 ± 0.002
313	3.96×10^8	-12307		0.23 ± 0.007
318	1.66×10^7	-10499		0.1 ± 0.006

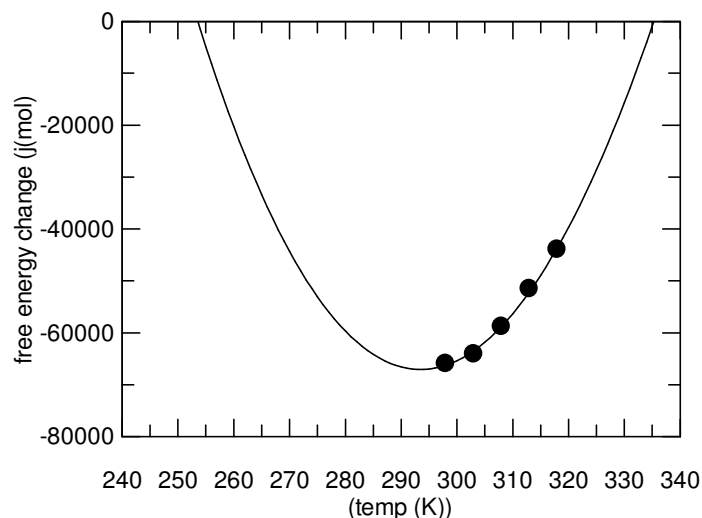


Figure 3.53 : Thermodynamics of unfolding of mutant *cmFDH*, Y160R. The free energy changes of unfolding in water (ΔG_w) over a range of temperatures (T) were determined from GdnHCl-induced equilibrium denaturation data and fitted to the equation 2, at a reference temperature of $T_0=298$ K.

The free energy change of Y160R decreases with increasing temperature. It has a T_m of 62 °C, a 1 °C decrease in the stability compared to that of the native protein, which corresponds to a decrease in the thermodynamic stability of 2.2 kcal/mol at 25 °C.

The results show that, at the reference temperature of 25 °C the enthalpy change on folding (ΔH) is favourable -41 ± 11 kcal/mol) and the heat capacity change (ΔC_p) is -5.6 ± 1 kcal/mol/K. The entropy change at 25 °C is unfavourable ($-T\Delta S = +25.3 \pm 0.04$ kcal/mol) (Fig. 3.53).

Insertion of a positively charged arginine residue instead of aromatic tyrosine residue causes a favourable enthalpy change and unfavourable entropy changes accompanied by a decrease in stability, compared to native *cmFDH*.

Y302R

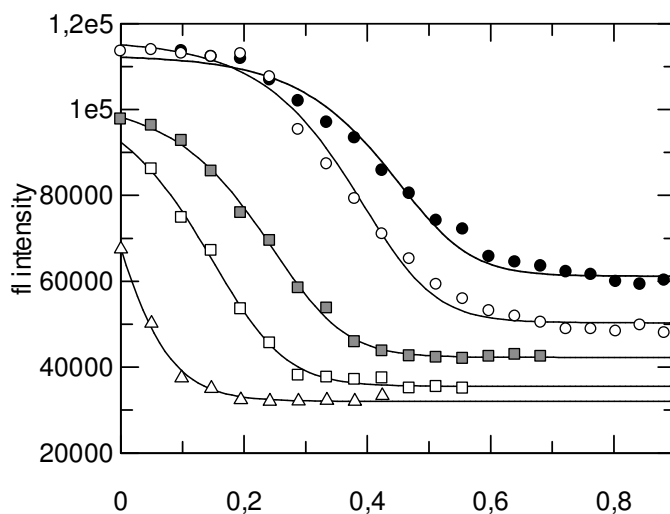


Figure 3.54 : GdnHCl-induced equilibrium unfolding transition of mutant Y302R in different temperatures: 25°C is closed circles, 30°C is open circles, 35°C is grey square, 40°C is open square and 45°C is open triangle.

Table 3.22: m , K_w , ΔG and $[\text{denaturant}]_{0.5}$ results of mutant Y302R from GdnHCl induced denaturation experiments.

Temp (K)	K_w	ΔG (cal/mol)	m (cal/mol M)	$[\text{GdnHCl}]_{0.5}$ (M)
298	6.60×10^{10}	-14742		0.43 ± 0.006
303	1.98×10^{10}	-14262		0.37 ± 0.004
308	9.91×10^8	-12699	-4.9 ± 1.6	0.23 ± 0.007
313	1.36×10^8	-11646		0.17 ± 0.007
318	1.86×10^6	-9116		0.05 ± 0.002

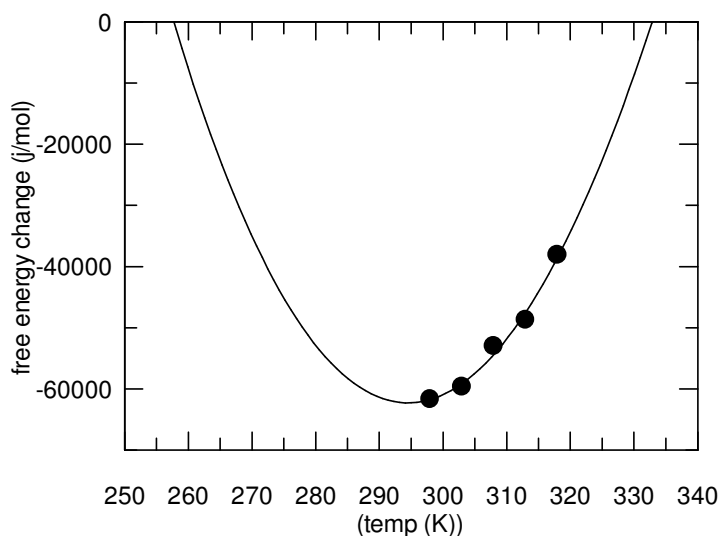


Figure 3.55 : Thermodynamics of unfolding of mutant *cmFDH*, Y302R. The free energy changes of unfolding in water (ΔG_w) over a range of temperatures (T) were determined from GdnHCl-induced equilibrium denaturation data and fitted to the equation 2, at a reference temperature of $T_0=298$ K.

The free energy change of Y302R decreases with increasing temperature. It has a T_m of 60 °C, a 3 °C decrease in stability compared to that of the native protein, which corresponds to an decrease in the thermodynamic stability of 3.2 kcal/mol at 25 °C.

The results show that, at the reference temperature of 25 °C the enthalpy change on folding (ΔH) is favourable approximately -37 ± 22 kcal/mol) and the heat capacity change (ΔC_p) is -6.2 ± 2.17 kcal/mol/K. The entropy change at 25 °C is unfavourable ($-T\Delta S = +21.7 \pm 0.07$ kcal/mol) (Fig. 3.55).

Insertion of a positively charged arginine residue instead of aromatic tyrosine residue in this position also causes a favourable enthalpy change and unfavourable entropy changes accompanied by a decrease in stability, compared to native *cmFDH*.

Table 3.23 and figure 3.56 summarize the results of the GdnHCl-induced unfolding transition at 25°C. The midpoint of thermal (T_m) denaturation for all mutants was obtained as the temperature where free energy change (ΔG_w) is equal to zero, from the plot of ΔG_w versus T (Prabhu and Sharp, 2005). Table 3.23 also compare the thermodynamic properties of mutants and native *cmFDH*.

Table 3.23: $[\text{GdnHCl}]_{0.5}$, m value, free energy changes recorded at 25°C to compare native and mutant *cm*FDHs.

	m_{GdnHCl} (cal/mol M)	$[\text{GdnHCl}]_{0.5}$ (D)	$\Delta[\text{GdnHCl}]_{0.5}$	$-\Delta G_{\text{GdnHCl}}$ (kcal/mol)	$\Delta\Delta G_{\text{GdnHCl}}$ (mut-native)
native <i>cm</i> FDH	-4.2 ± 0.008	0.85	-	17963	-
H13E	-4.5 ± 1	0.59	-0.26	16125	+1838
N147R	-5.3 ± 1.3	0.89	+0.04	21123	-3160
N187E	-4.7 ± 0.38	0.86	+0.01	19600	-1637
Q105R	-4.85 ± 0.9	1.02	+0.17	21166	-3203
N187E/Q105R	-4.7 ± 0.5	0.84	-0.01	17536	-400
N187E/N147R	-3.78 ± 0.77	0.72	-0.13	15745	+2218
Y160E	-4.06 ± 0.83	0.39	-0.46	13362	+4601
Y160R	-4.35 ± 0.55	0.59	-0.26	15765	+2198
Y302R	-4.9 ± 1.6	0.43	-0.42	14742	+3221

The free energy change between folded native form and unfolded denatured form of protein can be used to characterize the conformational stability of globular proteins. According to the results N147R, N187E and Q105R have better stability than native *cm*FDH and the other single or double mutants show worse stability. The m value changed only 1.1 cal/mol at maximum and 0.14 cal/mol at minimum.

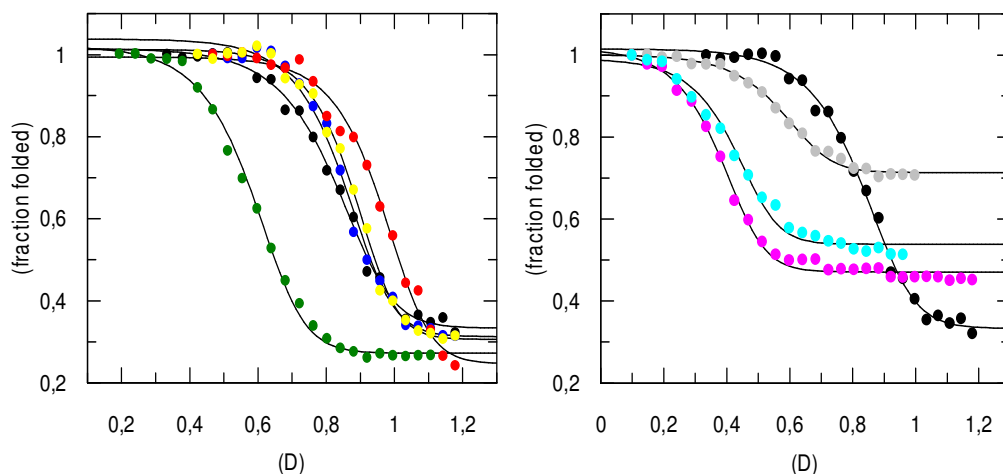


Figure 3.56 : Unfolding patterns: a. mutants designed according to homology model based on *ps*FDH (black circles: native *cm*FDH, blue circles: N187E, green circles: H13E, red circles: Q105R, yellow circles: N187R, b. mutants designed according to homology model based on *cb*FDH, pink circles: Y160E, grey circles: Y160R, light blue circles: Y302R.

Table 3.24: Thermodynamic properties of the native and surface electrostatic interaction mutants of *cmFDH* (T is 298K).

	T_m (°C)	ΔT_m	ΔH_{GdnHCl}	$-T\Delta S_{GdnHCl}$	ΔC_p $_{GdnHCl}$
	GdnHCl	(mut-native)	(kcal/mol)	(kcal/mol)	(cal/mol/K)
native <i>cmFDH</i>	63	0	27.5±18	-45.6±18	-10.5±1.8
H13E	60.5	-2.5	-24.8±14	+8.6±0.04	-7.4±1.3
N147R	65.5	+2.5	-60.3±22	+39.3±0.7	-5.9±2.1
N187E	68	+5	-16.5±2	-3.13±0.06	-6.9±2
Q105R	65.5	+2.5	-40.3±23	+19.3±0.07	-7.0±2.2
N187E/Q105R	54	-8	+166±29	-178±0.09	-25.8±2.8
N187E/N147R	59.5	-3.5	+22.9±2	-38.4±0.07	-10.6±2.17
Y160E	51	-12	+2.2±4.9	-14.9±0.01	-13.3±0.48
Y160R	62	-1	-41.4±11	+25.3±0.03	-5.6±1
Y302R	60	-3	-36.6±22	+21.7±0.07	-6.2±2.17

However it was detected that it is not exactly linear, increasing T_m correspondence to increasing free energy change as explained in the literature before (Rees and Robertson, 2001). ΔC_p and ΔH are the measurements of changes in accessible surface area because these quantities result primarily from changes in noncovalent interactions. If a protein is more thermostable it has also smaller ΔC_p which leads to a broader stability curve, conferring a higher T_m (Kumar and Nussinov, 2001; Johnson et al., 1997). In our study when a negative charge at position N187 or a positive charge at positions N147 and Q105 were introduced into native *cmFDH* individually, the ΔC_p values of these mutant proteins were clearly decreased (Tab. 3.24). While the most thermostable mutants have the smaller ΔC_p values, the double mutant N187E/Q105R and single mutant Y160E, which have the lowest thermostability according to comparison of T_m and ΔG values, have the largest ΔC_p values (Tab. 3.24). However, the heat capacity change of mutant N187E/N147R is the same as native *cmFDH*, it decrease the enthalpy as 4.5 kcal/mol and entropy as 8 kcal/mol causing the 2.2 kcal/mol destabilizing effect. On the other hand, destabilizing effect of H13E, Y160R and Y302R can not be explained with the approach that the larger ΔC_p cause the lower stability. H13E, Y160R and Y302R mutants have unfavorable ΔH and favourable ΔS at 298K in contrast to that native *cmFDH* shows. These mutants show that when histidine and tyrosine residues which

has aromatic side chains were replaced with glutamic acid and arginine residue which have the aliphatic straight side chain alter the configurational entropy by changing the entropy from favourable to unfavorable.

3.4.3.2 Urea induced denaturation

Experiments were performed as described in section 3.2.2.2. for each kinetically active mutant. Urea-induced unfolding transitions of mutants in different temperatures are shown in following figures (Fig. 3.57-3.73). Data were fitted to equation 1 to extract K_w and relationship of $\Delta G = -RT \ln K_w$ was used to calculate ΔG values (Tab. 3.25 to 3.33). The plots show the free-energy change of mutant H13E for the urea-induced unfolding transition as a function of temperature fitted to equation 2.4 as previously described (Figures 3.58, 60, 62, 64, 66, 68, 70, 72, 74).

The data obtained at different temperatures for all mutants is given in following part of this section, sequentially (H13E, N187E, Q105R, N147R, Y160E, Y160R, Y302R).

H13E

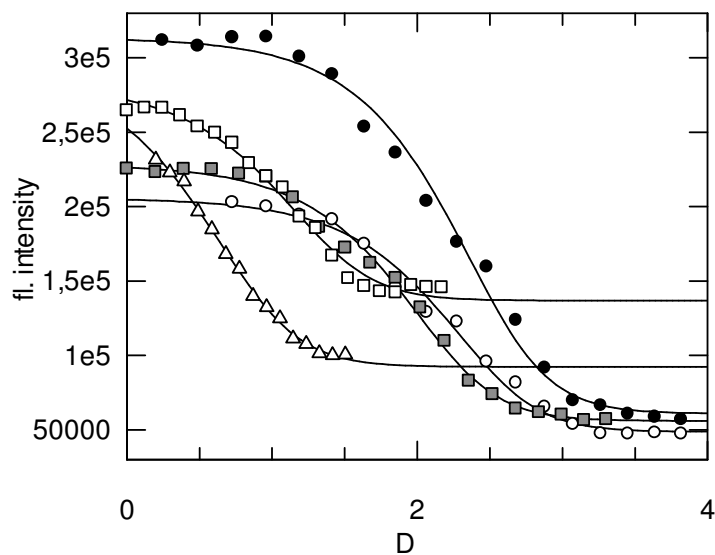


Figure 3.57 : Urea-induced equilibrium unfolding transition of mutant H13E in different temperatures: 25°C is closed circles, 30°C is open circles, 35°C is grey square, 40°C is open square and 45°C is open triangle.

Table 3.25: m , K_w , ΔG and $[\text{denaturant}]_{0.5}$ results of mutant H13E from urea induced denaturation experiments.

Temp (K)	K_w	ΔG (cal/mol)	m (cal/mol M)	$[\text{urea}]_{0.5}$ (M)
298	1.69×10^{11}	-15299		2.31 ± 0.05
303	1.27×10^{11}	-15381		2.22 ± 0.05
308	3.69×10^{10}	-14882	-1.04 ± 1	1.97 ± 0.06
313	9.32×10^8	-12839		1.14 ± 0.04
318	9.96×10^6	-10163		0.77 ± 0.02

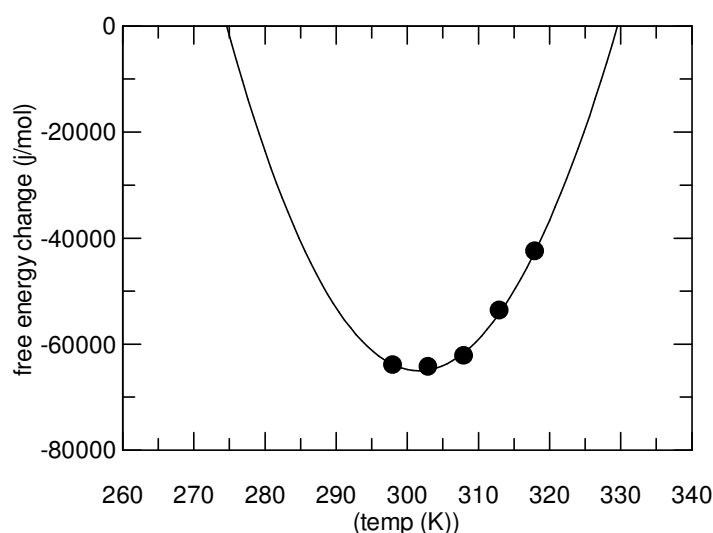


Figure 3.58 : Thermodynamics of unfolding of mutant *cmFDH*, H13E. The free energy changes of unfolding in water (ΔG_w) over a range of temperatures (T) were determined from urea-induced equilibrium denaturation data and fitted to the equation 2, at a reference temperature of $T_0=298$ K.

The free energy change of H13E decreases with increasing temperature. The results show that, at the reference temperature of 25°C the enthalpy change on folding (ΔH) is unfavourable approximately $+30 \pm 3.1$ kcal/mol and the heat capacity change (ΔC_p) is -12.4 ± 3 kcal/mol/K. The entropy change at 25°C is favourable ($-T\Delta S = -44.7 \pm 0.1$) kcal/mol) (Fig.3.58).

N187E

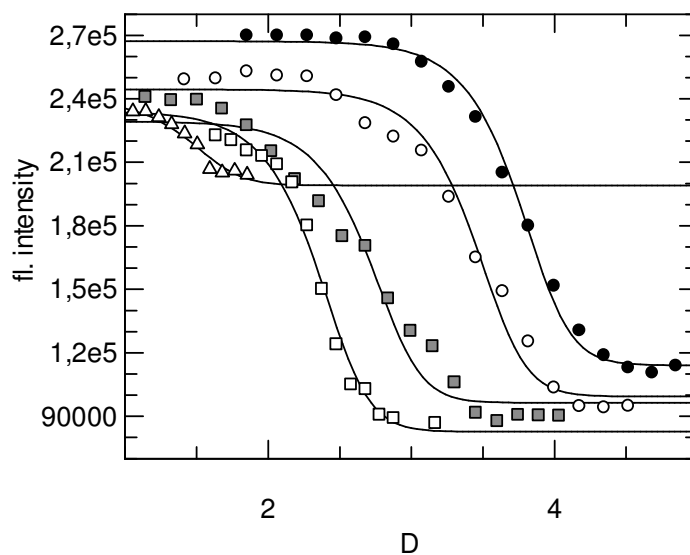


Figure 3.59 : Urea-induced equilibrium unfolding transition of mutant N187E in different temperatures: 25°C is closed circles, 30°C is open circles, 35°C is grey square, 40°C is open square and 45°C is open triangle.

Table 3.26: m , K_w , ΔG and $[\text{denaturant}]_{0.5}$ results of mutant N187E from urea induced denaturation experiments.

Temp (K)	K_w	ΔG (cal/mol)	m (cal/mol M)	$[\text{urea}]_{0.5}$ (M)
298	6.59×10^{19}	-27005		3.74 ± 0.01
303	5.76×10^{18}	-25986		3.48 ± 0.04
308	1.80×10^{16}	-22893	-1.88 ± 1	2.72 ± 0.05
313	1.04×10^{15}	-21498		2.37 ± 0.008
318	9.63×10^{11}	-17424		1.47 ± 0.02

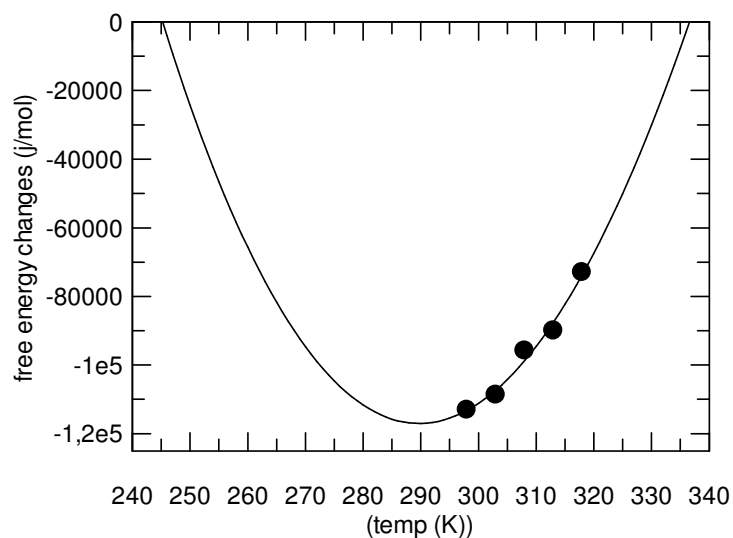


Figure 3.60 : Thermodynamics of unfolding of mutant *cmFDH*, N187E. The free energy changes of unfolding in water (ΔG_w) over a range of temperatures (T) were determined from urea-induced equilibrium denaturation data and fitted to the equation 2, at a reference temperature of $T_0=298$ K.

The free energy change of N187E decreases with increasing temperature. The results show that, at the reference temperature of 25 °C the enthalpy change on folding (ΔH) is favourable by approximately -92 ± 47 kcal/mol) and the heat capacity change (ΔC_p) is -7.75 ± 4.6 kcal/mol/K. The entropy change at 25 °C is unfavourable ($-T\Delta S = +65 \pm 0.15$ kcal/mol) (Fig.3. 60).

N147R

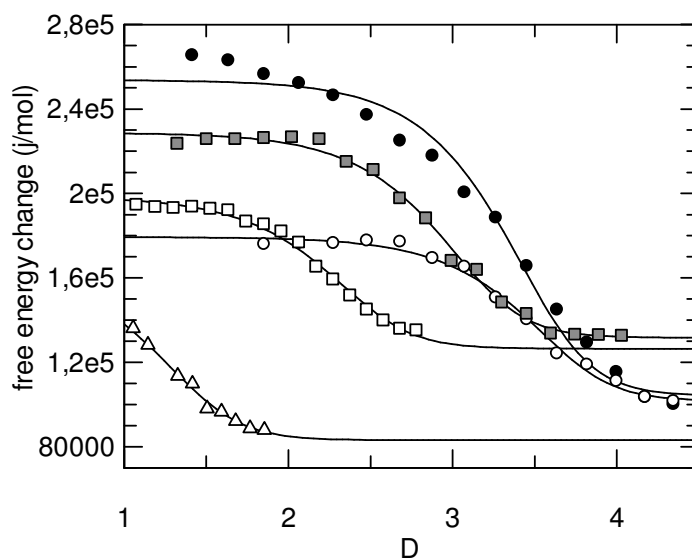


Figure 3.61 : Urea-induced equilibrium unfolding transition of mutant N147R in different temperatures: 25°C is closed circles, 30°C is open circles, 35°C is grey square, 40°C is open square and 45°C is open triangle.

Table 3.27: m , K_w , ΔG and $[\text{denaturant}]_{0.5}$ results of mutant N147R from urea induced denaturation experiments.

Temp (K)	K_w	ΔG (cal/mol)	m (cal/mol M)	$[\text{urea}]_{0.5}$ (M)
298	1.03×10^{15}	-20462		3.5 ± 0.08
303	2.07×10^{15}	-21217		3.47 ± 0.02
308	1.09×10^{14}	-19771	-1.32 ± 0.4	2.94 ± 0.02
313	2.50×10^{12}	-17746		1.85 ± 0.02
318	7.59×10^9	-15001		1.31 ± 0.03

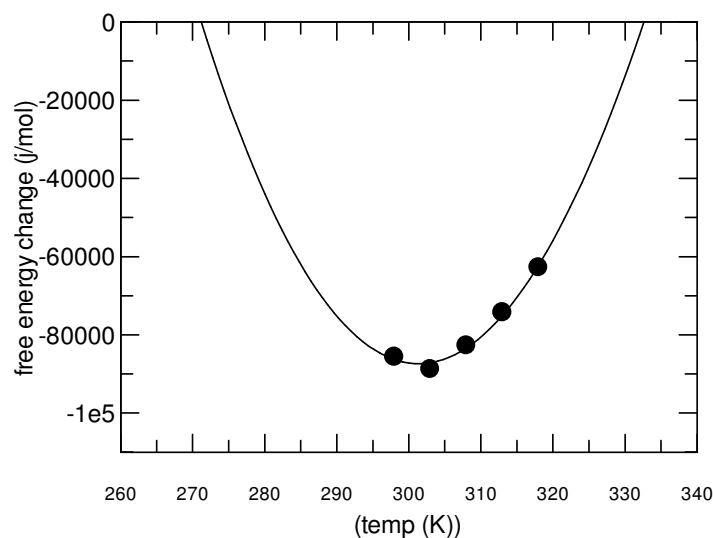


Figure 3.62 : Thermodynamics of unfolding of mutant *cmFDH*, N147R. The free energy changes of unfolding in water (ΔG_w) over a range of temperatures (T) were determined from urea-induced equilibrium denaturation data and fitted to the equation 2, at a reference temperature of $T_0=298$ K.

The free energy change of N147R decreases above 35°C (308K). The results show that, at the reference temperature of 25°C the enthalpy change on folding (ΔH) is unfavourable by approximately $+24 \pm 2.4$ kcal/mol) and the heat capacity change (ΔC_p) is -13.3 ± 2.3 kcal/mol/K. The entropy change at 25°C is favourable ($-T\Delta S = -45 \pm 0.08$ kcal/mol) (Fig. 3.62).

Q105R

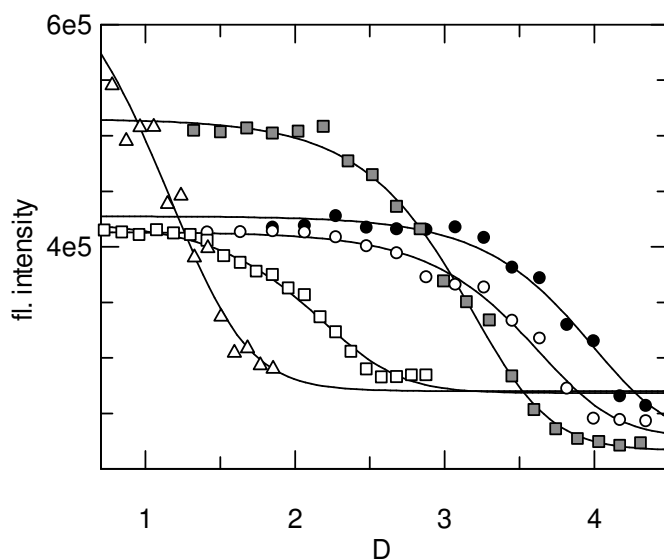


Figure 3.63 : Urea-induced equilibrium unfolding transition of mutant Q105R in different temperatures: 25°C is closed circles, 30°C is open circles, 35°C is grey square, 40°C is open square and 45°C is open triangle.

Table 3.28: m , K_w , ΔG and $[\text{denaturant}]_{0.5}$ results of mutant Q105R from urea induced denaturation experiments.

Temp (K)	K_w	ΔG (cal/mol)	m (cal/mol M)	$[\text{urea}]_{0.5}$ (M)
298	5.83×10^{14}	-20120		3.86 ± 0.05
303	1.11×10^{14}	-19457		3.68 ± 0.15
308	1.44×10^{13}	-18530	-1.1 ± 0.3	3.12 ± 0.03
313	1.43×10^{11}	-15971		2.15 ± 0.06
318	1.32×10^9	-13265		1.48 ± 0.02

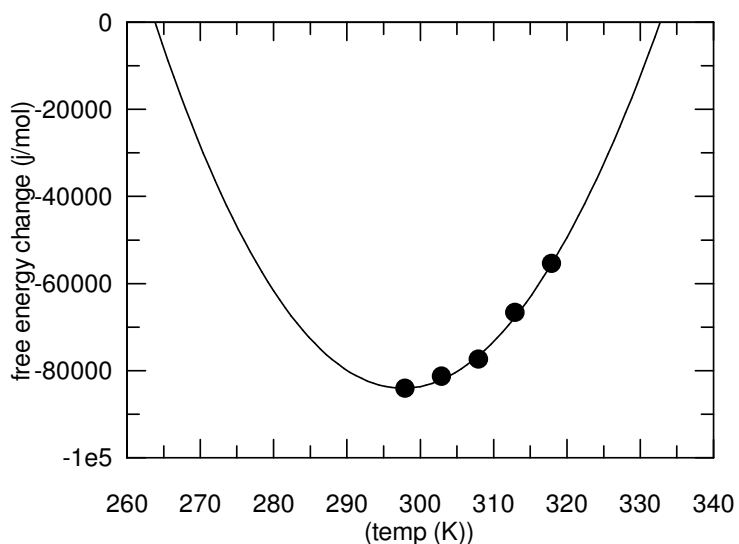


Figure 3.64 : Thermodynamics of unfolding of mutant *cmFDH*, Q105R. The free energy changes of unfolding in water (ΔG_w) over a range of temperatures (T) were determined from urea-induced equilibrium denaturation data and fitted to the equation 2, at a reference temperature of $T_0=298$ K.

The free energy change of Q105R decreases with increasing temperature. The results show that, at the reference temperature of 25 °C the enthalpy change on folding (ΔH) is favourable by approximately -24 ± 16 kcal/mol) and the heat capacity change (ΔC_p) is -10 ± 1.6 kcal/mol/K. The entropy change at 25 °C is unfavourable ($-T\Delta S = +3.9 \pm 0.05$ kcal/mol) (Fig. 3.64).

N187E/Q105R

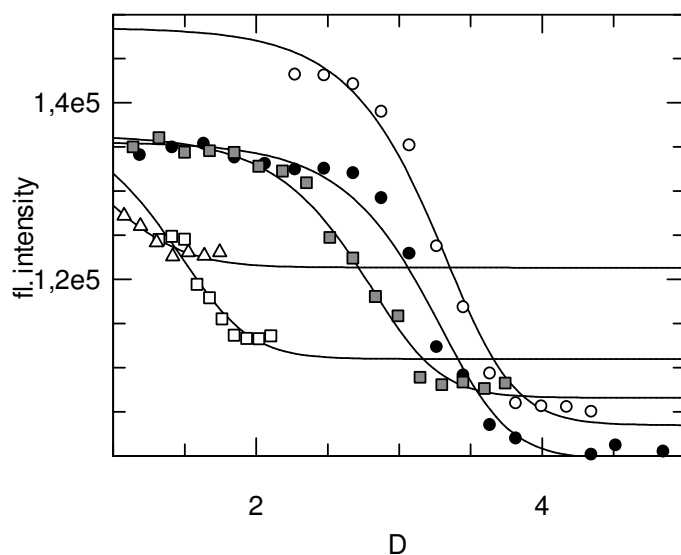


Figure 3.65 : Urea-induced equilibrium unfolding transition of mutant N187E/Q105R in different temperatures: 25°C is closed circles, 30°C is open circles, 35°C is grey square, 40°C is open square and 45°C is open triangle.

Table 3.29: m , K_w , ΔG and $[\text{denaturant}]_{0.5}$ results of mutant N187E/Q105R from urea induced denaturation experiments.

Temp (K)	K_w	ΔG (cal/mol)	m (cal/mol M)	$[\text{urea}]_{0.5}$ (M)
298	1.05×10^{14}	-19108		3.27 ± 0.01
303	8.62×10^{13}	-19303		3.19 ± 0.02
308	7.73×10^{12}	-18150	-1.2 ± 0.8	2.73 ± 0.03
313	1.01×10^{10}	-14319		1.6 ± 0.02
318	2.02×10^8	-12075		1 ± 0.02

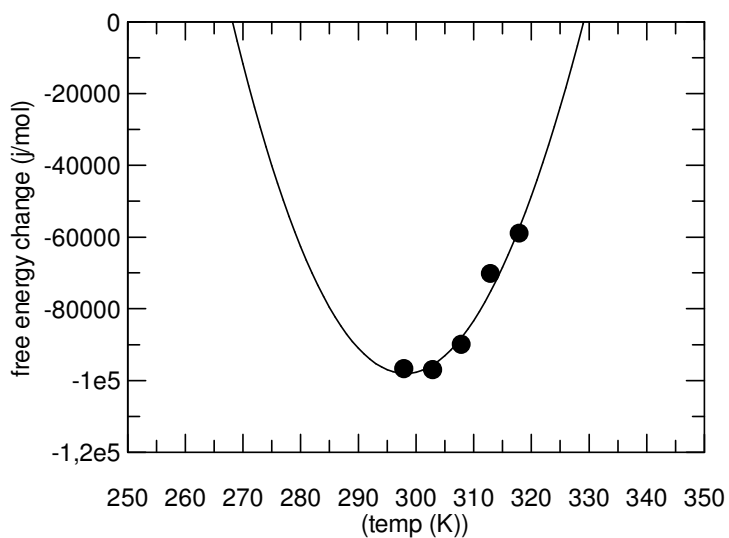


Figure 3.66 : Thermodynamics of unfolding of mutant *cmFDH*, N187E/Q105R. The free energy changes of unfolding in water (ΔG_w) over a range of temperatures (T) were determined from urea-induced equilibrium denaturation data and fitted to the equation 2, at a reference temperature of $T_0=298$ K.

The free energy change of N187E/Q105R decreases with increasing temperature. The results show that, at the reference temperature of 25 °C the enthalpy change on folding (ΔH) is favourable -2.3 ± 6.7 kcal/mol) and the heat capacity change (ΔC_p) is -13 ± 5 kcal/mol/K. The entropy change at 25 °C is favourable ($-T\Delta S = -17.9 \pm 0.2$ kcal/mol) (Fig. 3.66).

N187E/N147R

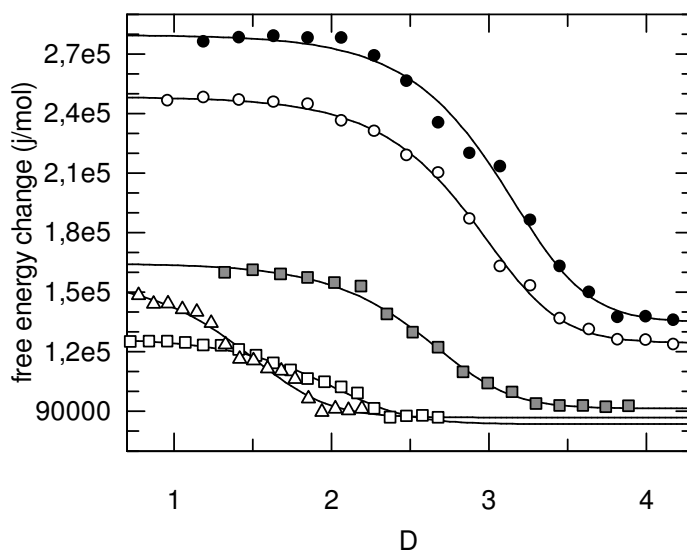


Figure 3.67 : Urea-induced equilibrium unfolding transition of mutant N187E/N147R in different temperatures: 25°C is closed circles, 30°C is open circles, 35°C is grey square, 40°C is open square and 45°C is open triangle.

Table 3.30: m , K_w , ΔG and $[\text{denaturant}]_{0.5}$ results of mutant N187E/N147R from urea induced denaturation experiments.

Temp (K)	K_w	ΔG (cal/mol)	m (cal/mol M)	$[\text{urea}]_{0.5}$ (M)
298	5.59×10^{13}	-18732		3.1 ± 0.04
303	2.33×10^{13}	-18518		2.9 ± 0.02
308	4.68×10^{12}	-17843	1.2 ± 0.1	2.6 ± 0.02
313	1.76×10^{11}	-16099		2 ± 0.05
318	2.23×10^8	-12138		1.5 ± 0.07

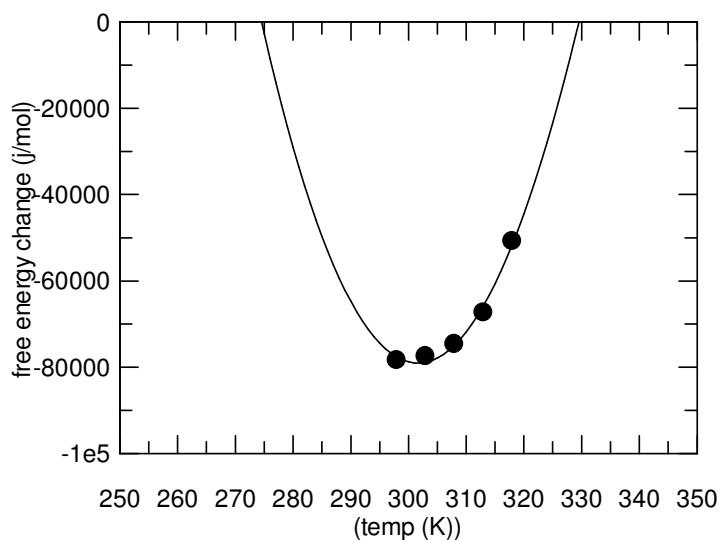


Figure 3.68 : Thermodynamics of unfolding of mutant *cmFDH*, N187E/N147R. The free energy changes of unfolding in water (ΔG_w) over a range of temperatures (T) were determined from urea-induced equilibrium denaturation data and fitted to the equation 2, at a reference temperature of $T_o=298$ K.

The free energy change of N187E/N147R decreases with increasing temperature. The results show that, at the reference temperature of 25 °C the enthalpy change on folding (ΔH) is favourable approximately -13 ± 10 kcal/mol) and the heat capacity change (ΔC_p) is -7.5 ± 1 kcal/mol/K. The entropy change at 25 °C is favourable ($-T\Delta S = -5.96 \pm 0.04$ kcal/mol) (Fig. 3.68).

Y160E

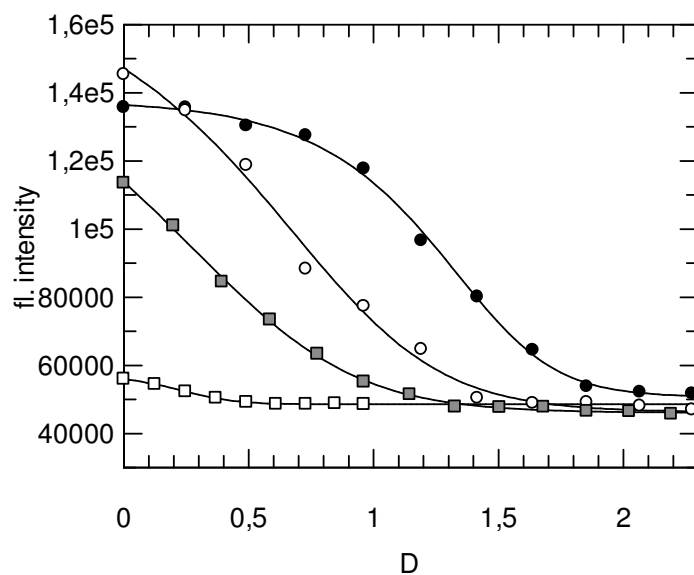


Figure 3.69 : Urea-induced equilibrium unfolding transition of mutant 160E in different temperatures: 25°C is closed circles, 30°C is open circles, 35°C is grey square, 40°C is open square.

Table 3.31: m , K_w , ΔG and $[\text{denaturant}]_{0.5}$ results of mutant Y160E from urea induced denaturation experiments.

Temp (K)	K_w	ΔG (cal/mol)	m (cal/mol M)	$[\text{urea}]_{0.5}$ (M)
298	3.55×10^{10}	-14375		1.3 ± 0.02
303	9.45×10^7	-11047	1.87 ± 1	0.7 ± 0.03
308	1.71×10^7	-10189		0.5 ± 0.02
313	8.79×10^7	-11371		0.24 ± 0.05

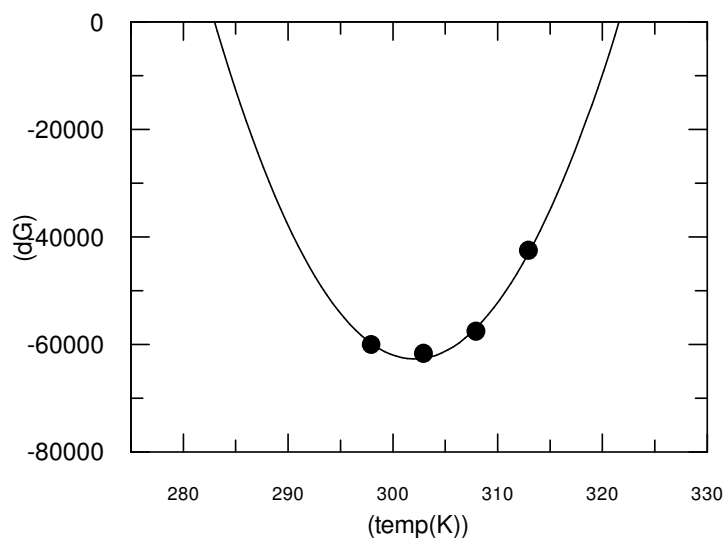


Figure 3.70 : Thermodynamics of unfolding of mutant *cm*FDH, Y160E. The free energy changes of unfolding in water (ΔG_w) over a range of temperatures (T) were determined from urea-induced equilibrium denaturation data and fitted to the equation 2, at a reference temperature of $T_0=298$ K.

The free energy change of N187E/N147R decreases with increasing temperature. The results show that, at the reference temperature of 25 °C the enthalpy change on folding (ΔH) is unfavourable 84 ± 26 kcal/mol and the heat capacity change (ΔC_p) is $-24,3 \pm 3.4$ kcal/mol/K. The entropy change at 25 °C is favourable ($-T\Delta S = -89.3 \pm 0.09$) kcal/mol) (Fig. 3.70).

Y160R

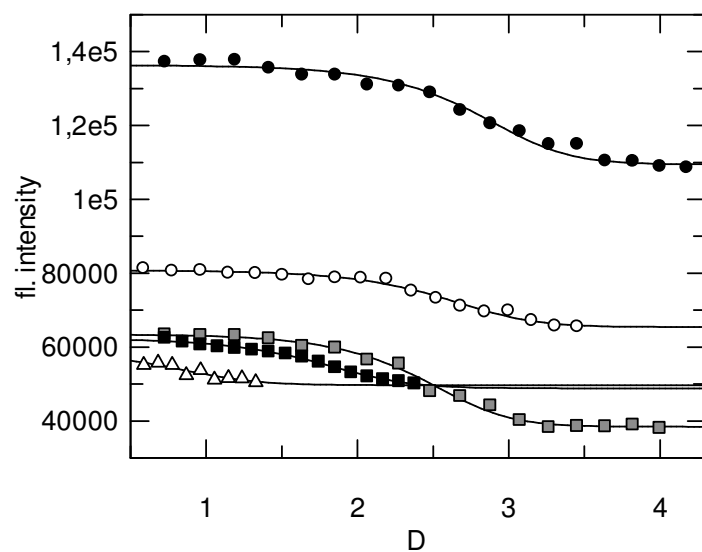


Figure 3.71 : Urea-induced equilibrium unfolding transition of mutant Y160R in different temperatures: 25°C is closed circles, 30°C is open circles, 35°C is grey square, 40°C is open square and 45°C is open triangle.

Table 3.32: m , K_w , ΔG and $[\text{denaturant}]_{0.5}$ results of mutant Y160R from urea induced denaturation experiments.

Temp (K)	K_w	ΔG (cal/mol)	m (cal/mol M)	$[\text{urea}]_{0.5}$ (M)
298	5.98×10^{12}	-16952		3.1 ± 0.2
303	2.01×10^{12}	-17335		2.7 ± 0.08
308	2.08×10^{12}	-17044	-1.14 ± 0.4	2.4 ± 0.15
313	4.13×10^{10}	-14694		1.9 ± 0.01
318	8.02×10^7	-12295		0.9 ± 0.03

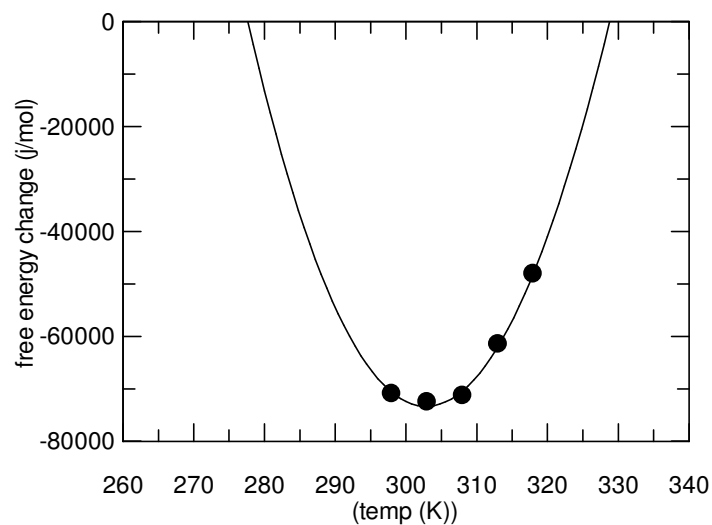


Figure 3.72 : Thermodynamics of unfolding of mutant *cmFDH*, Y160R. The free energy changes of unfolding in water (ΔG_w) over a range of temperatures (T) were determined from urea-induced equilibrium denaturation data and fitted to the equation 2, at a reference temperature of $T_0=298$ K.

The free energy change of Y160R after 40°C (313K). The results show that, at the reference temperature of 25 °C the enthalpy change on folding (ΔH) is unfavourable by approximately $+61 \pm 15.3$ kcal/mol) and the heat capacity change (ΔC_p) is -16.2 ± 1.5 kcal/mol/K. The entropy change at 25 °C is favourable ($-T\Delta S = -59 \pm 0.05$ kcal/mol) (Fig. 3.72).

Y302R

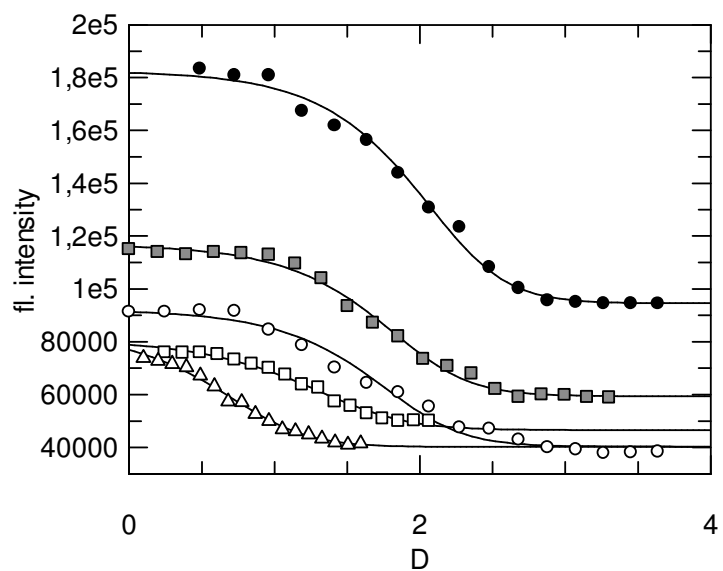


Figure 3.73 : Urea-induced equilibrium unfolding transition of mutant Y302R in different temperatures: 25°C is closed circles, 30°C is open circles, 35°C is grey square, 40°C is open square and 45°C is open triangle.

Table 3.33: m , K_w , ΔG and $[\text{denaturant}]_{0.5}$ results of mutant Y302R from urea induced denaturation experiments.

Temp (K)	K_w	ΔG (cal/mol)	m (cal/mol M)	$[\text{urea}]_{0.5}$ (M)
298	5.63×10^9	-13287		2 ± 0.05
303	2.03×10^{10}	-14279		1.73 ± 0.04
308	2.49×10^{10}	-14763	-1.1 ± 0.3	1.71 ± 0.02
313	1.21×10^9	-13006		1.3 ± 0.03
318	1.58×10^8	-10811		0.78 ± 0.02

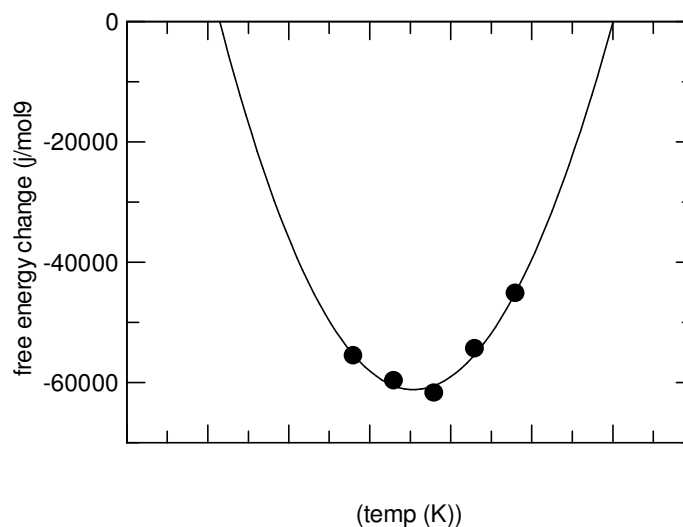


Figure 3.74 : Thermodynamics of unfolding of mutant *cmFDH*, Y302R. The free energy changes of unfolding in water (ΔG_w) over a range of temperatures (T) were determined from urea-induced equilibrium denaturation data and fitted to the equation 2, at a reference temperature of $T_0=298$ K.

The free energy change of Y302R decreases above 40°C (313K). The results show that, at the reference temperature of 25 °C the enthalpy change on folding (ΔH) is unfavourable approximately +98 ± 2 kcal/mol) and the heat capacity change (ΔC_p) is -15.2 ± 1.9 kcal/mol/K. The entropy change at 25 °C is favourable ($-T\Delta S = -111 \pm 0.07$ kcal/mol) (Fig. 3.74).

Table 3.34 summarizes the results of the urea-induced unfolding transition at 25°C to easily compare the results to each other. The midpoint of the thermal (T_m) denaturation for all mutants, is defined as the temperature where free energy change (ΔG_w) is equal to zero, obtained from the plot of ΔG_w versus T (Tab. 3.35). This table also compares the thermodynamic properties of mutant and native *cmFDH*.

The thermal dependence of the unfolding free energy changes obtained from both denaturants are shown together in figure 3.75.

Table 3.34: [urea]_{0.5}, m values and free energy changes recorded at 25°C to compare native and mutant *cm*FDHs.

	m _{urea} (cal/mol M)	[Urea] _{0.5} (D)	Δ [Urea] _{0.5}	-ΔG _{urea} (cal/mol)	ΔΔG _{urea} (mut-native)
native <i>cm</i> FDH	-1.57±0.6	3.93	-	24409	-
H13E	-1.04±1.2	2.31	-1.62	15299	+9110
N147R	-1.32±0.4	3.5	-0.43	20461	+3948
N187E	-1.88±1	3.74	-0.19	27005	-2596
Q105R	-1.1±0.3	3.86	-0.07	20119	+4290
N187E/Q105R	-1.2±0.8	3.1	-0.83	19108	+5301
N187E/N147R	-1.2±0.1	3.09	-0.84	18732	+5677
Y160E	-1.88±1	1.26	-2.67	14375	+10034
Y160R	-1.14±0.4	3.1	-0.83	16952	+7457
Y302R	-1.09±0.3	2	-1.93	14834	+9575

The estimation of the free energy of unfolding for a protein from different chemical (such as GdnHCl or urea) denaturations can be very different, depending on the nature of electrostatic interactions stabilizing the protein structure (Rashid et al., 2005). In our study, however, the estimation of free energy of unfolding from GdnHCl and urea denaturations are not same numerically, the results of the urea-induced denaturation experiments confirm the results of GdnHCl-induced denaturation experiments. The same mutants N147R, N187E and Q105R show better stability than native *cm*FDH. Other single or double mutants show worse stability compared to native *cm*FDH. T_m value of N147R, N187E and Q105R was increased 3, 7 and 3 °C, respectively. The m value changed by 0.53 cal/mol at maximum and 0.25 cal/mol at minimum (Tab. 3.34).

Table 3.35: Thermodynamic properties of the native and surface electrostatic interaction mutants of *cmFDH*.

	T_m (°C)	ΔT_m	ΔH_{urea}	$-T\Delta S_{\text{urea}}$	ΔC_p urea
	urea	(mut-native)	(cal/mol)	(cal/mol/K)	(kcal/mol/K)
.wt <i>cmFDH</i>	57	0	+4.85±4.8	-29.48±4.6	-17.02±0.16
H13E	56	-1	+29.94±10.	-45.15±0.035	-12.42±1.05
N147R	60	+3	+24.35±24	-44.9±0.08	-13.35±2.34
N187E	64	+7	-92.06±47	+64.95±0.16	-7.76±4.6
Q105R	60	+3	-24.04±16	+3.9±0.05	-10.06±1.6
N187E/Q105R	56	-1	-2.3 ± 6.7	-17.9 ±0.2	-13 ± 5
N187E/N147R	56	-1	+35.7±10.9	+54.2±0.04	-15±1
Y160E	49	-8	+84 ± 26	-89.3± 0.09	-24,3 ± 3.4
Y160R	56	-1	+61 ± 15.3	-59 ±0.05	-16.2 ± 1.5
Y302R	57	0	+98.09±2.0	-111±0.07	-15.17±1.96

The urea-induced denaturation experiments also confirmed that when the stability increases, the ΔC_p value decreases. Mutants N147R, N187E and Q105R which have the best T_m (Tab. 3.35) and ΔG values (Tab. 3.34), demonstrating increased thermostability, have the smallest ΔC_p values. The Y160E mutant which has the lowest T_m value has the largest ΔC_p . Although the best and worst mutants could be explained with this approach, it was observed that behaviour of mutants which have the nearly same T_m value as native *cmFDH* do not explain with this trend. These mutations, H13E, N187E/Q105R, N187E/N147R and Y160R decreased the thermostability by only 1°C and Y302R mutation did not affect the T_m value.

Tables 3.24 and 3.35 also show the melting temperatures of native and mutant *cmFDHs*. However GdnHCl and urea induced unfolding experiments give the different values, both of these denaturant predicted that N147R, N187E and Q105R mutations increased the melting temperature on the average of 2.75, 6, 2.75 °C. The T_m value difference between GdnHCl and urea experiments was ± 2 °C. The most dramatic increase in stability observed for the N187E mutant was 6 °C greater in average than the native *cmFDH*.

The m value of all mutants obtained from both in GdnHCl and urea transitions, which relates to the change in solvent exposure between the folded and the transition

state for unfolding, is very close to native *cmFDH* as shown in table 3.23 and 3.34. These results show that the mutations do not significantly change the core packing in *cmFDH* as expected.

The value of the urea or GdnHCl concentration at half-completion of the transition decreased with the increasing temperature. $[\text{urea}]_{0.5}$ and $[\text{GdnHCl}]_{0.5}$ for native *cmFDH* were indicated as 3.93 and 0.85, respectively at 25 °C. $[\text{urea}]_{0.5}/[\text{GdnHCl}]_{0.5}$ value shows that GdnHCl is 4.6 times more effective than urea in unfolding of *cmFDH*. N147R, N187E and Q105R mutants showed better $[\text{GdnHCl}]_{0.5}$ values than native and $[\text{urea}]_{0.5}$ values of these mutants were closest to native enzyme. The resistance of other mutant enzymes to unfolding by urea or GdnHCl were poorer than the native protein (Tab. 3.23 and 3.34).

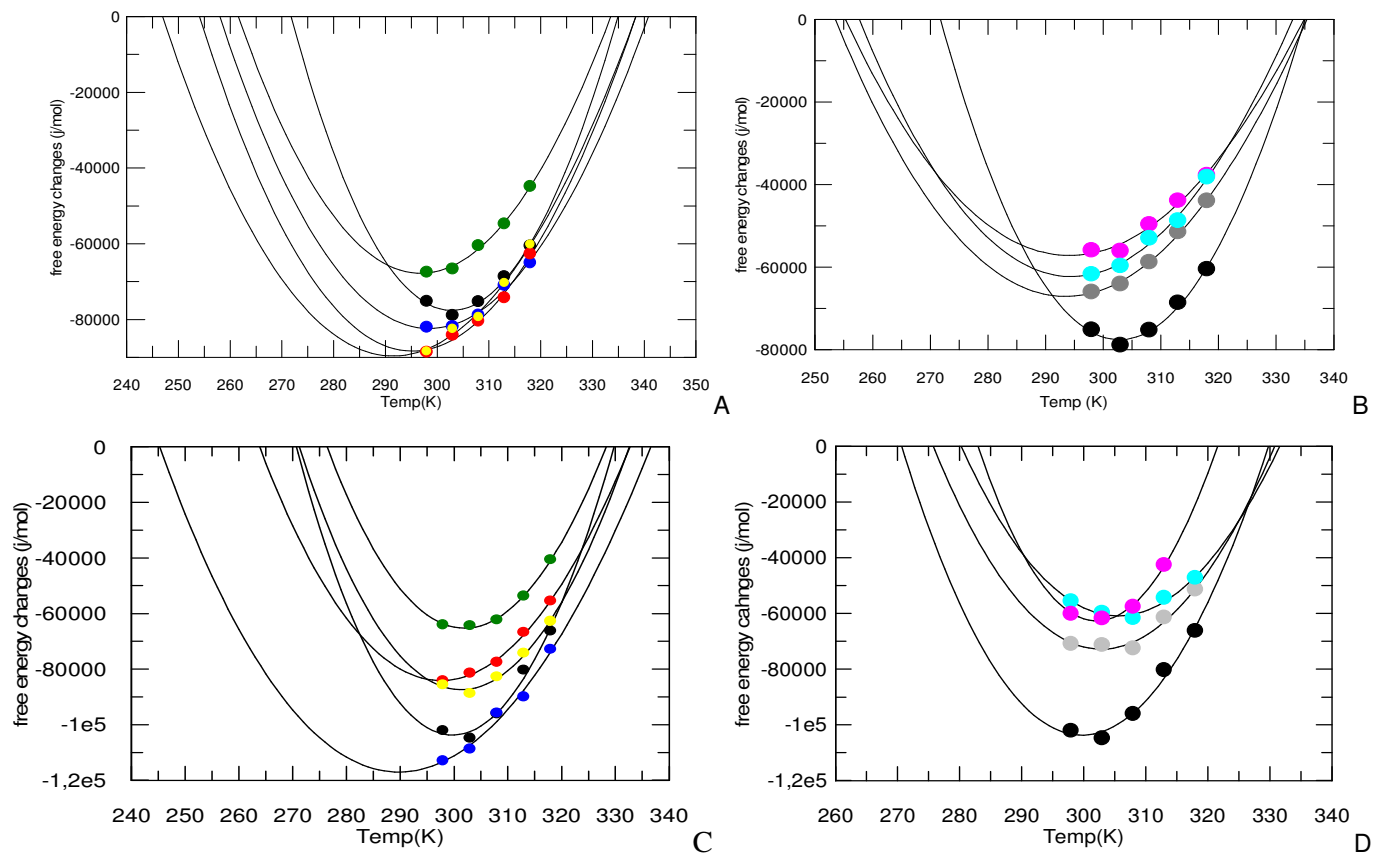


Figure 3.75 : A, B GdnHCl; C, D Urea induced unfolding of native and mutant *cmFDHs*. The free energy changes (ΔG) over a range of temperatures (T) were fitted to the equation 6. Black circles: native *cmFDH*, blue circles: N187E, green circles: H13E, red circles: Q105, yellow circles: N47R, pink circles: Y160E, grey circles: Y160R, light blue circles: Y302R.

3.4.4 Refolding Analysis

In order to determine the effect of the mutation on the folding kinetics, the process of renaturation from the fully unfolded state to folded active state was followed by measuring the regained enzymatic activity of the mutant proteins. The same experiment was performed for native *cmFDH*, see section 3.2.3. The measured activity of all mutants was plotted against time for refolding reactions performed at a series of protein concentrations. Refolding curves as a function of time of mutants as follows:

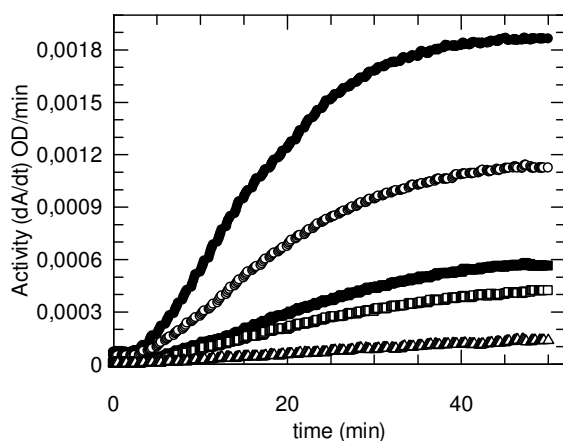


Figure 3.76 : Refolding of H13E mutant *cmFDH* followed by regain of activity.

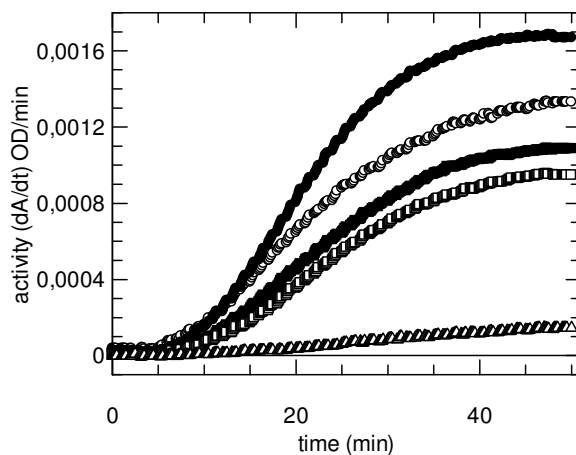


Figure 3.77 : Refolding of N187E mutant *cmFDH* followed by regain of activity.

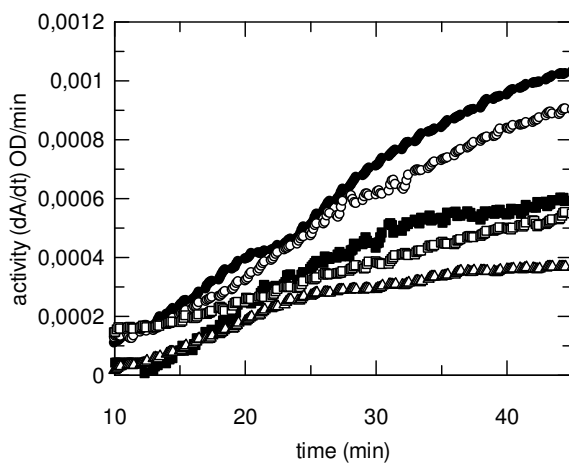


Figure 3.78 : Refolding of N147R mutant *cmFDH* followed by regain of activity.

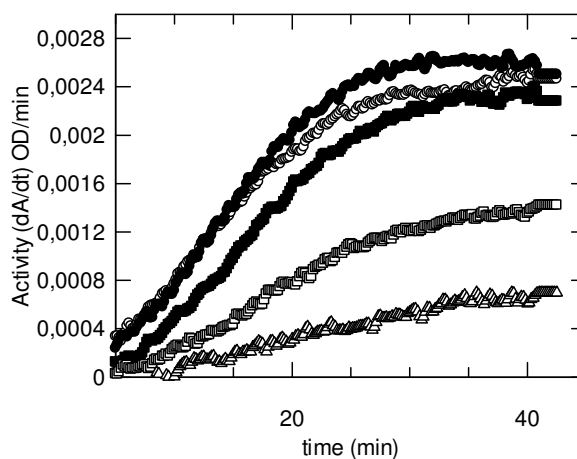


Figure 3.79 : Refolding of N187E/N147R mutant *cmFDH* followed by regain of activity.

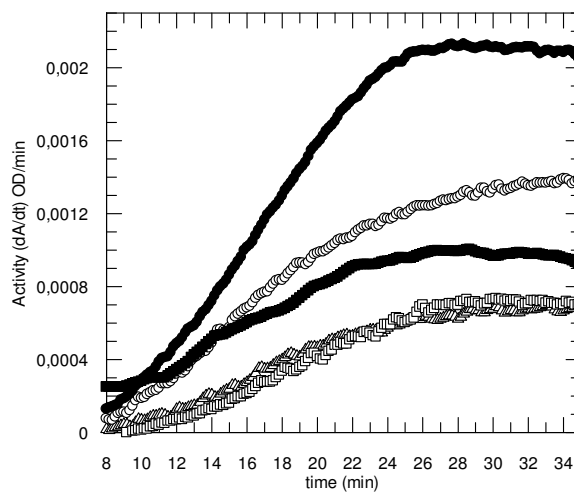


Figure 3.80 : Refolding of Y160E mutant *cmFDH* followed by regain of activity.

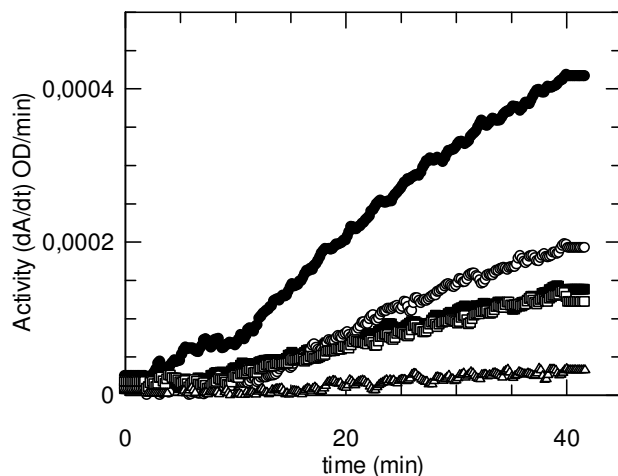


Figure 3.81 : Refolding of Y302R mutant *cmFDH* followed by regain of activity.

Considerable renaturation activity data could not be obtained for mutants Q105R, Y160R and N187E/Q105R. As described for native *cmFDH* refolding activity the reactivation curves of electrostatic interaction mutants have distinct lag phases showing that the refolding process is rate-limited by at least two steps occurring on the same time scale. The half time of refolding is obviously sensitive to protein concentration such as native *cmFDH*.

Refolding activity curves against to time were analysed in terms of $t_{1/2}$ versus total monomer concentration by using the approximation that the measured $t_{1/2} = 1/(k_{bi} \times M_0) + \ln 2 \times k_{uni}$, a uni-bi kinetic systems. The fitted yields values for the unimolecular folding and bimolecular association rate constants of all mutants (Fig. 3.82) are tabulated in table 3.36.

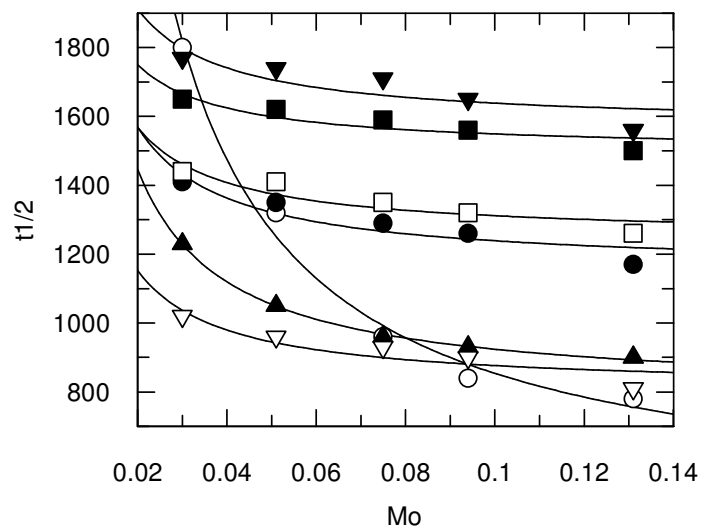


Figure 3.82 : The relationship between the half-time of refolding and reactant concentration. The refolding half-times were fitted to the equation; $t_{1/2} = 1 / (k_{bi} \times Mo) + \ln 2 \times k_{uni}$. Native *cmFDH* is open circles, H13E is closed circles, N187E is open squares, N147R is closed squares, N187E/N147R is facing up closed trinangle, Y160E is facing down open trianles and Y302R is facing down open triangles.

Table 3.36: Unimolecular folding and bimolecular association rate constants of all mutants.

proteins	$k_{bi} (M^{-1}s^{-1})$	$k_{uni} (s^{-1})$
Native <i>cmFDH</i>	2.4×10^4	1.6×10^{-3}
H13E	1.2×10^5	3.4×10^{-3}
N187E	1.6×10^5	3.7×10^{-3}
N147R	2.06×10^5	4.4×10^{-3}
N187E/N147R	7.5×10^4	2.4×10^{-3}
Y160E	1.49×10^5	2.4×10^{-3}
Y302R	1.54×10^5	4.6×10^{-3}

Electrostatic interaction mutants enhanced the the protein association rate constant significantly (Tab. 3.36), as shown experimentally before in the formation of the barnase:barstar complex (Schreiber and Fersht, 1996) and the colicin:Im9 interaction (Wallis et al., 1998).

3.5 Introduction of disulphide bridges into *cm*FDH structure

Comparison of homologous proteins from thermophilic and mesophilic sources in the literature prove that one of the most important strategies which has been used by evolution for protein thermostability is disulphide bridges (Thangudu et al., 2008). However, the introduction of extra disulfide bonds into proteins to increase the protein stability is not always successful in practice. The mechanism of stability gained from disulfide bridge structure is not still perfectly understood. Therefore there are many studies to understand the effect of disulfide bonds and cysteine residues on protein stability and attempts to improve stability by the addition of extra inter or intramolecular disulfide bridge into protein structures (Jeong et al., 2007; Davoodi et al., 2007; Yasukawa and Inouye, 2007). Some successful and unsuccessful examples of introduction of disulfide bridge studies published in recent years are summarized in the following table (3.37).

Table 3.37: Some examples of disulfide bridges have been introduced by site-directed mutagenesis into many systems.

Protein	Position of S-S bridges	Effect	Reference
Malate dehydrogenase	Thr187 disulfide bridges crossing the A–C and B–D interfaces	Stabilise	Bjork, et al. 2003
CD2	13 disulphide bridges (between surface of β -sheet structure)	Stabilise	Mason et al. 2005
Porcine odorant binding protein	C63-C155 (links the terminal α helix with a loop between the C and D β -sheets)	Stabilise	Parisi et al. 2005
Bacillus stearothermophilus No. 236 endo- β -1,4-xylanase	Between Ser100 and Asn150 at conserved region of family 11 xylanases	Stabilise	Jeong et al. 2007
E. coli thioredoxin	Intermolecular disulfide bonds (E101C-E101C, E101C-A105C, T89C-T89C, F102C-A105C, and D20CR73C)	No effect /Destabilise	Das et al. 2007
Leech carboxypeptidase inhibitor	Cys11–Cys34, Cys18–Cys62 and Cys22–Cys58 bridges on the structure of the β -sheet that is covalently connected to the α -helix by the Cys19–Cys43 disulfide bond.	Destabilise	Arolas et al. 2009
ribonuclease A	Folding (A4C/V118C, H105C/V124C, I107C/A122C) and unfolding (R10C/R33C, M30C/N44C, V43C/R85C) region	Stabilise	Pecher and Arnold, 2009

Because of its industrial importance, the FDH enzyme is one of several enzymes which have been subjected to disulfide bridge engineering to stabilize it against several factors. Cys residues of FDH enzymes from *Pseudomonas sp.101* (Odintseva et al., 2002), *Mycobacterium vaccae* (Yamamoto et al., 2005) and *Candida boidinii*, (Sluszyck et al., 2000) were engineered to overcome atmospheric oxidation of Cys residues. Disulfide bridges were introduced into the FDH enzyme from *Candida methylca* to improve the thermostability (Karagüler et al., 2007). The wild type *cmFDH* contains two cysteine residues buried in separate hydrophobic pockets but does not contain disulphide bridges, hence it is a good candidate for attempted stabilisation by this approach. Three pairs of cysteine residues were introduced into the *cmFDH* gene to construct three different disulphide bridged (T169/T226, V88/V112, M156/L159) mutants by Karagüler *et al.*(2007). Another attempt to introduce a disulfide bridge into *cmFDH* on the positions of A153 and I239 by mutating these residues to cysteine have been performed by the same group (unpublished data).

In this thesis, according to homology modelling of *cmFDH* based on *cbFDH* crystal structure which has amino acid sequence similarity higher than 90% to *cmFDH*, residues at positions 1 neighboring to N-terminal dimerization helix and 62 neighboring to functionally relevant residue 68 on the beginning point of two different beta-strands were selected to replace with cysteine residues to make a disulphide bridge in the N-terminal of catalytic domain of *cmFDH*. Firstly, the double mutant (M1C/D62C) was constructed and the effect on the properties of the FDH due to this disulphide bridge was investigated. After purification on a nickel–agarose column, enzyme assays were performed on both reduced and oxidised forms of the mutant proteins as described in Materials and Method section 2.3.1.1.

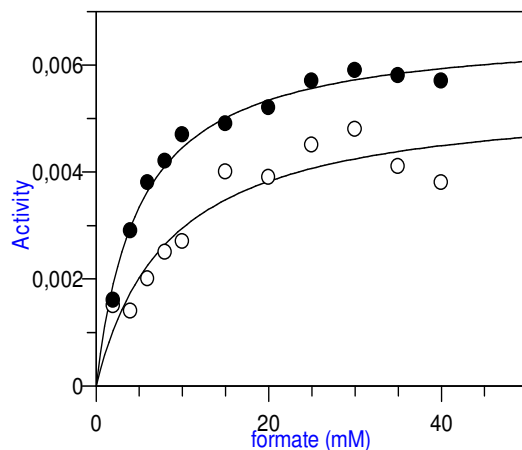


Figure 3.83 : Activity of disulphide bridge mutant M1C/D62C. Open circles show the activity in oxidised condition, closed circles show the activity in reduced condition.

Previous studies in the literature had been performed with respect to *ps*FDH crystal structure which has only 49 % similarity. However, residues selected to change according to homology model based on *cb*FDH 3D structure (> 90 % similarity) are more reliable in theory, the M1C/D62C disulphide bridge mutant has shown only 3.75 % and 1.4 % of the catalytic efficiency of native *cm*FDH in oxidised and reduced conditions, respectively (Fig. 3.83). Therefore, mutations M1C and D62C were investigated as single mutants, separately (Fig. 3.84) to be able to explain this unexpected result.

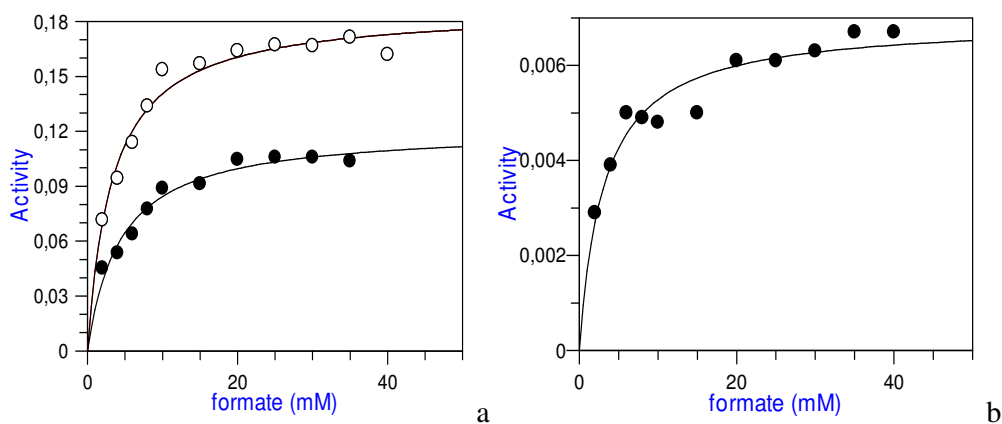


Figure 3.84 : Activity of single mutants, a. M1C, b. D62C, in oxidised and reduced conditions. Open circles show the activity in oxidised condition, closed circles show the activity in reduced condition.

The activity results of the 3 mutants and native *cm*FDH in both conditions are summarized in table 3.38. For native *cm*FDH there was almost no difference in

activity between oxidised and reduced conditions. Single mutant M1C and double disulfide mutant M1C/D62C have lower activity when the buffer conditions are reducing. On the other hand, it should be noted that the M1C single mutant has approximately 63 % better catalytic efficiency (k_{cat}/K_m) than native *cmFDH* in oxidised conditions. The other single mutant D62C has 6 % of the activity of native *cmFDH* in reducing conditions but it has no observable activity in oxidised conditions. Presumably this extra Cys residue causes a nontolerated defect on the catalytic machinery by rendering ineffective the neighboring residue P68 which is related to enzyme function on the catalytic domain.

The disulfide bridge mutants investigated in this work and the 3 disulfide bridge mutants in a previous study (Karaguler et al. 2007) on *cmFDH* did not increase thermostability. Moreover, only one of them could be tolerated to give a functional enzyme. Hence, it is clear that choosing sterically ideal sites for the insertion of disulphide bridges is crucial.

Table 3.38: Activity properties of disulphide bridge mutants in oxidised and reduced conditions.

Enzymes	reduced conditions			oxidised conditions		
	K_m (mM)	k_{cat} (sn^{-1})	k_{cat}/K_m ($sn^{-1} mM^{-1}$)	K_m (mM)	k_{cat} (sn^{-1})	k_{cat}/K_m ($sn^{-1} mM^{-1}$)
Native	4.42±0.8	1.2±0.009	0.29	4.75±0.3	1.13±0.1	0.24
M1C	4.39±0.6	0.8±0.004	0.18	3.33±0.4	1.25±0.0	0.38
D62C	3.13±0.5	0.046±0.0	0.015	No recordable activity		
M1C/D62C	8.44±2	0.036±0.0	0.0043	4.98±0.4	0.045±0.0	0.009

After the kinetic studies, thermal denaturation studies were performed for the active mutants M1C and M1C/D62C in both oxidised and reduced conditions. Values for temperatures at which 50 % activity remained under these conditions were recorded from the graphs in figure 3.85 and 3.86. For M1C, values for temperatures at which 50 % activity ($T_{0.5}$) remained of under oxidised and reduced conditions were measured to be 58.37 °C and 57.9 °C, respectively. For M1C/D62C, the ($T_{0.5}$) value was 55.02 °C in oxidised condition and 54.97 °C in reduced condition.

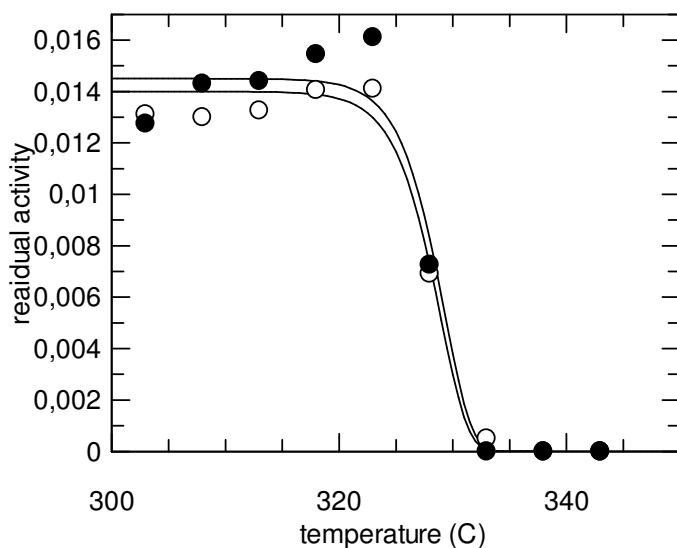


Figure 3.85 : The heat denaturation of M1C/D62C mutant was determined by measuring the rate of NADH production at 340 nm, after incubating protein samples for 20 min at a series of different temperatures. $T_{0.5}$ is 55.02 °C in oxidised condition (open circles) and 54.97 °C in reduced condition (closed circles).

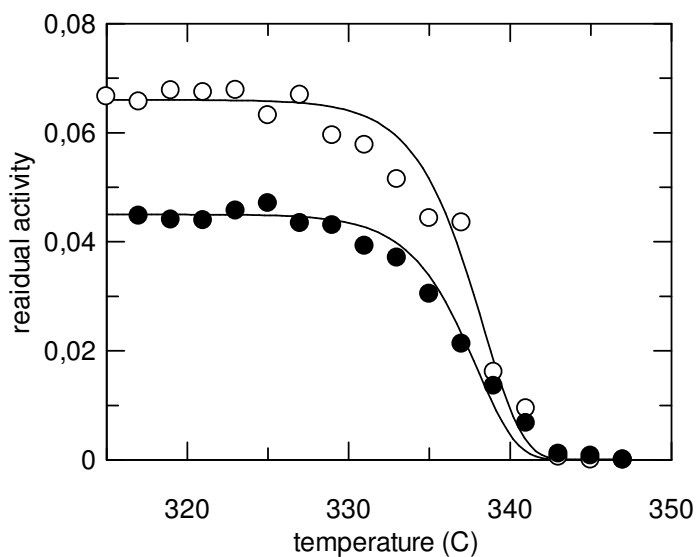


Figure 3.86 : The heat denaturation of M1C mutant was determined by measuring the rate of NADH production at 340 nm, after incubating protein samples for 20 min at a series of different temperatures. $T_{0.5}$ is 58.37 °C in oxidised condition (open circles) and 57.9 °C in reduced condition (closed circles).

The thermal denaturation experiments show that half life temperature ($T_{0.5}$) of M1C and M1C/D62C mutants do not change in oxidised or reduced conditions (figures 3.85 and 3.86). The $T_{0.5}$ value of M1C is 1.7 °C higher than native *cmFDH*.

The thermal denaturation data were fitted to the Arrhenius equation to calculate E_a and k_a values and the van't Hoff equations to calculate ΔH , ΔC_p and ΔS by combining equation 2.4 and 2.6 as explained before in section 3.2.7. The results are summarized in table 3.39.

For the M1C mutant E_a (activation enthalpy) and k_a (unfolding rate constant) were determined to be 94 kcal/mol and $1 \times 10^{57} \text{ s}^{-1}$, respectively. Results show that E_a and k_a values for M1C do not change in oxidized and reduced conditions and E_a is 3 kcal/mol higher than native *cmFDH* (91 kcal/mol), k_a is lower than that the value of native *cmFDH* ($2 \times 10^{57} \text{ s}^{-1}$). For the M1C/D62C double mutant E_a and k_a values increase in reducing conditions. Van't Hoff analysis show that while the unfavourable enthalpic barrier of both mutants increases in reducing conditions, the unfavourable heat capacity changes decrease. Entropy changes of M1C are favourable in reducing conditions but unfavourable in oxidizing conditions. Favourable entropy changes ($-T\Delta S$) increase in reducing conditions for the double mutant. The enthalpic barrier of M1C is about 11 kcal/mol higher than that native *cmFDH* has (5 kcal/mol). Native *cmFDH* has favourable entropic term (-5.5 kcal/mol at 298K) but M1C has unfavourable entropic term +2.4 kcal/mol at room temperature. The heat capacity change of M1C is 0.7 kcal/mol/K lower than native *cmFDH*. As a result, the increased stability can be explained by a decreased heat capacity change and an increased enthalpic term.

In order to characterize the M1C mutant more completely, because of its remarkable kinetic properties, guanidinium chloride and urea induced equilibrium unfolding experiment were performed at a series of temperatures in order to extract the thermal dependence of K_a .

The GdnHCl-induced unfolding transition of the M1C mutant at different temperatures is shown in Fig. 3.87. Data were fitted to equation 1 to calculate K_w and the $\Delta G = -RT \ln K_w$ relationship was used to calculate ΔG values (Tab. 3.40). The plot in Fig. 3.88 shows the free-energy change of mutant M1C as a function of temperature fitted to equation 2.4.

Table 3.39: Thermodynamic parameters for the disulphide bridge mutant and single cysteine mutant in oxidising and reducing conditions.

	ΔH		$-T\Delta S$		ΔC_p		E_a		k_a	
	(kcal/mol)		(kcal/mol)		(kcal/mol/K)		(kcal/mol)		(s^{-1})	
	O	R	O	R	O	R	O	R	O	R
M1C	16.4±2	60±2.7	+2.4±0.006	-38±0.008	1.3±0.6	0.09±0.1	94±0.5	94±0.7	1.2x10 ⁵⁷	1.5x10 ⁵⁷
M1C/D62C	74.5±7	153±1.3	-47.6±0.02	-119±0.004	5.4±4	1.3±0.7	91.5±0.2	93±1	2.2x10 ⁵⁷	1.8x10 ⁵⁸

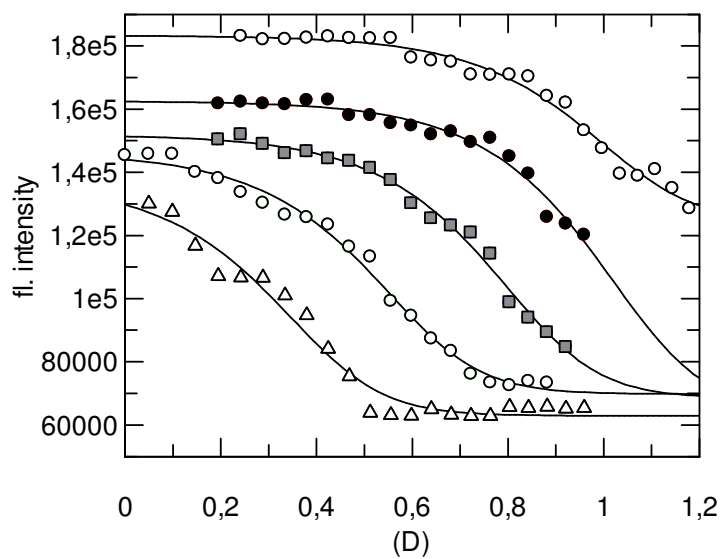


Figure 3.87 : GdnHCl -induced equilibrium unfolding curves of mutant M1C in different temperatures: 25°C is open circles, 30°C is closed circles, 35°C is grey square, 40°C is open square and 45°C is open triangle.

Table 3.40: m , K_w , ΔG and $[\text{denaturant}]_{0.5}$ results of mutant M1C from GdnHCl induced denaturation experiments.

Temp (K)	K_w	ΔG (cal/mol)	m (cal/mol M)	$[\text{GdnHCl}]_{0.5}$ (M)
298	1.53×10^{12}	-16603		1.1 ± 0.1
303	1.67×10^{12}	-16931		1.6 ± 0.3
308	1.30×10^{11}	-15655	-2.98 ± 0.1	1 ± 0.3
313	5.96×10^9	-13993		0.6 ± 0.06
318	4.64×10^8	-12601		0.4 ± 0.02

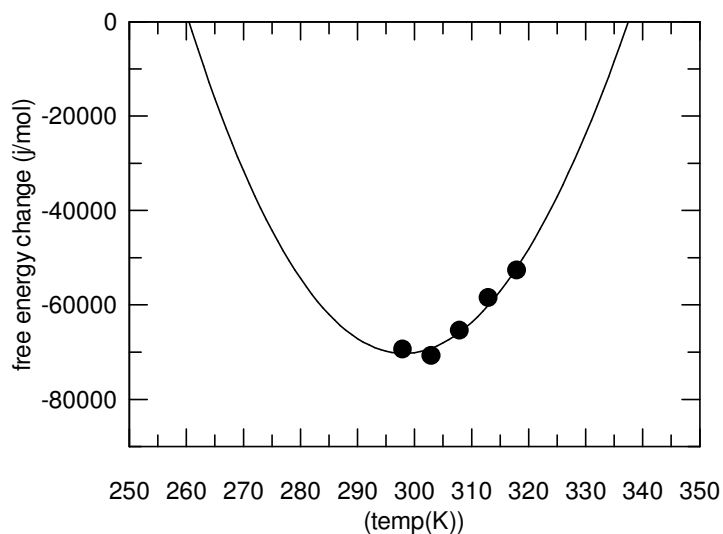


Figure 3.88 : Thermodynamics of unfolding of mutant *cmFDH*, M1C. The free energy changes of unfolding in water (ΔG_w) over a range of temperatures (T) were determined from GdnHCl -induced equilibrium denaturation data and fitted to the equation 2, at a reference temperature of $T_0=298$ K.

The results show that at the reference temperature of 25 °C the enthalpy change on folding (ΔH) is favourable, approximately -15.9 ± 2.8 kcal/mol and the heat capacity change (ΔC_p) is -6.75 ± 2.7 kcal/mol/K. The entropy change at 25 °C is favourable ($-T\Delta S = -0.88 \pm 0.09$ kcal/mol).

The urea-induced unfolding transitions of the M1C mutant at different temperatures is shown in Fig. 3.89. Data were fitted to equation 1 to calculate K_w and the $\Delta G = -RT \ln K_w$ relationship was used to calculate ΔG values (Tab. 3.41). The plot in Fig. 3.90 shows the free-energy change of mutant M1C for urea-induced unfolding transitions as a function of temperature fitted to equation 2.4 as previously described.

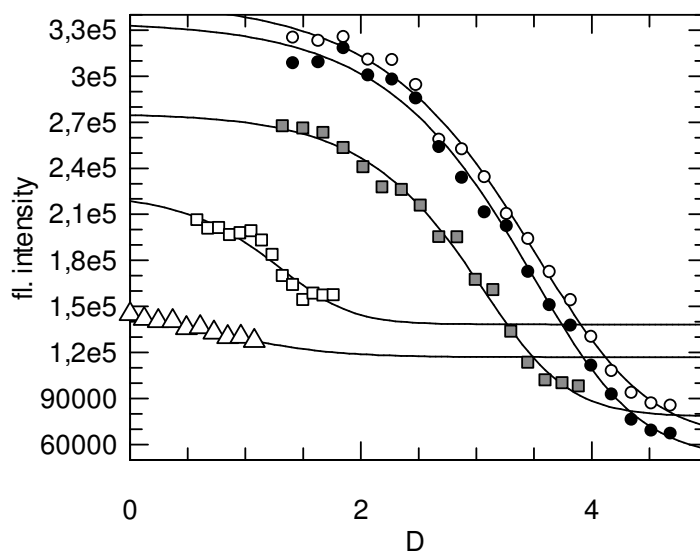


Figure 3.89 : Urea-induced equilibrium unfolding curves of mutant M1C in different temperatures: 25°C is open circles, 30°C is closed circles, 35°C is grey square, 40°C is open square and 45°C is open triangle.

Table 3.41: m , K_w , ΔG and $[\text{denaturant}]_{0.5}$ results of mutant M1C from urea induced denaturation experiments.

Temp (K)	K_w	ΔG (cal/mol)	m (cal/mol M)	$[\text{urea}]_{0.5}$ (M)
298	1.58×10^{11}	-15260		3.6 ± 0.1
303	1.47×10^{11}	-15469		3.5 ± 0.09
308	4.75×10^{10}	-15035	-0.7 ± 0.1	3.2 ± 0.3
313	3.98×10^8	-12310		2.5 ± 1.3
318	4.05×10^7	-11044		1.3 ± 0.01

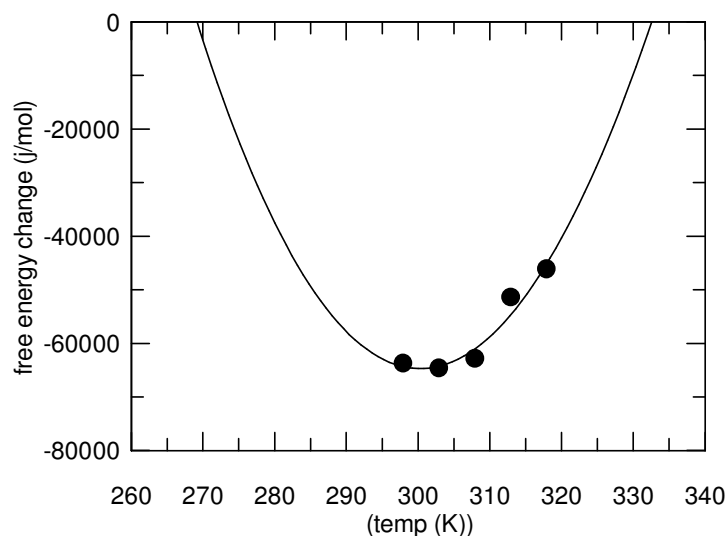


Figure 3.90 : Thermodynamics of unfolding of mutant *cmFDH*, M1C. The free energy changes of unfolding in water (ΔG_w) over a range of temperatures (T) were determined from urea-induced equilibrium denaturation data and fitted to the equation 2, at a reference temperature of $T_0=298$ K.

The results show that at the reference temperature of 25 °C the enthalpy change on folding (ΔH) is unfavourable, approximately $+6 \pm 4.4$ kcal/mol and the heat capacity change (ΔC_p) is -9.2 ± 4.2 kcal/mol/K. The entropy change at 25 °C is favourable ($-T\Delta S = -21.4 \pm 0.14$ kcal/mol).

Further evidence for the introduction of strain into the oxidised M1C mutant is afforded by the thermostability and denaturation experiments. According to GdnHCl and urea induced denaturation experiments, replacing the methionine residue by cysteine decreased the free energy gain on folding of the mutant by 1.4 and 9 kcal mol⁻¹, respectively at room temperature. The gain at the T_m value was calculated as +2°C from both GdnHCl and urea experiments. The favourable entropy change was indicated by alteration of Met1 residue to Cys in the folded state. However, different ΔG and T_m values was detected from different chemicals depending on the nature of electrostatic interactions stabilizing the protein structure, it is clear that Cys replacement at the first position slightly improved catalytic efficiency and stability.

In the literature there are several studies investigating the Met to Gln, Leu, Ile, Phe, Val, Ala or noncoded amino acid substitution at several positions of protein structure. It is considered that oxidation of methionine to the sulfoxide form may disrupt the structure and stability of enzymes (Oh et al., 2002). Substitution of methionine with

cysteine, which converts a hydrophobic residue into a more hydrophilic one, can markedly alter the properties of a protein (Dai et al., 2007). Methionine and cysteine are two sulfur-containing amino acids but site chain of Cys is shorter than Met. Therefore, probably, change of Met to Cys affects the catalytic efficiency of protein and increase the thermostability by providing a more sterically compact structure.

3.6 Site Saturation mutagenesis application on first residue of *cmFDH*

According to the results of characterization studies of M1C/D62C disulphide bridge mutants we decided to apply the site saturation mutagenesis strategy to the M1 residue which was shown to influence temperature stability according to the above results. After the generation of mutant library, mutants shown in table 3.42 were selected according to the screening method described in the Materials and Methods section, using 96 well plate analysis of 200 colonies. Steady state activity measurements and thermal denaturation experiments were performed for selected 8 mutants as described previously. Table 3.42 summarizes the results of kinetic measurements and the $T_{0.5}$ values.

Table 3.42: Activity and $T_{0.5}$ values of site saturation mutants on M1 position of *cmFDH*.

<i>cmFDH</i> M1 mutants	K_m (mM)	k_{cat} (sn ⁻¹)	k_{cat} / K_m (sn ⁻¹ mM ⁻¹)	$T_{0.5}$
Met1Cys	3.33±0.4	1.25±0.005	0.38	58.37±0.2
Met1Gln	2.87±0.4	0.39±0.002	0.1359	54.65±0.2
Met 1Gly	2.58±0.3	0.11±0.0005	0.0441	53.19±1.3
Met 1Asn	2.80±0.3	0.27±0.001	0.0986	53.27±1.8
Met 1Ala	4.02±0.45	0.42±0.002	0.1055	55.59±0.7
Met 1Arg	9.76±4.5	0.59±0.01	0.0609	55.80±3
Met 1Val	3.34±0.2	0.53±0.001	0.1603	52.55±0.5
Met 1Ser	4.49±0.5	0.87±0.004	0.1941	55.12±0.7
Met 1Leu	6.30±1	1.17±0.008	0.1861	56.57±0.2
Native <i>cmFDH</i>	4.75±0.3	1.12±0.1	0.24	56.7±0.2

The first residue of *cmFDH* corresponds to the 15th residue of recombinant 6xHis-tagged *cmFDH* (MKH₆HMHAGAQMKIVL...). Therefore, mutation on the start codon of the *fdh* gene does not affect the expression of enzyme. As shown by the

results of 8 mutations at this position, these alterations are tolerated (Tab. 3.42). If the K_m values are compared individually, except for Met1Arg and Met1Leu, all mutants have better affinity for the substrate formate than native *cmFDH*. On the other hand, while Met1Leu has a higher K_m value than native *cmFDH* for formate, it also has the best k_{cat} value among the site saturation mutants and the $T_{0.5}$ value of this mutant is almost the same as native *cmFDH*. When all mutants are compared in terms of catalytic efficiency, the best one is Met1Cys (Tab. 3.42).

When the results of thermal inactivation experiments are compared to each other as percentage of residual activity, it was observed that native *cmFDH*, M1C, M1Q and M1L mutants have the nearly same activity after incubation at 50 and 55°C. Among all mutants M1L has the best residual activity after incubation at 60°C, 17 %. Table 3.43 and figure 3.91 summarize the residual activities of enzymes after incubation at 50, 55 and 60 °C.

Remaining activity data were fitted to the Arrhenius equation to calculate E_a and k_a values and van't Hoff equations to calculate ΔH , ΔC_p and ΔS by combining equation 4 and 6 as explained before in section 3.2.7. The results are summarized in table 3.44.

With reference to the van't Hoff equation, calculated ΔG values at reference 30 show that cysteine, glutamine, leucine and alanine mutants all increased the stability by 2.5, 2.4, 2.3 and 1.5kcal/mol, respectively. The effect of glutamine and alanine substitution probably comes from side chains which have relatively greater polarity than the hydrophobic side chain of methionine. These side chain changes reduce the hydrophobicity and van der Waals interactions (Chin, D. and Means, A. R., 1996; Balog et al., 2003; Kim et al., 2001). Leucine and methionine have hydrophobic amino side chains and the van der Waals volume occupied by leucine is the same as for methionine. Introduction of the leucine can cause significant steric interferences and substantial movement in several nearby residues (Ann-Lipscomb et al., 1998). Methionine to leucine substitution may give either a stabilizing or destabilizing effect depending on the environment of the residues altered (Ann-Lipscomb et al., 1998; Pokkuluri et al., 2002). In this study the stabilizing effect of the M1L mutation comes from increased entropy at room temperature. Its higher enthalpy and entropy and lower heat capacity are the notable properties when compared to *native cmFDH*.

Asparagine and serine have destabilizing effects, by the 2.1 and 1.4 kcal/mol respectively. Arginine, valine and serine have little effect on the stability. The counterpart studies in the literature have shown that methionine substitutions to noncoded amino acids, valine, arginine and serine generally have minor or no effects on protein structure, being slightly stabilizing or destabilizing depending on the location (Yamniuk et al., 2009)

Table 3.43: Residual activities of native *cm*FDH and mutant enzymes after incubation in 50, 55 and 60 °C for 20 min. Residual activities were expressed relative to activities in room temperature (25 °C).

Temp.(°C)	Native <i>cm</i> FDH	M1C	M1Q	M1G	M1N	M1A	M1R	M1V	M1S	M1L
0	100	100	100	59	41	90	97	95,5	85	100
55	85.5	81	91.5	22	40	55.5	39.5	24	54	85
60	6.6	0.7	0	0	0	3	0	0	0	17

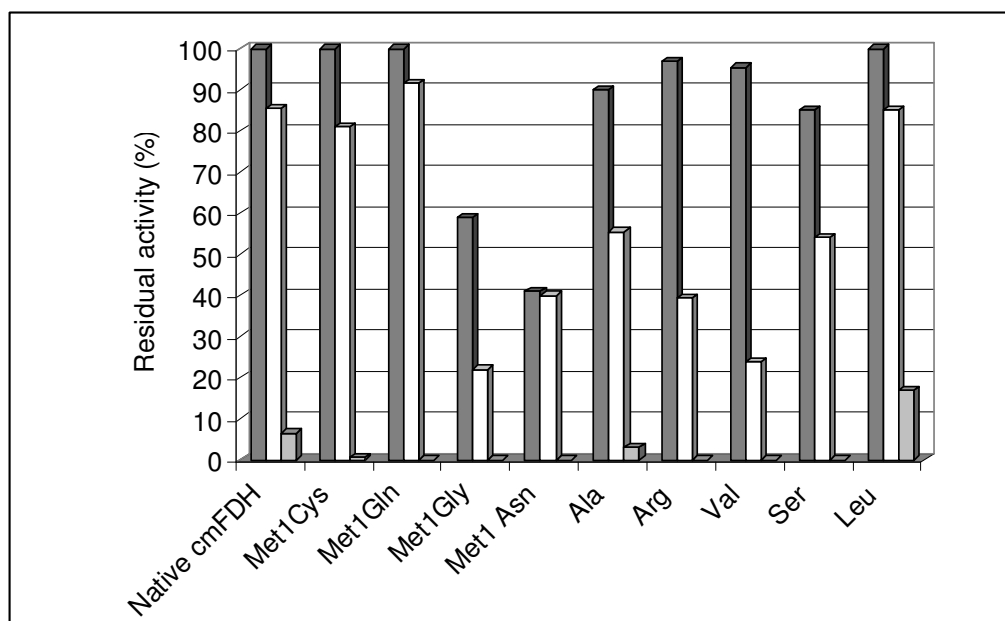


Figure 3.91 : Bar graph presentation of residual activities of native *cm*FDH and site saturation mutants after incubation in 50 (dark grey), 55 (white) and 60 °C (light grey) for 20 min. Residual activities were expressed relative to activities at room temperature (25 °C).

Table 3.44: Comparison of enthalpy, entropy, heat capacity change, activation enthalpy and rate constant values for the site saturation mutants.

Enzymes	ΔH (kcal/mol)	$-T\Delta S$ (kcal/mol)	ΔC_p (kcal/mol/K)	E_a (kcal/mol)	k_a (s ⁻¹)
M1C	16.4±2	+2.4±0.006	1.3±0.6	94±0.5	1.2x10 ⁵⁷
M1Q	57.7±3.5	-35.7±0.012	1.02±0.39	95±0.15	5.1 10 ⁵⁹
M1G	10.9±26	+9±0.08	3.2±1,4	90±0.3	6.5x10 ⁵⁶
M1N	35.3±27	-17.8±0.09	0.5±1.2	88±0.9	2.8x10 ⁵⁵
M1A	35.9±15	-15±0.05	2.1±0.9	92±0.5	4.7x10 ⁵⁷
M1R	17.8±23	+1.5±0.07	2.9±1.3	91.5±2	3 x10 ⁵⁷
M1V	37.7±15.8	-17.8±0.05	1.7±0.9	91±0.2	4 x10 ⁵⁷
M1S	-5.7±23	+23.8±0.07	3.2±0.9	90.6±0.7	8 x10 ⁵⁶
M1L	57.6±0.3	-35.7±0.3	0.65±0.3	93.8±0.3	3 x10 ⁵⁸
Native <i>cm</i> FDH	25±10	-5.5±0.003	2.0±0.5	91±0.7	2x10 ⁵⁷

4. CONCLUSION

The understanding of the factors leading to the thermostability of this enzyme contributes to our understanding of protein folding and stability, and it is also critical for designing an efficient FDH enzyme that can work at high temperatures. Such an enzyme is required for the regeneration of reduced cofactor in many enzyme-based synthetic approaches to the manufacture of fine chemicals within industrial and biotechnological areas such as medicine, pharmaceutical, food, detergents etc. When it is viewed from a broader perspective the analysis of the folding mechanism and stability of homodimeric *cm*FDH is a significant contribution to the understanding of the dimeric enzymes.

The folding mechanism and stability of native *cm*FDH were analysed by exposure to denaturing agents and to heat. Equilibrium denaturation data yielded a dissociation constant of about 10^{-13} M. Any populated intermediate state was not observed, only native dimer and unfolded monomers significantly populated. From the temperature-dependence of the free energy of folding, as measured by equilibrium chemical denaturation, the heat capacity change on folding is -10.5 ± 1.8 kcal/mol/K, almost exactly in line with the empirically predicted value for the unfolding of two subunit chains of 364 residues. These findings showed that homodimeric *cm*FDH unfolds by two state single transition model without intermediates in equilibrium. In the equilibrium one dimer is equal to two unfolded monomers including both folding and dissociation processes.

By fitting the rate constants for irreversible thermal unfolding, in the absence of chemical denaturant, to the integrated van't Hoff equation, we derive the following values for the transition state of unfolding ΔC_p , ΔH and ΔS of 2.0 kcal/mol/K , 25 kcal/mol and -5.5 kcal/mol at 298 K which can serve as parameters for predicting the rate of denaturation over a wide temperature range.

The kinetics of refolding and unfolding reactions revealed that the overall process comprises 2 steps, folding and assembly, representing a irreversible unimolecular-bimolecular kinetic model. In the first step a marginally stable folded monomeric

state is formed at a rate (k_1) of about $2 \times 10^{-3} \text{ s}^{-1}$ (by deduction k_{-1} is about 10^{-4} s^{-1}) and assembles into the active dimeric state with a bimolecular rate constant (k_2) of about $2 \times 10^4 \text{ M}^{-1} \text{ s}^{-1}$. The rate of dissociation of the dimeric state in physiological conditions is extremely slow ($k_{-2} \sim 3 \times 10^{-7} \text{ s}^{-1}$).

After the analysis of kinetic and thermodynamic properties of the folding and assembly of native *cmFDH*, the effect of electrostatic interaction on the surface of *cmFDH* was investigated in terms of folding and stability. Characterization studies performed by using two different chemical denaturation agents showed that association constant (K_a) of native and mutants decreased when the temperature of the equilibrium denaturation is increased. However GdnHCl and urea induced unfolding experiments give the different free energy change values because of the ionic properties of GdnHCl, results from both denaturant experiments confirm each other in terms of the stabilizing or destabilizing effect of a particular mutation. It is obvious that N147R, N187E and Q105R mutations increased the melting temperature on the average of 2.75, 6, 2.75 °C. The T_m value difference between GdnHCl and urea experiments was ± 2 °C. The most dramatic increase in stability observed for the N187E mutant was 6 °C in average in the absence of denaturant at 25°C. The mutants showed that increased numbers of electrostatic interactions can cause either stabilizing or destabilizing effect on the thermostability of this protein. According to equilibrium unfolding experiments we observed that mutations did not cause a change in the equilibrium unfolding mechanism.

For the native *cmFDH*, the data show that it is stabilized by an unfavourable enthalpic contribution and accompanied by a favourable entropic change at room temperature, in contrast to many proteins which are stabilized by a favorable enthalpic contribution (Pandya, et al, 1999; Kearney et al., 2007). When the thermodynamic properties of mutants and native *cmFDH* are compared it shows that additional electrostatic interactions have different effects on the enthalpy and entropy changes at room temperature. Based on the thermodynamic results, it is suggested that three of twelve mutations, N187E, Q105R and N147R, increased the stability of *cmFDH* by introducing favourable electrostatic interactions. Three of the nine positions selected to be changed were successful designs. This result corresponds to a 33 % accuracy of designing mutant to increase thermostability. On the other hand all the other positions of mutations are important because they all

have a measurable effect on the *cmFDH* folding and activity, hence contribute to our understanding of the interactions that stabilize or destabilize this protein.

The another point of interest concerns the effects of double mutants on stability. It is known that, stabilization effect are generally additive allowing significant stabilization to be achieved with a number of single-point mutations (Serov et al., 2005). In contrast, additive stabilizing effect of double mutants has not been observed in this thesis even though the corresponding single mutants have stabilizing effects. In the literature there are also examples of non-additive effects of distinct point mutations on the thermodynamic stability of proteins (Xian et al., 2006; Ann-Lipscomb et al., 1998).

The second strategy to increase the thermostability was the formation of a disulphide bridge. The improvement of thermal stability of FDH by introducing disulfide bridges is a difficult task since the previous studies resulted with a decrease in the enzyme stability (Slusarczyk et al., 2003, Karagüler et al., 2007). The structure of *cbFDH* which has 97 % identity with amino acid sequence of *cmFDH* provides a better model for rational design and also shows that the *cmFDH* model based on *psFDH* structure has reasonable quality apart from a poor loop prediction between residues 10 and 19. Nevertheless, the positions choosing as sterically ideal sites for the insertion of disulphide bridges did not give the desired success, M1C single mutant increased the T_m value 2 °C. When we investigated the disulphide bridge constructed between M1 and D62 residue we found that replacing the methionine residue by cysteines increased the free energy gain on folding of the mutant.

Finally, to elucidate this unexpected effect, site saturation mutagenesis approach was applied to this position to generate all feasible mutants. In the literature there are several studies investigating methionine to Gln, Leu, Ile, Phe, Val, Ala or noncoded amino acid substitution at several positions in protein structures but we could not find any study where the first residue of the protein amino acid chain was changed. Therefore, the position of the methionine substitution applied in this study is important in terms of being the first.

REFERENCES

- Akke, M. and Forsen, S.,** 1990: Protein stability and electrostatic interactions between solvent exposed charged side chains, *Proteins: Structure, Function and Genetics*, **8**, 23-29.
- Ali, M. and Imperiali, B.,** 2005: Protein oligomerization: How and why, *Bioorganic and Medicinal Chemistry*, **13**, 5013-5020.
- Allen, S., Holbrook, J.,** 1995: Isolation, sequence and overexpression of the gene encoding NAD-dependent formate dehydrogenase from the methylotrophic yeast *Candida methylca*, *Gene* **162**, 99-104.
- Alsallaq, R., Zhou, H.X.,** 2007: Prediction of protein-protein association rates from a transition-state theory, *Structure*, **15**, 2, 215-24.
- Alsop, E., Silver, M. and Livesay, D.R.,** 2003: Optimized electrostatic surfaces parallel increased thermostability: a structural bioinformatic analysis, *Protein Engineering*, **16**, 12, 871-874.
- Andreadeli, A., Flemetakis, E., Axarli, I., Dimou, M., Udvardi, M. K., Katinakis, P. and Labrou, N. E.,** 2009: Cloning and characterization of *Lotus japonicus* formate dehydrogenase: A possible correlation with hypoxia, *Biochimica et Biophysica Acta - Proteins & Proteomics*, **1794**, 6, 976-984.
- Andreadeli, A., Platis, D., Tishkov, V., Popov, V. and Labrou, N. E.,** 2008: Structure-guided alteration of coenzyme specificity of formate dehydrogenase by saturation mutagenesis to enable efficient utilization of NADP⁺, *FEBS Journal*, **275**, 3859–3869.
- Anfinsen, C. B.,** 1973: Principles that govern the folding of protein chains, *Science* **181**, 96, 223–230.
- Annaluru, N., Watanabe, S., Saleh, A. A., Kodak, T. and Makino, K.,** 2006: Site-directed mutagenesis of a yeast gene for improvement of enzyme thermostability, *Nucleic Acids Symposium Series*, **50**, 1, 281-282.
- Ann-Lipscomb, L., Gassner, N. C., Snow, S. D., Eldridge, A. M., Baase, W. A., Drew, D. L. and Matthews, W.,** 1998: Substitution shown in T4 lysozyme Context-dependent protein stabilization by methionine-to-leucine, *Protein Science*, **7**, 765-773.
- Arnold, F. H.,** 1998: Design by Directed Evolution, *Accounts of Chemical Research*, **31**, 125-131.
- Arnold, F. H.,** 2001: Combinatorial and computational challenges for biocatalyst design *Nature* , **409**, 253-257.

- Arolas, J. L., Castillo, V., Bronsoms, S., Aviles, F.X., Ventura, S.,** 2009: Designing Out Disulfide Bonds of Leech Carboxypeptidase Inhibitor: Implications for Its Folding, Stability and Function, *Journal of Molecular Biology*, **392**, 529–546.
- Baker, D.,** 2000: A surprising simplicity to protein folding, *Nature*, 405, 6782, 39–42.
- Baldwin, R. L.,** 2007: Energetics of Protein Folding, *Journal of Molecular Biology*, **371**, 283–301.
- Balog, E. M., Norton, L. E., Bloomquist, R. A., Cornea, R. L., Black, D. J., Louis, C. F., Thomas, D. D. and Fruen, B. R.,** 2003: Calmodulin Oxidation and Methionine to Glutamine Substitutions Reveal Methionine Residues Critical for Functional Interaction with Ryanodine Receptor-1, *The Journal of Biological Chemistry*, **278**, 18, 15615–15621.
- Banavar, J. R. and Maritan, A.,** 2007: Annual Review of Biophysics and Biomolecular Structure, *Annual Review Biophysics and Biomolecular Structure*, **36**, 261–80.
- Baryshnikova, E. N., Melnik, B. S., Finkelstein, A. V., Semisotnov, G. V. and Bychko, V. E.,** 2005: Three-state protein folding: Experimental determination of free-energy profile VA, *Protein Science*, **14**, 2658–2667.
- Bellotti, V., Nuvolone, M., Giorgetti, S., Obici, L., Palladini, G., Russo, P., Lavatelli, F., Perfetti, V. and Bellotti, G. M.,** 2007: The workings of the amyloid diseases, *Annals of Medicine*, **39**, 200–207.
- Berezovsky, N. I.,** 2008: Protein and DNA Thermostability, Physics and Evolution of Computational Biology Unit, Bergen Center, *Wiley Encyclopedia of Chemical Biology*, John Wiley & Sons, Inc.
- Betz, S. F.,** 1993: Disulfide bonds and the stability of globular proteins, *Protein Science*, **2**, 1551–1558.
- Bjørk, A., Dalhus, B., Mantzilas, D., Eijsink, V. G. H. and Sirevag, R.,** 2003: Stabilization of a Tetrameric Malate Dehydrogenase by Introduction of a Disulfide Bridge at the Dimer–Dimer Interface, *Journal of Molecular Biology*, **334**, 811–821.
- Bloom, J. D., Labthavikul, S. T., Otey, C. R. and Arnold, F. H.,** 2006: Protein stability promotes evolvability, *Proceedings of the National Academy of Science of the USA*, **103**, 15, 5869–5874.
- Bolivar, J. M., Wilson, L., Ferrarotti, S. A., Fernandez-Lafuente, R., Guisan, J. M., Mateo, C.,** 2007: Evaluation of different immobilization strategies to prepare an industrial biocatalyst of formate dehydrogenase from *Candida boidinii*, *Enzyme and Microbial Technology*, **40**, 4, 540–546.
- Bommarius, A. S., Broering, J. M., Chaparro-Riggers, J. F. and Polizzi, K. M.,** 2006: High-throughput screening for enhanced protein stability, *Current Opinion in Biotechnology*, **17**, 606–610.

- Bornscheuer, U. T. and Pohl, M.**, 2001: Improved biocatalysts by directed evolution and rational protein design, *Current Opinion in Chemical Biology*, **5**, 137–143.
- Bradford, M. M.**, 1976: A rapid and sensitive method for quantitation of microgram quantities of protein utilizing the principle of protein-dye-binding, *Analytical Biochemistry*, **72**, 248-54.
- Burton, S. G.**, 2003: Oxidizing enzymes as biocatalysts, *Trends Biotechnology*, **21**, 543–549.
- Cabra, V., Vázquez-Contreras, E., Moreno-Cárcamo, A., Arreguin-Espinosa, R.**, 2008: The effect of sulfhydryl groups and disulphide linkage in the thermal aggregation of Z19 α -zein, *Biochimica et Biophysica Acta*, **1784**, 7-8, July- 1028-1036.
- Chen, H. and Kihara, D.**, 2008: Estimating quality of template-based protein models by alignment stability, *Proteins*, **71**, 1255–1274.
- Chen, K., and Arnold, F. H.**, 1993: Tuning the activity of an enzyme for unusual environments: Sequential random mutagenesis of subtilisin E for catalysis in dimethylformamide, *Biochemistry*, **90**, 5618-5622.
- Chen, R.**, 2001: Enzyme engineering:rational redesign versus directed evolution, *Trends in Biotechnology*, **19**, 1, 13-4.
- Chen, Y., Ding, F., Nie, H., Serohijos, A. W., Sharma, S., Wilcox, K. C., Yin, S., Dokholyan, N. V.**, 2008: Protein folding: Then and now, *Archives of Biochemistry and Biophysics*, **469**, 4–19.
- Chin, D. and Means, A. R.**, 1996: Methionine to Glutamine Substitutions in the C-terminal Domain of Calmodulin Impair the Activation of Three Protein Kinases, *The Journal of Biological Chemistry*, **271**, 48, 30465–30471.
- Chistoserdova, L., Crowther, G. J., Vorholt, J. A., Skovran, E., Portais, J. C. and Lidstrom, M. E.**, 2007: Identification of a Fourth Formate Dehydrogenase in *Methylobacterium extorquens* AM1 and Confirmation of the Essential Role of Formate Oxidation in Methylophony, *Journal of Bacteriology*, 9076–9081.
- Cho, J. H. and Raleigh, D.P.**, 2006: Electrostatic Interactions in the Denatured State and in the Transition State for Protein Folding: Effects of Denatured State Interactions on the Analysis of Transition State Structure, *Journal of Molecular Biology*, **359**, 5, 1437-1446.
- Cho, J. H., Sato, S., Horng, J. C., Anil, B., Raleigh, D. P.**, 2008: Electrostatic interactions in the denatured state ensemble: Their effect upon protein folding and protein stability, *Archives of Biochemistry and Biophysics*, **469**, 1, 20-28.
- Chothial, C. and Lesk, A. M.**, 1986: The relation between the divergence of sequence and structure inproteins, *The EMBO Journal*, **5**, 4, 823-826.
- Chu, X., Yu, W., Wu, L., Liu, X., Li, N., Li, D.**, 2007: Effect of a disulfide bond on mevalonate kinase, *Biochimica et Biophysica Acta - Proteins & Proteomics*, **1774**, 12, 1571-1581.

- Chul Lee, S., Chang, Y. J., Min Shina, D., Hana, J., Seo, M. H., Fazelini, H., Maranasb, C. D., Kima, H. S.,** 2009: Designing the substrate specificity of d-hydantoinase using a rational approach, *Enzyme and Microbial Technology*, **44**, 170–175.
- Clarke, J., Hounslow, A. M. and Fersht, A. R.,** 1995: Disulfide Mutants of Barnase II: Changes in Structure and Local Stability Identified by Hydrogen Exchange, *Journal of Molecular Biology*, **253**, 505–513.
- Creighton, T.,** 1993: Chemical properties of polypeptides. In: *Proteins*, 2nd edn. W.H. Freeman and Company, New York.
- Daia, X. L., Sunb, Y. X. and Jiang, Z. F.,** 2007: Attenuated cytotoxicity but enhanced fibril of a mutant amyloid β -peptide with a methionine to cysteine substitution, *FEBS Letters*, **581**, 1269–1274.
- Dalton, J. A. R. and Jackson, R. M.,** 2007: An evaluation of automated homology modelling methods at low target–template sequence similarity, *Structural Bioinformatics*, **23**, 15, 1901–1908.
- Dar, T. A., Singh, L. R., Islam, A., Anjum, F., Moosavi-Movahedi, A. A. and Ahmad, F.,** 2007: Guanidinium chloride and urea denaturations of β -Lactoglobulin A at pH 2.0 and 25 °C: The equilibrium intermediate contains non-native structures (helix, tryptophan and hydrophobic patches), *Biophysical Chemistry*, **127**, 3, 140–148.
- Das, M., Kobayashi, M., Yamada, Y., Sreeramulu, S., Ramakrishnan, C., Wakatsuki, S., Kato, R and Varadarajan, R.,** 2007: Design of Disulfide-linked Thioredoxin Dimers and Multimers Through Analysis of Crystal Contacts, *Journal of Molecular Biology*, **372**, 1278–1292.
- Davies, N. M., Teng, X. V.,** 1997: Importance of Chirality in Drug Therapy and Pharmacy Practice: Implications for Psychiatry, *Advances in Pharmacy*, I, 3, 242–252.
- Davoodi, J., Wakarchuk, W. W., Carey, P. R., Surewicz, W. K.,** 2007: Mechanism of stabilization of *Bacillus circulans* xylanase upon the introduction of disulfide bonds, *Biophysical Chemistry*, **125**, 453–461.
- Decklerck, N.,** 1995: Hyperthermostable mutants of *Bacillus licheniformis* α -amylase: multiple amino acid replacements and molecular modelling *Protein Engineering*, **8**, 1029–1037.
- Dill, K. A.,** 1990: The meaning of hydrophobicity, *Science*, **250**, 297–298.
- Dominy, B.N., Minoux, H., Brooks, C.L.,** 2004: An electrostatic basis for the stability of thermophilic proteins, *Proteins: Structure, Function and Genetics*, **57**, 128–141.
- Doyle, S. M., Braswell, E. H. and Teschke, C. M.,** 2000: SecA folds via a dimeric intermediate, *Biochemistry*, **39**, 11667–11676.
- Dunn, C.R., Wilks H.M., Halsall D.J., Atkinson T., Clarke A.R., Murhead H., Holbrook J.J.,** 1991: Design and synthesis of new enzymes based on the lactate dehydrogenase framework, *Philosophical Transaction of Royal Society London B.*, **332**, 177–184.

- Eckstein, M., Daubmann, T. and Kragl, U.,** 2004: Recent Developments in NAD(P)H Regeneration for Enzymatic Reductions in One- and Two-Phase Systems, *Biocatalysis and Biotransformation*, **22**, 2, 89-96.
- Eijsink, V.G.H., Björkb, A., Gaseidnes, S., Sirevag, R., Synstad, B., Van den Burge, B., Vriend, G.,** 2004: Rational engineering of enzyme stability, *Journal of Biotechnology*, **113**, 105–120.
- Ellis, R. J.,** 2003: Protein Folding: Importance of the Anfinsen Cage, *Current Biology*, **13**, 881-883.
- Endo, T., Koizumi, S.,** 2001: Microbial conversion with cofactor regeneration using genetically engineered bacteria, *Advanced Synthesis and Catalysis*, **343**, 521-526.
- Eriksson T., Björkman, S., Roth, B., Fyge, A., Högländ, P.,** 1995: Stereospecific determination, chiral inversion in vitro and pharmacokinetics in humans of the enantiomers of thalidomide, *Chirality*, **7**, 1, 44-52.
- Fedorchuk, V.V., Galkin, A.G., Yasny, I.E., Kulakova, L.B., Rojkova, A.M., Filippova, A.A., Tishkov, V.I.,** 2002: Influence of interactions between amino acid residues 43 and 61 on thermal stability of bacterial formate dehydrogenases, *Biochemistry (Mosc.)*, **67**, 1145–1151.
- Fernandez-Lafuente, R.,** 2009: Stabilization of multimeric enzymes: Strategies to prevent subunit dissociation, *Enzyme and Microbial Technology*, **45**, 405–418.
- Folch, B., Rooman, M. and Dehouck, Y.,** 2008: Thermostability of Salt Bridges versus Hydrophobic Interactions in Proteins Probed by Statistical Potentials, *Journal of Chemical Information and Modeling*, **48**, 1, 119–127.
- Francs-Small, C., Ambard-Bretteville, C., Small, I. D., Remy, R.,** 1993: Identification of a major soluble protein in mitochondria from nonphotosynthetic tissues as NAD-dependent formate dehydrogenase. *Plant Physiology*, **102**, 4, 1171-1177.
- Ghosh, S. and Mandal, D. K.,** 2006: Kinetic stability plays a dominant role in the denaturant-induced unfolding of Erythrina indica lectin, *Biochimica et Biophysica Acta*, **1764**, 1021-1028.
- Grimsley, G.R., Shaw, K.L., Fee, L.R., Alston, R.W., Huyghues, B.M., Thurlkill, R.L., Scholtz, J.M. and Pace, C.N.,** 1999: Increasing protein stability by altering long-range coulombic interactions, *Protein Science*, **8**, 1843-1849.
- Gül Karagüler, N., Sessions, R. B. and Clarke' A. R.,** 2007: Effects of disulphide bridges on the activity and stability of the formate dehydrogenase from *Candida methylca*, *Biotechnology Letters*, **29**, 9, 1375-1380.
- Gül-Karagüler, N., Sessions, R. B., Clarke, A. R., Holbrook, J. J.,** 2001: A single mutation in the NAD-specific formate dehydrogenase from *Candida methylca* allows enzyme to use NADP, *Biotechnology Letters*, **23**, 283-287.

- Gül-Karagüler, N., Sessions, R.B., Moreton, K.M., Clarke, A.R., Holbrook, J.J.,** 2004: Estimating the energetic contribution of hydrogen bonding to the stability of *Candida methylica* formate dehydrogenase by using double mutant cycle, *Biotechnology Letters*, **26**, 1137-1140.
- Haki, G.D., Rakshit, S.K.,** 2003: Developments in industrially important thermostable enzymes, *Biosource Technology*, **89**, 17-34.
- Halliwell, C. M., Morgan, G., Chung-Pei, O., and Cass, A. E. G.,** 2001: Introduction of a (Poly)histidine Tag in L-Lactate Dehydrogenase Produces a Mixture of Active and Inactive Molecules., *Analytical Biochemistry*, **295**, 257–261.
- Hamza, M. A. and Engel, P. C.,** 2007: Enhancing long-term thermal stability in mesophilic glutamate dehydrogenase from *Clostridium symbiosum* by eliminating cysteine residues, *Enzyme and Microbial Technology*, **41**, 6-7,706-710.
- Hartl, F.U., Hayer-Hartl , M.,** 2002: Molecular chaperones in the cytosol: from nascent chain to folded protein, *Science*, **295**, 5561, 1852-1858.
- Haug, I. J., Skar, H. M., Vegarud, G. E., Langsrud, T., Draget, K. I.,** 2009: Electrostatic effects on β -lactoglobulin transitions during heat denaturation as studied by differential scanning calorimetry, *Food Hydrocolloids*, **23**, 8, 2287-2293.
- Hendsch, Z.S. and Tidor, B.,** 1994: Do salt bridges stabilize proteins? A continuum electrostatic analysis, *Protein Science*, **3**, 211-226.
- Hillisch, A., Pineda, L. F. and Hilgenfeld, R.,** 2004: Utility of homology models in the drug discovery process, *Drug Discovery Today*, **9**, 15, 659-69.
- Hilvert, D.,** 2001: Enzyme Engineering, *Chimia*, **55**, 867–869.
- Holbrook, J. J., Louise, C., Keyji , J., Hateley, John M.,** 2000: Chiral synthesis of 2-hydroxy carboxylic acids with a dehydrogenase United States Patent US6033882,
- Huang, O. and Quiñones, E.,** 2008: Assessment of the stability and unfolding pathways of azurin from *Pseudomonas aeruginosa* through the combination of denaturing osmolytes, *Archives of Biochemistry and Biophysics*, **477**, 1, 175-182.
- Hummel, W., Kula, M. R.,** 1989: Dehydrogenases for the synthesis of chiral compounds, *European Journal of Biochemistry*, **184**, 1–13.
- Hunter, M. G., Sunde, M., and Radford, S. E.,** 2000: Partially unfolded states of β 2-microglobulin and amyloid formation in vitro, *Biochemistry*, **39**, 8735–8746.
- Jacobson, M. and Sali, A.,** 2004: Comparative Protein Structure Modeling and its Applications to Drug Discovery, *Annual Reports In Medicinal Chemistry*, **39**, 259-273.
- Jaenicke R.,** 2000: Stability and stabilization of globular proteins in solution. *Journal of Biotechnology*, **79**, 3, 193-203.
- Jaenicke, R.,** 1991: Protein folding: local structures, domains, subunits, and assemblies. *Biochemistry*, **30**, 13, 3147–3161.

- Jeong, M. Y., Kim, S., Yun, C. W., Choi, Y. J., Chob, S. G.,** 2007: Engineering a *de novo* internal disulfide bridge to improve the thermal stability of xylanase from *Bacillus stearothermophilus* No. 236, *Journal of Biotechnology*, **127**, 300–309.
- Johannes, T. W., Woodyer, R., Zhao, H.,** 2007: Efficient Regeneration of NADPH using an Engineered Phosphite Dehydrogenase, *Biotechnology and Bioengineering*, **96**, 18-26
- Johnson, C. M., Oliveberg, M., Clarke, J. And Fersht, A. R.,** 1997: Thermodynamics of Denaturation of Mutants of Barnase with Disulfide Crosslinks, *Journal of Molecular Biology*, **268**, 198-208.
- Jormakka, M., Byrne, B. and Iwata, S.,** 2003: Formate dehydrogenase – a versatile enzyme in changing environments, *Current Opinion in Structural Biology*, **13**, 418–423.
- Karaguler, N.G., Sessions, R.B., Binay, B., Ordu, E.B. and Clarke, A.R.,** 2007: Protein engineering applications of industrially exploitable enzymes: *Bacillus stearothermophilus* LDH and *Candida methylica* FDH, *Biochemical Society Transactions*, **35**, 1610-1615.
- Karshikoff, A. and Ladenstein, R.,** 2000: Protein from thermophilic and mesophilic organisms essentially do not differ in packing, *Protein Engineering*, **11**, 10, 867-872.
- Kaup, B., Meyer, S. B., Sahm, H.,** 2005: D-mannitol formation from D-glucose in a whole cell biotransformation with recombinant E. coli, *Applied Microbiology and Biotechnology*, **69**, 397-403.
- Kearney, A., Avramovic, A., Castro, M. A. A., Carmo, A. M., Davis, S. J. and Merwe, P. A.,** 2007: The Contribution of Conformational Adjustments and Long-range Electrostatic Forces to the CD2/CD58 Interaction, *The Journal of Biological Chemistry*, **282**, 18, 13160-13166.
- Kim, Y. H., Berry, A. H., Spencer, D. S. and Stites, W. E.,** 2001: Comparint the effect on the protein stability of methionine oxidation versus mutagenesis: steps towards engineering oxidative resistance in proteins, *Protein Engineering*, **14**, 5, 343-347.
- Koivula, A.,** 1996: The active site of *Trichoderma reesei* cellobiohydrolase II: the role of tyrosine 169, *Protein Engineering*, **9**, 691-699
- Kortemme, T., Darby, N.J. and Creighton, T.E.,** 1996: Electrostatic Interactions in the Active Site of the N-Terminal Thioredoxin-like Domain of Protein Disulfide Isomerase, *Biochemistry*, **35**, 14503-14511.
- Kula, M. R., Wandrey, C.,** 1987, Continuous enzymatic transformation in an enzyme-membrane reactor with simultaneous NADH regeneration, *Methods in Enzymology*, **136**, 9–21.
- Kumar, S. and Nussinov, R.,** 2001: How do thermophilic proteins deal with heat, *Cellular and Molecular Life Sciences*, **58**, 1216-1233.
- Kumar, S. and Nussinov, R.,** 2002: Close range electrostatic, *ChemBiochem*, **3**, 7, 604-617.

- Kumar, S., Ma, B., Tsai, C. J. and Nussinov, R.,** 2000:Electrostatic Strengths of Salt Bridges in Thermophilic and Mesophilic Glutamate Dehydrogenase Monomers, *PROTEINS: Structure, Function, and Genetics*, **38**, 368–383.
- Kumar, S., Tsai, C.J., Nussinov, R.,** 2000: Factor enhancing protein stability, *Protein Engineering*, **13**, 839: 179-191.
- Kumar, S., Wolfson, H.J., Nussinov, R.,** 2001: Protein flexibility and electrostatic interactions, *IBM Journal of Research and Development*, **45**, 3-4, 499-512.
- Kundrotas, P. J. and Karshikoff, A.,** 2002: Modeling of denatured state for calculation of the electrostatic contribution to protein stability, *Protein Science*, **11**, 1681-1686.
- Kuzmic, P.,** 1996: Program DYNAFIT for analysis of enzyme kinetic data: application to HIV proteinase, *Analytical Biochemistry*, **237**, 260-273.
- Ladenstein, R. and Ren, B.,** 2006: Protein disulfides and protein disulfide oxidoreductases, in hyperthermophiles, *FEBS Journal*, **273**, 4170–4185.
- Ladokhin, A. S., Jayasinghe, S. and White, S. H.,** 2000: How to Measure and Analyze Tryptophan Fluorescence in Membranes Properly, and Why Bother?, *Analytical Biochemistry*, **285**, 2, 235-245.
- Lamzin, V. S., Aleshin, A. L., Stroskopytov, B. V., Yukhnevich, M. G., Popov, V. O., Harutyunyan, H. R. and Wilson, K. S.,** 1992: Crystal structure of NAD-dependent formate dehydrogenase, *European Journal of Biochemistry*, **206**,441 -452.
- Leach, A. R.,** 2001: Molecular Modelling, Principles and Applications, Chapter 10: Protein Structure Prediction, Sequence Analysis and Protein Folding, pp.550., Pearson Education Limited, Edinburgh Gate, England.
- Lee, B. and Vasmatzis, G.,** 1997: Stabilization of protein structures, *Current Opinion in Biotechnology*, **8**, 423-428.
- Lehmann, M. and Wyss, M.,** 2001: Engineering proteins for thermostability: the use of sequence alignments versus rational design and directed evolution, *Current Opinion in Biotechnology*, **12**, 371–375.
- Leung, D.W., Chen, E., Goeddel, D.V.,** 1989: A method for random mutagenesis of a defined DNA segment using a modified polymerase chain reaction, *Technique*, **1**, 11–15.
- Liese, A.,** 2005: Technical application of biological principles in asymmetric catalysis, *Advances in Biochemical Engineering Biotechnology*, **92**, 197–224.
- Liese, A., Vilella, M.,** 1999: Production of fine chemicals using biocatalysis, *Current Opinion in Biotechnology*, **10**, 595–603.
- Lill, H., Hisabori, T., Groth, G. and Bald, D.,** 2004: A thermostable enzyme as an experimental platform to study properties of less stable homologues, *Protein Engineering, Design & Selection*, **17**, 7, 553–555.

- Liu, W., Wang, P.**, 2007: Cofactor regeneration for suitable enzymatic biosynthesis, *Biotechnology Advances*, **25**, 369-384.
- Loladze, V.V. and Makhatadze, G.I.**, 2002: Removal of surface charge-charge interactions from ubiquitin leaves the protein folded and very stable, *Protein Science*, **11**, 174-177.
- Loladze, V.V., Ibarra-Molero, B., Sanchez-Ruiz, J.M. and Makhatadze, G.I.**, 1999: Engineering a Thermostable Protein via Optimization of Charge-Charge Interactions on the Protein Surface, *Biochemistry*, **38**, 16419-16423.
- Lutz, S., Bornscheuer, U. V.**, 2009: Protein Engineering chapter 3 page11, Wiley VCH Verlag GmbH &Co KGaA Weinheim.
- Maity, H., Mossing, M. C., Eftink, M. R.**, 2005: Equilibrium unfolding of dimeric and engineered monomeric forms of Cro (F58W) repressor and the effect of added salts: evidence for the formation of folded monomer induced by sodium perchlorate, *Archives of Biochemistry and Biophysics*, **434**, 93-107.
- Mallam, A. L. and Jackson, S.E.**, 2007: A comparison of the folding of two knotted proteins: YbeA and YibK. *Journal of Molecular Biology*, **366**, 2, 650-665.
- Mann, C. J., Matthews, C. R.**, 1993: Structure and stability of an early folding intermediate of Escherichia coli trp aporepressor measured by far-UV stopped-flow circular dichroism and 8-anilino-1-naphthalene sulfonate binding, *Biochemistry*, **32**, 5282-5290.
- Marshall, S. A., Lazar, G. A., Chirino, A. J. and Desjarlais, J. R.**, 2003: Rational design and engineering of therapeutic proteins, *Drug Discovery Today*, **8**, 212-221.
- Martinelle, M.**, 1996: The role of Glu87 and Trp89 in the lid of *Humicola lanuginosa* lipase, *Protein Engineering*, **9**, 519-524.
- Mas, J.M., Aloy, P., Martí-Renom, M.A., Oliva, B., Blanco-Aparicio, C., Molina, M.A., Llorens, R., Querol, E. and Avilés, F.X.**, 1998: Protein similarities beyond disulphide bridge topology, *Journal of Molecular Biology*, **284**, 3, 541-548.
- Mason, J. M., Cliff, M. J., Sessions, R. B. and Clarke, A. R.**, 2005: Low Energy Pathways and Non-native Interactions, The Influence of artificial disulfide bridges on the mechanism of folding, *The Journal Of Biological Chemistry*, **280**, 49, 40494-40499.
- Matthews, B. W.**, 1993: Structural And Genetic Analysis of Protein Stability *Annual Review of Biochemistry*, **62**, 139-60.
- Mayer, G., Kulbe, K.D., Nidetzky, B.**, 2002: Utilization of xylitol dehydrogenase in a combined microbial/enzymatic process for production of xylitol from D-glucose, *Applied Biochemistry*, **99**, 3, 577-590.
- McClellan, A. J., Scott, M. D., Frydman, J.**, 2005: Folding and quality control of the VHL tumor suppressor proceed through distinct chaperone pathways, *Cell*, **121**, 5, 739-48.

- McParland, V. J., Kad, N. M., Kalverda, A. P., Brown, A., Kirwin-Jones, P., Mei, G., Venere, A., Rosato, N. and Finazzi-Agro, A.,** 2005: The importance of being dimeric, *FEBS Journal*, **272**, 16–27.
- Northrup, S.H. and Erickson, H.P.,** 1992: Kinetics of protein-protein association explained by Brownian dynamics computer simulation, *Proceedings of the National Academy of Science of the USA, Biochemistry*, **89**, 3338-3342.
- Milla, M. E. and Sauer, R. T.,** 1994: p22 Arc Repressor: Folding Kinetics of a Single-Domain, Dimeric Protein, *Biochemistry*, **33**, 1125-1133.
- Monera, O. D., Kay, C. M. And Hodges, R. S.,** 1994: Protein denaturation with guanidine hydrochloride or urea provides a different estimate of stability depending on the contributions of electrostatic interactions, *Protein Science*, **3**, 1984-1991.
- Moro, F., Muga, A.,** 2006: Thermal Adaptation of the Yeast Mitochondrial Hsp70 System is Regulated by the Reversible Unfolding of its Nucleotide Exchange Factor, *Journal of Molecular Biology*, **358**, 5, 1367-1377.
- Moult, J.,** 2005: A decade of CASP: progress, bottlenecks and prognosis in protein structure prediction, *Current Opinion in Structural Biology*, **15**, 285–289.
- Muller GW.,** 1997: Thalidomide: From tragedy to new drug discovery, *ChemTech*, **27**, 21-25.
- Najera, H., Costas, M. and Fernandez-Velasco, D.A.,** 2003: Thermodynamic characterization of yeast triosephosphate isomerase refolding : insights into the interplay between function and stability as reasons for the oligomeric nature of the enzyme. *Biochemistry Journal*, **370**, 785-792.
- Nakamura, K., Aizawa, M., Miyawaki, O.,** 1988: In electro-enzymology coenzyme regeneration. Springer-Verlag, Berlin and Heidelberg, 87-161.
- Nollen, E. A. A. and Morimoto, R. I.,** 2002: Chaperoning signaling pathways: molecular chaperones as stress-sensing heat shock proteins, *Journal of Cell Science*, **115**, 2809-2816.
- Odintseva, E.R., Popova, A.S., Rojkova, A.M., Tishkov, V.I.,** 2002: Role of cysteine residues in stability of bacterial formate dehydrogenase, *Bull. Moscow Univ., Ser. 2 Chem.* **43**, 356–359.
- Oh, K. H., Nam, S. H. and Kim, H.S.,** 2002: Improvement of Oxidative and Thermostability of *N*-Carbamyl-D-Amino Acid Amidohydrolase by Directed Evolution, *Protein Engineering*, **15**, 8, 689–695.
- Oliveberg, M. and Fersht, A. R.,** 1996: Formation of electrostatic interactions on the protein-folding pathway, *Biochemistry*, **35**, 8, 2726–2737.
- Olson, B.J.S.C., Skavdah, M.Ramberg, H., Osterman, J. C., Markwell, J.,** 2000: Formate dehydrogenase in *Arabidopsis thaliana*: characterization and possible targeting to the chloroplast, *Plant Science*, **159**, 205–212.

- Pandya, M. J., Williams, P. B., Dempsey, C., Shewry, P. R. and Clarke, A. R.,** 1999: Direct kinetic evidence for folding via a highly compact, misfolded state, *The Journal of Biological Chemistry*, **274**, 38,. 26828–26837.
- Parisi, M., Mazini, A., Sorbi, R. T., Ramoni, R., Grolli, S., Favilla, R.,** 2005: Role of the disulphide bridge in folding, stability and function of porcine odorant binding protein: Spectroscopic equilibrium studies on C63A/C155A double mutant. *Biochimica et Biophysica Acta*, **175**, 30-39.
- Parker, M.J., Lorch, M., Sessions, R.B., Clarke, A.R.,** 1998: Thermodynamic properties of transient intermediates and transition states in the folding of two contrasting protein structures. *Biochemistry*, **37**, 2538-2545.
- Patel, R. N.,** 2004: Biocatalytic Synthesis of Chiral Intermediates, *Food Technology and Biotechnology* **42**, 4, 305–325.
- Pecher, P. and Arnold, U.,** 2009: The effect of additional disulphide bonds on the stability and folding of ribonuclease A, *Biophysical Chemistry*, **141**, 21–28.
- Perl, D. and Schmid, F.X.,** 2001: Electrostatic Stabilization of a thermophilic cold shock protein, *Journal of Molecular Biology*, **313**, 343-357.
- Permyakov, S. E., Makhatadze, G. I., Owenius, R., Uversky, V. N., Brooks. L., Permyakov, E. A., Berliner, L. J.,** 2005: How to improve nature: study of the electrostatic properties of the surface of α -lactalbumin, *Protein Engineering, Design & Selection*, **18**, 9, 425–433.
- Pokkuluri, P. R., Raffin, R., Dieckman, L., Boogaard, C., Stevens, F. J. and Schiffer, M.,** 2002: Increasing Protein Stability by Polar Surface Residues: Domain-Wide Consequences of Interactions Within a Loop Biosciences Division, *Biophysical Journal*, **82** , 391–398.
- Popov, V.O., Thiskov, V.I.,** 2003: NAD⁺-dependent formate dehydrogenase. From a model enzyme to a versatile biocatalyst, *Protein Structures: Kaleidoscope of Structural Properties and Functions*, 441-443.
- Prabhu, N. V. and Sharp, K. A.,** 2005: Heat capacity in Proteins, *Annual Review. of Physical Chemistry*, **56**, 521–48.
- Privalov, P. L.,** 1996: Intermediate states in protein folding. *Journal of Molecular Biology*, 258, 707–725.
- Prosinecki, V., Faisca, P. F. N. and Gomes, C. M.,** 2007: Conformational States and Protein Stability from a Proteomic Perspective, *Current Proteomics*, **4**, 44-52 44
- Radford, S. E., Gosal, W. S., Platt, G. W.,** 2005: Towards an understanding of the structural molecular mechanism of beta(2)-microglobulin amyloid formation in vitro, *Biochimica Et Biophysica Acta-Proteins and Proteomics*, **1753**, 1, 51-63.
- Ragone, R.,** 2000: How the Protein Concentration Affects Unfolding Curves of Oligomers, *Biopolymers*, **53**, 221–225.

- Rainer, J., and Rainer, R.,** 1989: Folding Proteins. In: Creighton T (ed) Protein Structure (a practical approach), 1st edn. IRL Press, Oxford.
- Rajagopalan, L., Chin, C. C. and Rajarathnam, K.,** 2000: Role of Intramolecular Disulfides in Stability and Structure of a Noncovalent Homodimer, *Biophysical Journal*, **93**, 2129–2134.
- Ramesh N .,** 2004: Biocatalytic Synthesis of Chiral Pharmaceutical Intermediates, *Food Technology and Biotechnology*, **42**, 4, 305–325.
- Rashid, F., Sharma, S. and Bano, B.,** 2005: Comparison of Guanidine Hydrochloride (GdnHCl) and Urea Denaturation on Inactivation and Unfolding of Human Placental Cystatin (HPC), *The Protein Journal*, **24**, 5, 283-292.
- Razvi, A and Scholtz, J. M.,** 2006: Lessons in stability from thermophilic proteins, *Protein Science*, **15**, 1569-1578.
- Rees, D. C. and Robertson, A. D.,** 2001: Some thermodynamic implications for the thermostability of proteins, *Protein Science*, **10**, 1187-1194.
- Reetz, M. F., Carballeira, j. D. and Vogel, A.,** 2006: Iterative Saturation Mutagenesis on the Basis of B Factors as a Strategy for Increasing Protein Thermostability, *Angewandte Chemie International Edition*, **45**, 7745 –7751.
- Reiersen, H. and Rees, A. R.,** 2000: Trifluoroethanol may form a solvent matrix for **assisted** hydrophobic interactions between peptide side chains, *Protein Engineering*, **13**, 11, 739-743.
- Relyea, H.A., Vrtis, J. M., Woodyer, R., Rinkus S. A., van der Donk, W. A.,** 2005: Inhibition and pH dependence of phosphite dehydrogenase, *Biochemistry*, **44**, 6640–6649.
- Riley, P. W., Cheng, H., Samuel, D., Roder, H. and Walsh, P. N.,** 2007: Dimer Dissociation and Unfolding Mechanism of Coagulation Factor XI Apple 4 Domain: Spectroscopic and Mutational Analysis, *Journal of Molecular Biology*, **367**, 558–573.
- Robertson, A.D., Murphy, K.P.,** 1997: Protein Structure and the Energetics of Protein Stability. *Chemical Reviews*. **97**, 5, 1251-1268.
- Robic, S., Guzman-Casado, M., Sanchez-Ruiz, J. M. and Marqusee, S.,** 2003: Role of residual structure in the unfolded state of a thermophilic protein, *Proceedings of the National Academy of Science of the USA*, **100** , 20, 11345–11349.
- Robinson-Rechavi, M., Alibés, A. and Godzik, A.,** 2006: Contribution of Electrostatic Interactions, Compactness and Quaternary Structure to Protein Thermostability: Lessons from Structural Genomics of *Thermotoga maritima*, *Journal of Molecular Biology*, **356**, 2, 547-557.
- Roca, M., Messer, B., Warshel A.,** 2007: Electrostatic contributions to protein stability and folding energy, *FEBS Letters* , **581**, 10, 2065-2071.

- Rodriguez, E., Wood, Z. A., Karplus, P. A. and Lei, X. G., 2000:** Site-Directed Mutagenesis Improves Catalytic Efficiency and Thermostability of *Escherichia coli* pH 2.5 Acid Phosphatase/Phytase Expressed in *Pichia pastoris*, *Archives of Biochemistry and Biophysics*, **382**, 1, 105-112.
- Rojkova, A.M., Galkin, A.G., Kulakova, L.B., Serov, A.E., Savitsky, P.A., Fedorchuk, V.V., Tishkov, V.I., 1999:** Bacterial formate dehydrogenase. Increasing the enzyme thermal stability by hydrophobization of alpha Helices, *FEBS Letters*, **445**, 183–188.
- Rubingh, D. N., 1997:** Protein engineering from a bioindustrial point of view, *Current Opinion in Biotechnology*, **8**, 4,417-422.
- Rudra, S.G., Shivhare, U. S., Basu, S. and Sarkar, B.C., 2008:** Thermal inactivation kinetics of peroxidase in coriander leaves. *Food and Bioprocess Technology*, **1**, 187–195.
- Rumfeldt, J. A.O., Galvagnion, C., Vassall, K. A., Meiering, E. M., 2008:** Conformational stability and folding mechanisms of dimeric proteins, *Progress in Biophysics and Molecular Biology* **98**, 61–84.
- Russo, A., Antignani, A., Giancola, C. and D'Alessio, G., 2002:** Engineering the refolding pathway and the quaternary structure of seminal ribonuclease by newly introduced disulfide bridges, *Journal of Biological Chemistry*, **277**, 48643-48649.
- Rutgers University, 2008, April 11,** Protein Data Bank Archives, 50000th Molecule Structure. *Science Daily*. Retrieved June 17.
- Sali, A. and Blundell, T. L., 1993:** Comparative protein modelling by satisfaction of spatial restraints, *Journal of Molecular Biology*, **234**, 779-815.
- Sambrook, J., Fritsch, E.F., Maniatis, T., Molecular Cloning-A Laboratory, Manual, 2nd Edn.;** Cold Spring Harbor Laboratory Press: USA, 1989.
- Sanchez, R. and Sail, A., 1997:** Advances in comparative protein-structure modelling, *Current Opinion in Structural Biology*, **7**, 206-214.
- Sarmentoa, A. C., Oliveiraa, C. S., Pereiraa, A., Esteves , V. I., Moirc, A.J.G., Saraivad, J., Pirese, E., Barros, M., 2009:** Unfolding of cardosin A in organic solvents and detection of intermediaries. *Journal of Molecular Catalysis B: Enzymatic*, **57**, 115–122.
- Schirwitz, K., Schmidt, A. and Lamzin, V. S., 2007:** High-resolution structures of formate dehydrogenase from *Candida boidinii*, *Protein Science*, **16**, 1146-1156.
- Schlosshauer, M. and Baker, D., 2004:** Realistic protein–protein association rates from a simple diffusional model neglecting long-range interactions, free energy barriers, and landscape ruggedness. *Protein Science*, **13**, 1660–1669.
- Schreiber, G., Fersht, A.R., 1996:** Rapid, electrostatically assisted association of proteins. *Nature Structural and Molecular Biology*, **3**, 5, 427-31.

- Seelbach, K., Riebel, B., Hummel, W., Kula, M. R., Tishkov, V. I., Egorov, A. M., Wandrey, C., Kragl, U., 1996: A novel, efficient regenerating method of NADPH using a new formate dehydrogenase, *Tetrahedron Letters*, **37**, 9, 1377-1380.
- Serov, A. E. , Popova, A. S and Tishkov, V. I. , 2002: The Kinetic Mechanism of Formate Dehydrogenase from Bakery Yeast, *Doklady Biochemistry and Biophysics*, **382**, 26–30.
- Serov, A.E., Odintzeva, E.R., Uporov, I.V., Tishkov, V.I., 2005: Use of Ramachandran plot for increasing thermal stability of bacterial formate dehydrogenase, *Biochemistry (Mosc.)*, **70**, 804–808.
- Serrano, L., Bycroft, M., Fersht A. R., 1991: Aromatic-aromatic interactions and protein stability. Investigation by double-mutant cycles. *Journal of Molecular Biology*, **218**, 2, 465-75.
- Shaked, Z., Whitesides, G. M., 1980: Enzyme-catalyzed organic synthesis: NADH regeneration by using FDH, *Journal of American Chemical Society*, **102**, 7104–7105.
- Slusarczyk, H., Felber, S., Kula, M.R., Pohl, M., 2000: Stabilization of NAD⁺-dependent formate dehydrogenase from *Candida boidinii* by site-directed mutagenesis of cysteine residues, *European Journal of Biochemistry*, **267**, 1280–1289.
- Spadiut, O., Leitner, C., Salaheddin, C., Varga, B., Vertessy, B. G., Tan, T. C., Divne, C., Haltrich, D., 2009: Improving thermostability and catalytic activity of pyranose 2-oxidase from *Trametes multicolor* by rational and semi-rational design. *FEBS Journal*, **276**, 3, 776-792.
- Spector, S., Wang, M., Carp, S.A., Robblee, J., Hendsch, O.Z.S Fairman, R., Tidor, B. and Raleigh, D.P., 2000: Rational Modification of Protein Stability by the Mutation of Charged Surface Residues, *Biochemistry*, **39**, 872-879.
- Stagg, L., Zhang, S. O., Cheung, M. S. and Stafshede, P. W., 2007: Molecular crowding enhances native structure and stability of protein flavodoxin, *Proceedings of the National Academy of Science of the USA* **104**, 48, 18976-18981.
- Stemmer, W. P. C., 1994: DNA shuffling by random fragmentation and reassembly: *In vitro* recombination for molecular evolution, *Proceedings of the National Academy of Science of the USA*, **91**, 10747-10751.
- Stevens, J.M., Armstrong, R.N., Dirr, H.W. , 2000: Electrostatic interactions affecting the active site of class sigma glutathione S-transferase, *Biochemistry Journal*, **347**, 193-197.
- Suárez, M. and Jaramillo, A., 2009: Challenges in the computational design of proteins, *Journal of the Royal Society Interface*, 1-15.
- Suzuki, K., Itai, R., Suzuki, K., Nakanishi, H., Nishizawa, H. K., Yoshimura, E. and Mori, S., 1998: Formate Dehydrogenase, an Enzyme of Anaerobic Metabolism, Is Induced by Iron Deficiency in Barley Roots, *Plant Physiology*, **116**, 725–732.

- Svensson, A.K.E., Bilsel, O., Kondrashkina, E., Zitzewitz, J.A. and Matthews, C.R.**, 2006: Mapping the Folding Free Energy Surface for Metal-free Human Cu,Zn Superoxide Dismutase. *Journal of Molecular Biology* **364**, 1084–1102.
- Svensson, J., Andersson, C., Reseland, J. E., Lyngstadaas P. R., Bülow, L.**, 2006: Histidine tag fusion increases expression levels of active recombinant amelogenin in *Escherichia coli*. *Protein Expression and Purification*, **48**, 11, 34-41
- Synowiecki, J., Grzybowska, B., Zdzieblo, A.**, 2006: Sources, properties and suitability of new thermostable enzymes in food processing, *Critical Reviews in Food Science and Nutrition*, **46**, 197-205.
- Takita, T., Aono, T., Sakurama, H., Itoh, T., Wada, T., Minoda, M., Yasukawa, K., Inouye, K.**, 2008: Effects of introducing negative charges into the molecular surface of thermolysin by site-directed mutagenesis on its activity and stability, *Biochimica et Biophysica Acta - Proteins & Proteomics*, **1784**, 3, 481-488.
- Tao, H. and Cornish, V. W.**, 2002: Milestones in directed enzyme evolution, *Current Opinion in Chemical Biology*, **6**, 858–864.
- Thangudu, R. R., Manoharan, M., Srinivasan, N., Cadet, F., Sowdhamini, R. and Offmann, B.**, 2008: Analysis on conservation of disulphide bonds and their structural features in homologous protein domain families *BMC Structural Biology*, **8**, 55, 1-22.
- Tigerstrom, A., Schwarz, F., Karlsson, G., Okvist, M. Ivarez-Ru´a, C.A.A, Maeder, D.,Robb, F.T and Sjolín, F.**, 2004: Effects of a Novel Disulfide Bond and Engineered Electrostatic Interactions on the Thermostability of Azurin, *Biochemistry*, **43**, 12563-12574.
- Tishkov, V. I and Zaitseva, E. A.**, 2008: Modern Trends in Biocatalytic Synthesis of Chiral Compounds, *Moscow University Chemistry Bulletin.*, **63**, 2, 111–113.
- Tishkov, V. I. and Popov, V. O.**, 2004: Catalytic Mechanism and Application of Formate Dehydrogenase *Biochemistry (Moscow)*, **69**, 11, 1252-1267.
- Tishkov, V. I., Popov, V.O.**, 2006: Protein engineering of formate dehydrogenase, *Biomolecular Engineering*, **23**, 89–110.
- Tramontano, A.**, 1998: Homology Modeling with Low Sequence Identity Methods: *A Companion to Methods in Enzymology*, **14**, 293–300.
- Trejo, F., Gelpi, J.L.I., Ferrer, A., Boronat, A., Busquets, M. and Cortes, A.**, 2001: Contribution of engineered electrostatic interactions to the stability of cytosolic malate dehydrogenase, *Protein Engineering*, **14**, 11, 911-917.
- Turner, N. J.**, 2003: Directed evolution of enzymes for applied biocatalysis, *Trends in Biotechnology*, **21**, 11, 474-8.
- Url-1** <<http://www.invitrogene.com>>, accessed at 01.05.2006.
- Url-2**<http://www.ch.embnet.org/MD_tutorial/pages/MD.Part2.html>, accessed at 04.11.2008.

- Url-3**<<http://www.ccl.net/cca/documents/molecular-modeling/node9.html>>, accessed at 04.11.2008.
- Url4**<http://www.wag.caltech.edu/publications/theses/alan/subsection1_4_0_2_2.html>, accessed at 04.11. 2008.
- Url-5**<http://cmt.dur.ac.uk/sjc/thesis_ppr/node21.html>, accessed at 04.11. 2008.
- Url-6**<<http://www.ncbi.nlm.nih.gov>>, accessed at 21.10. 2009.
- Uversky, V. N.**, 2003,: Protein folding revisited. A polypeptide chain at the folding – misfolding – nonfolding cross-roads: which way to go?, *Cellular and Molecular Life Sciences*, **60**, 1852–1871.
- Van der Donk, W. A. and Zhao, H.**, 2003: Recent developments in pyridine nucleotide regeneration, *Current Opinion in Biotechnology*, **14**, 421–426.
- Vassall, K.A., Stathopoulos, P.B., Rumfeldt, J.A.O., Lepock, J.R. and Meiering, E.M.**, 2006: Equilibrium Thermodynamic Analysis of Amyotrophic Lateral Sclerosis-Associated Mutant Apo Cu, Zn Superoxide Dismutases, *Biochemistry*, **45**, 7366-7379.
- Voutilainen, S. P., Boer, H., Alapuranen, M., Jänis, J., Vehmaanperä, J. and Koivula, A.**, 2009: Improving the thermostability and activity of *Melanocarpus albomyces* cellobiohydrolase Cel7B, *Applied Microbiology and Biotechnology*, **83**, 261-272.
- Vrtis, J. M., White, A. K., Metcalf, W. W., van der Donk, W.A.**, 2002: Phosphite dehydrogenase: versatile cofactor-regeneration enzyme, *Angewandte Chemie International Edition*, **41**, 3257–3259.
- Waldburg, C.D., Schildbach, J.F. and Sauer, R.T.**, 1995: Are buried salt bridges important for protein stability and conformational specificity?, *Nature*, **2, 2**, 122-128.
- Walker, J. M. and Rapley, R.**, 2008: Molecular Biomethods, 2nd Edition, chapter 35, pp587_HUmanaPress2008, TotowaUSA.
- Wallis, R., Leung, K.Y., Osborne, M.J., James, R., Moore, G.R., Kleanthous, C.**, 1998: Specificity in protein-protein recognition: conserved Im9 residues are the major determinants of stability in the colicin E9 DNase-Im9 complex, *Biochemistry*. **37**, 2, 476-85.
- Watanabe, T., Hattori, T., Tengku, S., Shimada, M.**, 2005: Purification and characterization of NAD-dependent formate dehydrogenase from the white-rot fungus *Ceriporiopsis subvermispota* and a possible role of the enzyme in oxalate metabolism, *Enzyme and Microbial Technology*, **37**, 1, 68-75.
- Wedemeyer, W. J., Welker, E., Narayan, M. and Scheraga, H. A.**, 2000: Disulfide Bonds and Protein Folding, *Biochemistry*, **39**, 15, 4207-16.
- Wei, J., Zhou, J., Xu T. and Lu, B.**, 2009: Rational Design of Catechol-2, 3-dioxygenase for Improving the Enzyme Characteristics, *Applied Biochemistry and Biotechnology*.

- Went, H. M., Benitez-Cardoza, C. G., Jackson, S. E.,** 2004: Is an intermediate state populated on the folding pathway of ubiquitin?, *FEBS Letters*, **567**, 333–338.
- Whitten, S.T. and Moreno, B.G.E.,** 2000: pH Dependence of Stability of Staphylococcal Nuclease: Evidence of Substantial Electrostatic Interactions in the Denatured State, *Biochemistry*, **39**, 14292-14304.
- Wichmann, R., Vasic-Racki, D.,** 2005: Cofactor regeneration at the lab scale, *Advence Biochemical Engineering/Biotechnology*, **92**, 225–260.
- Wickner, S., Maurizi, M. R. and Gottesman, S.,** 1999: Posttranslational Quality Control: Folding, Refolding, and Degrading Proteins, *Science*, **286**,1888-1893.
- Williams, G.J., Nelson, A.S., and Berry, A.,** 2004: Directed evolution of enzymes for biocatalysis and the life sciences, *Cellular and Molecular Life Science*, **61**, 3034-3046.
- Wong, T. S., Tee, K. L., Hauer, B., Schwaneberg, U.,** 2004: Sequence saturation mutagenesis (SeSaM): a novel method for directed evolution, *Nucleic Acids Research*, **32** , 3, 26.
- Woodyer, R., van der Donk, W. A., Zhao, H.,** 2006: Optimizing a biocatalyst for improved NAD(P)H regeneration: directed evolution of phosphite dehydrogenase, *Combinatorial Chemistry & High Throughput Screening*, **9**, 237-245.
- Woodyer, R., Zhao, H., van der Donk, W. A.,** 2005: Mechanistic investigation of a highly active phosphite dehydrogenase mutant and its application for NADPH regeneration, *FEBS*, **272**, 15, 3816-3827.
- Wu, W., Zhu, D. and Hua, L.,** 2009: Site-saturation mutagenesis of formate dehydrogenase from *Candida bodinii* creating effective NADP⁺-dependent FDH enzymes, *Journal of Molecular Catalysis B: Enzymatic*, **61**, 3-4, 157-161.
- Wunderlich, M. Martin, A., Staab, C. A. and Schmid, F. X.,** 2005: Evolutionary Protein Stabilization in Comparison with Computational Design, *Journal of Molecular Biology*, **351**, 1160–1168
- Xian, W., Connolly, P. J., Oslin, M., Hausrath, A. J. and Osterhout, J. J.,** 2006: Fundamental processes of protein folding: Measuring the energetic balance between helix formation and hydrophobic interactions, *Protein Science*, **15**, 2062–2070.
- Xiao, L. and Honig, B.,** 1999: Electrostatic Contributions to the Stability of Hyperthermophilic Proteins, *Journal of Molecular Biology*, **289**, 1435-1444.
- Xu, Z., Jing, K., Liu, Y., Cen, P.,** 2007: High-level expression of recombinant glucose dehydrogenase and its application in NADPH regeneration, *J. Ind. Microbiology and Biotechnology*, **34**, 1, 83-90.
- Yamamoto, H., Mitsuhashi, K., Kimoto, N., Kobayashi, Y., Esaki, N.,** 2005: Robust NADH-regenerator: improved alpha-haloketone-resistant formate dehydrogenase, *Applied Microbiology and Biotechnology*, **67**, 33–39.

- Yamniuk, A. P., Ishida, H., Lippert, D. and Voge, H. J.**, 2009: Thermodynamic Effects of Noncoded and Coded Methionine Substitutions in Calmodulin, *Biophysical Journal* , **96**, 1495–1507.
- Yang, H. M., Yao, B., Meng, K., Wang, Y. R., Bai, Y. G. and Wu, N. F.**, 2007: Introduction of a disulfide bridge enhances the thermostability of a *Streptomyces olivaceoviridis* xylanase mutant, *Journal of Industrial Microbiology & Biotechnology*, **34**, 3, 213-218.
- Yasukawa, K. and Inouye, K.**, 2007: Improving the activity and stability of thermolysin by site-directed mutagenesis, *Biochimica et Biophysica Acta*, **1774**, 1281–1288.
- Ying, Y., Zhang, W.**, 2008: Some properties of polyphenol oxidase from lily., *International Journal of Food Science & Technology*, **43**, 1, 102-107.
- Yokoigawa, K., Okubo, Y., Soda, K., Misono, H.**, 2003: Improvement in thermostability and psychrophilicity of psychrophilic alanine racemase by site-directed mutagenesis, *Journal of Molecular Catalysis. B, Enzymatic*, **23**, 2-6, 389-395.
- Young, J. C., Moarefi, I. and Hartl, F. U.**, 2001: Hsp90 : a specialized but essential protein-folding tool, *The Journal of Cell Biology*, **154**, 2, 267-274 .
- Young, J. C., Agashe, V. R., Siegers, K. and Hartl, F. U.**, 2004: Pathways of chaperone-mediated protein folding in the cytosol, *Nature Reviews Molecular Cell Biology*, **5**, 781.
- Yun, S., Urbanc, B., Cruz, L., Bitan, G., Teplow, D. B. and Stanley, H. E.**, 2007: Role of electrostatic interactions in amyloid β -protein (Ab) oligomer formation: A discrete molecular dynamics study, *Biophysical Journal*, **92**, 4064–4077.
- Zheng, I., Baumann, U. and Reymond, J. L.**, 2004: An efficient one-step site-directed and site-saturation mutagenesis protocol, *Nucleic Acids Research*, **32**, 14, 115.
- Zhou, H.X., Wong, K.Y. and Vijayakumar, M.**, 1997: Design of fast enzymes by optimizing interaction potential in active site, *Proceedings of the National Academy of Science of the USA, Biophysics* **94**, 12372–12377.
- Zawirska-Wojtasiak, R.**, 2006: Chirality and the nature of the food authenticity of aroma, *Acta Scientiarum Polonorum, Technology. Aliment*, **5**, 1, 21-36.
- Zwaning, R., Szabo, A. and Bagchi, B.**, 1992: Levinthal's Paradox, *Proceedings of the National Academy of Science of the USA*, **89**, 20-22.

APPENDICES

APPENDIX A.1 : Essential buffers and stock solutions used in study.

APPENDIX A.2 : Essential chemicals and biochemicals used in study.

APPENDIX A.3 : Map of pQE-2 expression vector used in study.

APPENDIX A.1: Essential buffers and stock solutions used in study.

Purification Buffers for 1000 ml

Lysis buffer :

50 mM NaH₂PO₄

300 mM NaCl

10 mM imidazole

Wash buffer:

50 mM NaH₂PO₄

300 mM NaCl

20 mM imidazole

Elution buffer :

50 mM NaH₂PO₄

300 mM NaCl

250 mM imidazole

Adjust pH of all buffers to 8.0 using NaOH.

10x TAGZyme Buffer for 500 ml

200 mM NaH₂PO₄

1.5 M NaCl 43.83 g

Adjust to desired pH with NaOH. Filter (0.2 µm) into a sterile storage vessel and store at 2–8°C.

LB medium for 1000 ml

10 g tryptone,

5 g yeast extract

10 g NaCl

LB agar: LB medium containing 15 g/liter agar

Ampicillin stock solution: 100 mg/ml in H₂O, sterile filter, store in aliquots at –20°C

IPTG (1 M): 238 mg/ml in H₂O, sterile filter, store in aliquots at –20°C

SDS-PAGE sample buffers

5x SDS-PAGE sample buffer: 0.225 M Tris·Cl, pH 6.8; 50% glycerol; 5% SDS; 0.05% bromophenol blue; 0.25 M DTT

SDS-PAGE tank buffer for 1000 ml

3.02 g Tris-Base

14.4 g Glycine

GdnHCl stock solution (10M): 47.7 g/100 ml in dH₂O

Urea stock solution (8M): 24 g/50 ml in dH₂O

APPENDIX A.2 : Essential chemicals and biochemicals used in study.

Chemical/Biochemical	Manufacturer	Catalog no
NAD ⁺ Free acid	Roche	10127973001
Formate	Aldrich	10 760-3
IPTG	Roche	11411446001
DTT	Roche	10 708 984 001
Ampicillin (anhydrous)	Sigma-Aldric	A2804
Bovine serum albumin	Sigma-Aldric	85041C
Bradford Reagent	Sigma-Aldric	B6916
T4 Ligase	Sigma-Aldric	D2886
Lysosyme	Sigma-Aldric	62971
DNA Marker	Fermentas	SM0193
Pst I	Sigma-Aldric	R7023
SacI	Sigma-Aldric	R5268
GeneTailor site directed mutagenesis system	Invitrogen	12397014
His-tagged protein stain	Invitrogen	LC6030
TAGzyme expression Kit	Qiagen	34300
Ni-NTA Agarose	Qiagen	30230
pQE-2 expression vactor	Qiagen	32932
DApase enzyme	Qiagen	34362
Qcyclase/pGAPase	Qiagen	34342
Tripton	Merck	1.07213.1000
NaCl	CarloErba	368257
Yeast Extract	LabM	MC1
Tris	Amresco	0826
NaH ₂ PO ₄	Riedel-de Haen	04269
Imidazole	Applichem	A1073,0100
Plasmid Isolation Kit	Roche	11754 785 001
Taq Polymerase	Fermentas	EP0401
Pfu Polymerase	Fermentas	EP0501
Platinum Polymerase	Invitrogen	11304,011
Unstained Protein Marker	Fermentas	SM0431
Prestained protein Marker	Fermentas	SM0441
SDS	Sigma	L-4390
GdnHCl	Biochemica	A 1499, 1000
Urea	Merck	1.08487.1000
Glycine	Merck	5.00190.1000
Ethanol	Riedel-de Haen	32221
Methanol	Riedel-de Haen	24229
Isopropanol	Merck	1.01040.2500
Acetic acid	Riedel-de Haen	27225
Primers	Operon	
Amoniumpersulphate	Sigma	A4418

APPENDIX A.3: Map of pQE-2 expression vector used in study.

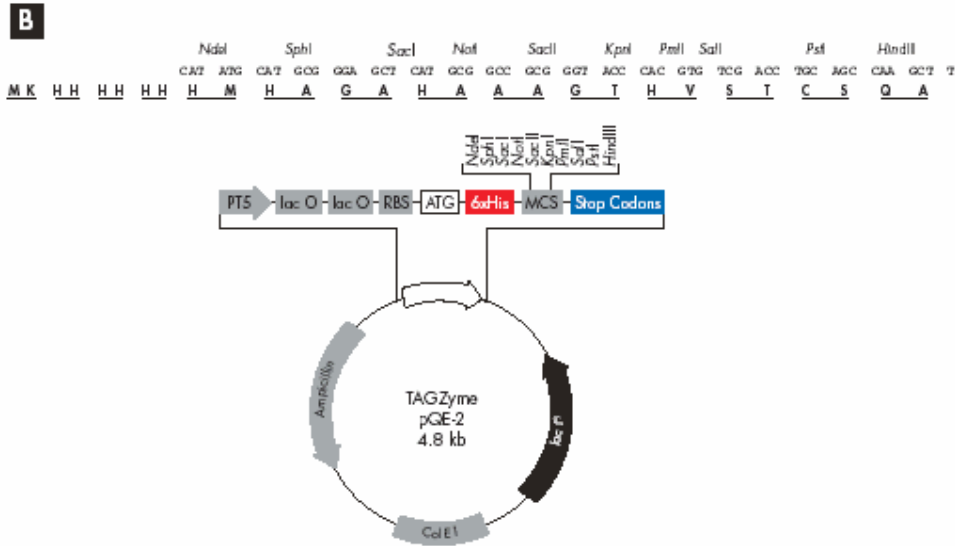


Figure A.1 : TAGZyme™ pQE-2 expression vector.



CURRICULUM VITAE

Candidate's full name: Emel Ordu

Place and date of birth: İstanbul, 1977

Permanent Address: Tantavi Mah. Köroğlu cad. Basiret sok. No:14/6
Ümraniye/İstanbul

Universities and Colleges attended:

Master of Science: Yıldız Technical University, Institute of Science and Technology,
Department of Biology.

Bachelor of Science: University of Istanbul, Faculty of Science, Department of
Biology.

High School: Pertevniyal High School.

Publications in SCI:

From Phd studies;

- Emel B. Ordu, Gus Cameron, Anthony R. Clarke, Nevin Gül Karagüler “Kinetic and thermodynamic properties of the folding and assembly of formate dehydrogenase” **FEBS Letters**, 583: 2887-2892, 2009.
- Emel Bıçakçı Ordu and Nevin Gül Karagüler, “Improving the purification of NAD⁺dependent formate dehydrogenase from *Candida methylica*”, **Prep. Biochem. and Biotech**, 37: 333-341,2007.
- N.G. Karaguler,, R.B. Sessions, B. Binay, E.B. Ordu and A.R. Clarke, “Protein engineering applications of industrially exploitable enzymes: *Bacillusstearothermophilus* LDH and *Candida methylica* FDH, **Biochemical Society Transactions**, 35: 1610-1615, 2007.
- Emel B. Ordu, Richard B. Sessions, Anthony R. Clarke, Nevin Gül Karagüler “Effect of surface electrostatic interactions on the stability and folding of formate dehydrogenase from *Candida methylica*”Submitted in Feb.2010.
- Emel B. Ordu, Richard B. Sessions, Anthony R. Clarke & Nevin Gül Karagüler, “ Site Saturation Mutagenesis Application on the first residue of *Candida methylica* Formate Dehydrogenase Based on Results of Introduction a Disulphide Bridge to Increase Thermostability “ to be submitted in May 2010.

From MSc studies;

- Bıçakçı, E., Memon, A. R., An Efficient and Rapid *in vitro* Regeneration System For Metal Resistant Cotton. *Biologia Plantarum*, 9 (3): 415-417, 2005.

Publications in congress

- Ordu E. B., Sessions R. B., Clarke A. R., Gül-Karagüler N. “NAD⁺-dependent formate dehydrogenase from *Candida methylica* with the increased thermostability” ProStab 2009, 8th International Conference on Protein Stabilisation 2009, 14th - 17th April 2009, Graz, Avustria. Poster.
- Ordu EB, Sessions RB, Clarke AR, Gul-Karaguer N, Increasing the thermostability of NAD(+)-dependent formate dehydrogenase from *Candida methylica* by homology modeling based on strategy of optimization of protein surface electrostatic interactions, *FEBS JOURNAL* (275) 226-226, JUN 2008.
- Kahraman M, Ordu EB, Karaguler NG, Tamerler C ,Media optimization on *Escherichia coli* with pQE-2 carrying FDH gene in molasses-based medium, *FEBS JOURNAL* (275) 362-362 , JUN 2008.
- Doluca O, Ordu, E. B, Kisakesen HI, Sessions RB, Clarke AR, Tamerler C, Gul-Karaguler N, Effects of cysteine/cystine engineering on thermal stability of formate dehydrogenase from *Candida methylica*, *FEBS Journal* (275) 398-398, JUN 2008.
- Yelboga, E, Candan Z, Binay B, Ordu EB, Sessions RB Clarke AR, Gül-Karaguler N, Crucial residues in NAD+/NADP+ specificity of formate dehydrogenase from *Candida methylica*, *FEBS Journal* (275)234-234, JUN 2008.
- Barış Binay, Kemal Şanlı, Emel Ordu, Nevin Gül Karagüler, Application of Computational Methods to Design Thermostable *Candida methylica* FDH” International Enzyme Engineering Symposium in Kusadasi Turkey), 1-5 October, 2008.
- Ordu E, Moreton KM., Binay B., Doluca, O., Yelboğa E., Kahraman M., Yeşiladalı K.S., Sessions R. B., Clarke A.R., Tamerler, C., Gül-Karagüler N. “Production of enzyme based compounds for Pharmaceutical Industry” 5th International Symposium on Pharmaceutical Chemistry, September 5-7, 2007 Istanbul, TURKEY, poster.
- Bıçakçı E., Sessions R. B., Clarke A. R., Gül-Karagüler N., “Increasing the thermostability of NAD⁺-dependent formate dehydrogenase from *Candida methylica* by optimization of surface electrostatic interaction” ProStab 2007, 7th International Conference on Protein Stabilisation 2007, 11th - 14th April 2007,, Exeter, UK, poster.
- Osman Doluca, , Bıçakçı E., Binay B., , Sessions R. B., Clarke A.R., Tamerler, C., Gül-Karagüler N., “Enhancing Thermal Stability of Formate Dehydrogenase from *Candida methylica* by cysteine/cystine engineering” ProStab 2007, 7th International Conference on Protein Stabilisation 2007, 11th - 14th April 2007, Exeter, UK., poster.

- Yelboga, E., Binay B. Bıçakçı, E., Session RB., Clarke, AR, Gül Karagüler N. “ Alteration the coenzyme specificity of formate dehydrogenase from *Candida methylca*” ProStab 2007, 7th International Conference on Protein Stabilisation 2007, 11th - 14th April 2007, Exeter, UK. , poster.
- E. Bıçakçı, B. Binay, R.B. Sessions, A.R. Clarke, N. Gül Karagüler “Protein engineering application on pharmaceutically Important Enzymes:LDH and FDH. PROTEOMICS- Protein Structure and Function Workshop with international partipation, 20-23 September 2006, Antalya-Türkiye, poster.
- SOPHIED Integrated Project - 1st Plenary Meeting, Serial Focused Research Meetings – Workshop, October 10-13, 2005, MOBGAM.
- E. Bıçakçı and A.R. Memon “ Screening and selection of cotton genotypes resistant to Cd Toxicity”, pp 105,1st Scientific Workshop And Management Committee Meeting,14-16 June 2005, Pisa - Italy
- Emel Bıçakçı, Abdülrezzak Memon, “Farklı pamuk genotiplerinin Cd, Cu ve Ni streslerine karşı gösterdikleri tepkilerin incelenmesi ve karşılaştırılması.” XIII. Biyoteknoloji Kongresi, Çanakkale, 25-29 Ağustos 2003, pp.77., poster
- Emel Bıçakçı, Abdülrezzak Memon, “Screening and in vitro regeneration of Metal Resistant Cotton Grown in Turkey.” 28th International Meeting of The Federation of European Biochemical Societies, İstanbul, 20-25 Ekim 2002., poster
- Memon, A.R., Bıçakçı, E., Ozdemir, A. and Gencer, O., 2001., Chama, Greece. In-vitro regeneration of different cotton genotypes in Turkey and development of stress resistant cotton. The Inter- Regional Cooperative Research Network on Cotton. pp.15-16.
- Memon, A. R., Özdemir,A., Cevher, B., Bıçakçı, E., Kumbaracı, M., Gencer, O., 2000., Adana -TURKEY. Characterization and Expression of Heavy Metal Induced Genes in Cotton Grow Southern Region of Turkey. The Inter- Regional Cooperative Research Network on Cotton. pp.253-257.